

# **CRANFIELD INSTITUTE OF TECHNOLOGY**

**COLLEGE OF AERONAUTICS**

**DEPARTMENT OF AVIONICS**

**ELECTRONIC SYSTEM DESIGN GROUP**

**PhD THESIS**

**ACADEMIC YEAR 1993-1994**

**GEORGE PAMPALOS**

**THEORY AND DESIGN OF AN ELECTRODELESS PORTABLE CONDUCTIVITY METER**

**SUPERVISOR**

**R. ANDREW**

## ACKNOWLEDGEMENTS

I am greatly indebted to Mr R. Andrew for his expert supervision and advice throughout the course of this work and to Mr G. Young for his advice and guidance.

The technical assistance and advice of Mr J. Hackett and Mr D. Slater as well as several members of ESD staff is greatly appreciated.

I also owe many thanks to my fellow students at ESD for their friendship and moral support.

The financial support of "ΠΑΓΧΙΑΚΟ ΙΔΡΥΜΑ ΥΠΟΤΡΟΦΙΩΝ Ι. Δ. ΠΑΤΕΡΑ" during part of my study at Cranfield is also acknowledged and appreciated.

Last but not least I would like to express my gratitude to my family for their constant encouragement and unending support.

*To all I have lost during the years of my stay at Cranfield*

## ABSTRACT

The method of electrodeless conductivity measurement using two coils wound on toroidal ferrite cores in close proximity, coupled by the induced current in the electrolyte and operating in the audio range of frequencies has been used in process control since its introduction in the 1950s. It presents several advantages over the traditional method of measuring conductivity most important of which are stability, ruggedness, and maintenance free operation. Its major disadvantage is the large sample size required for correct operation.

Despite its long established use in industry with various configurations of probe design, there is no published theory of its operation. A model of the probe operation is presented which takes into account the pattern of current flow induced in the electrolyte. This allows the electrolyte to be modelled as a resistance and the effect of geometrical factors upon this resistance is described. The operation of the probe can be represented by an equivalent circuit and theoretical expressions for the cell constant are derived. The correctness of this theory is confirmed by practical measurements. Factors affecting the performance of the probe such as operating frequency, cable length and coupling have been examined.

The design and development of a conductivity meter which operates with an existing electrodeless sensor is described. It comprises analog circuitry which interfaces the sensor to a microcontroller. The microcontroller provides synchronisation, analog circuit control, calculations, display update, and interfacing with a small keyboard. A requirement that the meter be portable necessitated the minimisation of component count, cost and power consumption. Addition of reference curves for various chemicals stored in the microcontroller's EEPROM allows the instrument to be used as a concentration meter.

# CONTENTS

<b>CHAPTER 1: INTRODUCTION</b>	<b>1</b>
1.1 Definition of electrolytic conductivity	1
1.2 Common applications of conductivity measurement	4
1.3 Brief history and methods of quantitative conductivity measurement	4
1.4 Literature review of electrodeless conductivity	10
1.5 Objectives of this work	15
 <b>CHAPTER 2: THE ELECTRODELESS SENSOR</b>	 <b>18</b>
2.1 Introduction	18
2.2 Investigation of the electric field in the electrolyte	18
2.2.1 Formulation of difference equation	18
2.2.2 Approximation of difference equation	23
2.2.3 Solution of difference equation	27
2.2.4 Solution for varying probe dimensions	35
2.2.4.1 Effects of varying bore depth	36
2.2.4.2 Effects of varying bore radius	39
2.2.4.3 Effects of toroidal core cross section	40
2.2.4.4 Effects of solution volume around the conductivity probe	40
2.2.5 Derivation of an expression for the cell constant	40
2.3 Equivalent circuit modelling of the conductivity sensor	53
2.3.1 Formulation of an equivalent circuit model	53
2.3.2 Examination of factors affecting the model probe performance	56
2.3.2.1 Effects of variations in the cable resistance on the probe output	58
2.3.2.2 Effects of variations of coupling coefficients on the output current	60

2.3.2.3 Effects of operating frequency on the output current	60
2.3.2.4 Comparison of model and actual probe outputs	67

## **CHAPTER 3: THE HARDWARE PART OF THE CONDUCTIVITY METER 72**

3.1 Introduction	72
3.2 The analog circuit of the conductivity meter	72
3.2.1 Power supply	75
3.2.2 Oscillator	75
3.2.3 Current to voltage converter	76
3.2.4 Amplification/range selection	76
3.2.5 Phase sensitive detector (PSD)	77
3.2.6 Voltage limiter	79
3.2.7 Voltage level shifter	80
3.2.8 The temperature measurement circuit	81
3.2.9 Voltage to frequency (V/F) converter	82
3.2.10 Oscillator amplitude measurement	82
3.2.11 Error considerations in the analog circuit	83
3.3 The digital circuit	86
3.3.1 The microcontroller	86
3.3.2 The display driver	86
3.3.3 The display	87
3.3.4 The keyboard	87

## **CHAPTER 4: THE SOFTWARE PART OF THE CONDUCTIVITY METER 88**

4.1 Introduction	88
4.2 The MC68HC11-a brief overview	88
4.2.1 Memory map - the INIT register	89
4.2.2 Resets and interrupts	90
4.2.3 Real time interrupts and the pulse accumulator system	92

4.3 The program timing	94
4.4 General structure of the software	95
4.5 The subroutines of the program	105
4.5.1 The keyboard handling routines	106
4.5.2 The multiplication routines	118
4.5.3 The display routines	122
4.5.4 Conductivity compensation against oscillator amplitude variations	125
4.5.5 Compensation of temperature measurement against reference voltage variations	126
4.5.6 The temperature compensation/concentration determination routines	127
4.5.7 The autoranging algorithm	141
4.5.8 The key parsing algorithm	143
4.6 Calibration procedure	156
4.7 Error measurements in uncompensated conductivity measurements	157
 CHAPTER 5: CONCLUSIONS	164
5.1 Summary	164
5.2 Suggestions for further work	166
 REFERENCES	169
 APPENDIX 1: TABLES OF DATA FOR THE SOLUTIONS REFERENCE CURVES	172
 APPENDIX 2: LIST OF COMPONENTS	176

# LIST OF FIGURES

1.1	Conductivity variation with temperature and concentration	5
1.2	Wheatstone bridge for conductivity measurement	7
1.3	Four electrode DC system	9
1.4	HF conductimetric cells	10
1.5	Basic components of an electrodeless system	11
1.6	Probe design suitable for immersion in the electrolytic solution	12
1.7	Externally mounted toroidal coil configuration	13
2.1	Probe cross section	19
2.2	Tube of current around probe	20
2.3	Element of current tube	21
2.4	Current tube with infinitesimal gap	22
2.5	Voltage conventions shown on a cross section of the probe	22
2.6	Definition of area under investigation	23
2.7	Typical point of grid	25
2.8	Grid boundaries	29
2.9	Structure of program giving the solution of Laplace's equation	30
2.10	Potential distribution around probe section	31
2.11	Potential distribution for large bore radius	32
2.12	Element volumes for vertical current flow calculation	34
2.13	Element volume for horizontal current flow calculation	35
2.14	Variation of $\sigma/l$ with $b$	37
2.15	Variation of $\sigma/l$ with $1/a^2$	38
2.16	Current and voltage variation with bore depth	41
2.17	Bore and remaining solution resistance variation with bore depth	42
2.18	Current and bore edge voltage variation with bore radius	43
2.19	Bore and remaining solution resistance variation with bore radius	44
2.20	Current and bore edge voltage variation with probe cross section	45



2.21	Bore and remaining solution resistance variation with probe cross section	46
2.22	Current and bore edge voltage variation with horizontal solution area from probe to container edge	47
2.23	Bore and remaining solution resistance variation with horizontal solution area from probe to container edge	48
2.24	Current and bore edge voltage variation with vertical solution area	49
2.25	Bore and remaining solution resistance variation with vertical solution area	50
2.26	Variation of solution resistance outside the cell bore with c for several values of a	52
2.27	Effects of scaling on cell constant	54
2.28	Network equivalent of the conductivity probe	55
2.29	Variation of output current amplitude with cable resistance	59
2.30	Variation of output current phase with cable resistance	61
2.31	Output current amplitude variation with coupling coefficients ( $R_c=0.20\Omega$ )	62
2.32	Output current amplitude variation with coupling coefficients ( $R_c=0.05\Omega$ )	63
2.33	Variation of output current phase with coupling coefficients ( $R_c=0.20\Omega$ )	64
2.34	Variation of output current phase with coupling coefficients ( $R_c=0.05\Omega$ )	65
2.35	Output current and phase variation with operating frequency	66
2.36	Comparison of model and actual probe output	68
2.37	Current variation in the solution	70
2.38	Current variation in the drive circuit	71
3.1	Block diagram of the conductivity measuring system	73
3.2	The analog part of the conductivity meter	74
3.3	The digital part of the conductivity meter	85

4.1	System memory map	91
4.2	Main timer system related registers	93
4.3	Initialisation section	96
4.4	Real time interrupt service routine	99
4.5	Pulse accumulator overflow interrupt service routine	106
4.6	Keyboard connections to microcontroller	108
4.7	Keyboard scanning routine	109
4.8	Key debouncing algorithm	113
4.9	Key release test	116
4.10	16×16 multiplication routine	119
4.11	Special multiplication routine	121
4.12	Main display routine	123
4.13	Conductivity compensation against oscillator amplitude variations	128
4.14	Temperature measurement compensation against voltage reference variations section	129
4.15	General structure of the memory block for storing chemical data of 18°C curve	130
4.16	Method of concentration and $\sigma_{18}$ determination	132
4.17	Temperature compensation/concentration determination section	135
4.18	Subroutine for the calculation of conductivity at solution temperature using the stored reference curve	140
4.19	The autoranging algorithm	144
4.20	General structure of key parsing algorithm	147
4.21	Table driven algorithm for key depression interpretation	149
4.22	Permissible transitions table	150
4.23	Stable state table	151
4.24	Table of addresses of action routines of the key parsing algorithm	152
4.25	New input code derivation section of key parsing algorithm	153
4.26	New stable state derivation section of key parsing algorithm	155
4.27a	Instrument response curve (range ×1)	158
4.27b	Instrument response curve (range ×10)	159
4.27c	Instrument response curve (range ×100)	160

4.28a Instrument error curve (range x1)	161
4.28b Instrument error curve (range x10)	162
4.28c Instrument error curve (range x100)	163

# CHAPTER 1

## INTRODUCTION

### 1.1 Definition of electrolytic conductivity

Electrolytes are a class of materials which conduct electricity by means of positively and negatively charged molecular or atomic charge carriers; these are called ions and this kind of conduction is called ionic conduction. Positively charged ions are called cations and negatively charged ones are called anions because they move towards the cathode and the anode respectively. This kind of conduction differs from the electronic conduction of metals and semiconductors in that there is transport of material when charge is carried; no matter is transferred (other than electrons) in electronic conduction. As a result there is chemical change involving formation or removal of ionic charges at the cathode or anode. Many materials whether gaseous, solid or liquid exhibit ionic conduction under certain circumstances. However we must distinguish materials in which ions are not inherently present, but have to be generated using considerable amounts of energy, from those in which ions naturally exist. The former are insulators at low potentials and only conduct after high voltages have been applied. The latter are called electrolytes and include ionic compounds. Further discussion will be focused entirely on these and their most interesting property, conductance.

When an acid, base or salt is dissolved in water, a considerable proportion becomes spontaneously dissociated into positive and negative ions. These ions have increased mobility, leading to increased conductance of the solution compared to solid electrolytes which in general are poor conductors. In general electrolytic solutions obey Ohm's law, except under abnormal conditions such as

very high voltages or very high frequency currents. Since by Ohm's law the current flowing through a given conductor (under the influence of an EMF) is inversely proportional to its resistance  $R$ , the quantity  $1/R$  is a measure of conducting ability and is termed conductance; this used to be expressed in reciprocal ohms ( $\text{ohm}^{-1}$ ) sometimes called mhos but today the name Siemens is mostly used. The resistance of a conductor varies directly as its length  $l$  and inversely as its area  $a$ , that is

$$R = \rho \frac{l}{a}$$

where  $\rho$  is a constant called specific resistance or resistivity of the particular conducting material. The specific conductance or conductivity is defined as  $1/\rho$ , is denoted by  $\sigma$  and is usually expressed in  $\text{mS/cm}$ .

The solvents usually employed are intrinsically poor conductors. Most often conductivity water (ie water obtained through careful and repeated distillation) is used but also some organic solvents with very low conductivity are popular. Solvents themselves present some (small) degree of dissociation leading to some error in the measurement of solution conductivity, particularly in the lowest conductivity ranges. For example, water ionises as:



This leads to a minimum conductivity of the purest water of  $0.04 \mu\text{S/cm}$  at  $18^\circ\text{C}$ .

The value of conductivity for a specific electrolyte solution is mainly affected by two factors: electrolyte concentration and solution temperature. As expected, higher concentration of the solution leads to increased conductivity (at a fixed temperature) due to the larger number of charge carriers. This relation however is not linear, especially at high concentrations. Among the factors influencing this nonlinearity are:

**Viscosity**; according to Stoke's law, ionic velocity (and consequently conductivity) is inversely proportional to solution viscosity.

**Degree of dissociation**; ionic concentration can be very much different from total electrolyte concentration, as indicated by the electrolyte's dissociation constant

(e.g. weak electrolytes).

**Ionic association**; while strong electrolytes (i.e. electrolytes with high degree of dissociation) are completely dissociated in solutions, association as "ion pairs" might reduce the ionic concentration.

**Asymmetry effect**; according to the Debye Huckel theory, positive ions find themselves among negative ions. Positive and negative ions travel in opposite directions, therefore asymmetric charge gradients can be formed, thus reducing the effect of the driving force.

**Electrophoretic effect**; when an ion moves in some viscous medium, it can be considered to drag along with it quantities of solution in its vicinity. As a result, the neighbouring ions do not move through a stationary medium. This can further restrict the ions' mobility with obvious effects on conductivity. The electrophoretic effect is again a function of concentration.

Attempts have been made to calculate the conductivity of electrolytic solutions taking into account all of the above mentioned factors and specific equations have been established; however they are not of much practical use as they apply only to very low concentrations. The most common practice today (especially in conductometric instrumentation) is to use calibration curves of measured behaviour of conductivity versus concentration at various temperature values.

The other most important factor influencing the value of conductivity is temperature. Some of the temperature related factors are:

**Viscosity**; as mentioned above, conductivity varies inversely with viscosity. Usually this is the most significant temperature related factor affecting conductivity, as it affects the mobility of ions; it varies as about 2% per degree Celsius.

**Dissociation constant**; the degree of dissociation for an electrolytic solution is again a function of temperature.

**Density**; in general an increase in temperature leads to a decrease in conductivity.

Again it is more preferable to use calibration curves for temperature

compensation, should it be needed, than attempting to establish some temperature dependent relationship for each of the above two factors. Conductivity variations with temperature and concentration are also solution composition dependent and usually are similar to these shown in figure 1.1. In order that conductivity values are comparable, they are usually referred to either 18 °C or 25 °C.

## **1.2 Common applications of conductivity measurement**

The measurement of conductivity as a means of concentration determination find is widely used in industry. The diversity of applications can be seen in the following examples:

In chemical streams, when solution strength has to be measured and controlled.  
In food industry for the determination of the strength of the solutions used for fruit peeling.

In waste streams, as way of determining the amount of dissolved solids.

In pulp and paper industry, for the control of white liquor fed to digestors.

In steam boilers, for the control of reduction of dissolved solids and checking the quality of the condensate.

In reverse osmosis, where conductivity is used to monitor equipment performance.

In monitoring drinking water quality.

In monitoring semiconductor rinse water.

In mineral extraction plants for the measurement and control of acid concentration in leach pulps.

In conductimetric titration for the determination of the acid - base balance point.

## **1.3 Brief history and methods of quantitative conductivity measurement**

In 1776 Henry Cavendish described to the Royal Society [1] his attempts to imitate the effects of the torpedo, a fish that can deliver strong electric shocks. In that presentation he also compares the conductivity of distilled and pure water to that of various metals; his conductivity ratios are surprisingly close to modern

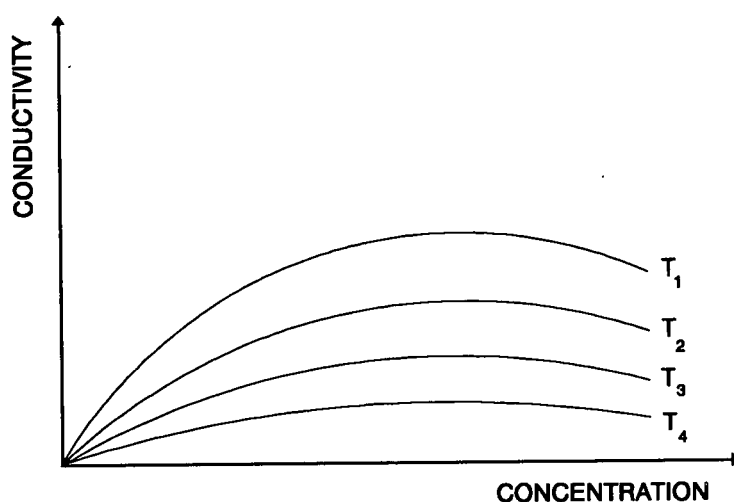


Figure 1.1 Conductivity variation with temperature and concentration

values if allowance is made for temperature variations. Cavendish never published how he obtained these results or the method he had used. It is worth mentioning that at the time he conducted his experiments only static and frictional electricity was available. His records were preserved and later examined and published by J.C. Maxwell [2]. From these records it appears that Cavendish used a pair of glass tubes filled with the solution under investigation. On one end of each tube a sliding electrode was attached so that the effective liquid path could be altered. On the other end fixed electrodes were attached, and these were connected to the outside surfaces of parallel connected Leyden jars. By adjusting the position of the sliding electrodes so that using the shocks he received when touching the knob of each jar with one hand and the sliding electrode with the other, he could determine the relative conductivity of the liquids in the tubes.

Twenty years later the electric battery was invented, allowing more precise electricity measurements using DC currents. It was soon realised however that with the electrodes being in contact with the solution several problems can develop; firstly the discharge of ions with the transfer of electrons results in reduction of the ionic concentration and secondly in most cases these discharged ions affect the surface of the electrodes and consequently the resistance in the vicinity of the electrodes.



One of the earliest and most successful approaches to measurement was conducted by E.N. Horsford [3]. He had been using a well varnished wooden trough with two partitions inserted, supporting two plate electrodes; one of the partitions could slide along the trough therefore the length and depth of the solution column could be adjusted. By changing the length of this column he would adjust the series connected variable resistor so that the series connected galvanometer would give the same reading as before. The difference in the two values of the variable resistor would then represent the difference in resistance of the liquid column. The aim of this method was to eliminate the error due to the above mentioned electrolysis effect. In that way the resistance of the liquid column was compared to that of the wire composing the variable resistor.

The electrolysis effects can be minimised by replacing the DC source with an AC one. Any electrolysis occurring during the first half of each cycle is reversed during the second half, therefore the chemical change in the vicinity of the electrodes is reversed and the overall state of electrodes and solution remains unchanged. This method was first described and used by Kohlrausch in 1869 [4]. The frequency he used was approximately 1000Hz and was provided by a buzzer or small induction coil; the shape of the waveform though, was far from pure sinusoidal. This frequency allowed the use of a telephone receiver as a balance point detector of the Wheatstone bridge he employed. The principle of this method which is still in use today can be seen in figure 1.2.

The variable capacitor in that figure was added later by researchers as it was found it was necessary to offset the inherent capacitance of the solution/electrode interface in the conductivity cell. When balance in resistance and capacitance has been achieved, the following equation holds:

$$\frac{R_1}{R_2} = \frac{R_3}{R_4}$$

With the value of  $R_3$  determined the conductivity of the solution in the calibrated conductivity cell can then easily be derived.

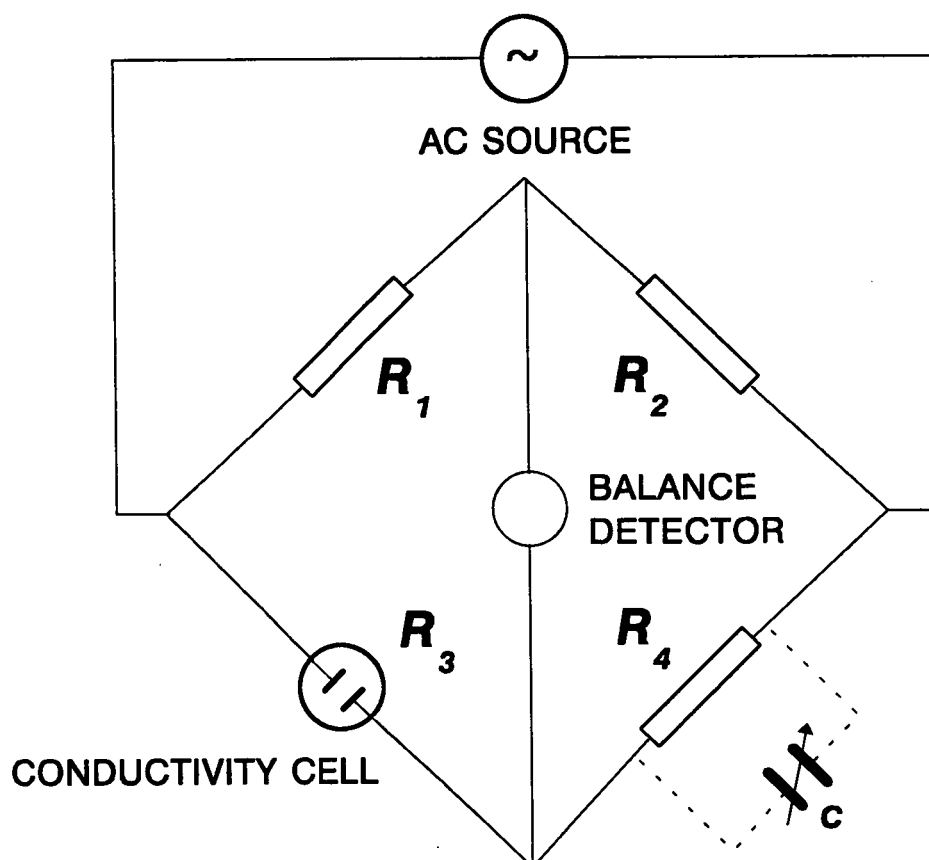


Figure 1.2 Wheatstone bridge for conductivity measurement

Kohlrausch and his co-workers studied the methods and principles of conductivity measurements during the last quarter of last century and produced results which are still considered to be very precise.

Further advances in technology led to the design of improved components and subsequent use of them in superior systems for conductivity measurement. Washburn and Bell [5] used a bridge circuit with an improved AC 1000Hz source, a tuned telephone detector, and platinum film resistors to minimise the capacitive and inductive effects of the wirewound equivalents used until then.

In spite of the obvious advantages of AC measurement methods the interest in DC methods did not cease to exist. Marie and Noyes [6] measured the conductivity of several acids using two hydrogen electrodes and obtained results very close to those of Kohlrausch especially for dilute solutions. They were also using a Wheatstone bridge which could operate on AC current as well. Another

approach was to measure the voltage drop between two electrodes placed in the liquid column between the two main electrodes of the system, when a fixed current was passing. This method has been employed and refined by several workers [7], [8] and more extensively by Gordon and Gunning [20]. The principle of this four electrode system can be seen in figure 1.3.

As electronic component technology progressed, stable high frequency oscillators were designed and constructed. This gave researchers the ability to perform conductivity measurements with electrodes not in contact with the solution. This method is usually called high frequency conductometry or oscillometry and the frequencies employed are in the range 1 to 10 MHz. This method can operate in either inductive or capacitive mode. In the inductive mode the solution holding vessel is placed within the coil as seen in figure 1.4(a); The susceptibility of the solution plays the important role in this configuration.

In the capacitive method the electrodes take the form of metal bands or plates bonded on the external surface of the cell (as seen in figure 1.4(b)). At high frequencies the impedance of the solution becomes a complex function of its resistance, dielectric constant and the capacitance of the circuit. The theory, methods and applications of high frequency conductometry have been extensively reviewed by Pungor [10]. According to Light [11] this method does not appear to be used much today.

This however was not the first electrodeless method to be invented. Back in 1860 Beetz attempted to induce currents in conductive solutions by the motion of a magnet [4]. In 1880 Guthrie and Boys [12] presented a rather complicated method for electrodeless conductivity measurement. They suspended a vessel containing the conductive solution by a torsion wire in the field of powerful rotating magnets, and calculated the conductivity by the force needed to oppose the motion of the liquid. Despite the difficulties they encountered, the results obtained compared very well with those of Kohlrausch.

In 1926 another electrodeless method appeared; S. Ruben [13] used a coil to induce high frequency currents (not mentioning the range of frequencies he used though) in a cylindrical vessel placed into a coil. Then he measured the signal

given by another secondary coil placed on the same axis with the first one; He claimed that the secondary coil signal was inversely proportional to the conductivity of the solution in the vessel.

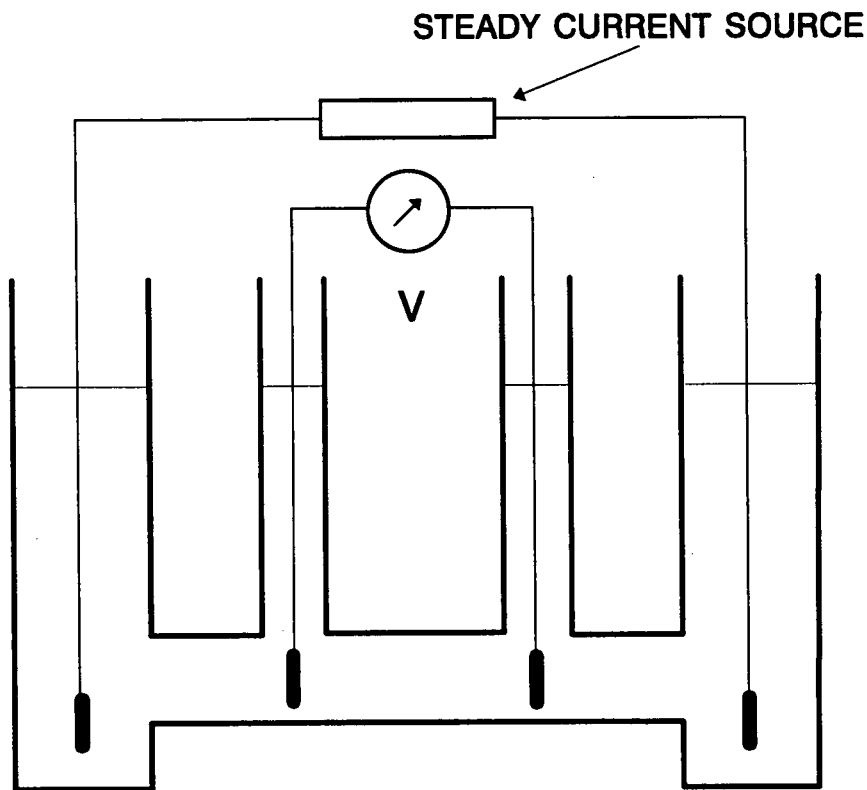


Figure 1.3 Four electrode DC system

A system that is now of great industrial importance appeared in the late 40s/ early 50s. In 1947 Matthew Relis wrote a thesis at M.I.T. titled "An electrodeless method for measuring the low frequency conductivity of electrolytes". The principle of this method can be seen in figure 1.5. The conductivity probe consists of two closely spaced coils toroidally wound on ferrite cores, coaxially situated (this is not shown in figure 1.5 for clarity) and placed in some kind of waterproof casing. This system is immersed in the electrolytic solution under investigation. An oscillator of stable amplitude and frequency energises the drive coil. This induces a closed loop current in the solution, which in turn induces a current

proportional to the solution conductivity in the pickup coil.

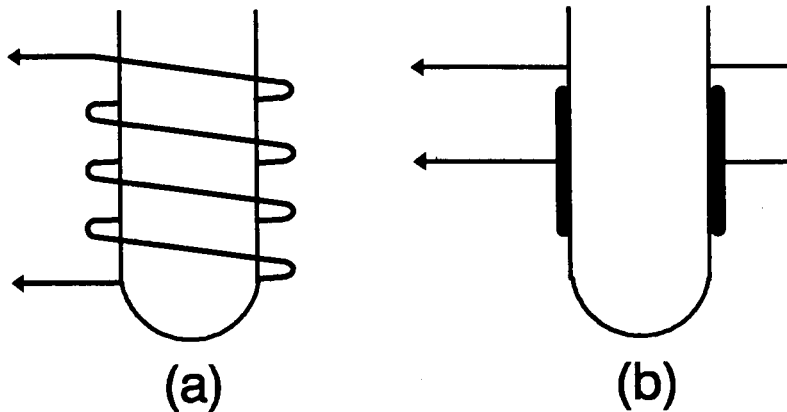


Figure 1.4 HF conductimetric cells

This is then amplified and sent to a display or some recording device. Relis reported that earlier attempts to measure conductivity using a similar kind of sensor had been made in 1920 by Piccard and Frivolt in Switzerland [15]. This kind of measurement has since been known as "electrodeless" and its history and subsequent developments and applications are the subject of the next section.

#### 1.4 Literature review of electrodeless conductivity.

Relis was eventually granted a patent for his invention in 1951 [16]. In that patent the conductivity probe is described in detail together with the design of the associated instrumentation. The coils are wound on toroids of ferromagnetic material and enclosed in shields of split design to avoid closed conducting loops around them. This shielding is necessary for the reduction of the capacitive coupling between the two coils. Despite the use of copper shields however there was still some pick up signal causing measurement errors. Magnetic leakage was recognised to be another source of errors and Relis tried to minimize it by rotating the one coil with respect to the other. Non uniform (ie with permeability anomalies) cores still were found to be a source of error. He then added a circuit that injected a signal cancelling the effects of stray field coupling in the pickup

coil.

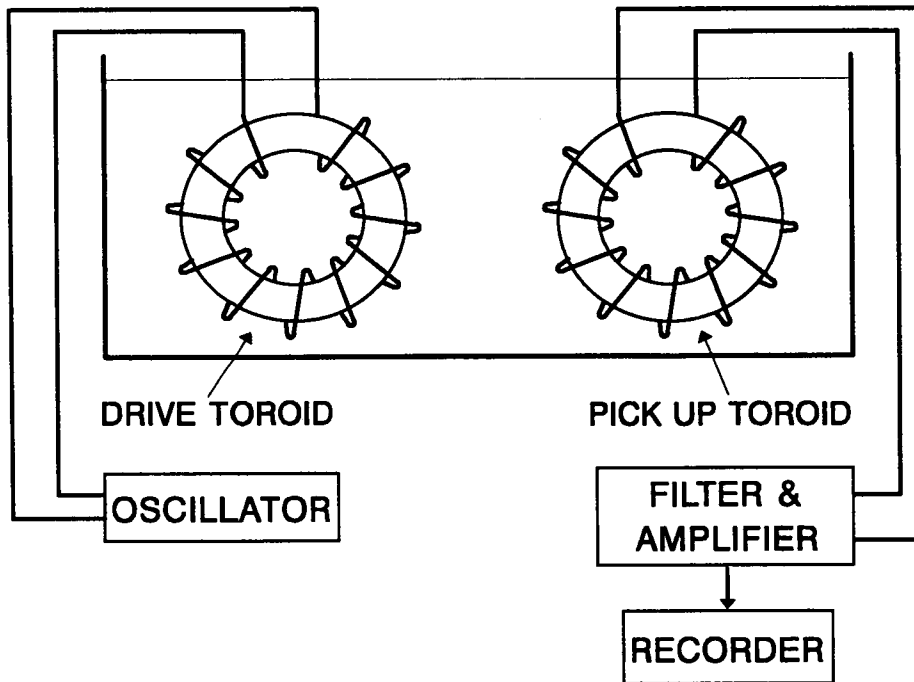


Figure 1.5 Basic components of an electrodeless system

A probe design suitable for immersion in conductive solutions, similar to that designed by Relis can be seen in Figure 1.6.

Following the Relis patent many improvements and variations mainly to the design of the conductivity probe appeared, but the basic design and principles essentially remained the same.

In 1955 Fielden was granted a patent [17] for an instrument using a variation of the probe design. In his patent the coils were mounted on the external surface of a non conductive pipe having the form of a loop, as seen in figure 1.7. A balancing winding containing a variable resistor going through the holes in the center of the toroids was also provided. The toroids were able to slide along the pipe on different planes and this was claimed to reduce greatly the pickup signals between the coils. This method appeared to be very promising for use with process solutions; it had however two problems: first, there was the possibility

of loss of some of the current in the electrolyte, through the ground of the piping system; second, the large solution loop paths created the equivalent of large cell constants.

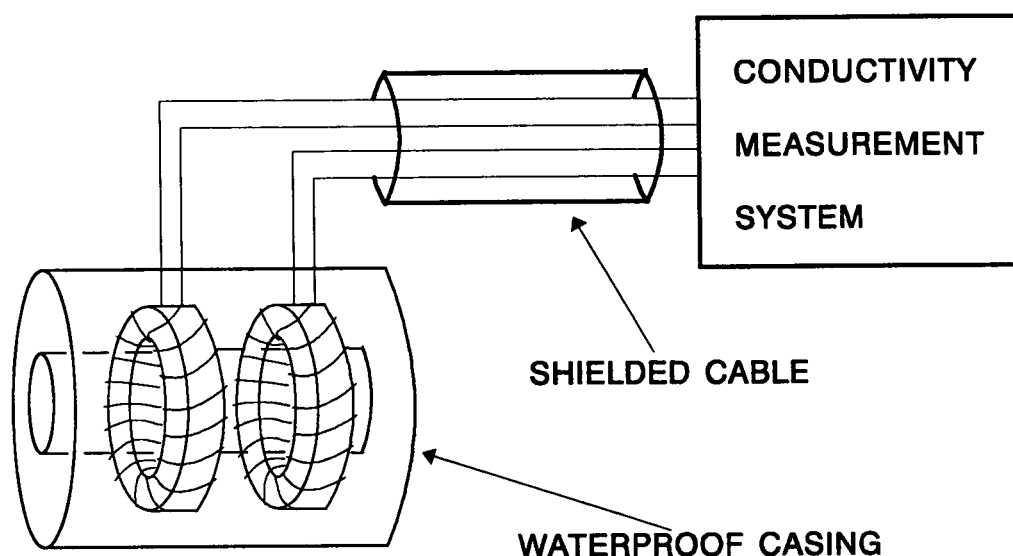


Figure 1.6 Probe design suitable for immersion in the electrolytic solution

An improved method of mounting the coils externally to the solution piping was presented by Sperry in 1968 [18]. He had used two drive coils mounted on the solution loop pipe which induced additive currents within the loop and cancelling ones in the inlet and outlet pipes. The latter ones were connected to metal sections and were grounded in order to provide return paths for the currents flowing in the inlet and outlet pipes. Two pick up coils were employed as well, one mounted on the loop and another on either the inlet or the outlet pipe. The former was used to measure the amount of current in the electrolyte. The latter would indicate whether any leakage current was present; if there were, the currents induced by the two drive coils were balanced until it disappeared. With this arrangement the problem of leakage currents was claimed to be eliminated; however the problem of the large equivalent cell constant remained.

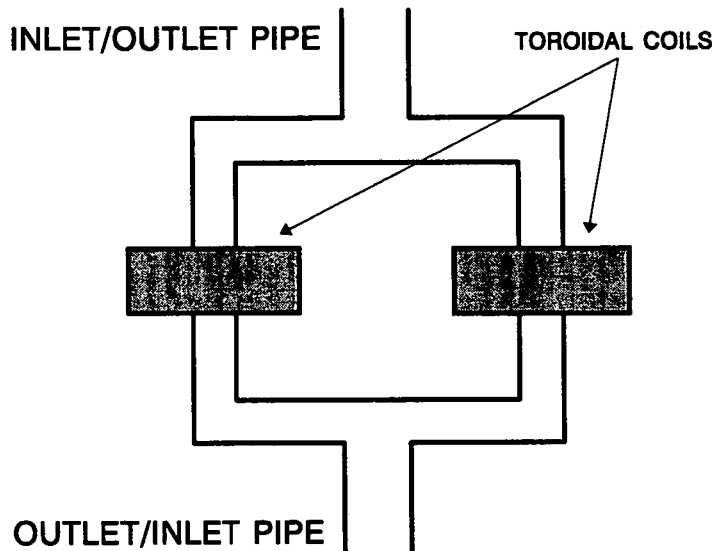


Figure 1.7 Externally mounted toroidal coil configuration

Rosenthal [19] and Kidder [20] also presented systems with externally mounted toroids. The latter used a conductive wire to close the solution loop rather than a complete solution loop. He also used a temperature sensor in contact with the solution and electrically included in both the drive and pickup circuits in order to provide automatic temperature compensation.

Gross took further steps in the sensor design. In his first patent [21] he pointed out that the method of compensation provided by Relis could prove ineffective particularly at low conductivity ranges, as the injected signal is not linear with the conductivity signal. According to his patent the winding on each of the cores starts at one point, continues up to a point near the starting one, and then again backwards until the starting point is met. This method of winding is used on both the drive and pickup coils, and can be repeated many times on each of them until the desired number of turns is achieved. He claimed that using this method of winding together with high permeability ferromagnetic core materials, low conductivity measurements can be made without the need of external compensating networks, as coupling due to electrostatic and magnetic effects is thus minimised. He also claimed that there is no need for shielding around the



toroids if such an arrangement is used. This method could not however eliminate coupling due to asymmetries in the ferrite cores. In another patent [22] he proposed cores made from stacked ring punchings and rotating them until the pickup due to the stray magnetic field is minimised. As this method can prove expensive and permeable shields can also be asymmetric themselves, he proposed ordinary conductive material shields placed over the core and under the coil winding. Gross also found that the thickness of the shields greatly affects the attenuation of stray signals in the pickup coil and also their phase. Finally for improved stray signal rejection he used additional shields over the windings.

The ruggedness of this method makes it suitable for use in corrosive, abrasive and in general hostile environments. The application in process industries is obvious, where the use of conventional contacting electrode systems requiring regular maintenance would be a definite disadvantage. The method was first used for the measurement of seawater salinity (around 48mS/cm) [14], [16], [23]. Koski [24] designed and patented an electrodeless system suitable for use in nuclear plants. In another publication [25] he described a probe suitable for use in high temperature and pressure environments. Rosenberger [26] designed a complete system for controlling the amount of dissolved solids in a slurry liquid stream employing an electrodeless sensor. The design and test results for electrodeless systems used for the control of acid concentrations in leach pulps have also been published [27], [28].

The development of the microprocessor and its successor, the microcontroller, with their vast applications in industry greatly affected the design of instruments for conductivity measurement and control. The microprocessor is now used to perform processing functions previously handled by hardware, thus leading to more accurate data in a more useful form; it also leads to reduced component count and hardware costs and increased reliability. An example of such an instrument and its abilities is described by K.M. Queeney and J.E. Downey in their paper titled "Applications of a microprocessor based electrodeless conductivity monitor" [29].

Despite its long established application in industry the electrodeless method

did not receive extensive literature review. Stock [31] discusses it together with other methods of conductivity measurement and Light [11] presents a more detailed review of the method and its applications.

There has also been a general lack of laboratory test equipment using the above described electrodeless method. This is mainly due to the probe size and the sample size required. The size of the probes is of the order of centimeters and consequently a sample size ranging from several hundreds of milliliters to several liters is necessary in order that a complete loop in the solution is formed.

Finally, theoretical treatment of the sensor operation is generally lacking possibly because the greatest interest in the method lies in its industrial application rather than the actual way it operates. Efforts for an equivalent network modelling have appeared in some publications [25], [27], [28]. The theoretical investigation of the way the sensor operates is the subject of the next chapter.

### **1.5 Objectives of this work**

This project started when LTH Electronics of Luton, a company involved in the design of industrial measurement and control systems, required to develop a portable conductivity meter that would employ an electrodeless sensor of the type described in figure 1.6 of the previous section. At that time they were producing portable conductivity meters which however were built around conventional graphite electrode sensors. They were also producing analog conductivity measurement and control systems using electrodeless sensors, but these could not be adapted for portable use because of their size and power consumption.

Their requirements were to build a compact, electrodeless conductivity meter using microcontroller technology (they proposed the use of Motorola's 68HC11), which would lead to reduced component count and consequently overall size, cost and power consumption. In addition the microcontroller resources could allow storage of known behaviour of conductivity versus concentration for a number of chemical solutions. The meter should be able to display conductivity in mS/cm, both compensated and uncompensated, respective concentration in % by weight for several solutions, and finally, the solution temperature. The

accuracy requirements were a maximum of 2% over a 10 to 500mS/cm range. Solution temperatures to be measured should be in the range 0 to 100°C. All the components used should be low cost and commonly available on the market. Finally, the meter should be "user friendly".

In the course of search for literature on electrodeless conductivity measurement, no analysis of the sensor operation was found to have been published; therefore effort could be placed on the study of the sensor operation and the various parameters affecting it. This is the subject of chapter 2.

The design of the conductivity meter should be aimed at achieving a best compromise of accuracy and cost. As far as the cost is concerned, that includes the cost of components, construction and initial calibration. Besides, the cost of use must be given consideration, ie power consumption and recalibration.

As far as the operation is concerned, after studying the requirements and assessing the capabilities of the 68HC11 and common analog and digital components available on the market, the following decisions were taken:

- Ranges of measurement: 2 to 19.99mS/cm, 20 to 199.9mS/cm and 200 to 1999mS/cm. Changes between ranges should be done automatically.
- Solution temperature range 0 to 100°C.
- Frequency of operation in the audio range. Finally 15KHz was decided upon, so that the amplifiers had adequate gain-bandwidth product.
- Accuracy target as set by the company.
- Power provided by a 9V alkaline battery.
- Display used: 3½ digit LCD.
- For demonstration reasons, six reference curves at 18°C were decided to be stored. Each would have an identification number from 1 to 6.
- Four control keys functioning as follows:
  - \* A key that would display conductivity when pressed.
  - \* A key that would display the code number for the reference curve when pressed once, and a consecutive depression would cause this code to change to that corresponding to the next curve.
  - \* A key that would cause the solution temperature to one decimal digit of

resolution to be displayed.

\* Finally a key that would cause the respective concentration in % by weight of the respective chemical to be displayed.

Chapters 3 and 4 describe the realisation of a conductivity meter matching the above requirements as close as possible.

# CHAPTER 2

## The electrodeless sensor

### 2.1 Introduction

In this chapter the theory of the operation of the electrodeless sensor described in the previous chapter is presented. First a numerical method is employed to derive the pattern of current flow within the electrolytic solution and to determine how this is affected by different probe parameters; it also allows calculations of resistances and currents flowing in the electrolyte. Then the sensor is modelled as an equivalent electrical network; this gives a picture of the relative magnitudes of currents, voltages and phase angles of interest.

### 2.2 Investigation of the electric field in the electrolyte

#### 2.2.1 Formulation of difference equation

We start by considering a simplified vertical cross section of the conductivity probe depicted in figure 1.6 of the previous chapter as seen in figure 2.1. Clearly the probe is symmetrical around the axis  $z_1z_2$ . The alternating magnetic field produced by the drive coil is confined within the ferrite core; assuming a closely wound coil of many turns, no external magnetic field should exist. The whole space around the probe section is considered to be filled with a solution of conductivity  $\sigma$ .

The time changing magnetic field in the toroid core induces an electric field in the conductive solution according to Maxwell's equation:

$$\oint_l \vec{E} \cdot d\vec{l} = - \iint_s \frac{\partial \vec{B}}{\partial t} \cdot d\vec{S} \quad (2.2.1)$$

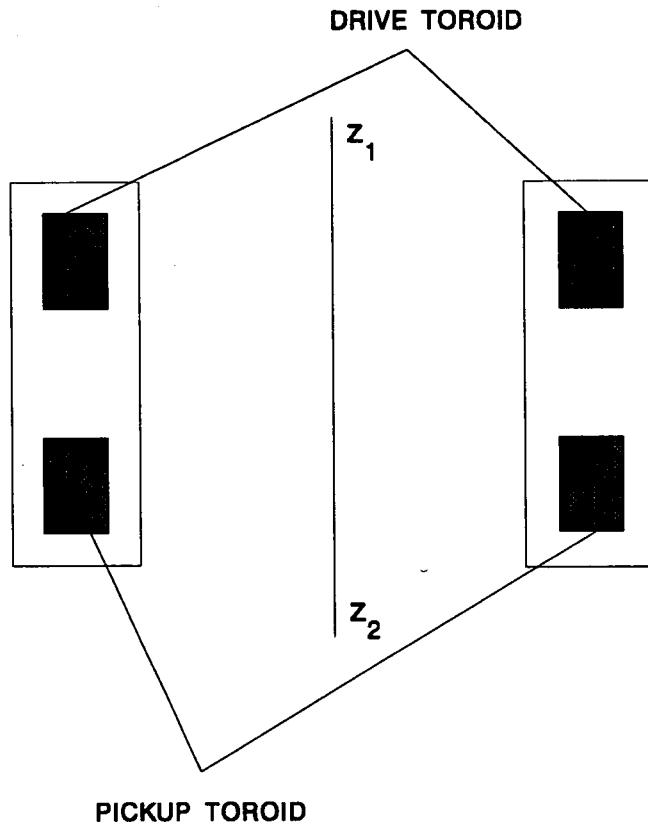


Figure 2.1 Probe cross section

where  $B$  is the magnetic field cutting any surface  $s$  bounded by the line  $l$  and  $E$  is the electric field along the line  $l$ . This equation can be written in differential form as:

$$\vec{\nabla} \times \vec{E} = -\frac{\partial \vec{B}}{\partial t} \quad (2.2.2)$$

The current induced in the electrolytic solution has no divergence as there is no free charge therefore it is solenoidal. In this case tubes of current can be constructed having walls parallel with the current flow. For conductive media

$\vec{J} = \sigma \vec{E}$  where  $\sigma$  is the conductivity of the material inside the tube, and the

electric field is also parallel with the walls of the tube. Assuming no current flowing through the walls of the tube, the current through any cross section  $a$  is:

$$I = \int_a \vec{J} \cdot d\vec{s} = \text{constant} \quad (2.2.3)$$

(see figure 2.2). Because the electric field in the tube is also solenoidal, no scalar potential can be defined.

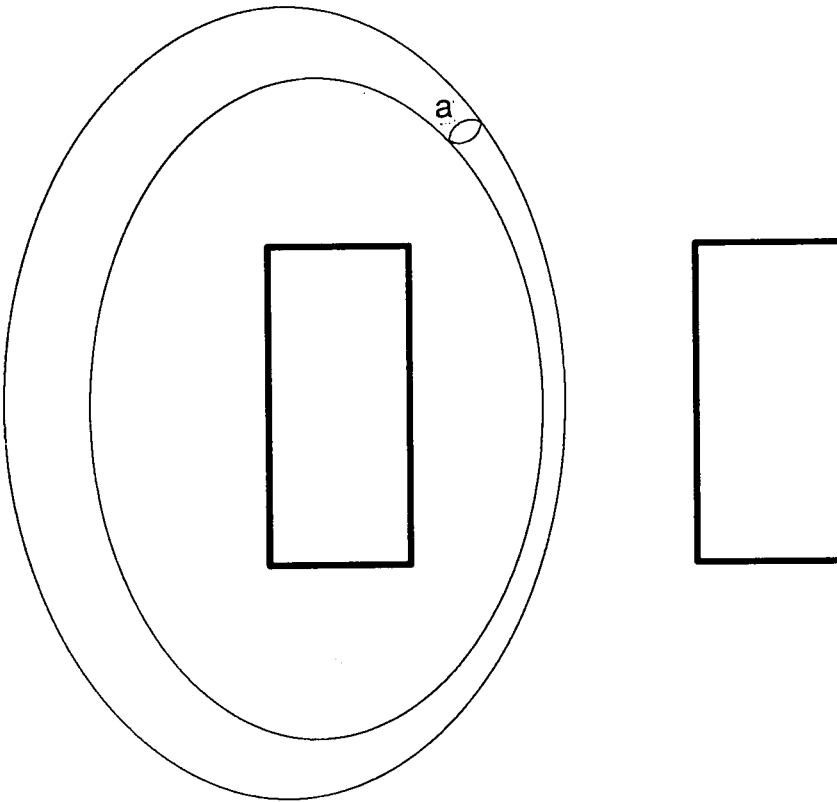


Figure 2.2 Tube of current around probe

If however elementary sections of the tube are considered (figure 2.3), the current can be thought to be driven by the potential difference between the two ends of the tube. This assumption allows us to consider a break of infinitesimal width at any point of the tube, as seen in figure 2.4, with the current driven by

a potential  $V = \int \vec{E} \cdot d\vec{l}$  ; assuming that the currents in the electrolyte make no

contribution to the magnetic field, this integral is independent of path and the instantaneous current flow can be deduced by solving the electrostatic field problem shown in figure 2.5. Now a scalar potential  $U$  can be defined as

$\vec{E} = -\vec{\nabla}U$  . Since in the conducting region the the current is constant,

$$\vec{\nabla} \cdot \vec{J} = 0 \text{ , or } \sigma \vec{\nabla} \cdot \vec{E} = 0 \text{ , or}$$

$$\vec{\nabla}^2 U = 0 \quad (2.2.4)$$

This is Laplace's equation for the area around the probe, filled with electrolytic solution.

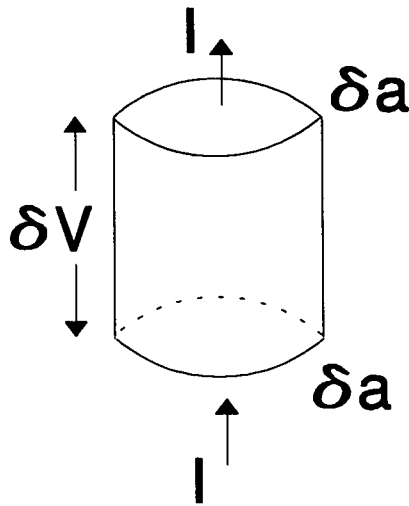


Figure 2.3 Element of current tube

If the integral  $\int \vec{E} \cdot d\vec{l}$  is not independent of path, as is the case when the magnetic field associated with the currents in the electrolyte is considered, then this method cannot be used.

The above assumptions allow further simplification of the area under investigation. By choosing the potential distribution of figure 2.5, the area around



the probe has reflection around the plane represented by the axis  $r_1r_2$ . Considering also the radial symmetry around the axis  $z_1z_2$  (see figure 2.1), we conclude that it is only necessary to solve the problem for the area shown in figure 2.6.

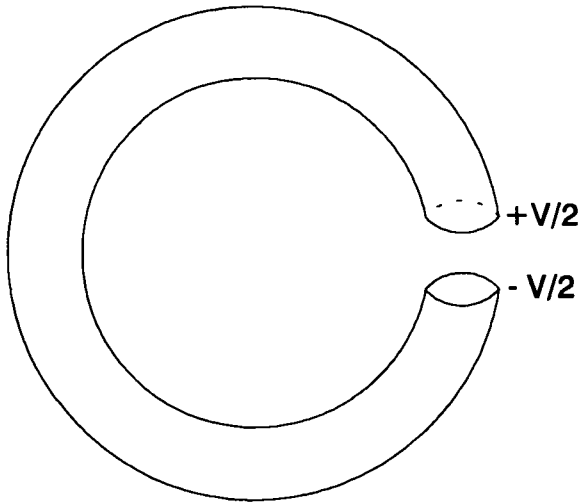


Figure 2.4 Current tube with infinitesimal gap

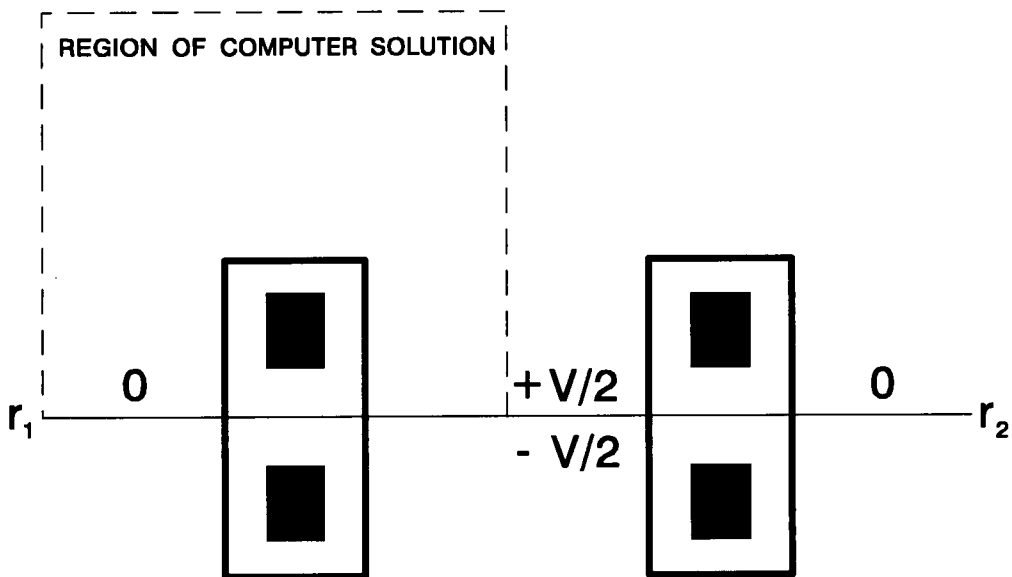


Figure 2.5 Voltage conventions shown on a cross section of the probe

In that figure, the boundaries BC, CD, DE, FG, GH and HA are reflective surfaces (ie no current flows through them), while EF is kept at a steady potential and AB at zero potential.

To analyse the potential distribution around the probe, Laplace's equation (2.2.4) has to be solved.

### 2.2.2 Approximation of difference equation

Since the problem has cylindrical symmetry, the equation is written in cylindrical coordinates as follows:

$$\frac{\partial^2 U}{\partial r^2} + \frac{1}{r} \frac{\partial U}{\partial r} + \frac{1}{r^2} \frac{\partial^2 U}{\partial \phi^2} + \frac{\partial^2 U}{\partial z^2} = 0 \quad (2.2.5)$$

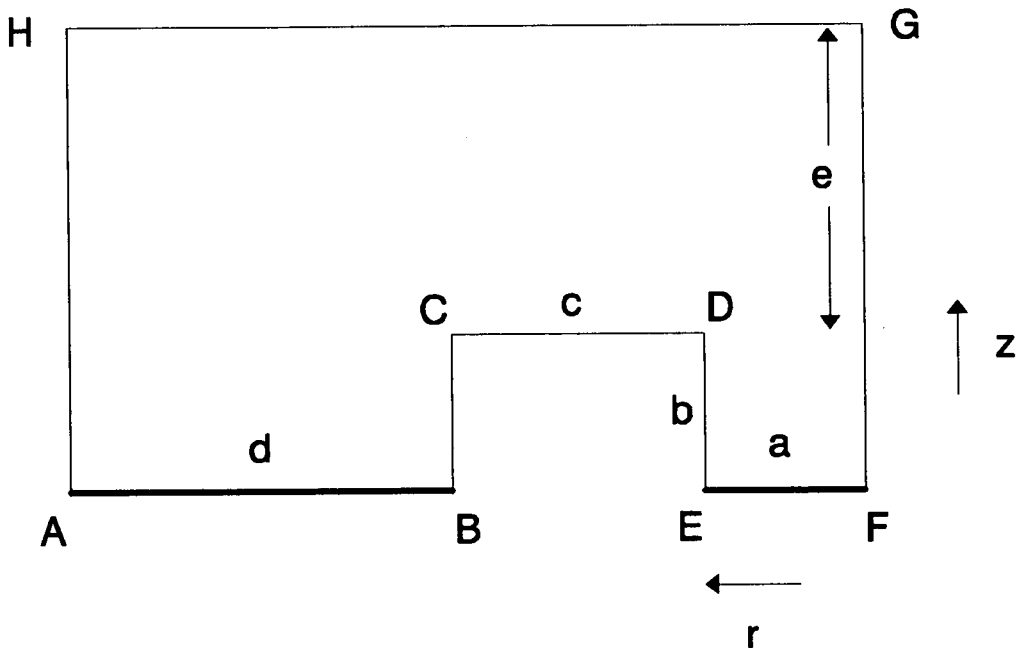


Figure 2.6 Definition of area under investigation

The third term in equation (2.2.5) is zero due to the symmetry of the problem therefore the equation can be rewritten as:

$$\frac{\partial^2 U}{\partial r^2} + \frac{1}{r} \frac{\partial U}{\partial r} + \frac{\partial^2 U}{\partial z^2} = 0 \quad (2.2.6)$$

The direction of  $r$  and  $z$  axes is taken as shown in figure 2.6.

To solve equation 2.2.6 we use the finite difference approximation method. We start by dividing the conductive solution area in small squares of width  $h$  and height  $k$ . Clearly, each point of the grid has coordinates  $r = ih$  and  $z = jk$ . Solutions of equation 2.2.7 are computed for the points on the intersection of horizontal and vertical lines.

The next step is to write finite difference approximations for the first and second derivatives. Considering a typical point of the grid as shown in figure 2.7, the second derivatives along the  $r$  and  $z$  axis can be derived from Taylor's expansion [32] respectively as:

$$\left(\frac{\partial^2 U}{\partial r^2}\right)_{i,j} = \frac{U_{i+1,j} + U_{i-1,j} - 2U_{i,j}}{h^2} \quad (2.2.7)$$

$$\left(\frac{\partial^2 U}{\partial z^2}\right)_{i,j} = \frac{U_{i,j+1} + U_{i,j-1} - 2U_{i,j}}{k^2} \quad (2.2.8)$$

A first derivative approximation along the  $r$  axis is:

$$\left(\frac{\partial U}{\partial r}\right)_{i,j} = \frac{U_{i+1,j} - U_{i-1,j}}{2h} \quad (2.2.9)$$

Substituting equations 2.2.7, 2.2.8 and 2.2.9 into 2.2.6, we take the following expression:

$$\frac{U_{i+1,j} + U_{i-1,j} - 2U_{i,j}}{h^2} + \frac{1}{ih} \frac{U_{i+1,j} - U_{i-1,j}}{2h} + \frac{U_{i,j+1} + U_{i,j-1} - 2U_{i,j}}{k^2} = 0 \quad (2.2.10)$$

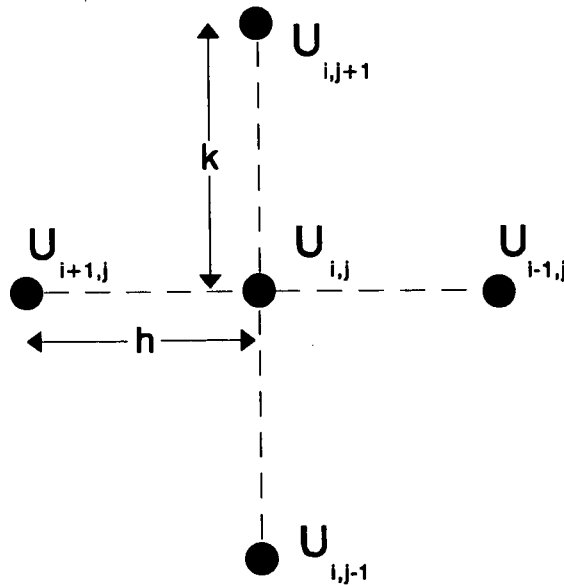


Figure 2.7 Typical point of the grid

From this equation the potential at a typical point of the grid can be deduced as:

$$U_{i,j} = \frac{ih^2(U_{i,j+1} + U_{i,j-1}) + ik^2(U_{i+1,j} + U_{i-1,j}) + \frac{k^2}{2}(U_{i+1,j} - U_{i-1,j})}{2i(h^2 + k^2)} \quad (2.2.11)$$

This equation gives the potential value for a point as a function of the potentials of the four surrounding points. Equation 2.2.11 is valid for all points inside the grid.

For points on the boundaries of the grid, special considerations have to be made.

For points belonging to a right hand reflective boundary (figure 2.8a), we replace  $U_{i-1,j}$  with  $U_{i+1,j}$ , therefore equation 2.2.11 gives:

$$U_{i,j} = \frac{h^2(U_{i,j+1} + U_{i,j-1}) + 2k^2 U_{i+1,j}}{2(h^2 + k^2)} \quad (2.2.11a)$$

For points on a left hand reflective boundary (figure 2.8b) we replace  $U_{i+1,j}$  with  $U_{i-1,j}$ , so equation 2.2.11 gives:

$$U_{i,j} = \frac{h^2(U_{i,j+1} + U_{i,j-1}) + 2k^2 U_{i-1,j}}{2(h^2 + k^2)} \quad (2.2.11b)$$

For points on a bottom reflective boundary (figure 2.8c) we replace  $U_{i,j-1}$  with  $U_{i,j+1}$ , therefore from equation 2.2.11 we have:

$$U_{i,j} = \frac{2ih^2 U_{i,j+1} + ik^2(U_{i+1,j} + U_{i-1,j}) + \frac{k^2}{2}(U_{i+1,j} - U_{i-1,j})}{2i(h^2 + k^2)} \quad (2.2.11c)$$

In the case of a top reflective boundary (figure 2.8d), we replace  $U_{i,j+1}$  with  $U_{i,j-1}$  and equation 2.2.11 gives:

$$U_{i,j} = \frac{2ih^2 U_{i,j-1} + ik^2(U_{i+1,j} + U_{i-1,j}) + \frac{k^2}{2}(U_{i+1,j} - U_{i-1,j})}{2i(h^2 + k^2)} \quad (2.2.11d)$$

For the corner point on the upper left of the conductive area (figure 2.8e), we replace  $U_{i+1,j}$  with  $U_{i-1,j}$  and  $U_{i,j+1}$  with  $U_{i,j-1}$ , therefore from equation 2.2.11:

$$U_{i,j} = \frac{k^2 U_{i-1,j} + h^2 U_{i,j-1}}{h^2 + k^2} \quad (2.2.11e)$$

Finally, for the corner point on the upper right of the conductive area (figure 2.8f), we replace  $U_{i-1,j}$  with  $U_{i+1,j}$  and  $U_{i,j+1}$  with  $U_{i,j-1}$ , therefore from equation 2.2.11:

$$U_{i,j} = \frac{k^2 U_{i,j-1} + h^2 U_{i+1,j}}{h^2 + k^2} \quad (2.2.11f)$$

The set of equations 2.2.11 and 2.2.11a to 2.2.11f define the potential for every point of the grid.

### 2.2.3 Solution of difference equation

For the solution of Laplace's equation an iterative method has been chosen. This method consists of scanning successively through each point of the grid and calculating the potential using whichever equation from the set described above is appropriate each time. For each point, the most recent values for the surrounding points are used. The formula suitable for iteration is:

$$U_{i,j}^{(k)} = U_{i,j}^{(k-1)} + r_{i,j} \quad (2.2.12)$$

where  $r_{i,j}$  is the residual value for each point examined, and the superscripts  $k$  and  $k-1$  denote the number of successive passes across the grid.

Assuming that the "sweeping" of the formula 2.2.12 across the grid takes place from right to left and from bottom to top, the residual value is defined as:

$$r_{i,j} = \frac{ih^2(U_{i,j+1}^{(k-1)} - U_{i,j-1}^{(k)}) + ik^2(U_{i+1,j}^{(k-1)} - U_{i-1,j}^{(k)}) + \frac{k^2}{2}(U_{i+1,j}^{(k-1)} - U_{i-1,j}^{(k)}) - 2i(h^2 + k^2)U_{i,j}^{(k-1)}}{2i(h^2 + k^2)} \quad (2.2.13)$$

The procedure is terminated when the residual value is reduced to zero, i.e.  $|r_{i,j}| < \epsilon$  for every point of the grid.

Since a large number of points (finer grid) can be required for a more detailed study of the field, the speed of convergence must be increased; hence the method of successive over-relaxation (SOR) [33] has been employed. This method uses the formula:

$$U_{i,j}^{(k)} = U_{i,j}^{(k-1)} + w r_{i,j} \quad (2.2.14)$$

where the parameter  $w$  is called overrelaxation factor and lies in the range

$1 \leq w < 2$ . This formula is again swept across the grid, until  $|r_{ij}| < e$  for every point.

The structure of the program employing the SOR method to find the solution of Laplace's equation can be seen in figure 2.9. A typical output of this program gives potential patterns like those of figure 2.10.

Examining solutions for several combinations of probe dimensions, it can be found that the equipotentials in the bore are horizontal until nearly the edge of that area, particularly when the volume of the solution is very large compared to the probe. This can lead to simplified (rough) calculations of bore and rest of the solution resistance calculations as will be seen later in this section.

Another observation is that for a large bore diameter the equipotentials indicate that the majority of current flow occurs closely to the probe section (figure 2.11).

The solution of Laplace's equation for the solution area can also give some values for the magnitude of current flow; this can be achieved by adding (integrating) the contributions of elementary surfaces across the grid, as follows:

Consider the elementary volumes along the  $r$  axis, as shown in figure 2.12. The current flowing vertically across each one of those volumes is:

$$\Delta I = J \Delta S \quad (2.2.15)$$

where  $J$  is the current density and  $\Delta S$  is the top and bottom area of each of these volumes. Recalling that the electric field and current density in a conductor are

related as  $J = \sigma E$ , and for this particular problem  $E = \frac{\Delta V}{\Delta z}$ , the vertical current

density can be written as:

$$J = \sigma \frac{\Delta V}{k} \quad (2.2.16)$$

where  $\Delta V$  is the potential difference between the top and bottom surfaces of each elementary volume. The top (and bottom) area of an elementary volume

at  $r = ih$  from the bore center considering  $360^\circ$  angle can be found as:

$$\Delta S = 2\pi ih^2 \quad (2.2.17)$$

Combination of equations (2.2.15), (2.2.16) and (2.2.17) yields an expression for the current flowing vertically through each elementary volume:

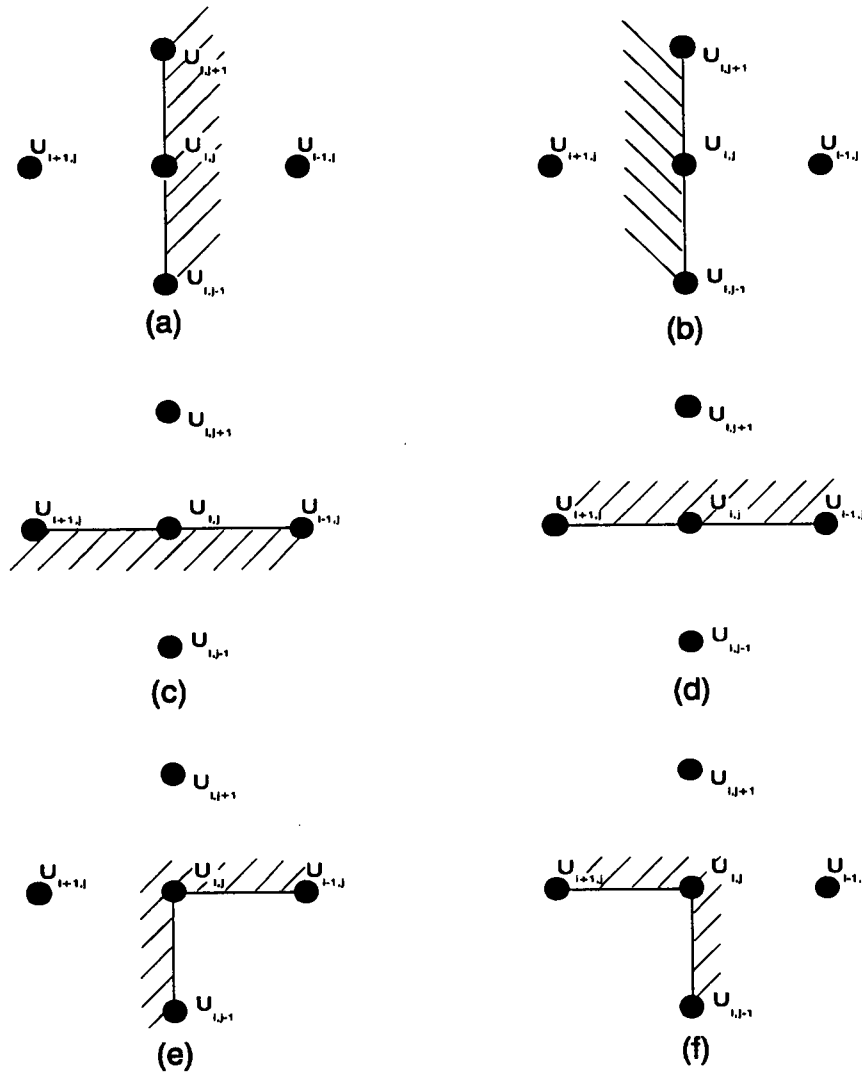


Figure 2.8



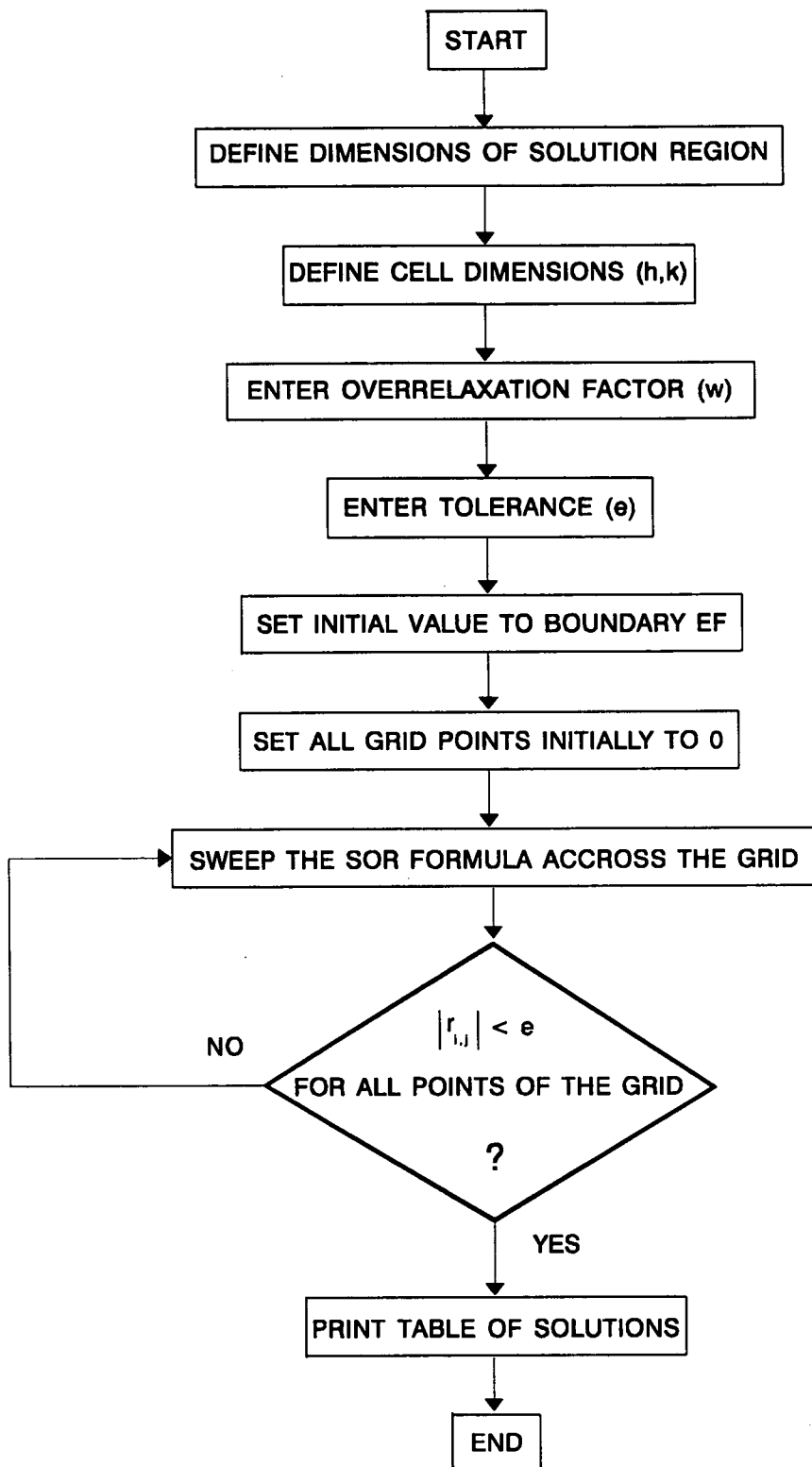


Figure 2.9

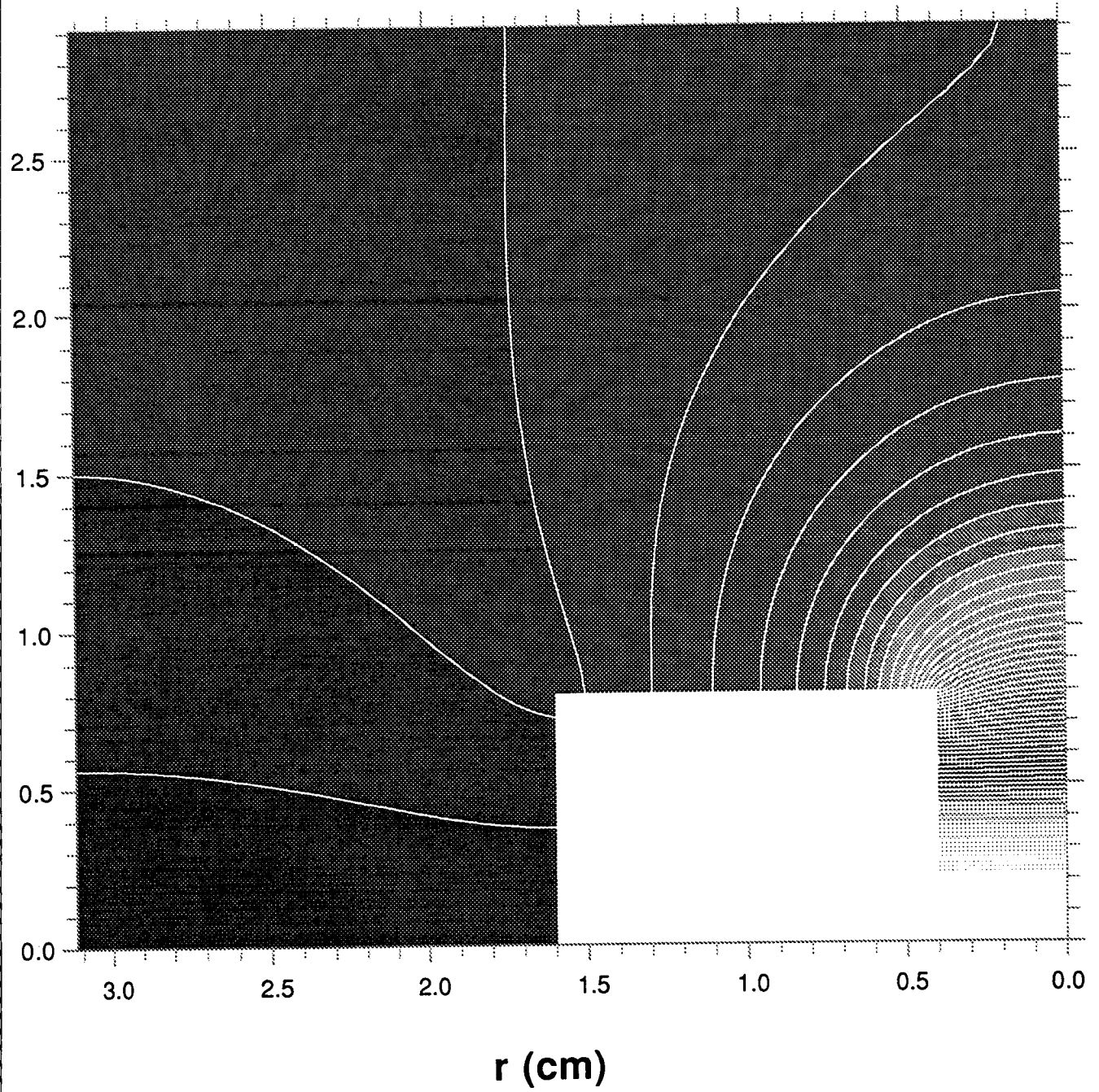


Figure 2.10 Potential distribution around probe section

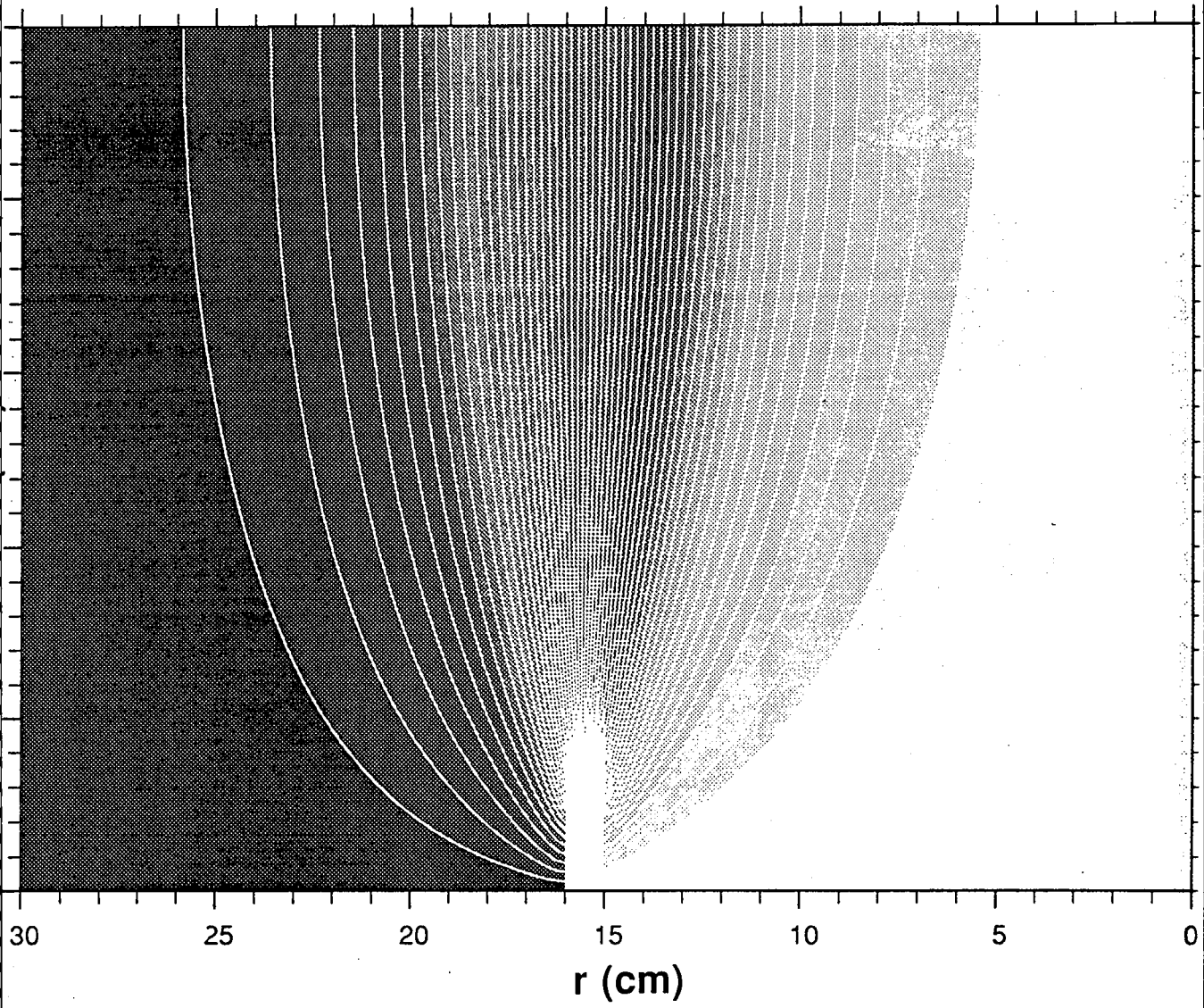


Figure 2.11 Potential distribution for large bore radius

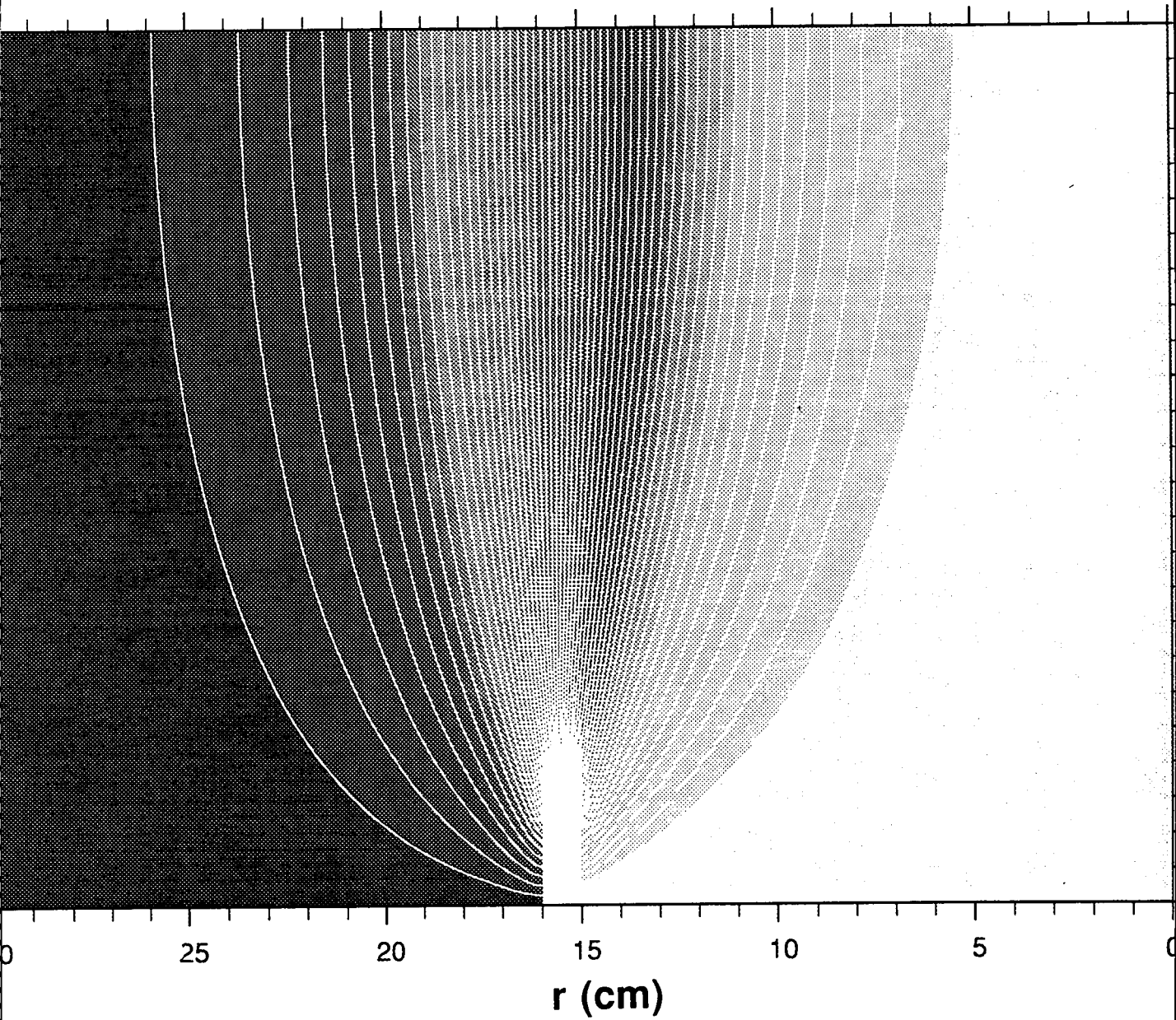


Figure 2.11 Potential distribution for large bore radius

$$\Delta I = 2\pi i \sigma \Delta V \frac{h^2}{k} \quad (2.2.18)$$

or,

$$\frac{\Delta I}{\sigma} = 2\pi i \Delta V \frac{h^2}{k} \quad (2.2.19)$$

For point 0 (ie elementary volume around the bore center)  $\Delta S = \frac{\pi h^2}{4}$ , therefore

$$\frac{\Delta I}{\sigma} = \pi \Delta V \frac{h^2}{k} \quad (2.2.20)$$

Equations 2.2.19 and 2.2.20 can give a value for the current passing through a surface, when integrated along the direction of the  $r$  axis. The value at the edges of the cross section (points A,B and E in figure 2.6) is half that given from equation 2.2.19.

Application of equations 2.2.18 and 2.2.20 for the current entry and exit sections of the conductive area around the probe (surfaces parallel to AB and EF in figure 2.6) has shown close agreement of the final values, which, as expected, improves with the number of points used to analyse the field around the respective surfaces.

A similar method can be employed to derive a value for the current flowing through a vertical surface. Consider the elementary volume in figure 2.13. The vertical surface on the right of the volume (after integrating for  $360^\circ$ ) can be found as:

$$\Delta S = 2\pi(i - \frac{1}{2})hk \quad (2.2.21)$$

The density of the current through this surface can be found as:

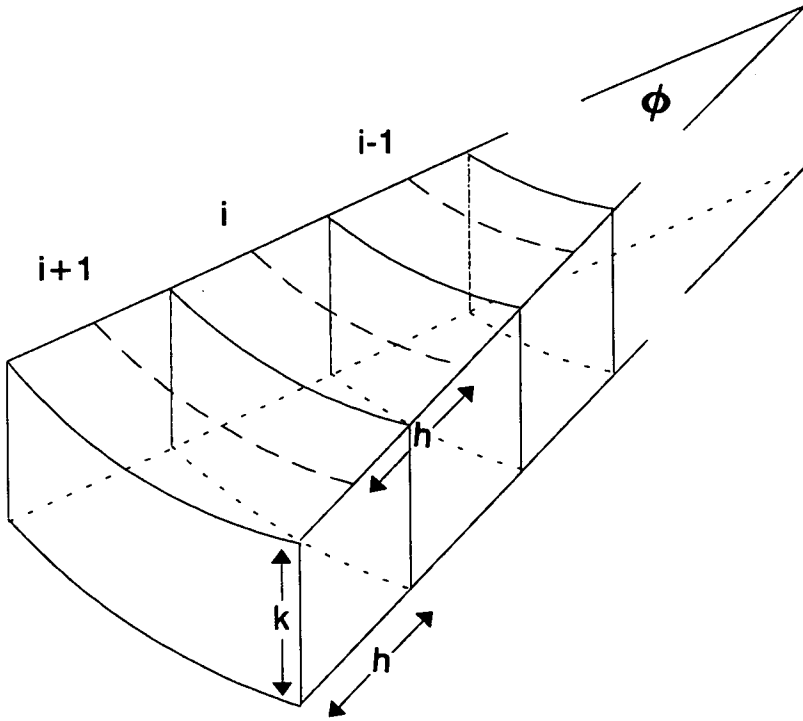


Figure 2.12 Element volumes for vertical current flow calculation

$$J = \sigma \frac{U_i - U_{i-1}}{h} = \sigma \frac{\Delta U_{i,i-1}}{h} \quad (2.2.22)$$

Substituting equations 2.2.21 and 2.2.22 in 2.2.15 we have an expression for the current:

$$\Delta I = 2\pi\sigma \Delta U_{i,i-1} \left(i - \frac{1}{2}\right)k \quad (2.2.23)$$

or,

$$\frac{\Delta I}{\sigma} = 2\pi \Delta U_{i,i-1} \left(i - \frac{1}{2}\right)k \quad (2.2.24)$$

Adding the current values for stacked elementary volumes gives the total value for the current flowing through a vertical surface. Again, for the first and last elementary volumes, the correct current value is half that given by equation 2.2.24. In this particular application two different vertical surfaces have been used; one on the left of point D and one on the right of point C (see figure 2.6).

Comparison of the current values given by the above equations are a check of the method of analysing the field around the conductivity probe. Several runs of the program have shown that the difference in current values are of the order of 1%, especially when a large number of points is used for the cell bore (ie more accuracy is achieved). The values of currents flowing in the electrolyte described from now on are the average of the values taken for the four surfaces described above.

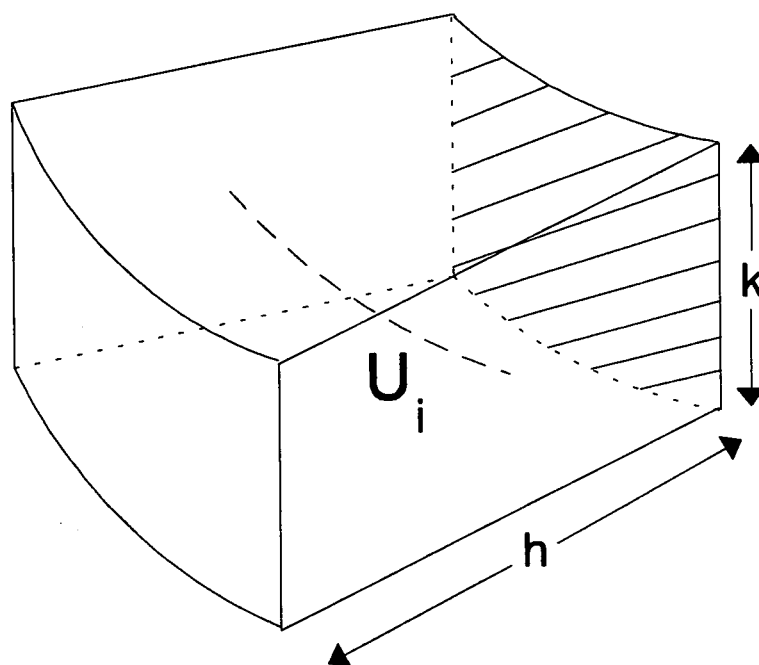


Figure 2.13 Element volume for horizontal current flow calculation

#### 2.2.4 Solution for varying probe dimensions

Now that the main procedures of the program have been explained, it can be used to examine some of the properties of the probe and the surrounding electrolytic solution.

We start by considering a probe with basic dimensions  $a = EF = 0.25\text{cm}$ ,  $b = DE = 1.50\text{cm}$ ,  $c = CD = 1.25\text{cm}$ ; the basic dimensions of the solution area are  $a + c + d = 12\text{cm}$  where  $d = AB$  and  $b + e = 15\text{cm}$ , where  $e$  is the distance between the top of the probe section and the top boundary of the solution area (figure 2.6). We examine the effect of changing the probe dimensions (one at a time) on the current in the solution and the resistance of the latter. As seen above, the dimensions of the whole solution area are large compared to the probe dimensions, therefore the equipotentials within the cell bore are nearly horizontal, so that the bore can be considered as a cylindrical conductor with its top and bottom surfaces at a nearly steady potential. The rest of the solution (from the bore edge and over) is considered to be another conductor. Initial potential value for the surface  $EF$  is set to 10,000. The grid cell dimensions are  $h = 0.0625\text{cm}$  and  $k = 0.125\text{cm}$ , resulting in an 192 by 120 grid.

The program described in section 2.2.3 gives values of  $I/\sigma$  for several probe dimensions. Examination of the variation of values for  $\sigma/I$  with bore depth ( $b$ ) shows a linear variation (figure 2.14). This is an indication that the solution resistance varies linearly with  $b$ . The intercept with the vertical axis gives a value for the resistance of the solution outside the bore. In a similar manner, the values of  $\sigma/I$  given by the program for several values of bore radius show that it varies linearly with  $1/a^2$  (figure 2.15).

#### 2.2.4.1 Effects of varying bore depth

Variation of  $b$  with  $a, c, d$  and  $e$  fixed, gives current-to-conductivity ratio and voltages across the top surface of the bore as shown in figure 2.16. In that figure  $V_{ave}$  denotes the average potential at the bore edge.

Using these values, approximate calculations for the bore and rest of the solution resistances can be made. The bore resistance can be derived from the formula:

$$\frac{10,000 - V_{ave}}{I/\sigma} \equiv \sigma R_b \quad (2.2.23)$$



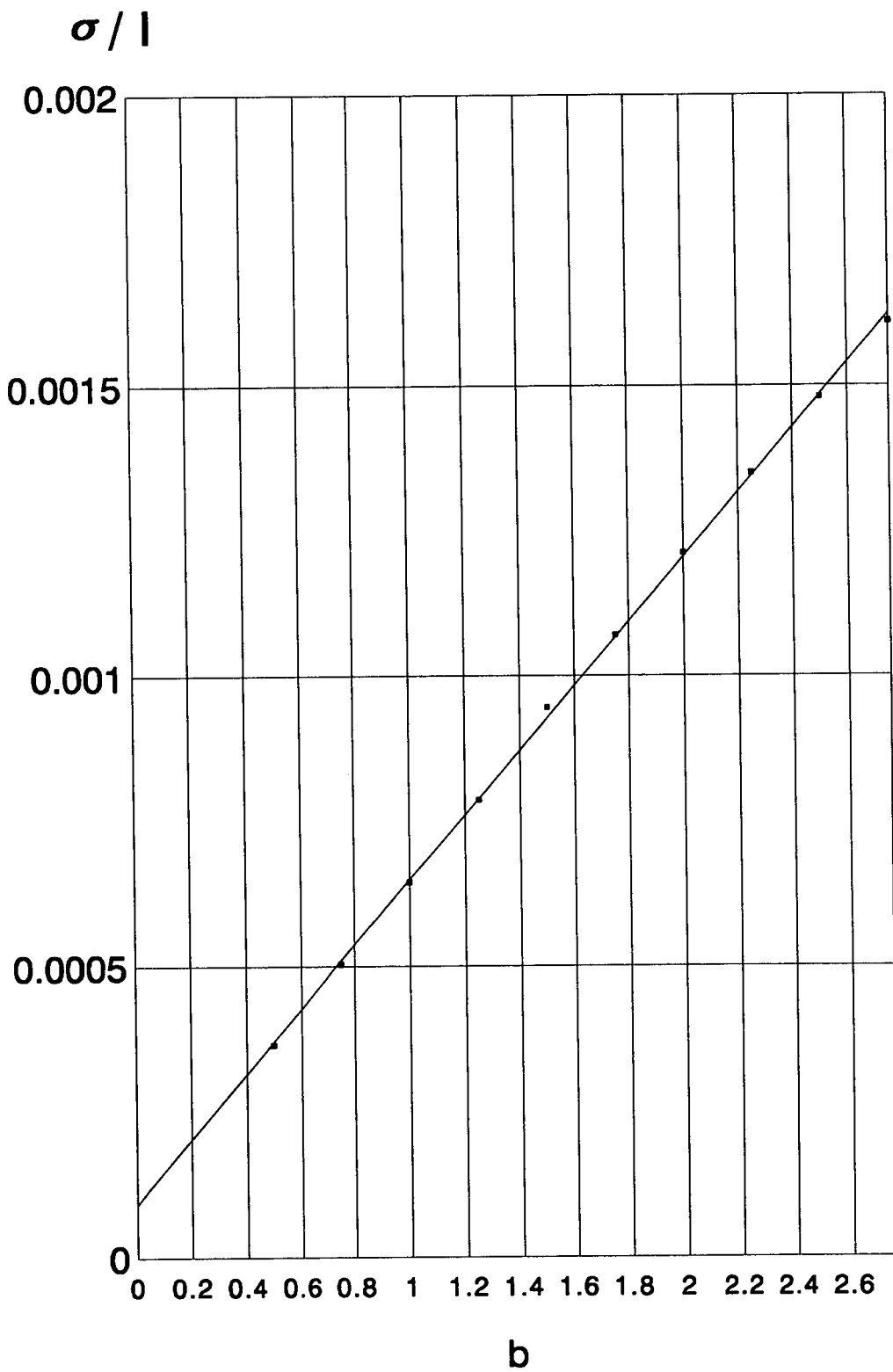


Figure 2.14 Variation of  $\sigma/l$  with  $b$

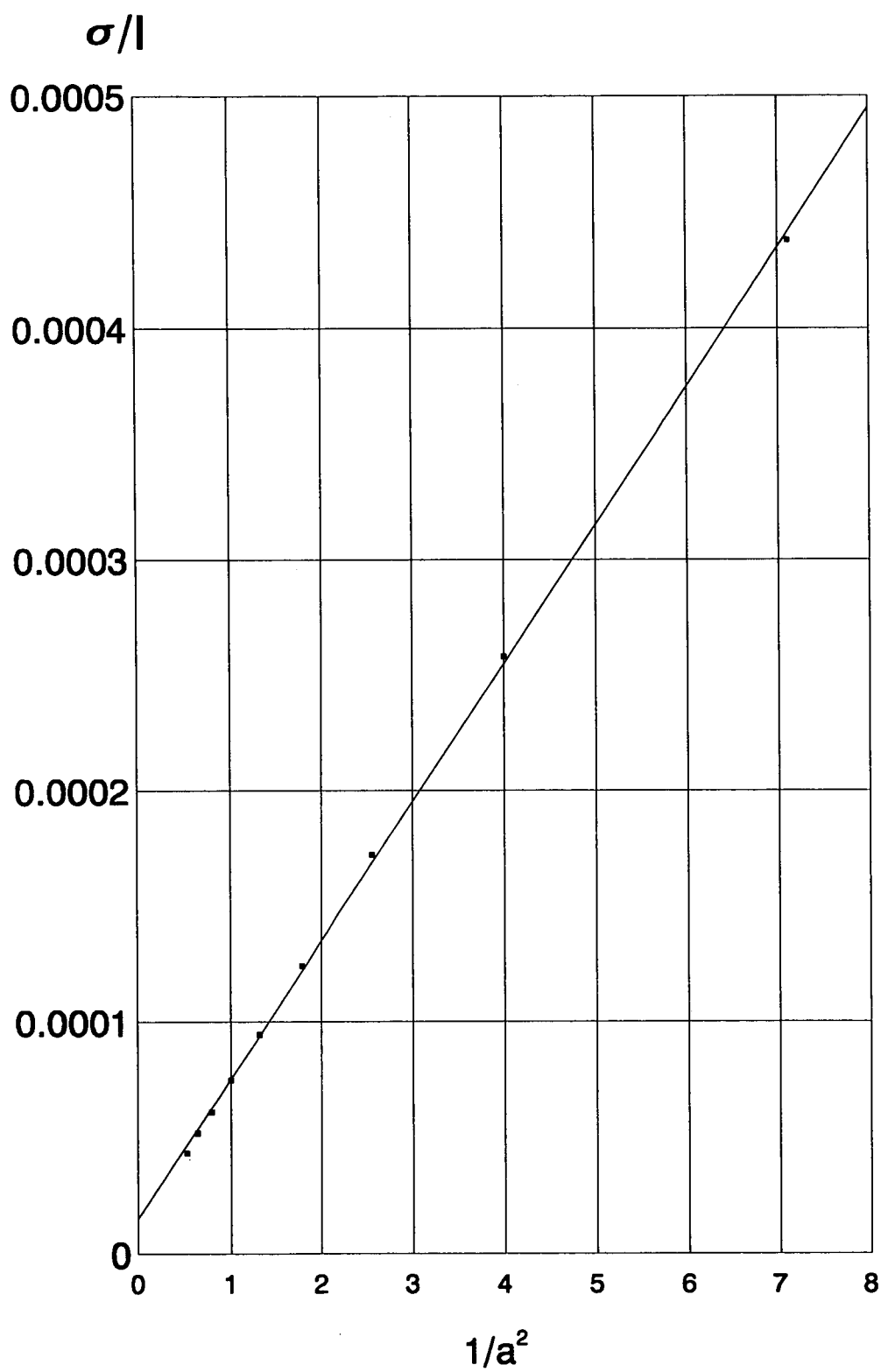


Figure 2.15 Variation of  $\sigma/l$  with  $1/a^2$

which gives the bore resistance multiplied by conductivity of the solution. For the rest of the volume of the solution, the following formula is used:

$$\frac{V_{ave}}{I/\sigma} \equiv \sigma R_r \quad (2.2.24)$$

In this formula  $R_r$  denotes the resistance of the rest of the solution, outside the bore. that the convention for the solution area under investigation (section 2.2.1 and figure 2.6) leads to calculated values for resistances divided by 2.

Variation of the bore depth ( $b$ ) with all the other dimensions remaining fixed, gives the resistance values shown in figure 2.17. In that figure (and all subsequent ones of the same nature) there has also been included the theoretical bore resistance-conductivity product:

$$\frac{b}{\pi a^2} \equiv \sigma R_b \quad (2.2.25)$$

so that comparison with the results of the program can be made. The theoretical values and values calculated by the program, are seen to be very close while the resistance of the solution outside the bore remains practically unaffected by changes in its depth. From the above two diagrams it can be seen that increased bore depth leads to reduced current in the solution; this can be attributed to the increasing bore resistance as the depth increases.

#### 2.2.4.2 Effects of varying bore radius

Next the variation in the current and bore edge voltage with changing bore radius ( $a$ ) is examined, with the rest of dimensions kept constant. Figure 2.18 shows the variation of these quantities with  $1/a^2$  rather than  $a$ . Figure 2.19 shows the respective resistance variations in the solution calculated using equations 2.2.23 and 2.2.24. It can be seen that increased bore cross section leads to increased currents due to larger bore cross section (smaller resistance). In figure 2.19 the variation of the bore resistance - theoretical and the one given by the program - as well as the resistance of the rest of the solution with  $1/a^2$  can be

seen. Again the two bore resistances - expected and calculated by the program - can be seen to be in agreement.

#### **2.2.4.3 Effects of toroidal core cross section**

The same procedure is followed for a changing probe section width (c) with all the other dimensions kept constant. Figure 2.20 shows the current and bore edge voltage variation with c. As expected, the latter does not change appreciably since the bore dimensions remain unchanged. Figure 2.21 shows the resistances variation with c. An expected drop in the total current value due to the increased path length from "source" to "sink" leads to respective increases in the resistance of the bore and remaining solution.

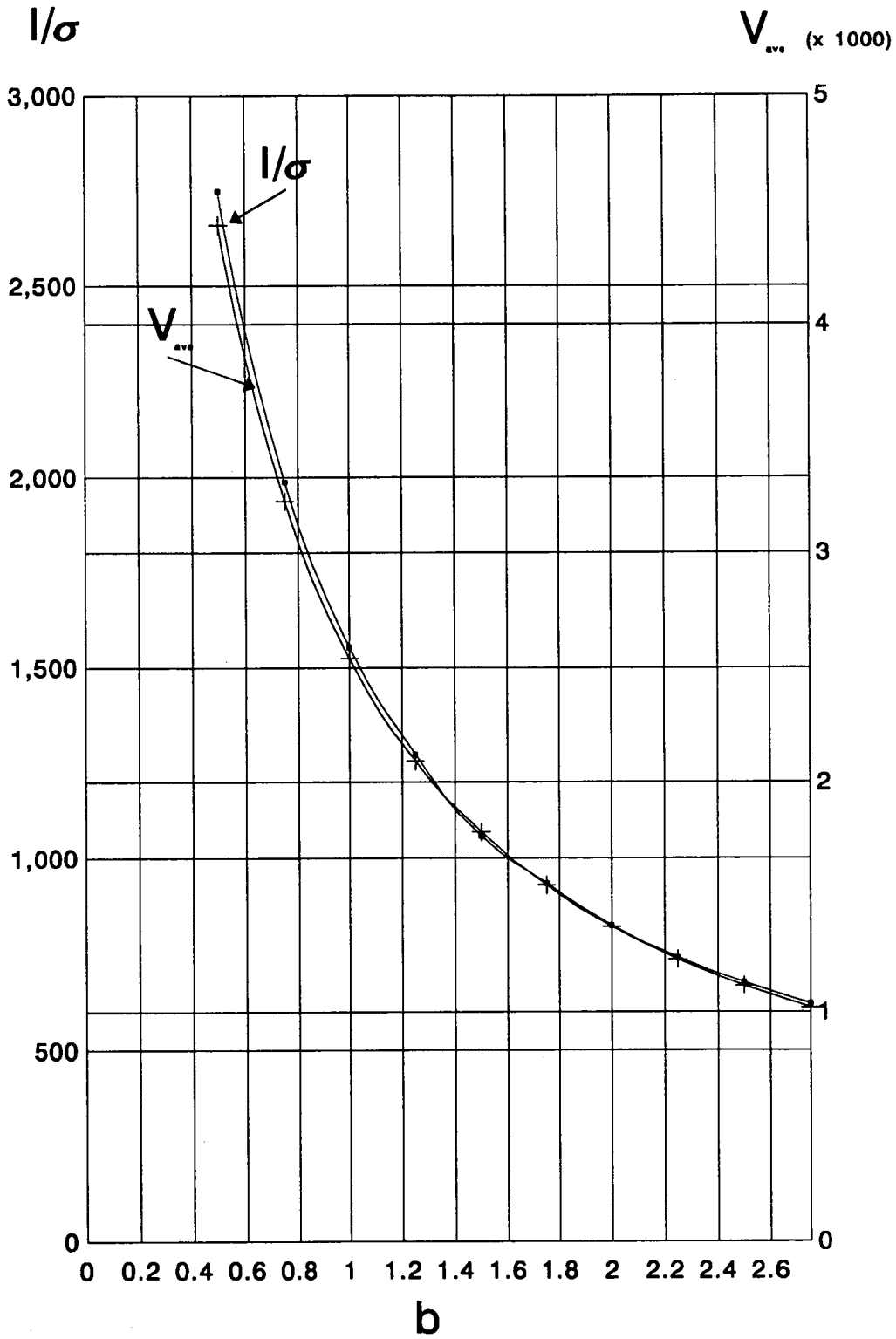
#### **2.2.4.4 Effects of solution volume around the conductivity probe**

Changes in the horizontal distance from the edge of the probe to the left hand vertical boundary of the solution area (d) leave the current, bore edge potential (figure 2.21) as well as solution resistances (figure 2.23) practically unchanged provided that it is large compared to the total horizontal probe dimensions. However, when d starts approaching the values of the horizontal probe dimensions, the current values start decreasing with consequent increase in the total resistance. This situation represents the case of using the probe in small solution samples (ie with container dimensions in the order of those of the probe) or as an in line sensor in process control pipes. Obviously, the reduction of current leads to measurement errors in this case.

Changes in the distance from the bore edge to the horizontal top boundary (e), has little effect until this dimension approaches those of the bore; in this case, the bore edge voltage is becoming slightly higher with the resistances changing accordingly (see figures 2.24 and 2.25).

#### **2.2.5 Derivation of an expression for the cell constant**

From figures 2.16 to 2.25 it can be seen that the calculated resistance of the bore is in close agreement with the theoretically expected, ie  $b/(\pi a^2)$ . As the total

Figure 2.16 Current and voltage variation with bore depth ( $b$ )

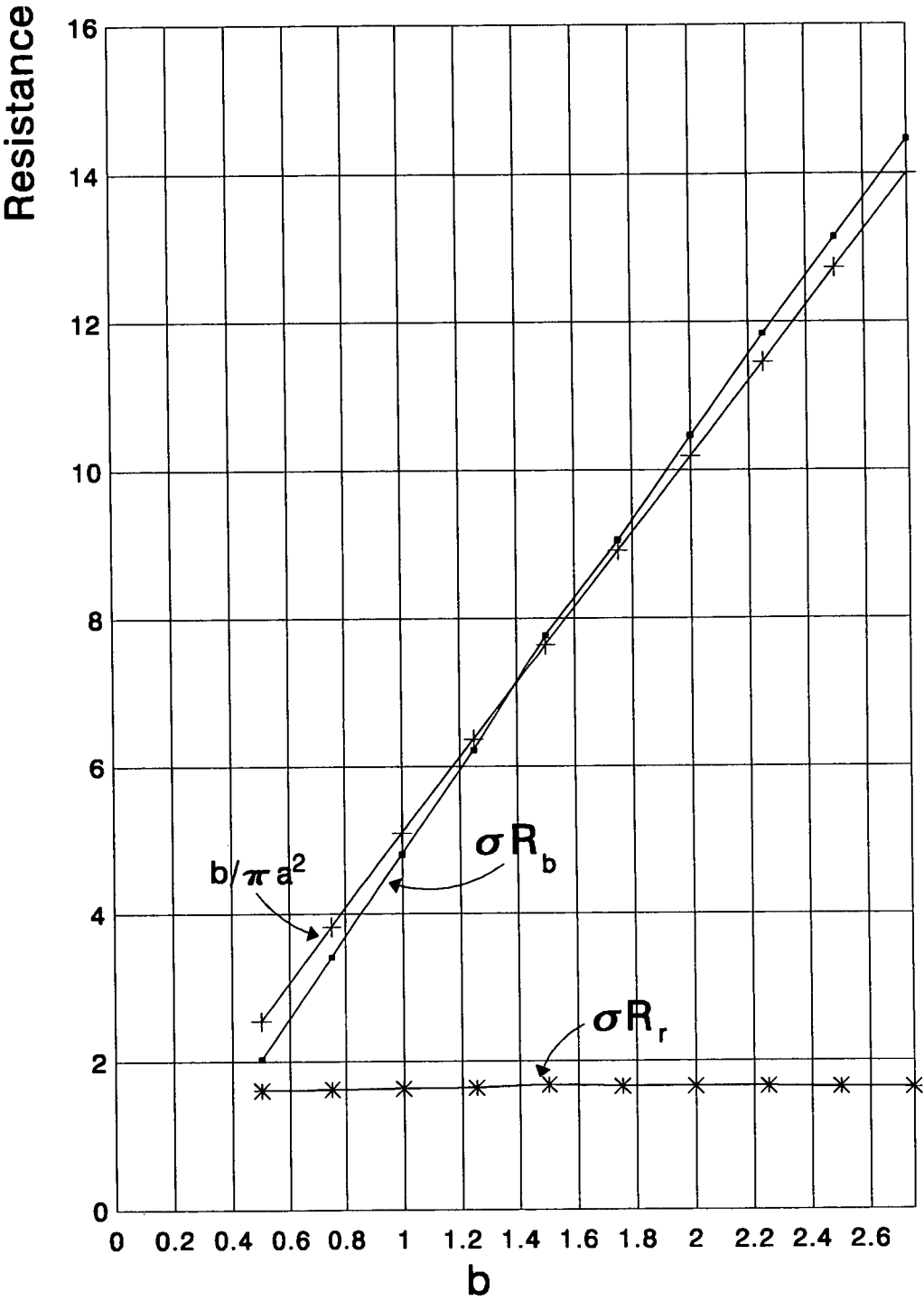


Figure 2.17 Bore and remaining solution resistance variation with bore depth ( $b$ )

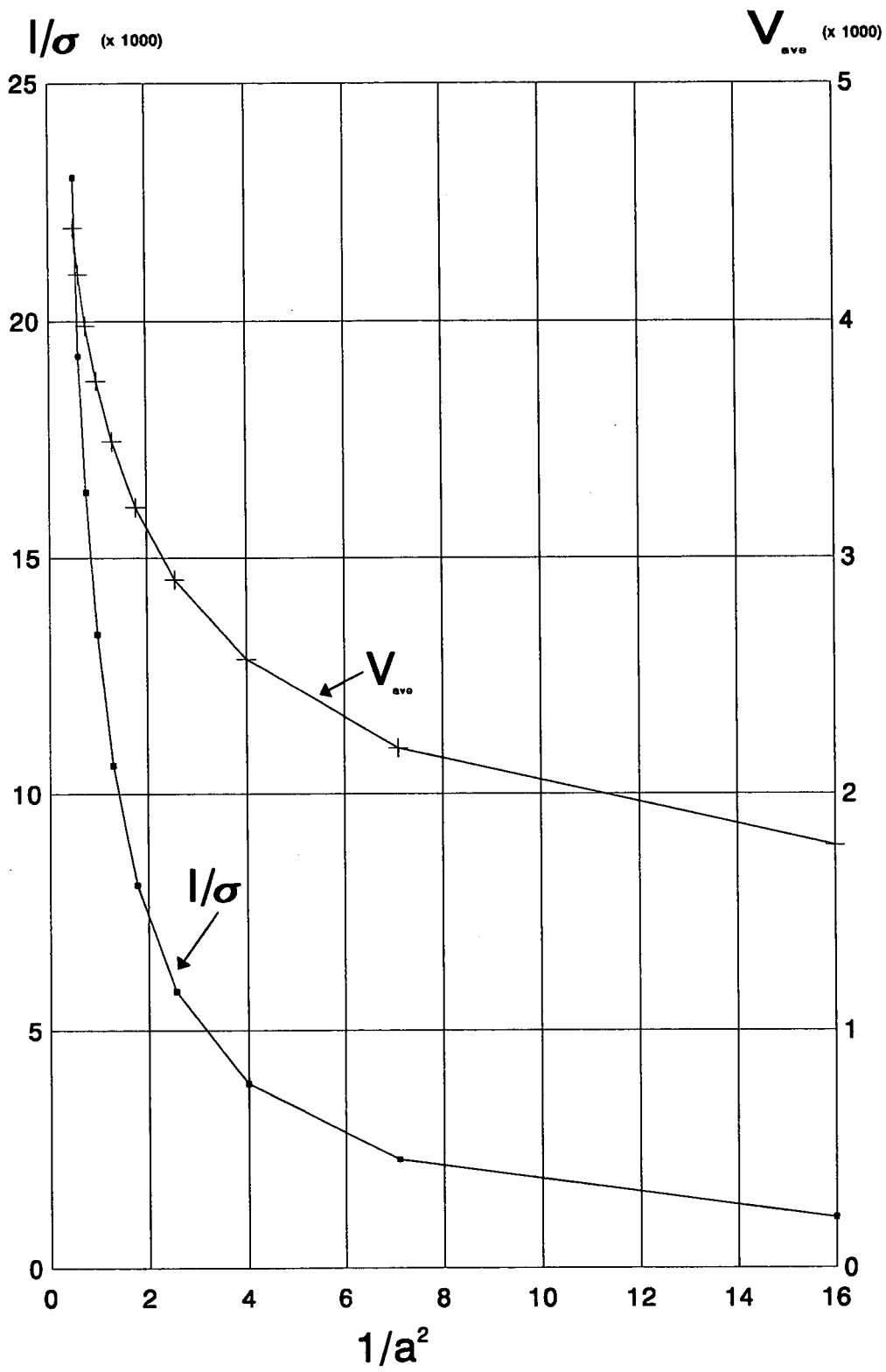


Figure 2.18 Current and bore edge voltage variation with bore radius (a)

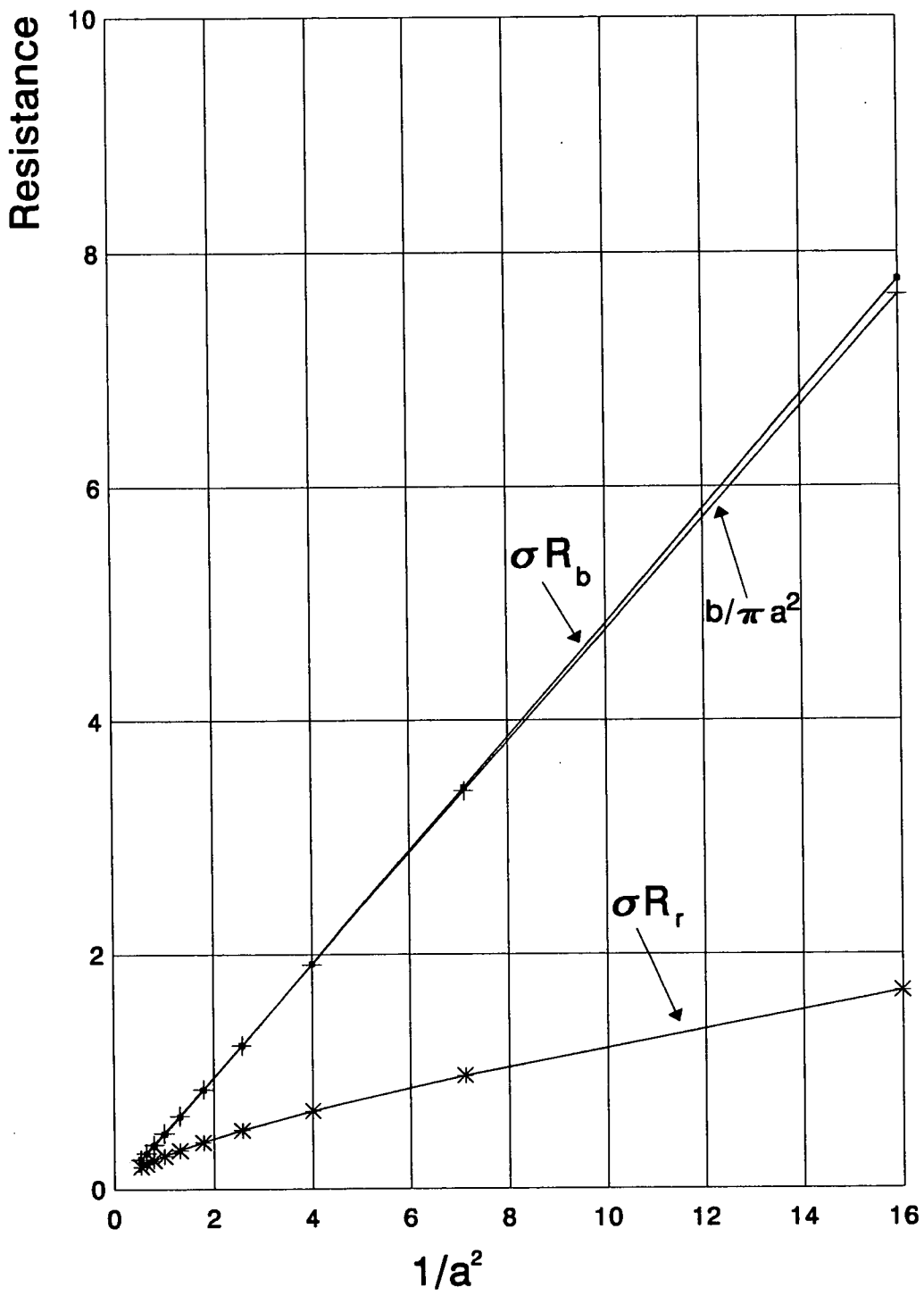


Figure 2.19 Bore and remaining solution resistance variation with bore radius (a)



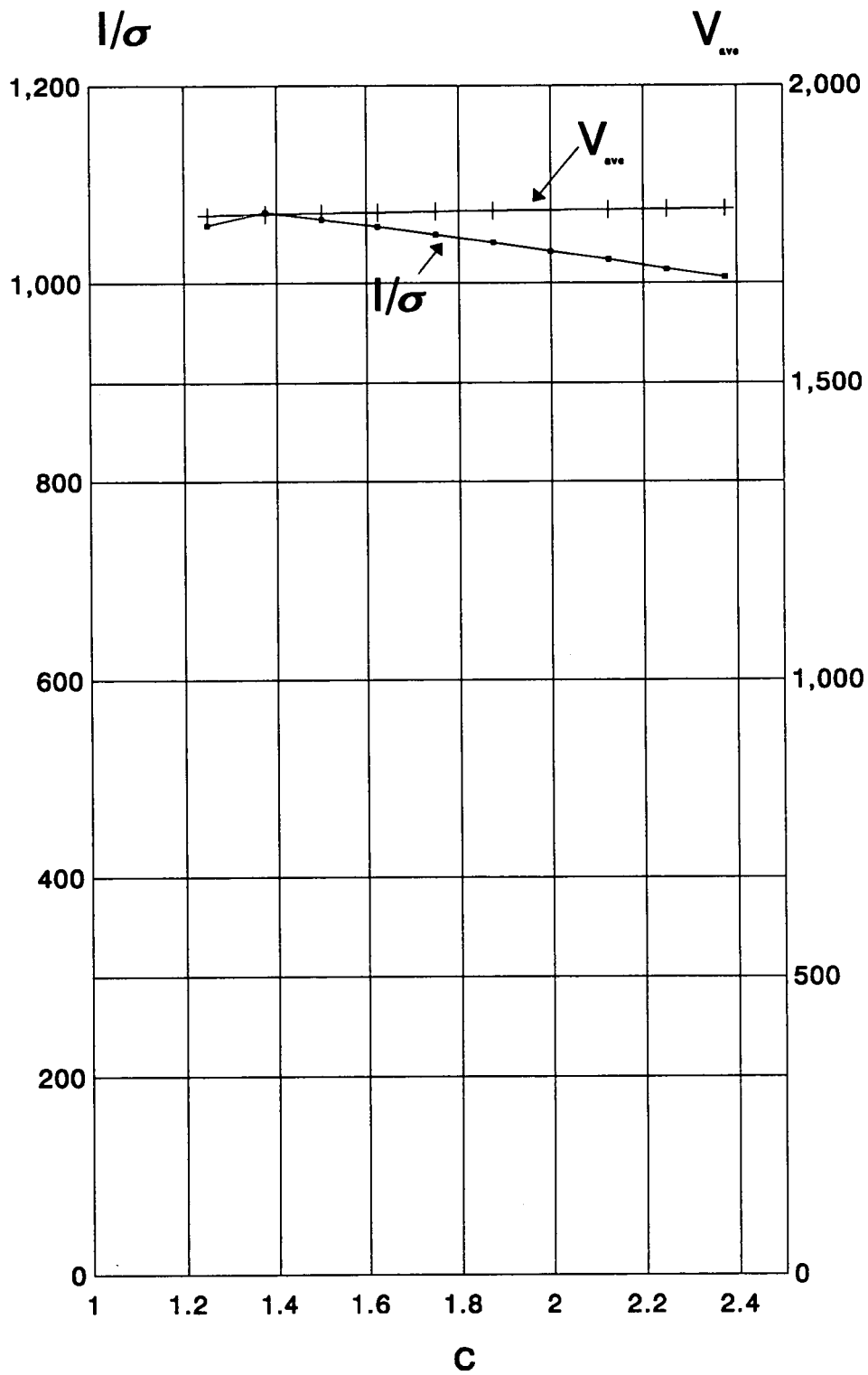


Figure 2.20 Current and bore edge voltage variation with probe cross section (c)

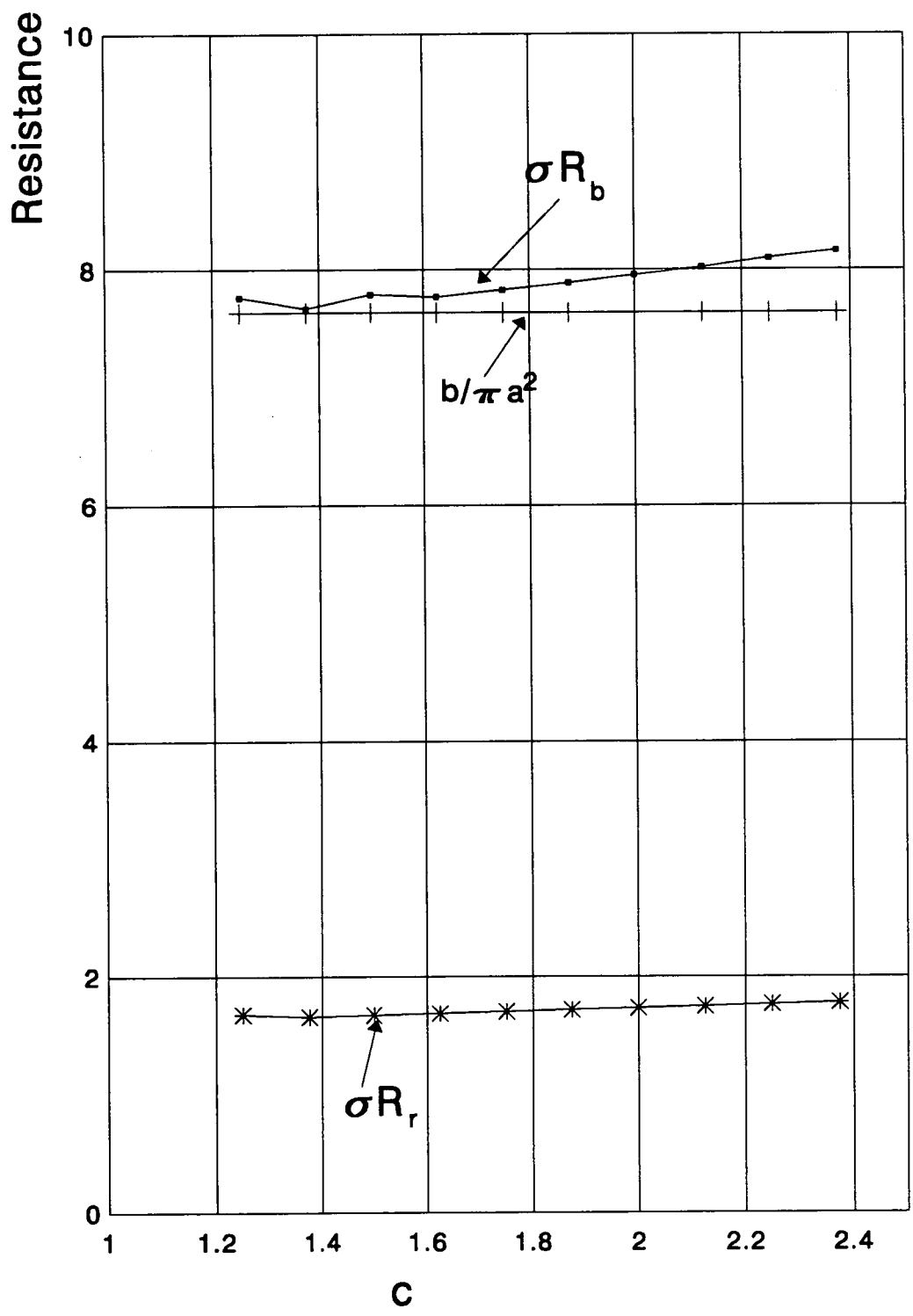


Figure 2.21 Bore and remaining solution resistance variation with probe cross section ( $c$ )

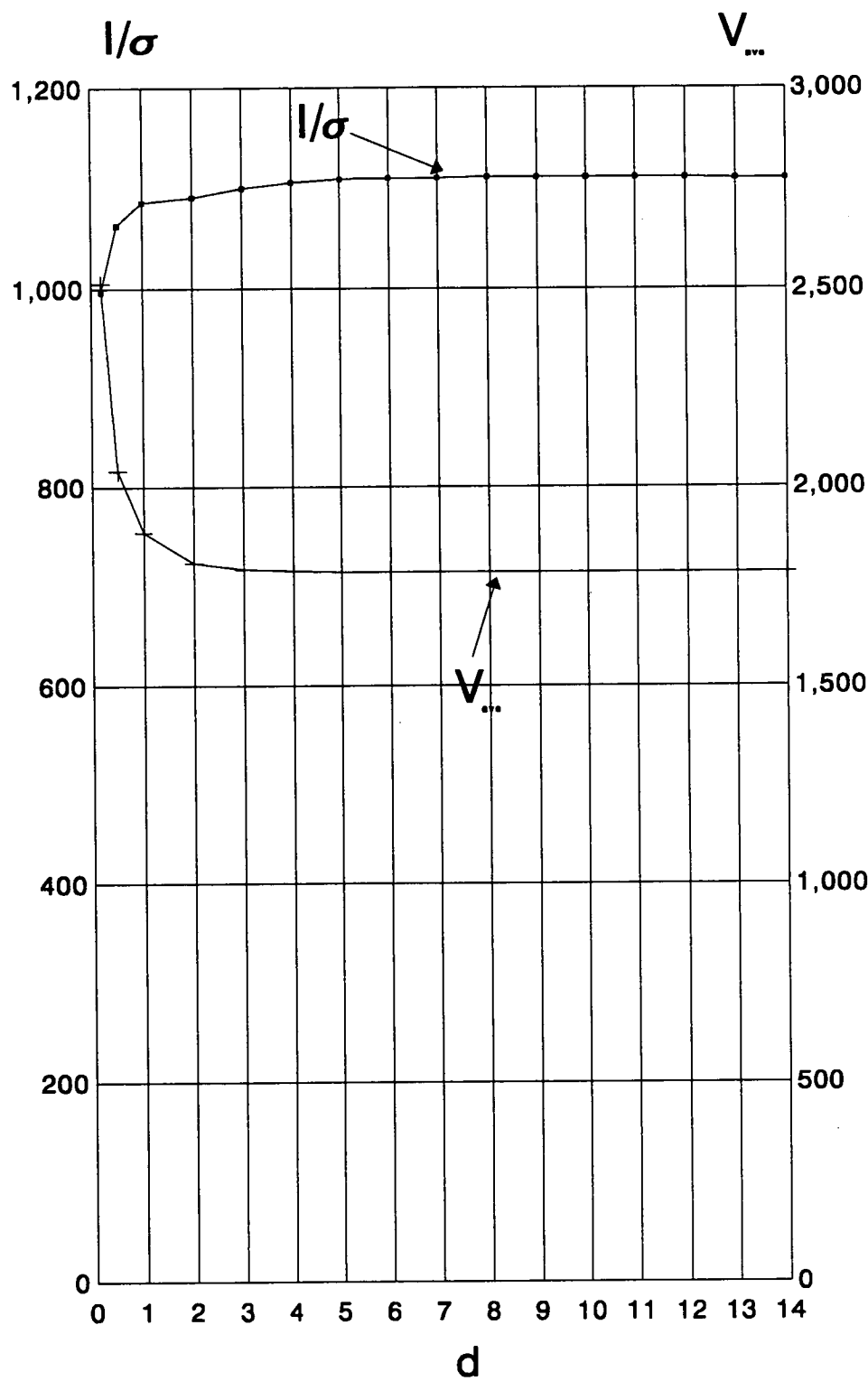


Figure 2.22 Current and bore edge voltage variation with horizontal solution area from probe to container edge ( $d$ )

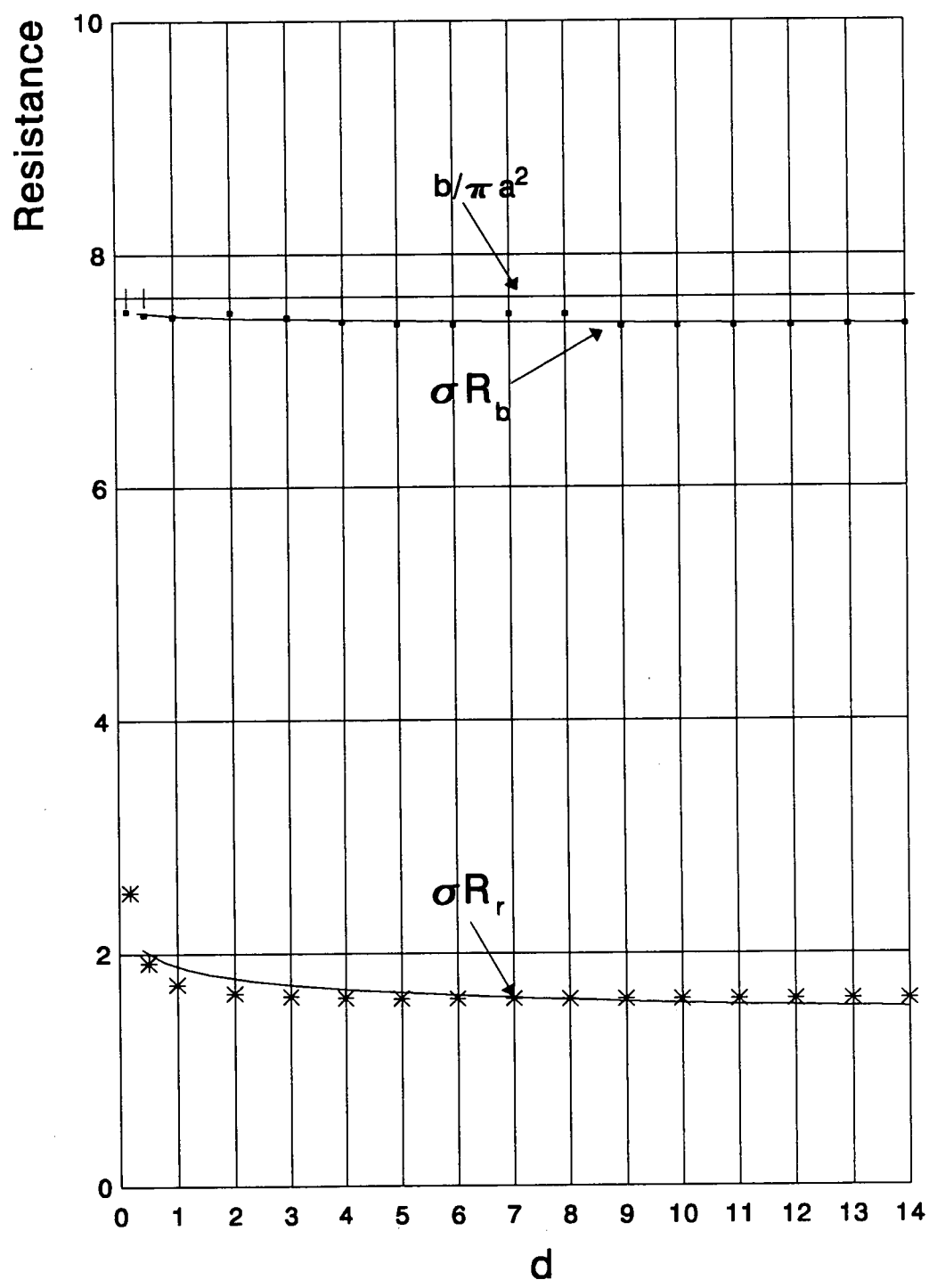


Figure 2.23 Bore and remaining solution resistance variation with horizontal solution area from probe to container edge ( $d$ )

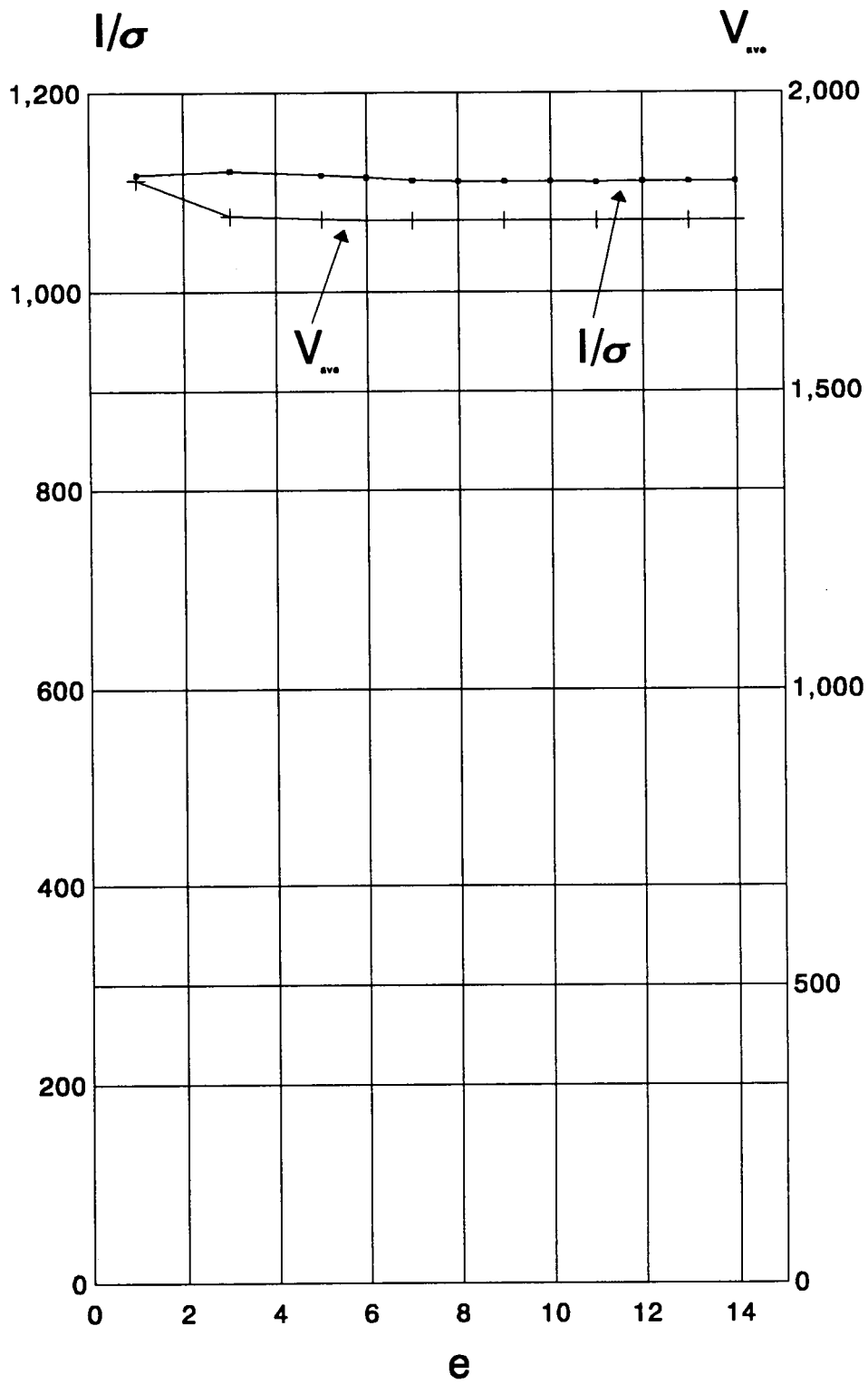


Figure 2.24 Current and bore edge voltage variation with vertical solution area ( $e$ )

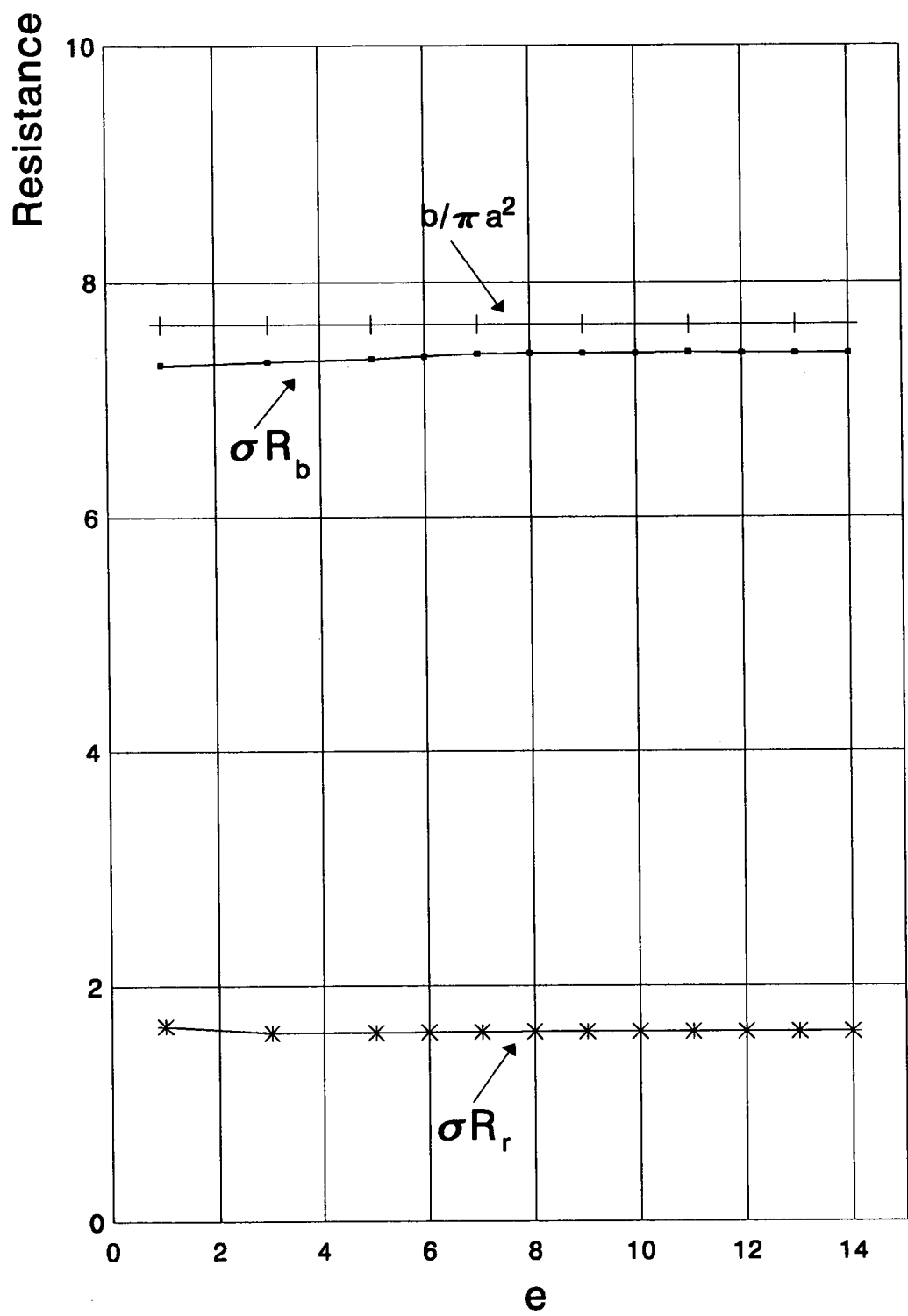


Figure 2.25 Bore and remaining solution resistance variation with vertical solution area ( $e$ )

resistance of the electrolyte is the sum of the bore resistance and that of the remaining solution, a further term must be added to the last expression.

Figure 2.17 shows that the resistance of the solution outside the bore shows no dependence on  $b$  for the range of dimensions examined. The same can be said for variations of  $d$  and  $e$ , unless these dimensions become sufficiently small to approach the horizontal and vertical ones of the probe respectively. Figure 2.19 shows a strong dependence on  $a$  and figure 2.21 a slight, but definite dependence on  $c$ . Therefore the relationship of the solution resistance outside the bore with  $a$  and  $c$  has to be investigated.

On figure 2.26  $\sigma R_r$  is plotted against  $c$  for several values of  $a$ . It is clear that the two quantities are linearly related, that is

$$\sigma R_r = rc + s \quad (2.2.28)$$

with  $r$  and  $s$  being functions of  $a$ .

Analysis of the values for  $r$  and  $s$  shows a linear variation with  $1/a^2$  and  $1/a^{1.3}$  respectively. Using the method of least squares to derive the regression coefficients for  $r(1/a^2)$  and  $s(1/a^{1.3})$  and substituting the them in 2.2.28, we can derive an expression for the resistance of the solution outside the cell bore:

$$\sigma R_r = 6.586 \cdot 10^{-3} \frac{c}{a^2} + 7.6832 \cdot 10^{-3} c + 0.2467 \frac{1}{a^{1.3}} + 0.0141 \quad (2.2.29)$$

The unit is  $\text{cm}^{-1}$  provided that  $a$  and  $c$  are in cm.

If  $R_s$  denotes the total resistance of the solution around the probe, the cell constant can be derived from the following expression:

$$\sigma R_s = \sigma R_b + \sigma R_r \quad (2.2.30)$$

Taking also into account the factor of 2 introduced by the conventions for the area under investigation, the expression for the cell constand can be written as:

$$\sigma R_s = \frac{2b}{\pi a^2} + 1.317 \cdot 10^{-2} \frac{c}{a^2} + 1.537 \cdot 10^{-2} c + 0.4934 \frac{1}{a^{1.3}} + 0.0282 \quad (2.2.31)$$

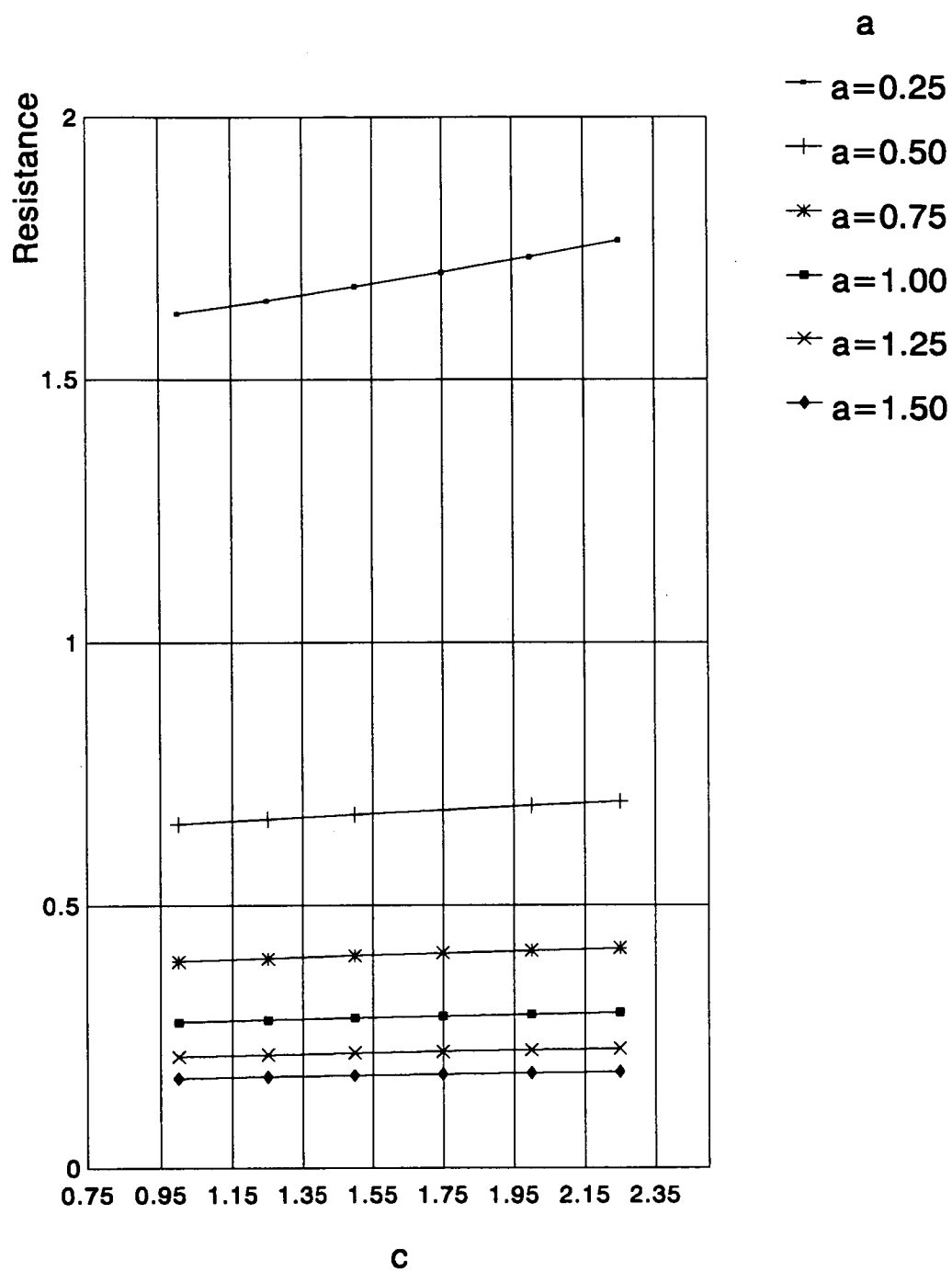


Figure 2.26 Variation of solution resistance outside the cell bore with  $c$  for several values of  $a$



Application of equation 2.2.31 on the probe used in this work for which  $a=0.46\text{cm}$ ,  $b=1.2\text{cm}$  and  $c=1.35\text{cm}$ , gives a cell constant of  $5.097\text{cm}^{-1}$ .

With an expression of the cell constant determined, the effects of scaling (ie variation of all probe dimensions by the same factor simultaneously) can be investigated. Figure 2.27 shows the effect of varying scale factor on the cell constant: it can be seen that the latter is inversely proportional to the scale factor; this is expected since the term  $2b/(\pi a^2)$  is dominant in expression 2.2.31. The dimensions of the probe also indicate the volume of the sample required for correct operation: for a large probe (with a diameter of  $10\text{cm}$  for example) a sample volume of several litres is required to avoid reduction of the signal amplitude due to "wall effect". For the lower conductivity ranges, where a smaller cell constant is required, a larger probe and sample volume must be used.

## 2.3 Equivalent circuit modelling of the conductivity sensor.

### 2.3.1 Formulation of an equivalent circuit model

The conductivity probe can be considered as an equivalent circuit comprising two transformers. The drive coil can be considered as the primary coil of the first transformer, with the solution loop forming its secondary. For the second transformer the solution loop can be considered as its primary, with the pickup coil forming the secondary winding. This arrangement can be seen in figure 2.28. In that figure  $R_J$ ,  $R_S$  and  $R_L$  denote the resistance of the drive circuit (voltage source, drive coil resistance, cable and connector resistances), the resistance of the electrolytic solution and the resistance of the pickup circuit (pickup coil, first stage of signal conditioning circuit input resistance, cable and connector resistances) respectively.  $M_{12}$  and  $M_{34}$  denote the mutual inductances of transformers  $T_1$  and  $T_2$  respectively. Assuming coupling coefficients  $m$  and  $n$  for the transformers  $T_1$  and  $T_2$  respectively, we can write

$$m = \frac{M_{12}}{\sqrt{L_1 L_2}} \quad (2.3.1)$$

and

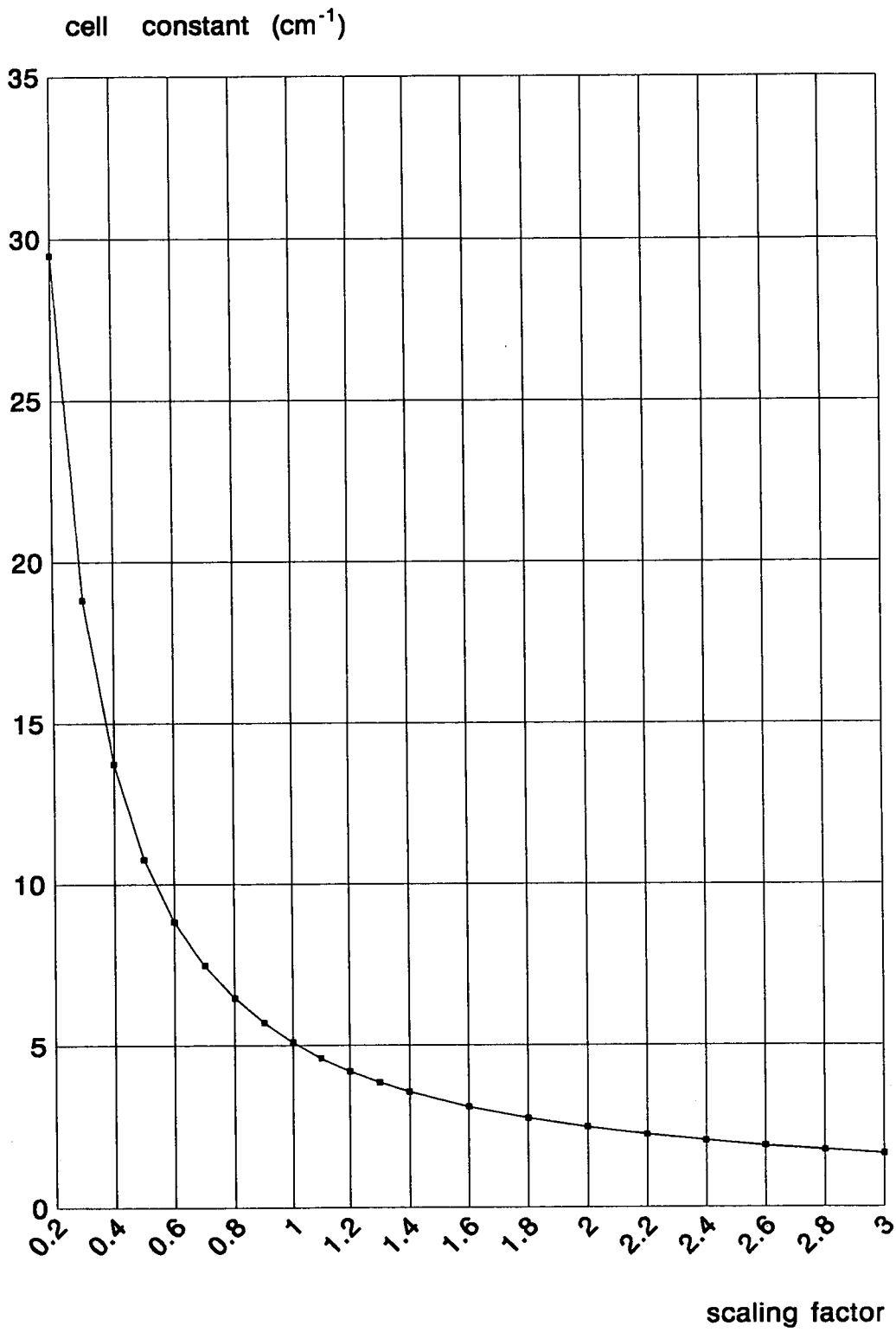


Figure 2.27 Effects of scaling on cell constant

$$n = \frac{M_{34}}{\sqrt{L_3 L_4}} \quad (2.3.2)$$

Applying Kirchoff's voltage law for the three current loops shown in figure 2.28, we derive the following set of equations (expressed in the s-domain):

$$R_1 I_1(s) + s L_1 I_1(s) + s M_{12} I_2(s) = V_s(s) \quad (2.3.3)$$

$$s L_2 I_2(s) + R_s I_2(s) + s L_3 I_2(s) + s M_{34} I_3(s) + s M_{12} I_1(s) = 0 \quad (2.3.4)$$

$$s L_4 I_3(s) + R_L I_3(s) + s M_{34} I_2(s) = 0 \quad (2.3.5)$$

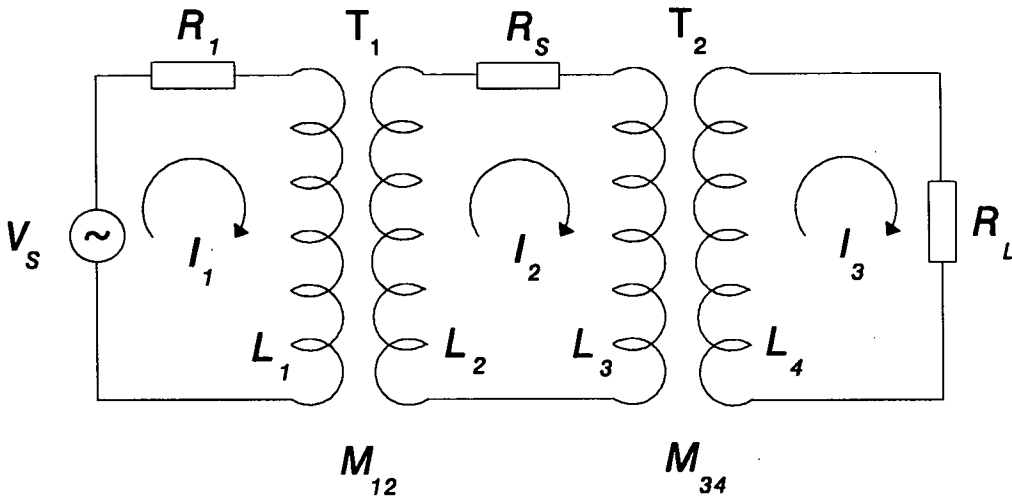


Figure 2.28 Network equivalent of the conductivity probe

This system of equations can be written in matrix form, after substituting equations 2.3.1 and 2.3.2 as:

$$\begin{bmatrix} R_1 + s L_1 & s m \sqrt{L_1 L_2} & 0 \\ s m \sqrt{L_1 L_2} & R_s + s L_2 + s L_3 & s n \sqrt{L_3 L_4} \\ 0 & s n \sqrt{L_3 L_4} & R_L + s L_4 \end{bmatrix} \begin{bmatrix} I_1(s) \\ I_2(s) \\ I_3(s) \end{bmatrix} = \begin{bmatrix} V_s(s) \\ 0 \\ 0 \end{bmatrix} \quad (2.3.6)$$

or,

$$AI = V \quad (2.3.7)$$

The determinant of this matrix can be found as:

$$\begin{aligned} D = & R_1 R_s R_L + s(L_2 R_1 R_L + L_3 R_1 R_L + L_4 R_1 R_s + L_1 R_s R_L) + \\ & + s^2(L_2 L_4 R_1 + L_3 L_4 R_1 (1 - n^2) + L_1 L_2 R_L (1 - m^2) + L_1 L_3 R_L + L_1 L_4 R_s) + \\ & + s^3(L_1 L_2 L_4 (1 - m^2) + L_1 L_3 L_4 (1 - n^2)) \end{aligned} \quad (2.3.8)$$

The matrix equation 2.3.6 then yields the following solutions:

$$I_1(s) = \frac{R_s R_L + s(L_4 R_s + L_2 R_L + L_3 R_L) + s^2(L_2 L_4 + L_3 L_4 (1 - n^2))}{D} V_s(s) \quad (2.3.9)$$

$$I_2(s) = \frac{-m\sqrt{L_1 L_2}(s R_L + s^2 L_4)}{D} V_s(s) \quad (2.3.10)$$

$$I_3(s) = \frac{s^2 m n \sqrt{L_1 L_2 L_3 L_4}}{D} V_s(s) \quad (2.3.11)$$

### 2.3.2 Examination of factors affecting the model probe performance

As seen in the expressions 2.3.11 the performance of a particular probe (ie the output current ( $I_3$ ) and its phase) depends on  $R_1$ ,  $R_L$ , the coupling coefficients of the model transformers, and the operating frequency, assuming a fixed number of turns and fixed toroidal cores. This subsection will mainly examine how each of these factors affects the performance of the modelled probe. The probe used in this work can be considered as a typical electrodeless sensor and its performance will be compared to that of the model of sensor developed in the

previous section.

The inductances involved are calculated from the formula

$$L = \frac{N^2}{R} \quad (2.3.12)$$

where  $N$  is the number of turns and  $R$  the reluctance of the magnetic circuit defined as

$$R = \frac{l}{\mu S} \quad (2.3.13)$$

where  $l$  is the length,  $S$  the cross section and  $\mu$  the permeability of the magnetic circuit.

Assuming identical cores (ferromagnetic material and dimensions) for the drive and pickup circuit and considering the coils  $L_2$  and  $L_3$  to be composed of one turn around the toroidal core, with  $L_1$  having 48 turns and  $L_2$  6 turns, the following inductance values can be derived:

$$L_1 = 6.5\text{mH}$$

$$L_2 = L_3 = 0.00282\text{mH}$$

$$L_4 = 0.102\text{mH}.$$

If the source driving the probe is chosen to be a feedback operational amplifier, its output resistance has a typical value of fractions of  $1\text{m}\Omega$ , therefore it can be ignored in the expression for  $R_i$ . If  $R_c$  denotes the combination of cable and connector resistances, which is obviously the same for the drive and the pickup circuits since identical cables and connectors run from the circuit board to the sensor connected through the same block connector, the following expressions can be written for the drive and pickup circuit resistances:

$$R_1 = R_d + R_c \quad (2.3.14)$$

and

$$R_L = R_p + R_c \quad (2.3.15)$$

where  $R_d$  and  $R_p$  denote the resistances of the drive and pickup coil and have the approximate values of  $0.356\Omega$  and  $0.044\Omega$  for the actual sensor respectively.

A suitable expression for the calculation of the output current can be written by using phasor representation for equations 2.3.8 and 2.3.11:

$$\begin{aligned} D = & R_1 R_s R_L + j\omega (L_2 R_1 R_L + L_3 R_1 R_L + L_4 R_1 R_s + L_1 R_s R_L) - \\ & - \omega^2 (L_2 L_4 R_1 + L_3 L_4 R_1 (1-n^2) + L_1 L_2 R_L (1-m^2) + L_1 L_3 R_L + L_1 L_4 R_s) - \\ & - j\omega^3 L_1 L_4 (L_2 (1-m^2) + L_3 (1-n^2)) \end{aligned} \quad (2.3.16)$$

and

$$I_3 = \frac{-\omega^2 mn \sqrt{L_1 L_2 L_3 L_4}}{D} V_s \quad (2.3.17)$$

Taking the voltage source in figure 2.28 as phase reference, that is:

$$V_s = V_m \angle 0^\circ \quad (2.3.18)$$

we can examine the effect of cable resistance, operating frequency and transformer coupling on the phase and magnitude of the sensor output current.

The solution resistances used in the following sections, represent values over the conductivity range of the probe used for this project.

### 2.3.2.1 Effects of variations in the cable resistance on the probe output

This is shown in figure 2.29 for the output current amplitude of the modelled sensor. It can be seen that small variations of cable resistance have no noticeable effect on the amplitude of the output current, which maintains its

linearity throughout the conductivity range.

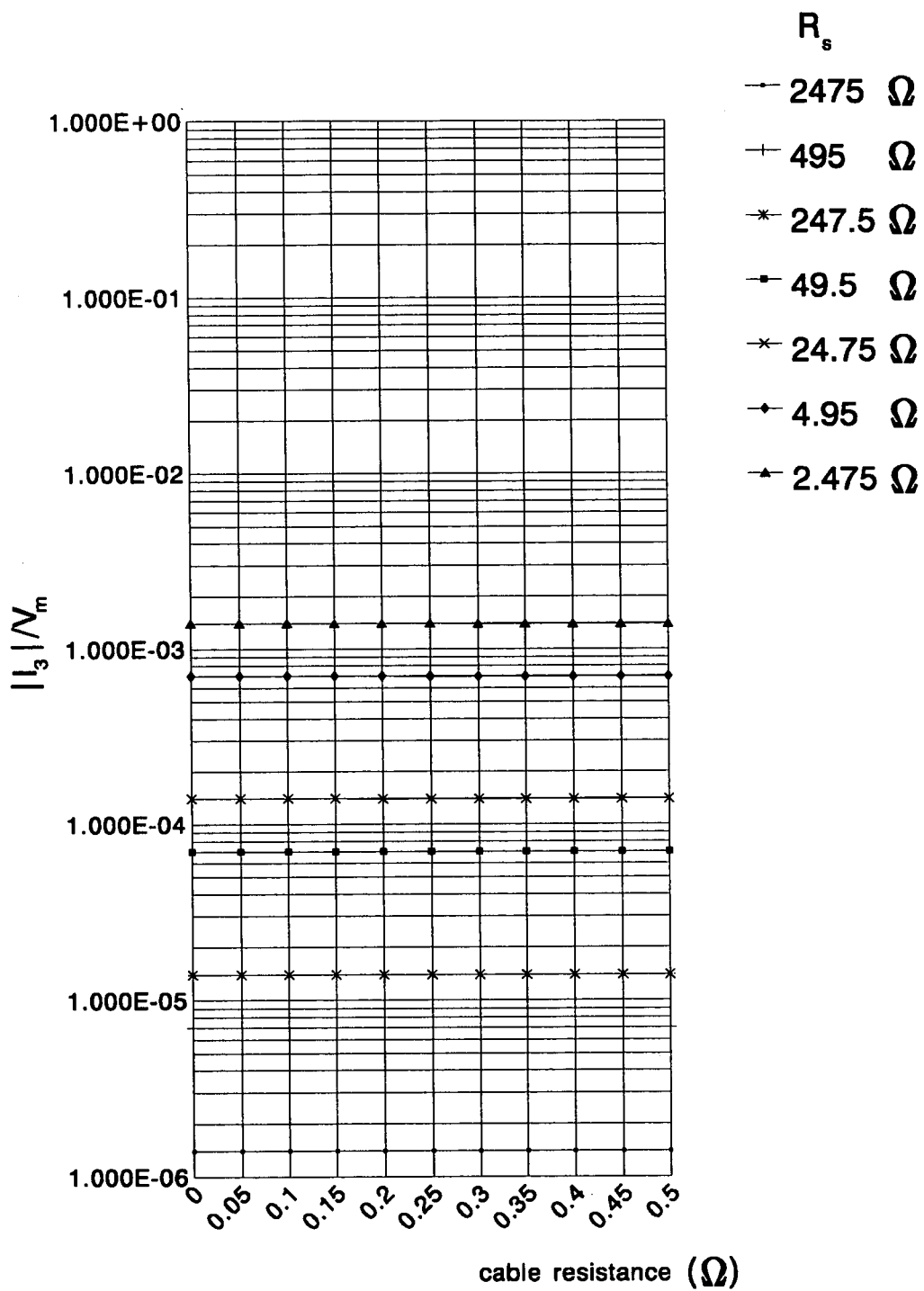


Figure 2.29 Variation of output current amplitude with cable resistance  
( $f=15\text{KHz}$ , coupling 100%,  $R_d=0.356\Omega$ ,  $R_p=0.044\Omega$ )

In figure 2.30 the effects of this variation on the phase of the output current are shown. This variation is linear, with a slope of about 6.6 degrees per  $\Omega$  of cable resistance. The small offset represents the effect of the resistances of the coils; if these are assumed to have no resistance, the phase angle is calculated as 0. Figure 2.30 also shows some tendency of the phase to change with solution resistance, as the cable resistance increases. This is obviously a most unwanted effect, which itself indicates that cable resistances should be kept as small as possible

### **2.3.2.2 Effects of variations of coupling coefficients on output current**

Separate examination of the variation of coupling coefficients of transformers  $T_1$  and  $T_2$  (see figure 2.28) shows that this variation has symmetrical effects on the magnitude and phase of the model output current and equal to the effect of the product of the two coefficients. As a very high coupling coefficient is expected due to the very high relative permeability of the toroidal core material, the product in the range 98 to 100% has been considered. In figures 2.31 and 2.32, the variation of output current amplitude with coupling for  $R_c=0.20$  and  $0.05\Omega$  respectively. It is clear that there is only a slight drop in amplitude as the coupling reduces; also linearity of magnitude is retained throughout the conductivity range. Figures 2.33 and 2.34 show the respective phase variations. It can be seen that phase varies linearly with coupling, but reduced coupling leads to nonlinearly varying slope throughout the conductivity range, though reduced cable resistance can lead to smaller spread of phase values. This is one more indication for minimisation of cable and connector resistances.

### **2.3.2.3 Effects of operating frequency on output current**

Figure 2.35 shows the variation in output current amplitude and phase with the operating frequency. It can be seen that the amplitude remains unaffected, while its linearity is retained throughout the conductivity range. Phase variation is more evident, and it remains the same for all conductivity values. Although there is phase variation, the absolute values of angles are small for small cable



resistances.

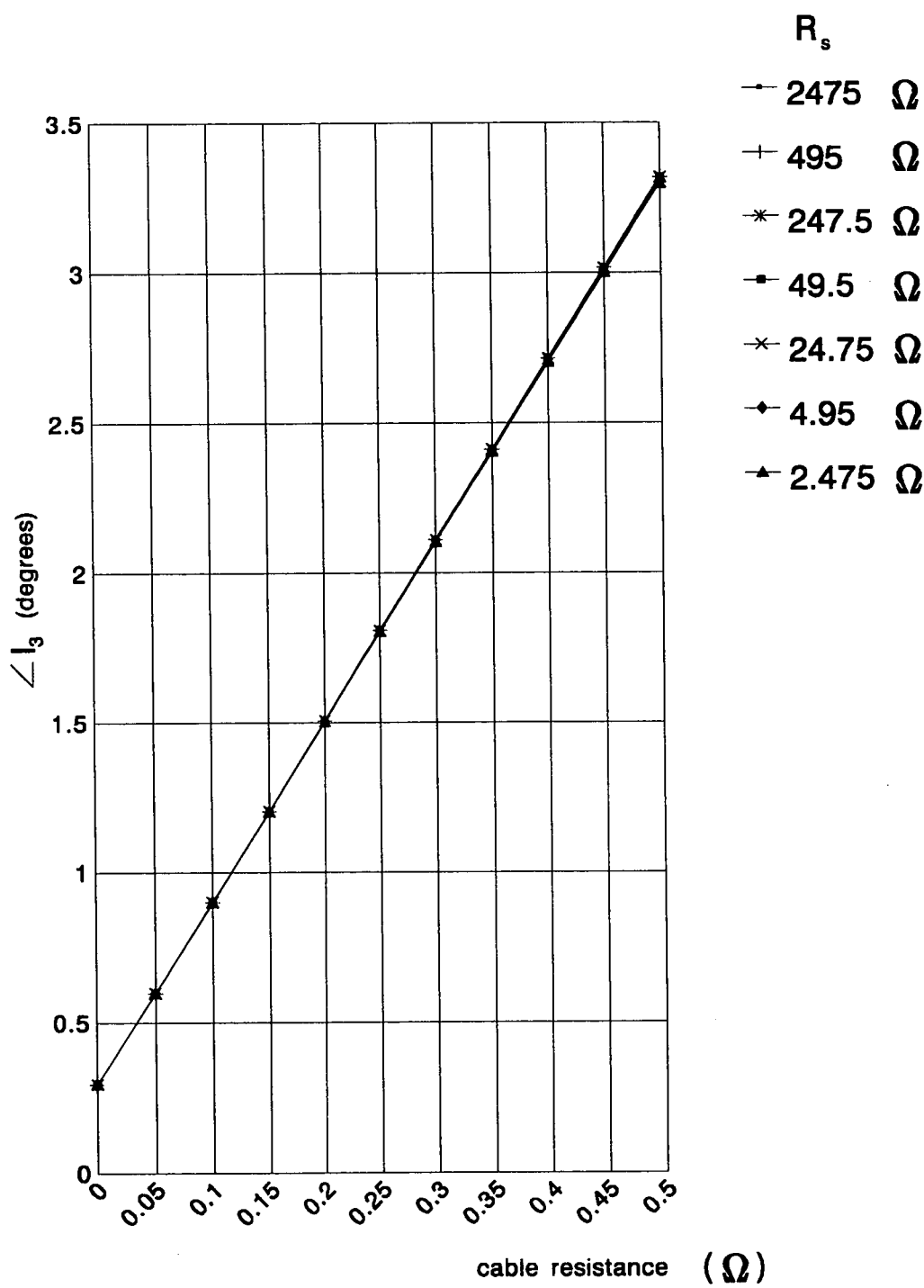


Figure 2.30 Variation of output current phase with cable resistance  
( $f=15\text{KHz}$ , coupling 100%,  $R_d=0.356\Omega$ ,  $R_p=0.044\Omega$ )

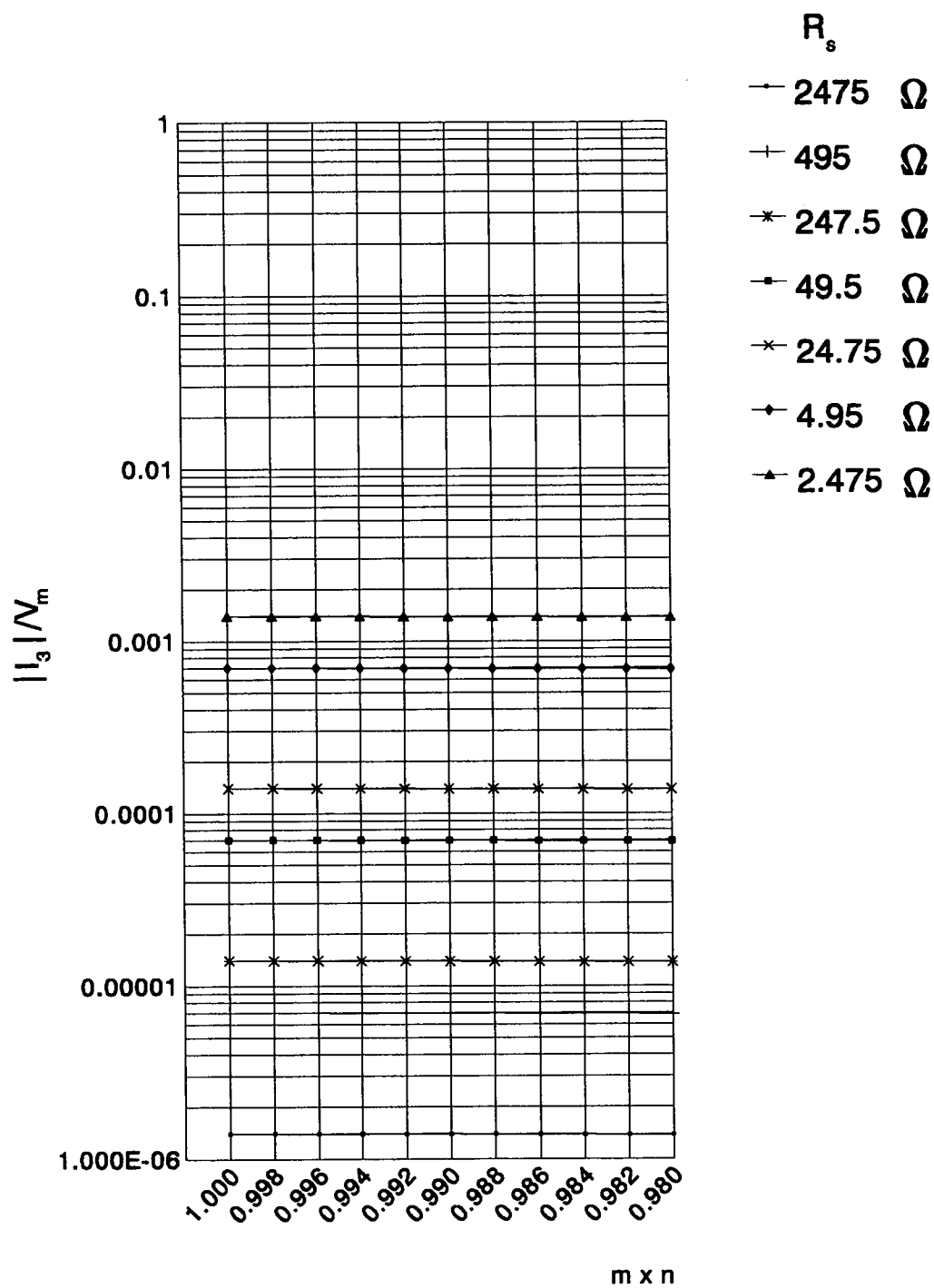


Figure 2.31 Output current amplitude variation with coupling coefficients  
 ( $f=15\text{KHz}$ ,  $R_d=0.356\Omega$ ,  $R_p=0.044\Omega$ ,  $R_c=0.20\Omega$ )

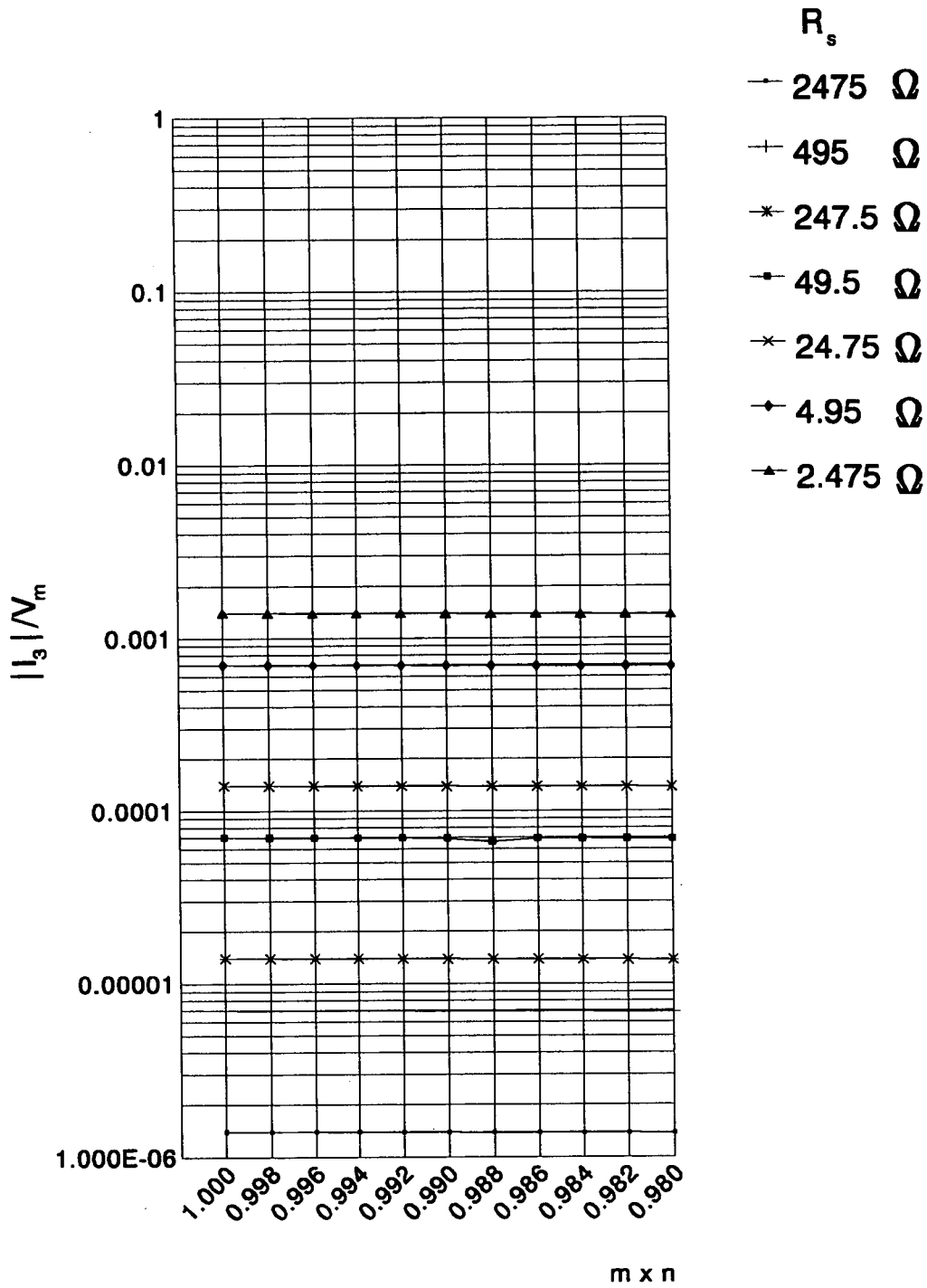


Figure 2.32 Output current variation with coupling coefficients  
 ( $f=15\text{KHz}$ ,  $R_d=0.356\Omega$ ,  $R_p=0.044\Omega$ ,  $R_c=0.05\Omega$ )

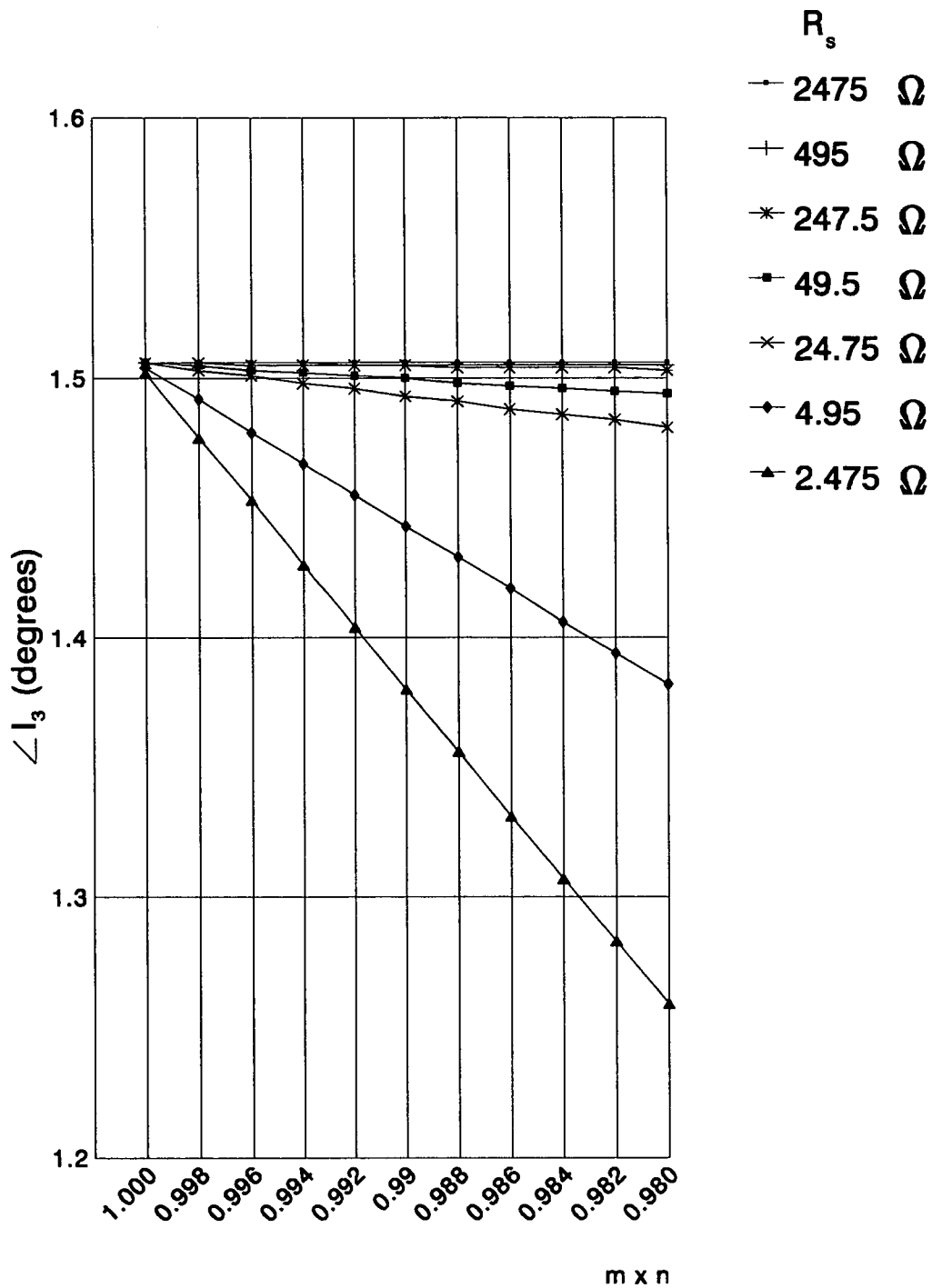


Figure 2.33 Variation of output current phase with coupling coefficients  
 ( $f=15\text{KHz}$ ,  $R_s=0.356\Omega$ ,  $R_p=0.044\Omega$ ,  $R_c=0.20\Omega$ )

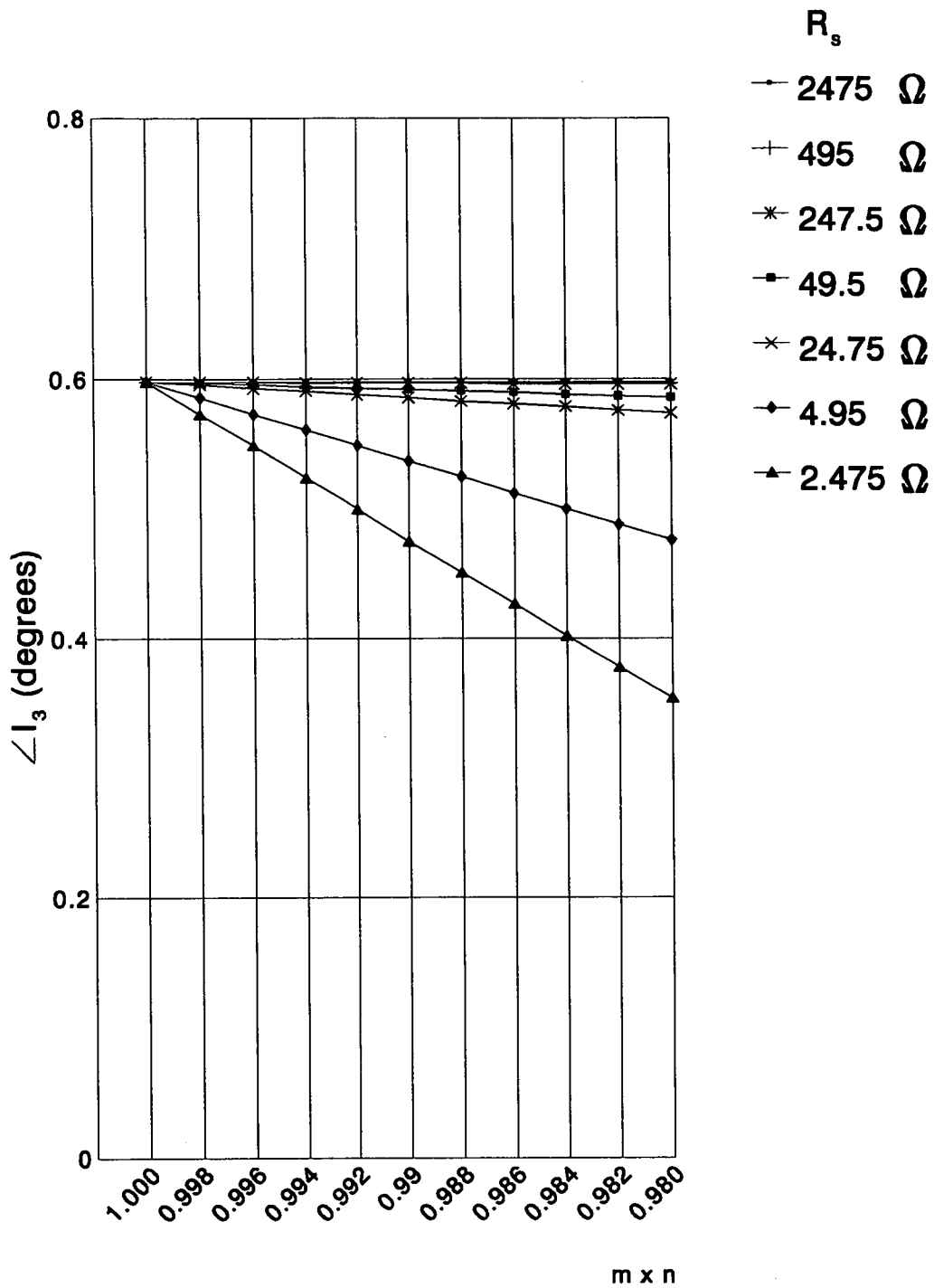


Figure 2.34 Output current phase variation with coupling coefficients  
 ( $f=15\text{KHz}$ ,  $R_d=0.356\Omega$ ,  $R_p=0.044\Omega$ ,  $R_c=0.05\Omega$ )

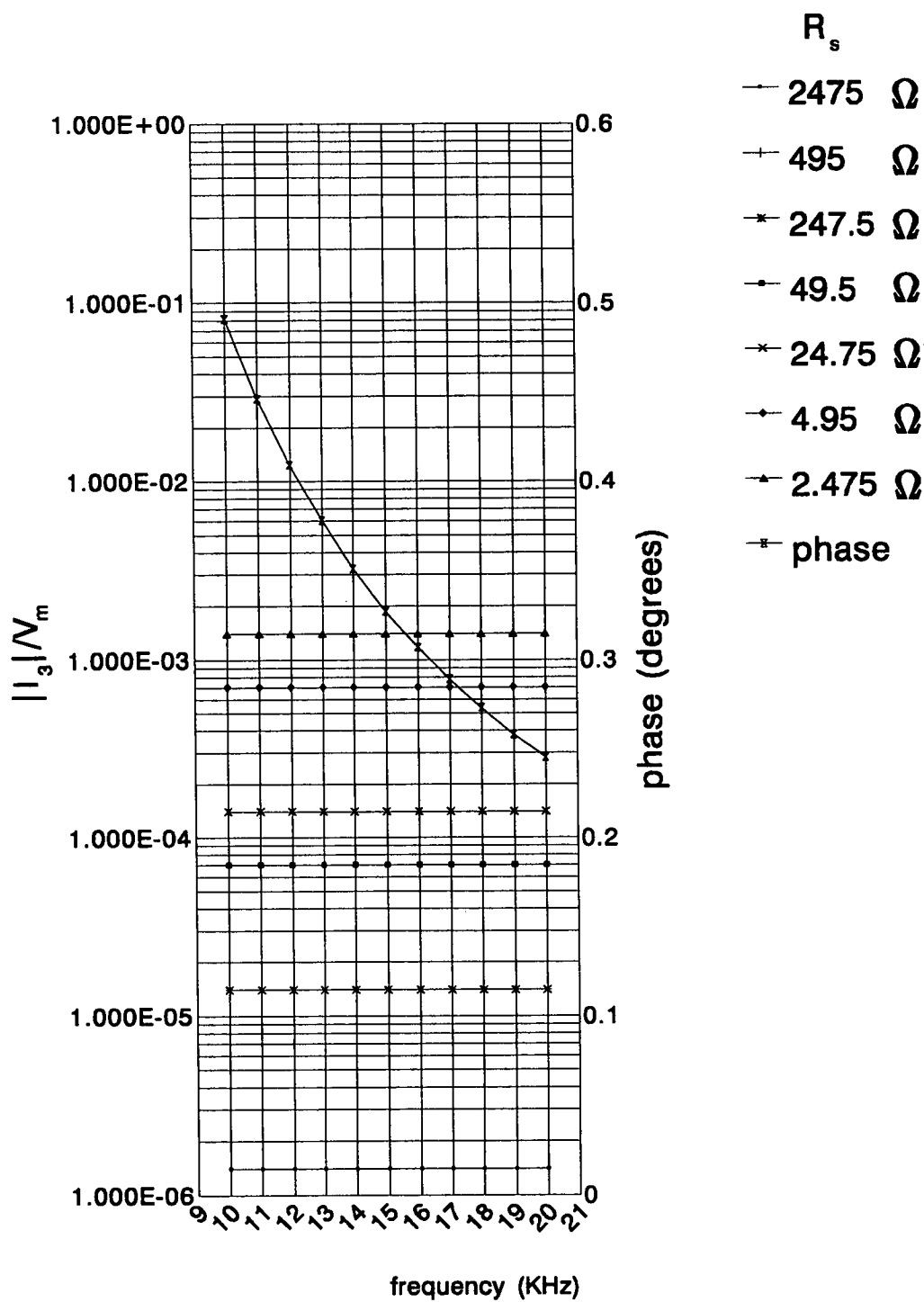


Figure 2.35 Output current and phase variation with operating frequency (coupling 100%,  $R_d=0.356\Omega$ ,  $R_p=0.044\Omega$ ,  $R_c=0\Omega$ )

### 2.3.2.4 Comparison of model and actual probe outputs

A comparison of the output current amplitude given by the model probe with that of the actual probe used for this work, can be seen in figure 2.36. It can be seen that these values are in very close agreement. In that figure several values for phase angles have also been plotted, and as expected the latter take reduced values for smaller cable resistances. In practice the phase angle was too small to be measured accurately, especially for the smaller values in the conductivity range, where the signal is obscured by high levels of noise, but it was thought to be less than 1 degree. For the model-derived values of current, coupling was taken to be 100%. Also, when current measurements were made, the cable length was kept to a minimum.

These comparisons show that the two transformer model is a good approximation of conductivity sensor. Therefore it can be used as a basis for the design of this kind of electrodeless sensors. It would be a good approximation to consider the output current in real situations to be given by equation 2.3.17, with  $R_1=R_L=0$ , and  $m=n=1$  (justified by the comparison between measured phase values and calculated as seen in figure 2.36), if low resistance cable, good quality connectors (or cable soldered directly to the circuit board), and even thicker wire for the coil windings (in the actual probe the wires were only 0.3mm in diameter) are used.

Then (on the assumption that the voltage source is taken as reference),

$$I_3 = \frac{-\omega^2 M_{12} M_{34}}{-\omega^2 L_1 L_4 R_s} \angle 0^\circ = \sqrt{\frac{L_2 L_3}{L_1 L_4}} \frac{V_m}{R_s} \angle 0^\circ = \frac{1}{N_1 N_4} \frac{V_m}{R_s} \angle 0^\circ \quad (2.3.19)$$

or,

$$I_3 = \frac{1}{N_1 N_4} \frac{V_m}{\text{cell constant}} \sigma \angle 0^\circ \quad (2.3.20)$$

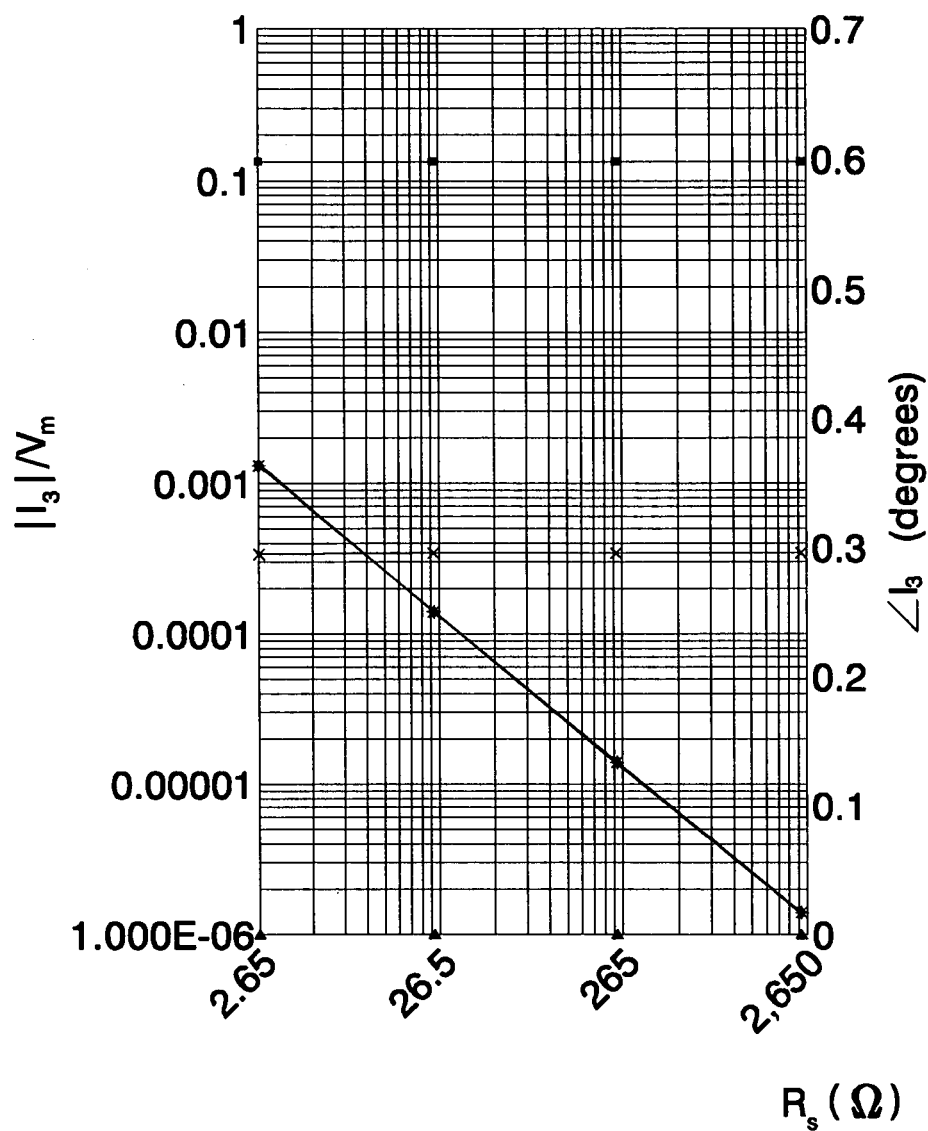


Figure 2.36 Comparison of model and actual probe output ( $f=15\text{KHz}$ )



As far as the further processing of the sensor output is concerned, it has been shown that the current amplitude is relatively immune to varying cable length, fluctuations in the frequency of operation and coupling, while its phase is sensitive to all of these factors. The actual phase values however show little deviation from the value of  $0^\circ$ , therefore the output signal can be processed by a system insensitive to small deviations. The phase sensitive detector described in the next chapter, is a building block ideally suited to this role.

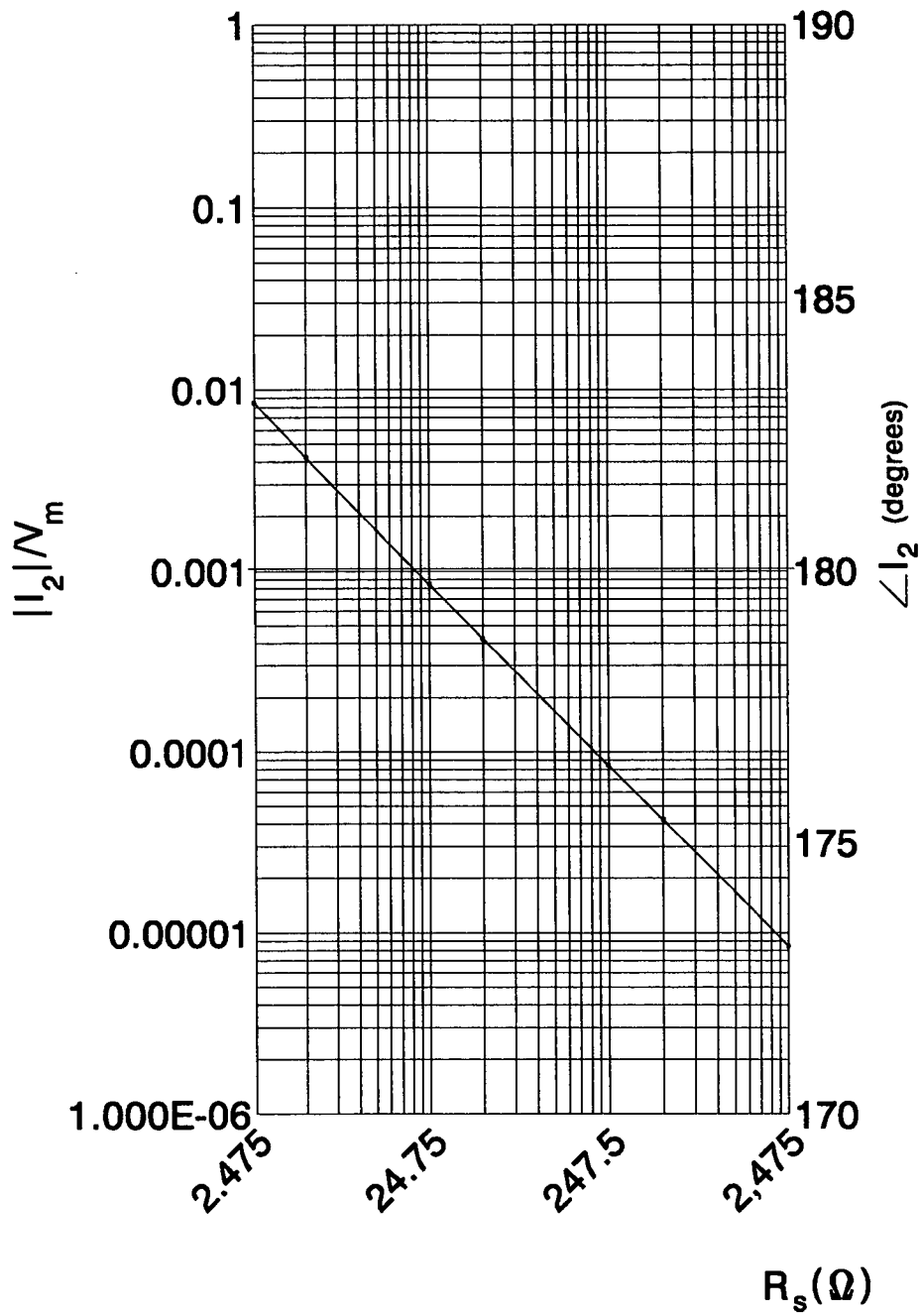
Equation 2.3.10 also gives an expression for the current in the electrolyte. Figure 2.37 shows its phase and magnitude variation for several values of solution resistance.

Considering the ideal case (ie  $R_1=R_L=0$ ) equation 2.3.10 gives:

$$I_2 = \sqrt{\frac{L_2}{L_1} \frac{V_m}{R_s}} \angle 180^\circ = \frac{1}{N_1} \frac{V_m}{\text{cell constant}} \sigma \angle 180^\circ \quad (2.3.21)$$

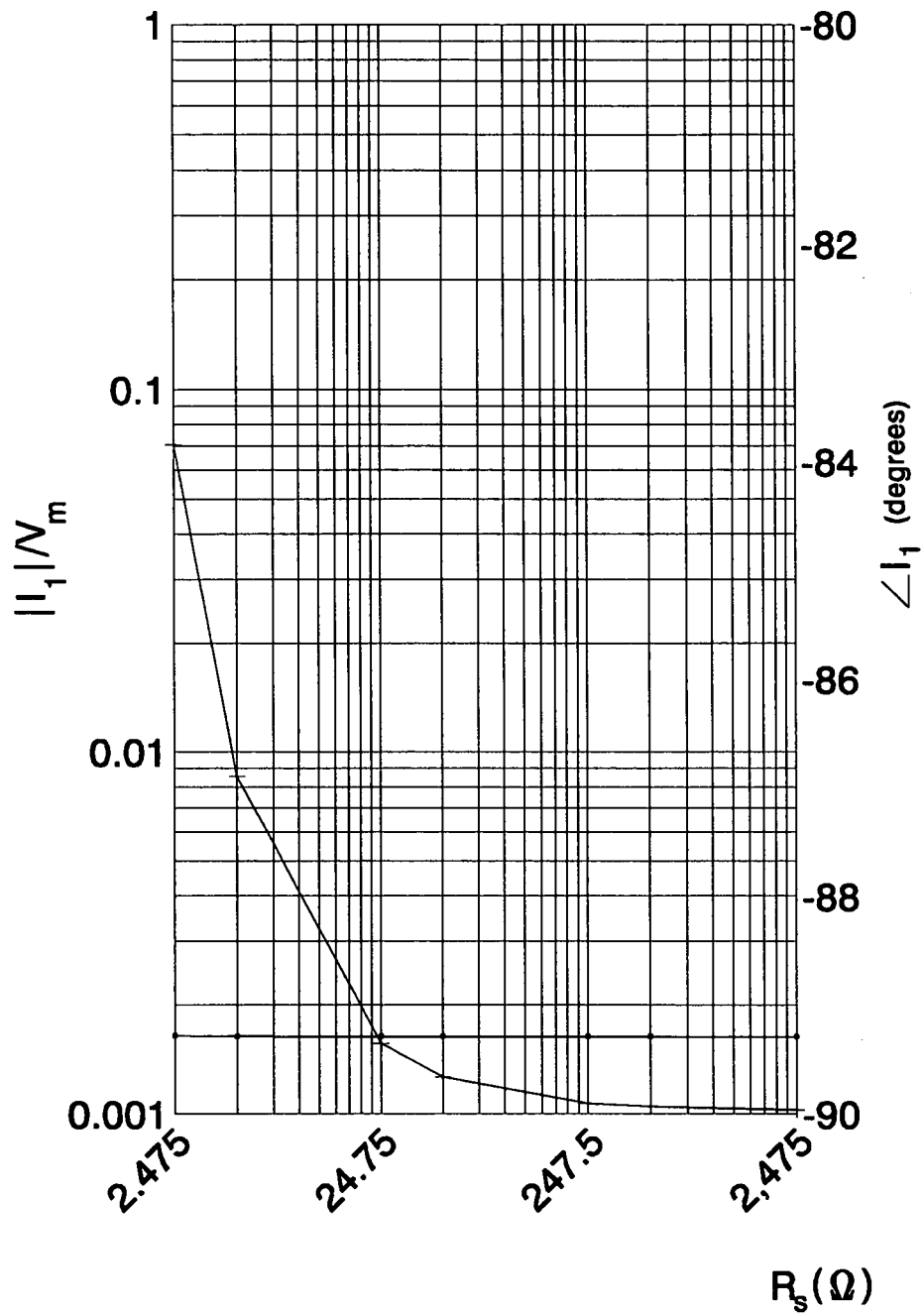
In figure 2.38 variation of the current in the drive circuit for several values of solution resistance can be seen. The effect of changing solution resistance on the current amplitude is minimal while the phase difference with the voltage source is very close to  $90^\circ$ , as expected from a circuit that is mainly inductive. In the ideal case equation 2.3.9 gives the following expression for the drive circuit current:

$$I_1 = \frac{V_m}{\omega L_1 R_s} \sqrt{\omega^2 L_2^2 + R_s^2} \angle \tan^{-1}\left(-\frac{R_s}{\omega L_2}\right) \quad (2.3.22)$$



$$\rightarrow |I_2|/N_m \rightarrow \angle I_2$$

Figure 2.37 Current variation in the solution ( $f=15\text{KHz}$ , coupling 100%,  $R_D=0.356\Omega$ ,  $R_P=0.044\Omega$ ,  $R_C=0.05\Omega$ )



$$|I_1|/N_m + \angle I_1$$

Figure 2.38 Current variation in the drive circuit ( $f=15\text{KHz}$ , coupling 100%,  $R_D=0.356\Omega$ ,  $R_P=0.044\Omega$ ,  $R_C=0.05\Omega$ )

# CHAPTER 3

## THE HARDWARE PART OF THE CONDUCTIVITY METER

### 3.1 Introduction

This chapter describes the hardware part of the conductivity meter. The main objective as mentioned in chapter 1 was to achieve a best compromise between accuracy and cost, using a small number of components thus minimising size, cost of production and power consumption. Part of that has been achieved by performing wherever possible the required tasks using software rather than hardware. The block diagram of the system can be seen in figure 3.1.

The hardware can be divided in two parts: The digital part, responsible for the general control of the system and data collection, processing and display, and the analog part which drives the conductivity probe and translates its output signals to a form readable by the microcontroller.

### 3.2 The analog circuit of the conductivity meter

This part consists of a sinusoidal oscillator driving the conductivity probe (drive coil), a current to voltage converter connected to its output, an amplification stage for the control of the range, a phase sensitive detector, a voltage limiter for the conductivity signal, the temperature measurement circuit, a voltage level shifter and a voltage to frequency converter. The schematic

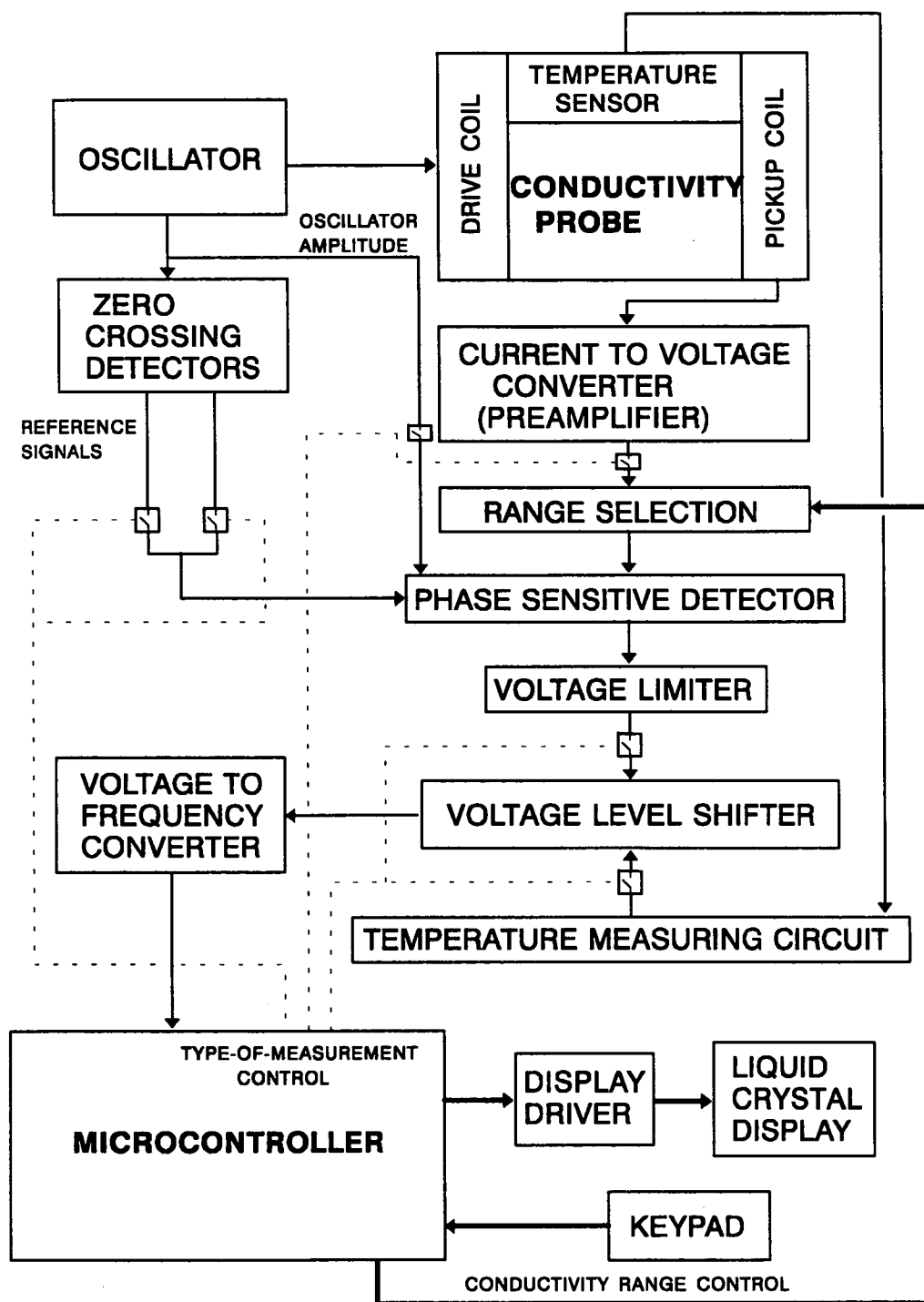
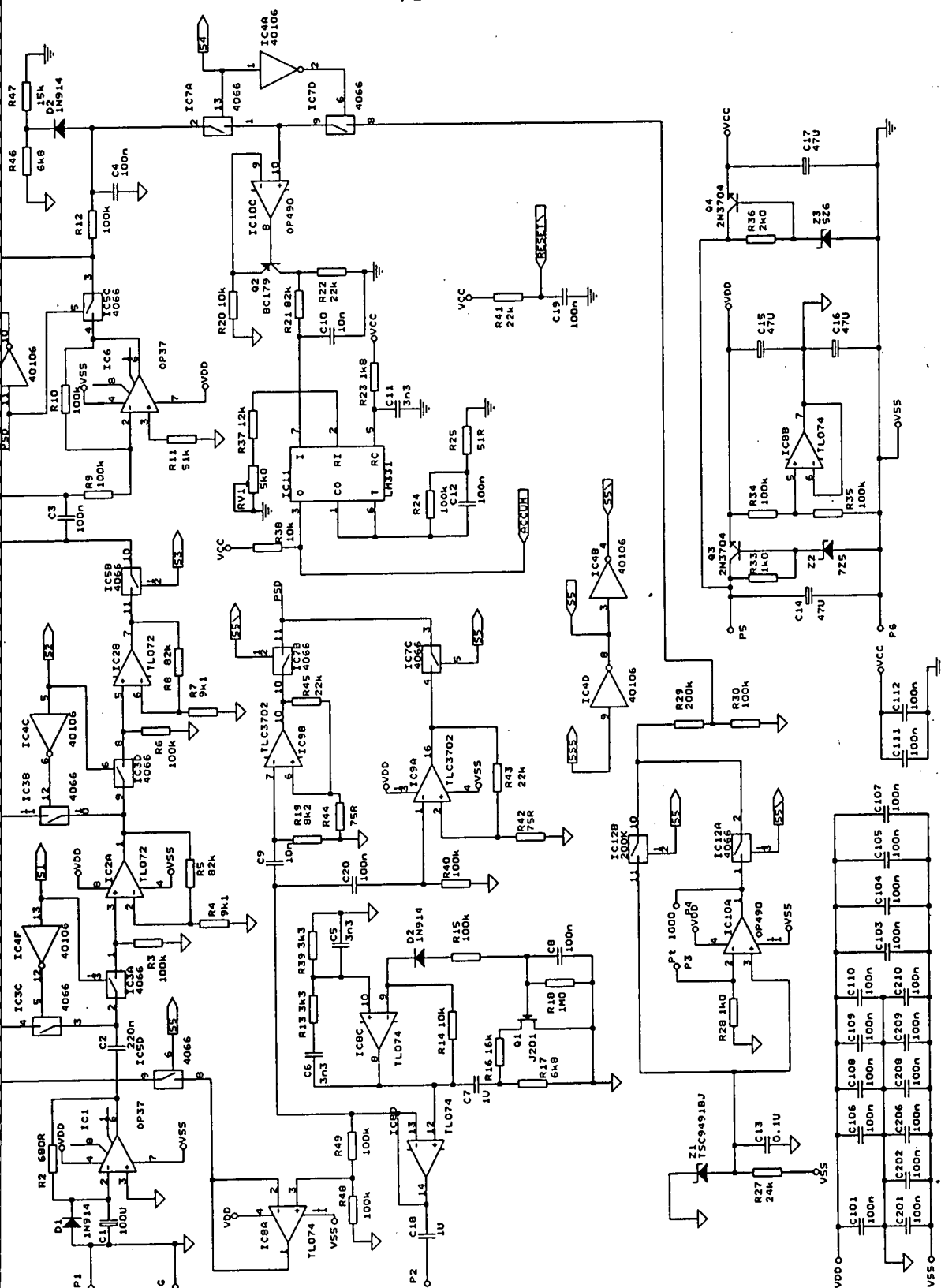


Figure 3.1 Block diagram of the conductivity measuring system



**Figure 3.2 The analog part of the conductivity meter**

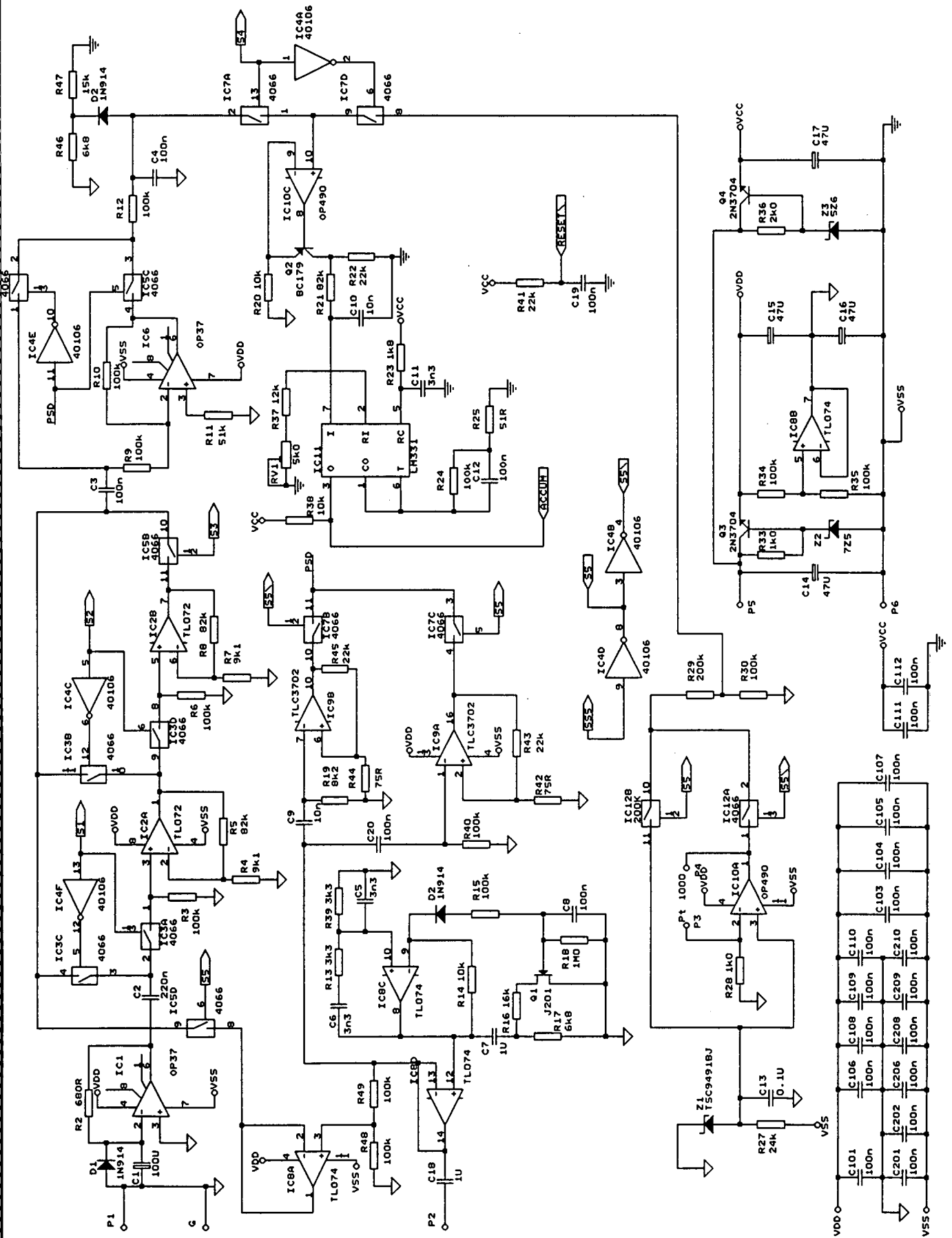


Figure 3.2 The analog part of the conductivity meter

diagram of the analog part of the system can be seen in figure 3.2.

### 3.2.1 Power supply

A single 9V battery provides power to the system; its voltage is stabilised using a standard voltage regulator to around 7V. A  $\pm 3.5\text{V}$  split supply is derived from that, with the mid point serving as analog ground, to be used by the operational amplifiers and the analog switches. A second supply, stabilised to 5V is derived from the battery voltage to power the digital circuitry: microcontroller, display drivers, and voltage to frequency converter. In figure 3.2, the  $+3.5\text{V}$  supply is denoted by VDD, the digital ground/ $-3.5\text{V}$  by VSS and the 5V supply by VCC.

### 3.2.2 Oscillator

A Wien bridge oscillator has been used to drive the conductivity probe; it has been chosen for the very low distortion sinusoidal output it produces, excellent frequency stability and the relatively small number of components required to realise. Stable frequency is of great importance, since it is one of the three factors affecting the probe's output signal. While compensation for oscillator amplitude variations can easily be provided, this is not the case for frequency variations as the output signal of the probe (its phase in particular as has been shown in chapter 2), changes over the entire range of measurement with changes in frequency. The positive feedback network C6/R13 and C5/R39 of amplifier IC8C provides a frequency of around 15 KHz. In practice it has been found that after sharp temperature variations to levels outside the proposed operational temperature of the system (0 to 70 °C), the oscillator output waveform saturates or becomes distorted before the frequency changes more than 1%. Its value has been maintained nearly constant over repeated on-off switching over a long period of time. The negative feedback network of the oscillator includes a JFET which acts as a voltage controlled resistor. A J201 transistor has been selected for its low cut off voltage (1.5 V max). The amplitude of the oscillator output must be adjusted



to around  $3V_{pp}$ . Precise adjustment is not necessary, since software allows variations of oscillator amplitude as well as small offsets. The oscillator output is buffered by the unity gain amplifier IC8D to avoid loading the oscillator and reducing its frequency stability. The input impedance of the drive coil is only about  $600\ \Omega$  at 15 KHz. A capacitor (C18) blocks any DC components present in the drive signal.

### 3.2.3 Current to voltage converter

This consists of amplifier IC1 and resistor R2. Its function is to convert the alternating current induced in the pick-up coil to a proportional voltage. Capacitor C1 is used to limit the zero frequency gain of this stage. Feedback resistor's R2 value has been selected to give an amplitude of around  $2.8V_{pp}$  at the output of IC1 when conductivity of the solution is 2000 mS/cm. This configuration makes signal preamplification easy and flexible. A suitable amplifier for this stage should have a low input offset voltage since the current-to-voltage converter is essentially an inverting amplifier with very low input resistance. An OP37 type operational amplifier with a maximum input offset voltage of 0.22mV has been found to be satisfactory in this respect, although its power consumption is relatively increased (around 2mA with  $\pm 3.5V$  supply at 25 °C). A small capacitor (C2) at the output of this stage removes the dc offset due to the input offset voltage of the OP37.

### 3.2.4 Amplification/range selection

After preamplification the conductivity signal is fed to the range selection stage. Each of the two amplifiers of this stage (IC2A and IC2B respectively), provide an amplification of 10 and therefore amplification by 1, by 10 and by 100 is available. These, in conjunction with the analog switches S1, S2, and S3 make three measurement ranges available, namely 2 to 19.99 mS/cm, 20 to 199.9 mS/cm and 200 to 1999 mS/cm. The operational amplifiers used in this stage are of the type TL07x; they have been chosen for their sufficient unity gain bandwidth (3MHz typical) and the relatively low current they draw (about

1.3mA with  $\pm 3.5V$  supply). The analog switches used at this stage, are of the type 4066 with supply current of the order of  $\mu A$ . They are powered by the analog supply voltages, so that the analog signals pass through them without distortion. The problem of controlling these switches with TTL signals from the microcontroller has been overcome by employing level shifting transistors; their inputs are TTL signals while the outputs are at the analog supply voltages. Obviously this configuration introduces inversion of the control signal. A transistor array (ULN2002A) has been used rather than discrete components for space saving reasons. The two inverters IC4C and IC4F which form part of switches S1 and S2 have been connected in such a way so that when the microcontroller comes out of reset the gain is set to times 100 so that no amplifier outputs are connected together. Again, capacitive coupling (C3) is used at this stage, which eliminates the DC component of the signal.

### 3.2.5 Phase sensitive detector (PSD)

This stage consists of the inverting amplifier IC6, the analog switches IC5A and IC5C and the low pass filter R12-C4. A phase sensitive detector is a circuit with two inputs: one is the signal input  $E_s \cos(\omega t + \theta)$  and the other is the reference input  $E_r \cos \omega t$ . The output has the mean value

$$V_o = 2 \frac{E_s}{\pi} \cos \theta \quad (3.2.1)$$

When  $\theta = 0^\circ$  the PSD operation is the same as that of a precision full wave rectifier and the output is

$$V_o = 2 \frac{E_s}{\pi} \quad (3.2.2)$$

Because of the  $\cos \theta$  factor in equation 3.2.1 the PSD is insensitive to small variations of the phase angle around the ideal of  $0^\circ$ , effectively acting as an ideal full wave rectifier. Signals whose phase is equal to  $90^\circ$  are completely rejected.

When the input signals do not have exactly the same frequency as the

reference signal the long term average tends to zero. Therefore the PSD acts also as a narrow band pass tracking filter with very good noise rejection. The bandwidth is set by the output low pass filter section R12-C4 and can be shown to be equal to  $1/(\pi R12 C4)$ , centered around the frequency of the reference signal.

The reference signals in the present application is derived from the sinusoidal oscillator and is a square wave with levels VSS and VDD, driving the analog switches IC5A and IC5C. It should be noted that there are also pass bands at the odd harmonics of the operating frequency as these are present in the reference signal.

The two reference signals are used as follows:

- One for the measurement of the oscillator amplitude, provided by the comparator IC9A. The high pass filter C20-R40 balances the phase shift introduced by the high pass filter section formed by C3 and R9.
- A second for the measurement of conductivity provided by the comparator IC9B. The high pass filter C9-R19 balances the phase shift of the sensor output signal and all shifts introduced by the amplification stages. It is clear that if R19 is replaced by a variable resistor, it can be used to compensate for variable cable resistances since, as shown in chapter 2, the resistance of the cable affects significantly the phase of the sensor output current. The first amplification stage could be located within the probe to avoid cable and connector resistance effects. However this involves the possible exposure of the amplifier circuitry to high temperatures; in addition, more supply lines should be incorporated in the connecting cable.

The operational amplifier employed at the inverting part of the phase sensitive detector is an OP37. It was chosen for its low noise and very small input offset voltage. Since the auto ranging algorithm (discussed in chapter 4) keeps the input of the phase sensitive detector at about 0.28 to 2.8  $V_{pp}$ , an output offset of around 0.4mV can be considered insignificant.

The resistor networks R44-R45 and R42-R43 provide some hysteresis for the comparators IC9B and IC9A to avoid any oscillation problems.

The analog switches IC5A and IC5C are controlled by the reference signals in such a way that the rectified signal is negative with respect to the analog ground. This is necessary for the correct operation of the voltage level shifting stage described below.

The above mentioned reference signals are selected by the analog switches IC7B and IC7C, which are operated under program control.

Finally, the time constant for the low pass filter R12-C4 is 10ms, much larger than the period of the measured signals (0.067ms).

### 3.2.6 Voltage limiter

The signal, now converted to a proportional negative with respect to the analog ground DC voltage passes through a voltage limiter (voltage clamp). The latter consists of the diode D2 and resistors R46 and R47.

Addition of this stage has proved to be necessary, to eliminate the following problem :

Suppose the circuit measures conductivity in the lowest range ( $\times 100$ ), and conductivity rises sharply to a level extending to an upper range. The range selection algorithm still keeps the amplification to  $\times 100$ , causing the amplitude of the signal to reach the supply voltages. Distortion of the signal then follows, but even if this does not occur, the voltage level shifter will saturate as its output range is limited (it starts saturating when the input signal exceeds about 1.1V). A false signal is then read by the voltage to frequency converter and eventually by the microcontroller; the latter adjusts then the range according to the false reading, and the system locks up at some incorrect conductivity value. In most cases the system ends up locked at some value in the  $\times 10$  range; the saturation voltage is too small to cause lock up in the  $\times 1$  range. The only way to exit this situation is then either to reset the microcontroller so that the range can be re-established during the initialisation section of the program or to reduce the conductivity reading (by taking the conductivity probe out of the solution) provided that this lock up condition has been noticed. Although the system is supposed to be used in a slowly changing

conductivity environment compared with microcontroller speeds, the above mentioned lock up situation can occur even when the system is on and the probe suddenly immersed in a highly conductive solution.

In this application reference for the voltage limiter is provided by the voltage divider R46-R47. As can be seen from figure 3.2, the limiting voltage is set to about -1.1V with respect to the analog ground. The requirement for this circuit is that the Thevenin equivalent of the reference network is much smaller than the series resistance (R12).

### 3.2.7 Voltage level shifter

This consists of IC10C, R20, R22 and Q2. The function of this stage is to convert the negative-with-respect-to analog ground conductivity/temperature signal, to a signal of proportional magnitude, but referred to the digital ground (VSS), so that it can be further used by the voltage-to-frequency converter.

This stage operates as follows: The inverting and non inverting inputs of the operational amplifier IC10C are considered to be essentially at the same voltage level, that is the conductivity/temperature DC voltage. Since this voltage is negative with respect to the analog ground a current will flow through resistor R20. A current of nearly equal value then passes through resistor R22 thus generating a voltage at the collector of Q2. It is obvious that the voltage at the output of the level shifter has 2.2 times the magnitude of that at the input of this stage, if 10 and 22K resistors are used for R20 and R22 respectively. This gives a maximum conductivity voltage not exceeding 2V with respect to the digital ground (VSS). In order that the currents through resistors R20 and R22 are of the same magnitude, the large signal current gain of the transistor must be as close to unity as possible. A transistor of the type BC179 has been chosen, with an  $h_{FE}$  between 140 and 900.

The input of the voltage level shifter can be either conductivity/oscillator amplitude signal or temperature signal, corresponding to the temperature of the solution. The two different input signals are selected by means of the

switches IC7A and IC7D, which are operated under program control.

### 3.2.8 The temperature measurement circuit

This is built around a voltage reference (Z1) of -1.23V with respect to the analog ground. This voltage is the input to the non-inverting amplifier IC10A. The feedback resistor of the amplifier IC10A is a temperature dependent platinum wire resistor (type Pt 1000) mounted on the probe, with a temperature coefficient of  $3.85\Omega/^{\circ}\text{C}$  and a resistance of  $1000\Omega$  at  $0^{\circ}\text{C}$ . With this configuration the output voltage of IC10A ranges from -2.460 to -2.934V with respect to the analog ground, for a range of temperatures 0 to  $100^{\circ}\text{C}$ . These voltages cannot be used directly by the voltage level shifter as they would cause it to saturate. The voltage divider R29-R30 reduces the respective range to about -0.812 to -0.968V.

The operational amplifier used for the temperature measurement circuit is of the type OP490G, a very low power circuit which draws only 0.080mA (maximum) per amplifier. The maximum offset voltage of these amplifiers varies from 0.5 to 1 mV according to the version; a better version obviously achieves more accurate temperature measurement should it be needed. The fourth amplifier of the package is used for the voltage level shifter (IC10C).

In order that the magnitude of the voltage reference is measured, another line between this and the voltage divider R29-R30 is included. Switches IC12A and IC12B are controlled by the same line determining the type of signal (ie oscillator amplitude or conductivity) at the input of the PSD. As will be shown in chapter 4, the operation

$$\frac{N_{TEMP}}{N_{REF}} - 2 \quad (3.2.3)$$

where  $N_{TEMP}$  and  $N_{REF}$  are the number of pulses corresponding to temperature and voltage reference signals, should give a rate of change same as that of the temperature sensor and a result of 0 for a temperature of  $0^{\circ}\text{C}$ . This equation will be implemented in the final temperature derivation section of the microcontroller

software (section 4.5.5).

### 3.2.9 Voltage to frequency (V/F) converter

This consists of IC11 (LM331) with some additional gain setting external resistors and capacitors. Its output is a TTL level (VSS to VCC) pulse train of frequency proportional to the applied input voltage.

Referring to figure 3.2, the output frequency is:

$$f_{out} = \frac{V_i}{2.09} \frac{R37 + R_{RV1}}{R24} \frac{1}{R23 C11} \quad (3.2.4)$$

where the input voltage  $V_i$  is measured in Volts. In this application the V/F converter is adjusted to give a maximum frequency of about 20KHz for an input voltage in the area of 2V DC. The maximum output frequency has been selected to reduce linearity error at high frequencies. Care has been taken so that all ancillary components are stable, with low temperature coefficients. RV1 is used to compensate for component tolerances. As will be shown in chapter 4, exact value of the slope of the V/F characteristic is unimportant, since ratiometric measurements are performed. Another possibility is to find an acceptable value for the combination R37-RV1 and then replace it with a fixed value resistor, thus making calibration of the system purely a matter of software. This could be an improvement if the meter is to be used in a harsh environment. The pulse train from the V/F converter, is finally received by the pulse accumulator of the microcontroller for further processing.

### 3.2.10 Oscillator amplitude measurement

As has been shown in chapter 2 (equation 2.3.20), the sensor output current is proportional to the amplitude of the source in the drive coil circuit. This amplitude can vary as a result of component tolerances aging and temperature variations. Therefore if this amplitude is measured at regular intervals, ratiometric measurements (ie conductivity value derived from the ratio of conductivity to

oscillator amplitude signal) can be performed, leading to elimination of the above influences in the final conductivity measurement.

A resistor network R48/R49 divides the oscillator amplitude by 2 and the resulting signal is fed directly to the phase sensitive detector through the buffer IC8A. Amplitude division is necessary as a mere  $3V_{pp}$  causes the input signal to the V/F converter to exceed the 2V DC limit. However if voltage division is used, signals of 2 to  $4V_{pp}$  can easily be accommodated.

### 3.2.11 Error considerations in the analog circuit

As mentioned in the previous section oscillator amplitude measurements provide a way of eliminating several errors in the conductivity measurements. As seen in figure 3.2, the oscillator amplitude signal and conductivity signal follow the same path after the range selection stage. Therefore any influences to subsequent stages up to the microcontroller would have the same effect on the conductivity and oscillator amplitude signals and would not affect the conductivity to oscillator amplitude ratio. It follows that if errors are to be calculated in the conductivity measurement circuit, only the errors in the voltage divider R48/R49, the current-to-voltage converter and the amplification stages need to be calculated. Taking also into account that the signals involved are AC and capacitors are used at the end of each stage to remove the DC components, we conclude that only component errors have to be considered.

In the case of the voltage divider R48/R49 the worst case error occurs when the errors in R48 and R49 have opposite signs. For 1% resistors the worst case error is 1%. For the current-to-voltage converter the error in the feedback resistor (R2) is taken as the error of this stage (1%). For each of the  $\times 10$  amplification stages, the worst case error occurs when the errors in the resistors of the gain network (R5/R4 or R8/R7) have opposite signs, and in that case it is 1.8% for each stage.

When the circuit is in the  $\times 1$  range the final value of conductivity depends on the ratio of the current-to-voltage converter gain and that of the voltage divider R48/R49. Therefore the worst case error in this case occurs when the errors in



the individual stages take opposite signs and amounts to 2%.

In the  $\times 10$  range the error of one amplification stage is added. The worst case error occurs when the error in the voltage divider R48/R49 takes opposite sign to those of the current-to-voltage converter and amplification stage. It is then 3.8% of the measurement.

In a similar manner when the circuit is in the  $\times 100$  range maximum error occurs when the error in the voltage divider takes opposite sign to those of all the other stages considered, and is calculated as 5.6%.

In the case of the temperature measurement circuit it can be seen in figure 3.2 that the voltage reference signal follows the same path as the temperature signal after the voltage divider stage R29/R30. Therefore for a ratiometric measurement taking into account the value of the reference voltage (equation 3.2.3) the errors to be considered are those introduced by the amplification stage IC10A. This measurement is performed using DC signal therefore the offset voltages of the amplifier IC10A have to be taken into account in addition to component errors.

For an amplifier of the type OP490G the maximum input offset voltage over the operating temperature range ( $-40$  to  $+85^{\circ}\text{C}$ ) is 1.5mV, and the input bias current 25nA. The input bias current causes an output offset voltage between 0.025 and 0.035mV for the range of temperatures measured and can be considered insignificant compared to the range of output voltages. The output offset voltage due to the input offset voltage varies according to the measured temperature from 3 to 3.58 mV.

The worst case error in gain for the amplifier feedback network is not exceeding 1.2% if R28 is a 1% tolerance resistor and the error in the Pt1000 sensor is specified as 1% maximum in the 0 to  $100^{\circ}\text{C}$  range. Therefore, assuming again same sign for the errors in gain and output offset voltages, the worst case fractional error in the output of IC10A can be calculated as 1.3% over the temperature range, with the maximum values near the  $0^{\circ}\text{C}$  measurement.

The digitisation error (ie the  $\pm 1$  count ambiguity at the measurement of the V/F converter pulses over a fixed time interval) must also be considered.

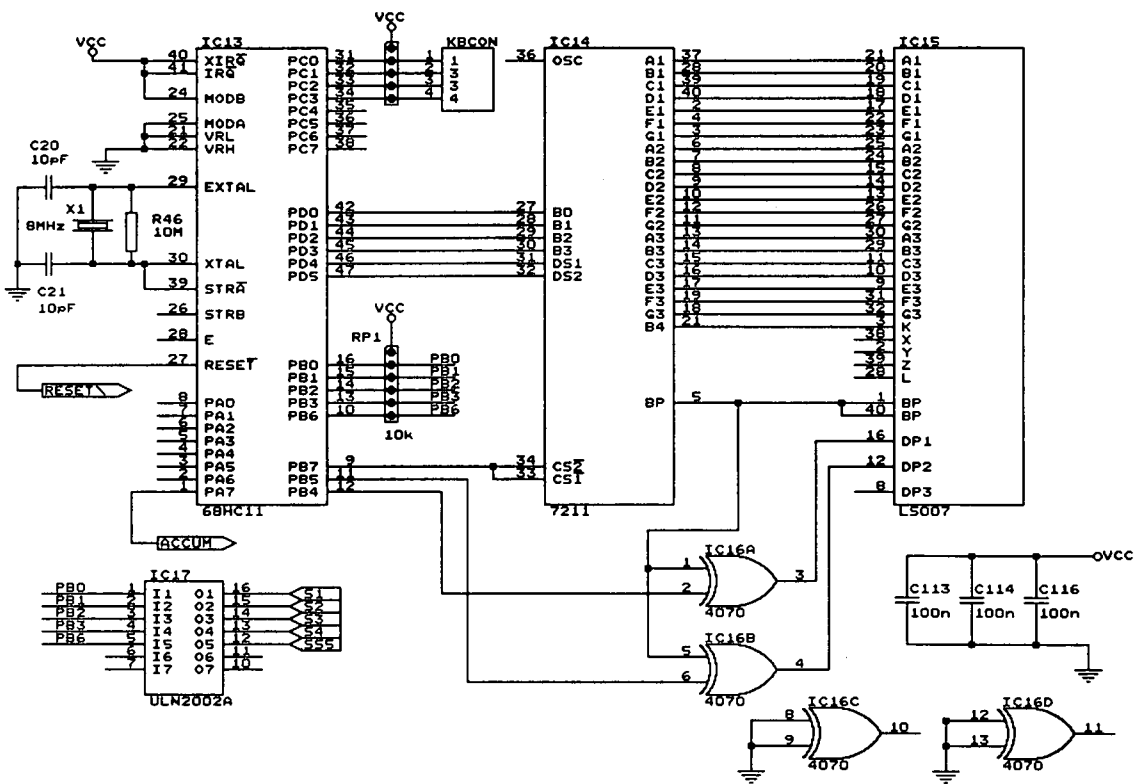


Figure 3.3 The digital part of the conductivity meter

In the case of conductivity it ranges from 0.37 to 0.089% (worst case fractional error) over an 163.84ms interval for the conductivity to oscillator amplitude ratio for the end values of each of the three ranges.

In the case of temperature measurement the number of pulses measured is greater so the  $\pm 1$  count error for the temperature to voltage reference signal gives a worst case fractional error from 0.093 to 0.096% for the end values of the temperature measurement range. Clearly these values are insignificant compared to the gain and offset errors in the temperature measurement circuit.

It can be seen that in the above error calculations always fractional error (ie  $|\Delta M|/M$  where  $M$  is the measured quantity) and the worst case has been considered, that is the signs of the individual contributions such that they add instead of cancelling; in practice it is quite possible that errors cancel each other, resulting in a much smaller value for the overall error of the system.

### 3.3 The digital circuit

This part of the system is much simpler and straightforward than the analog one. A schematic diagram can be seen in figure 3.3. It consists of the microcontroller, the display driver, the display and some additional digital circuits.

#### 3.3.1 The microcontroller

IC13 is the microcontroller, a Motorola 68HC811A8 device. The version selected has 8K of EEPROM rather than the ROM of the 68HC11A8. This version, though more expensive, was chosen for the ease of program updating, calibration parameter changing and it also gives added flexibility in chemical curve data location, alteration or addition. Besides it is far better suited for small volume production. The microcontroller is hardwired for single chip operation, by grounding the MODA and MODB pins. All these aspects will be discussed in more detail in chapter 4.

#### 3.3.2 The display driver

IC14 is the display driver, a CMOS 7211AM device. The data lines of this

chip are connected to an output port pins rather than the system data bus. The latter would be more preferable since it would place the display driver in the address space of the microcontroller, thus making the port pins available for control purposes. However, as the microcontroller operates in single chip mode in order to save space and power, address and data lines are not brought out of the chip.

### **3.3.3 The display**

IC15 is a standard 3 1/2 digit liquid crystal display. The 7211 device can only produce output codes to drive digits, therefore external EX-OR gates had to be provided to drive the decimal points on the display (IC16A and IC16B); they are driven directly by the microcontroller.

### **3.3.4 The keyboard**

KBCON is an arrangement of push-button switches and resistors which constitute the keyboard of the system. The actual arrangement will be shown in chapter 4, where the key debouncing algorithm is presented and explained.

ULN2002A is the transistor array used to transform VSS to VCC (TTL) level switch control signals from the microcontroller to VSS or VDD signals respectively.

# CHAPTER 4

## THE SOFTWARE PART OF THE CONDUCTIVITY METER

### 4.1 Introduction

This chapter describes the software written into the microcontroller; its role is to control the analog interface so that the desired quantities are measured at specified times, the collected data is processed and then sent to the display according to the user's demand.

The language used was standard Motorola assembly. It was preferred to a high level language (a C compiler was available) because it offers better control of on chip devices, well defined and controllable routine execution times and finally reduced program space.

Before any program sections are discussed, the microcontroller resources associated with this work must be shown, so that understanding of the former becomes more complete. The names of devices and registers in this chapter are the same as used in Motorola's MC68HC11 reference manual [31].

### 4.2 The MC68HC11 - a brief overview

The MC68HC11 is a microprocessor with several other peripheral devices incorporated in a single chip. There is RAM, ROM, EEPROM, and I/O devices like serial and parallel ports, even an analog to digital converter in some versions. It has a 16 bit address bus, therefore it has a 64K address space and an 8 bit data bus. It can operate in either single chip mode, in which case the address and data bus are not brought out of the chip, or in expanded mode, where the (multiplexed) address and data bus become available to the user, at the expense of two parallel ports, which however can be recovered with the addition



REG3-REG0 are the highest order hex digits of the first address location of the RAM and registers respectively. The INIT register is placed at location \$103D initially on reset and can only be altered during the first 64 cycles after reset. This mechanism ensures that the position of RAM and registers cannot be changed accidentally during program execution due to software error.

In the present application RAM and registers have been placed within the first 256 bytes of the memory map (\$0000 to \$00FF) with the registers occupying the locations \$0000 to \$003F, leaving 192 bytes for the stack and variables. If registers are placed in the locations mentioned above, then their individual bits can be acted upon by the bit manipulating instructions using their direct addressing mode. This is a very useful feature as individual bits of these registers are intensively used throughout the program. Also, if RAM variables are placed within the base of the address space, the instructions that use the direct addressing mode assume that the upper eight bits of the address are 0s; therefore these instructions take less program space, and operate faster than the equivalent ones using extended addressing mode. The same can be said for the reading or writing to the memory mapped registers (usually the case of using the parallel ports). In the environment of this application with so frequent references to RAM variables and registers, both of the above mentioned features offer considerable program space and time savings.

After the above discussion, the memory map of the system is formed as seen in figure 4.1.

#### **4.2.2 Resets and interrupts**

In the 68HC11, every possible source of interrupt has a unique vector. All on chip peripheral systems can generate individual maskable interrupts, under certain conditions which can only be recognised if the global mask interrupt bit in the condition code register is clear. There are also non maskable interrupts like reset and others associated with software safety mechanisms which are not used in the present work, therefore they need not be discussed.

For each source of interrupt there is a -local- flag bit to indicate that service

is required and an interrupt enable bit that enables the flag to generate a hardware interrupt request. Therefore it is up to the programmer to define which sources will generate interrupts and which can be handled by periodic polling. The former scheme is used with the timer and pulse accumulator, as will be shown later.

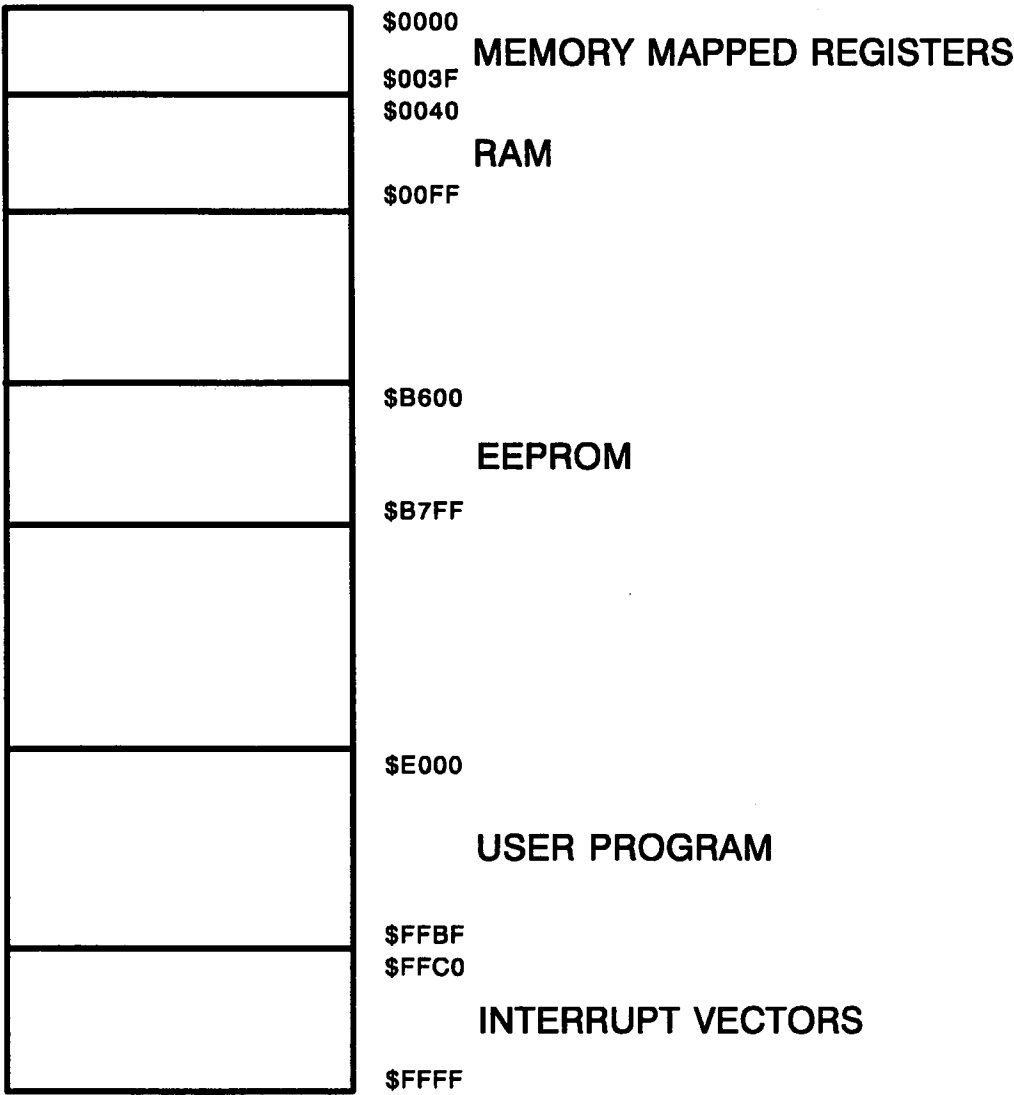


Figure 4.1 System memory map

The interrupts are classified according to priority of service; for example a real time interrupt has higher priority than a pulse accumulator interrupt.



However the user can elevate any of the maskable interrupts to the highest (maskable) priority by appropriate programming of the HPRIO register. The program developed does not change the priorities as the system works satisfactorily and it is easier to understand provided that the interrupt service routines are kept within certain time limits, which will be explained in one of the following sections (section 4.4).

Once an interrupt service routine starts, other interrupts cannot be serviced before the end of the current one and therefore become pending, irrespective of their priority. The CPU however sorts the pending interrupts according to their priority. This scheme indicates that all interrupt service routines should be kept as short as possible.

After reset or power on, the program counter is loaded with the contents of locations \$FFFE-\$FFFF therefore program execution starts from that address. In the present application these locations contain \$E000, the start of the on chip program memory area.

#### **4.2.3 Real time interrupts and the pulse accumulator system**

The 68HC11 operates with an 8MHz crystal oscillator. This frequency is divided by 4 to the internal PHASE 2 (PH2) clock and the external E clock. All operations inside and outside the CPU are referenced to these two clocks which have 90° phase difference. For the rest of the discussion it is assumed that the clock rate is 2MHz (500ns period).

The heart of the main timer system in the CPU is a 16 bit free running counter. It starts from \$0000 after reset and then counts up continuously. When it reaches \$FFFF it rolls over to \$0000, sets an overflow flag and carries on counting. As long as the microcontroller runs in the normal operating mode there is no way to interrupt, reset or alter in any way the value of the counter. However the counter can be read at any time to provide time reference.

The clocking rate of the counter-timer can be any of the four available programmable rates (1, 4, 8 and 16). A rate of 1 has been selected therefore there is an overflow after 65,536 counts, or 32.768 ms. The prescale value is

selected by programming the bits PR0 and PR1 of TMSK2 in figure 4.2.

The real time interrupt (RTI) function of the MC68HC11 can be used to generate hardware interrupts at a fixed periodic rate. There are four different RTI rates available. These are a function of the bus frequency (E clock) and the value of the programmable bits PTR1 and RTR0 of PACTL register in figure 4.2. In this application these bits are programmed to have both the value of 1 resulting in an interrupt rate request of 32.768 ms. As will be shown later, this rate is the base of the software part of the meter as it defines the duration of the measuring intervals and synchronises all the tasks performed by the CPU. The local flag set at the end of each RTI period is the RTIF bit in TFLG2 and the interrupt mask bit is the RTII in TMSK2; when the latter is 0, then interrupts are inhibited and the RTI system can operate in polled mode.

DDRA7	PAEN	PAMOD	PEDGE	0	0	RTR1	RTR0	PACTL (\$0026)
0	0	0	0	0	0	0	0	RESET

TOI	RTII	PAOVI	PAII	0	0	PR1	PR0	TMSK2 (\$0024)
0	0	0	0	0	0	0	0	RESET

TOF	RTIF	PAOVF	PAIF	0	0	0	0	TFLG2 (\$0025)
0	0	0	0	0	0	0	0	RESET

X	X	X	X	X	X	X	X	PACNT (\$0027)
-	-	-	-	-	-	-	-	RESET

Figure 4.2 Main timer system related registers

The pulse accumulator is an 8 bit counter system, which can be configured in gated time accumulation mode, or event counting mode. The latter mode of

operation is employed in the system developed to measure the number of pulses produced by the V/F converter over a fixed period of time. The output of the V/F converter is connected to bit 7 of PORT A which in this case serves as a clock trigger for the pulse counter. Normally this is configured as input by writing a 0 in DDRA7 bit of PACTL. The mode of operation is selected through the PAMOD bit of PACTL; a 0 written in this bit puts the system in the event counting mode.

Configuration and operation of the pulse accumulator system can be fully controlled by the user program. The system can be enabled or disabled at any time by writing an 1 or a 0 respectively to the PAEN bit of PACTL register. The event counter starts running then, until it overflows. Upon overflow, the PAOVF status bit is set to 1 and if interrupts are enabled (by writing an 1 in PAOVI bit of TMSK2), a hardware interrupt request is generated. In the present application the interrupt service routine consists of nothing but an increment of a RAM variable (named OVNO in the program), since PACNT is only 8 bits wide, an insufficient quantity for the number of pulses which have to be collected. The end result is a 16 bit number which consists of OVNO (upper byte) and PACNT (lower byte). The option of triggering the counter with rising or falling edge of the input signal (bit PEDGE of PACTL) is of no importance since we are only interested in the number of pulses and not the edges.

### **4.3 The program timing**

The main requirement from the meter as far as timing is concerned, was the update of the display for every quantity required two and a half times per second. This is an acceptable rate for the human eye, and is used in many instrument designs. Therefore all the necessary data collection, processing and display update should be completed within cycles of duration around 400ms each.

If the RTI system is configured to generate a hardware interrupt every 32.768ms as discussed in the previous section, then this time interval can

form the basic element of the system's timing: twelve of these intervals can compose a single measurement cycle of duration 393.22ms, during which all necessary tasks can take place, and is managed by the RTI service routine. Then one cycle can follow another, thus providing continuous measurements. In addition, each of the 32.768ms intervals is given a unique identity number within the measurement cycle, providing in this way a time reference for the various tasks to be performed. Therefore the workload of the RTI service routine can be spread evenly over the available time, since this is the very routine that manages nearly every task performed by the system after the end of initialisation.

#### **4.4 General structure of the software**

The software contains of an initialisation section during which on chip devices are initialised, algorithms are set to their initial states, global variables are given their initial values and interrupts are enabled. Some initial measurements need also to be performed. One is a measurement of the oscillator amplitude so that a value is available when the first Real Time Interrupt occurs. A second and very important measurement for the operation of the system is a conductivity measurement with the probe assumed out of the solution; this measurement yields a value for the offset in the measurement, ie stray signal induced in the pick up coil in the absense of a conductive loop linking the two coils. This signal comes from magnetic flux escaping from the drive coil due to inhomogenous ferromagnetic core material and non uniformly wound coils, as well as capacitive coupling of the two coils. In the present application the sensor used does not employ the winding techniques applied by several researchers [21], [22], [28], therefore significant stray coupling is expected, despite the use of copper shields. The value of the measured stray signal is stored in a RAM variable and subtracted from subsequent conductivity measurements. After completion of all these tasks control of the system is left to the real time and pulse accumulator overflow interrupt service routines.

A flowchart showing the structure of the initialisation section can be seen in figure 4.3. The flowchart of figure 4.4 shows the structure of the Real Time

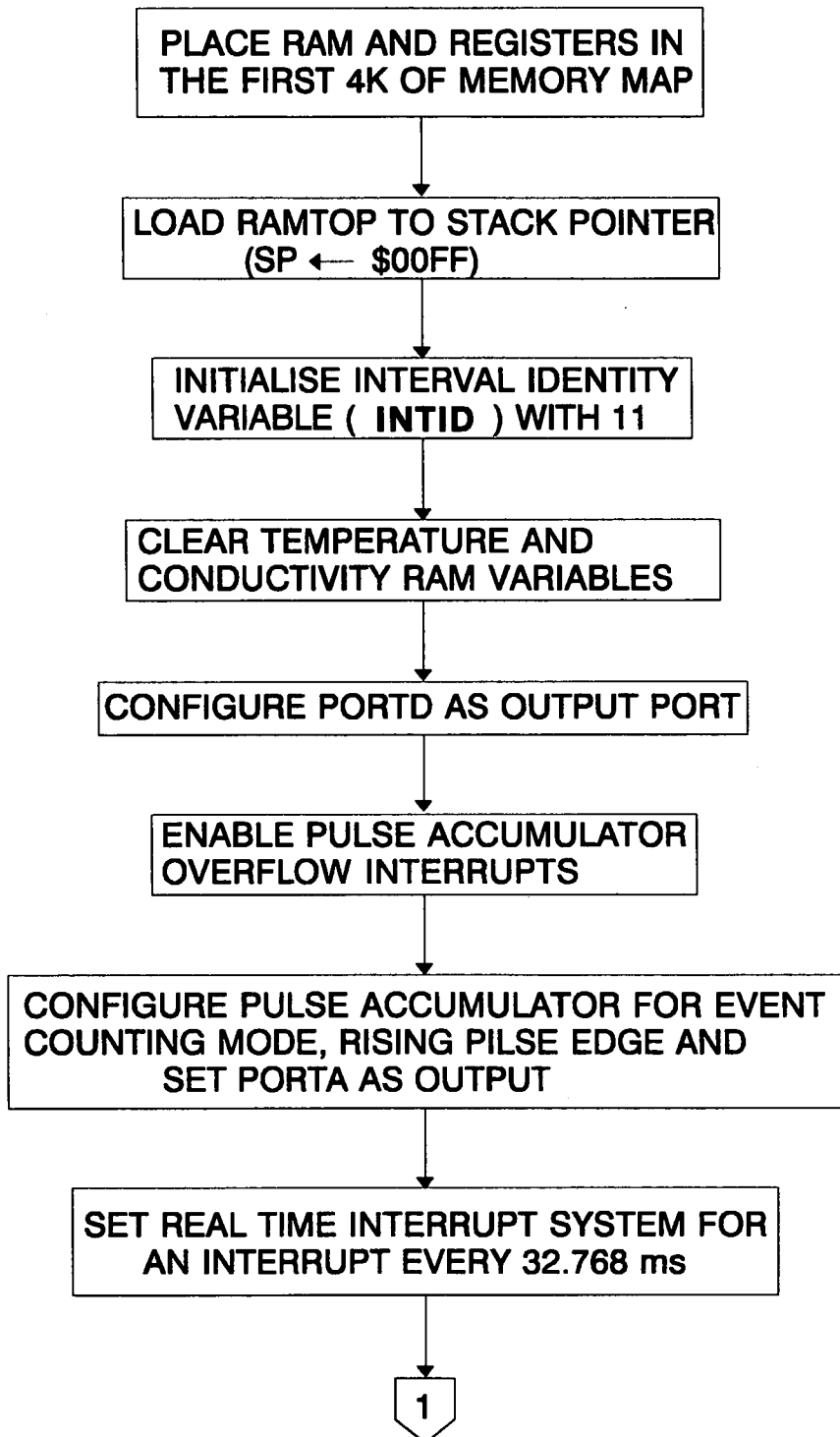


Figure 4.3 Initialisation section

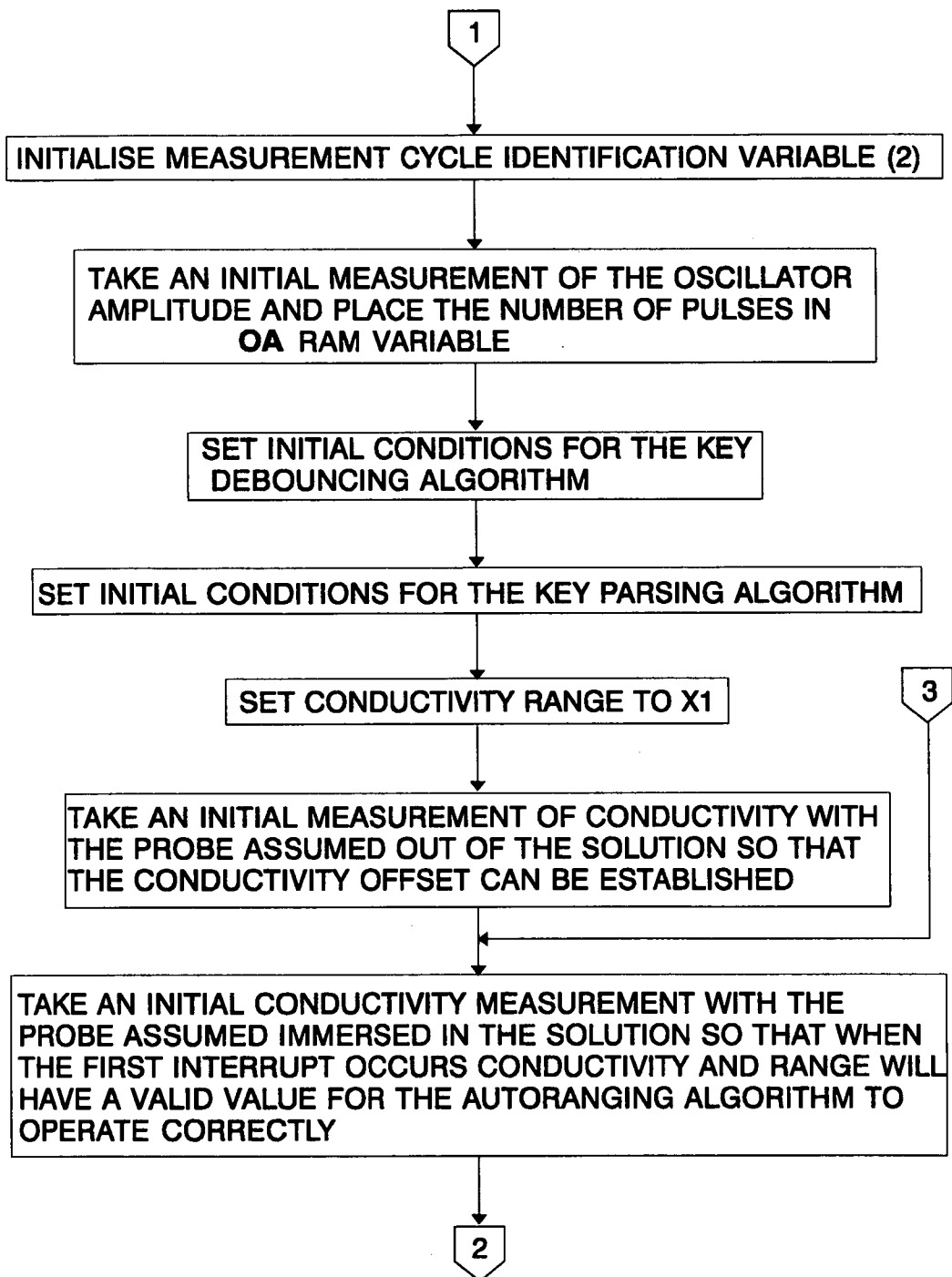


Figure 4.3 (Continued)

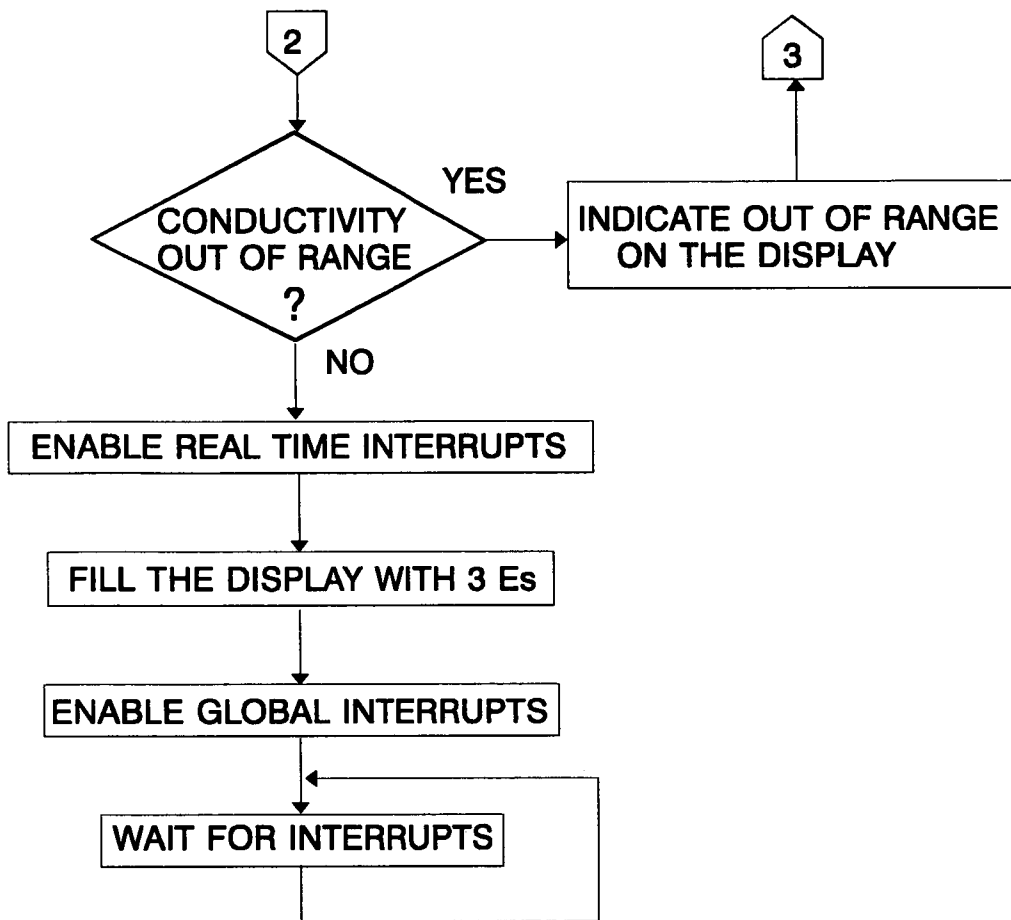


Figure 4.3 (Continued)

Interrupt service routine (named SYNC\_ISR in the program). The INTID RAM variable holds the number that identifies each of the 32.768ms intervals within each measurement cycle; its values range from 11 to 0, updated at the end of each 32.768ms interval. The role of another RAM variable must be explained here too; the OSMC variable is used to identify each of the measurement cycles. It takes the values 9 to 0 and is updated at the end of each measurement cycle. Every 10th cycle the conductivity and temperature measurement intervals are used to measure the oscillator amplitude and value of temperature reference (Z1) respectively, by setting the appropriate value to the SS5 signal (figure 3.2).

As can be seen from the flowchart of figure 4.4, temperature is measured during intervals #10 through to #6 (inclusive) and conductivity during intervals

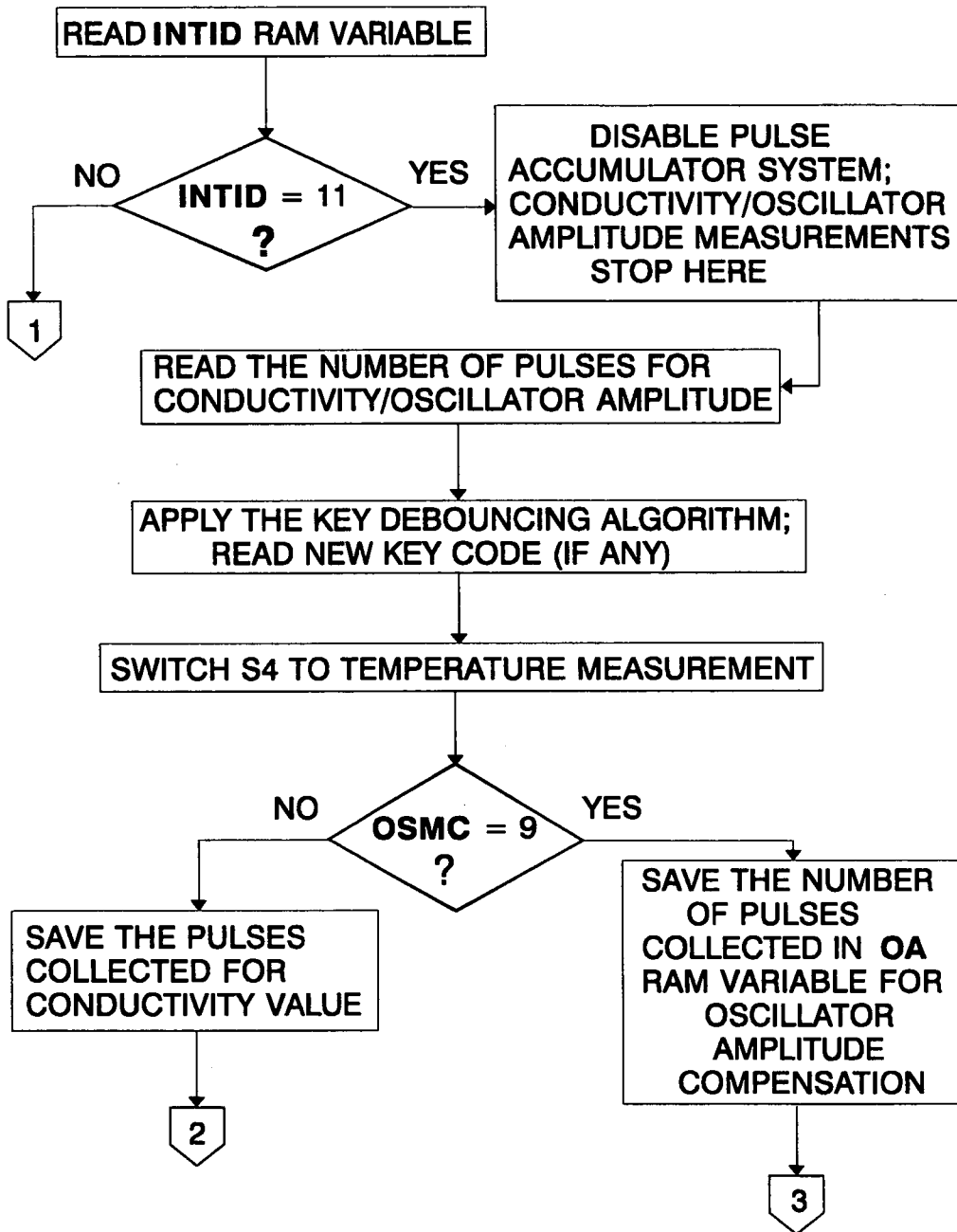


Figure 4.4 Real time interrupt service routine



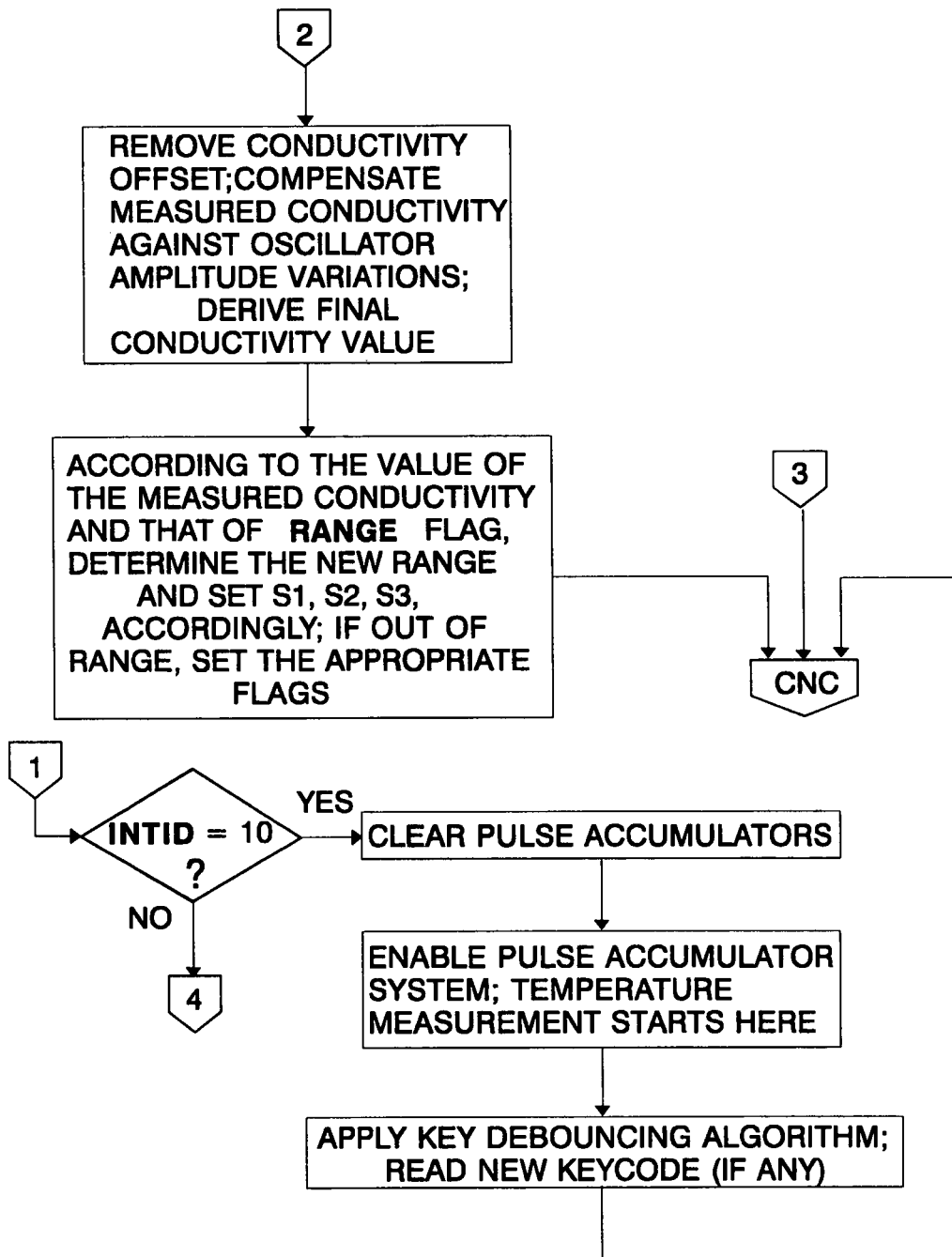


Figure 4.4 (continued)

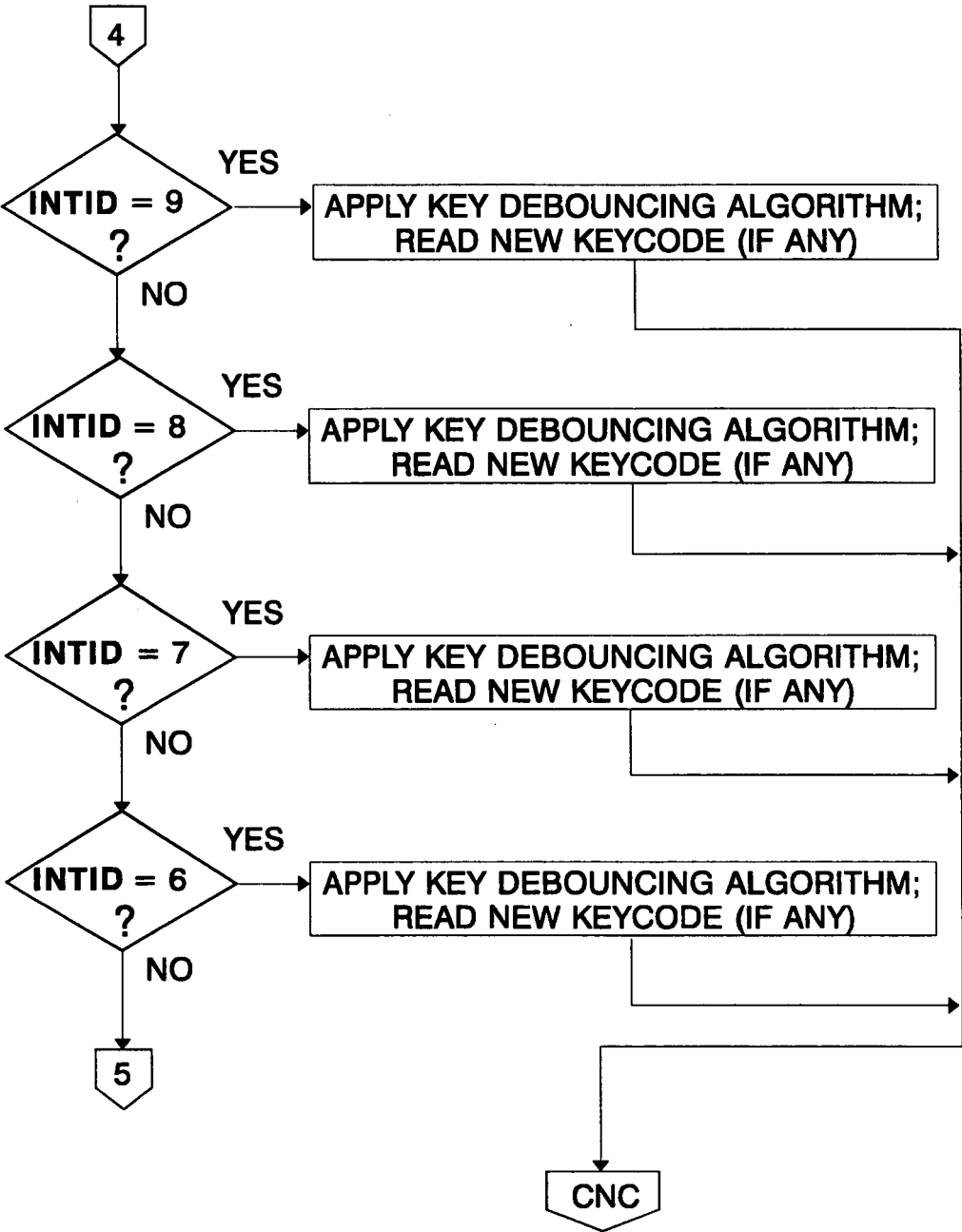


Figure 4.4 (Continued)

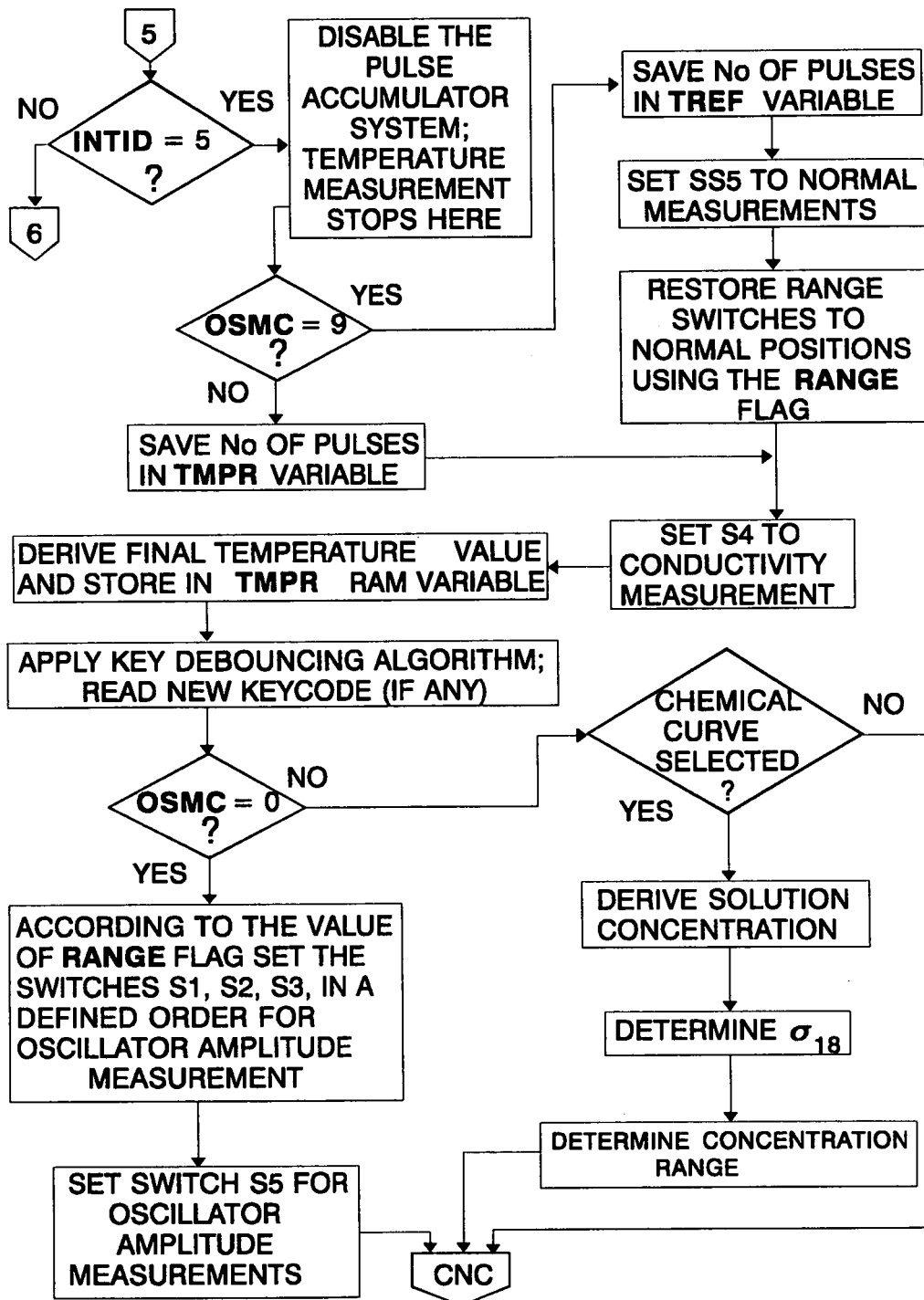


Figure 4.4 (continued)

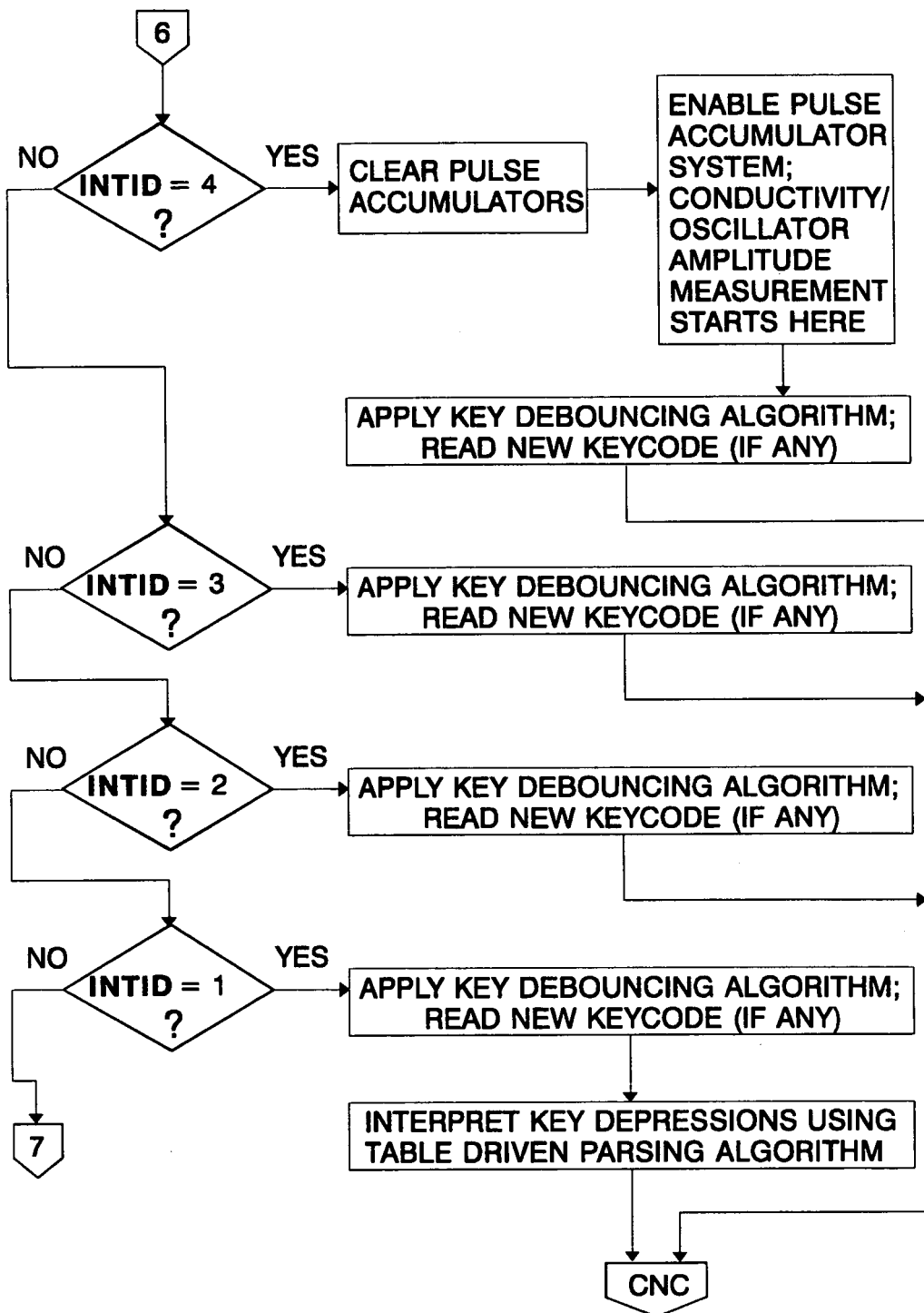


Figure 4.4 (Continued)

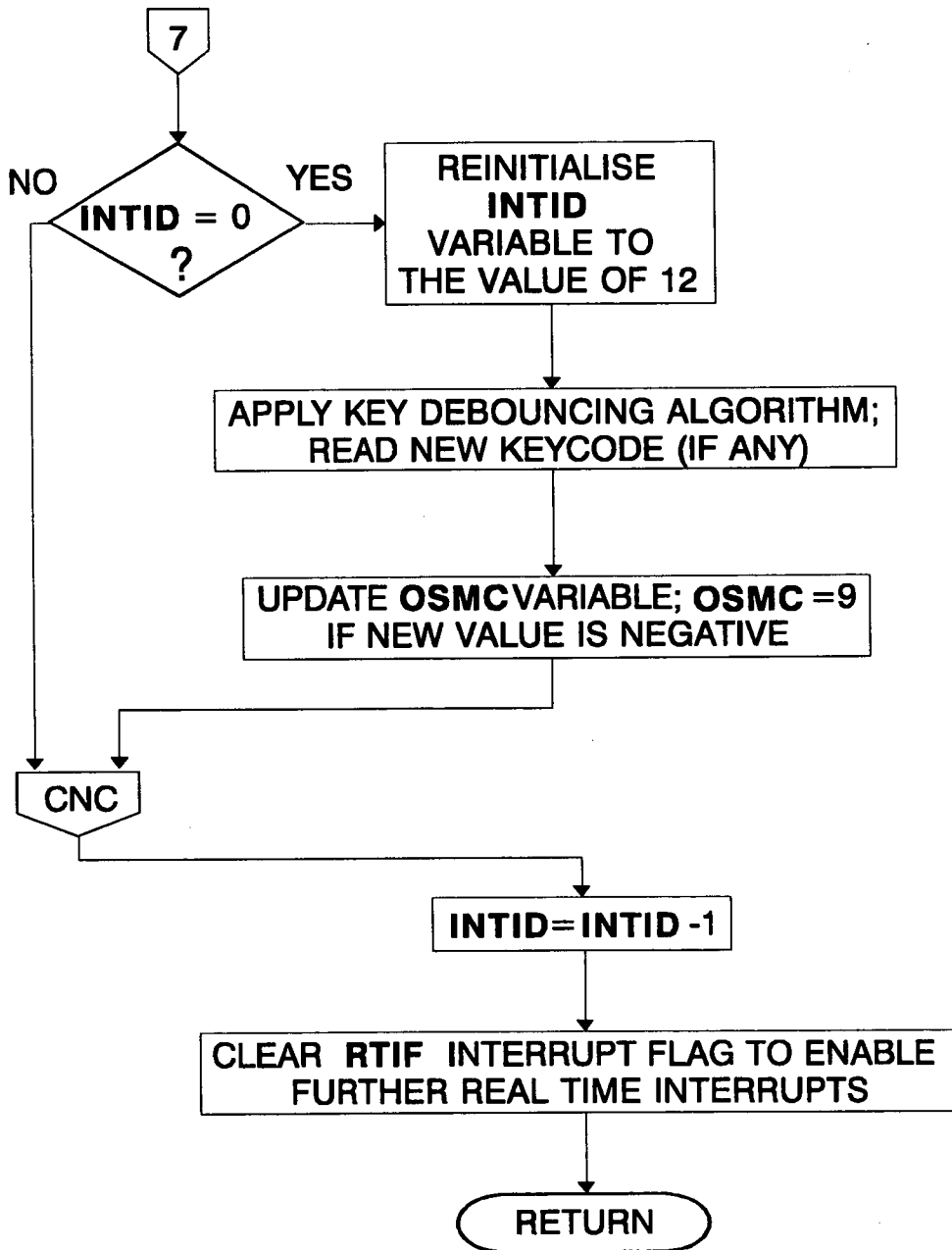


Figure 4.4 (continued)

#4 through to #0 (inclusive). The duration of all measurements is about 163.84ms and the same time interval is used for the measurements during the initialisation section, so that the same methods of data processing and the same conversion factors are used. In figure 4.4 S1, S2, S3, S4 and S5 denote the

control signal to the respective analog switches used in the circuit of figure 3.2.

It can be seen in figure 4.4 that SYNC\_ISR involves routines that by microcontroller timing standards can have considerable length (ie in the order of ms). Considering the interrupt latency scheme employed in the 68HC11 described in section 4.2.2, the maximum permissible length of SYNC\_ISR can be determined in order that measurements are performed correctly, as follows:

Suppose that the pulse accumulator system requests service immediately after the real time interrupt service routine starts. The former interrupt cannot be serviced before the end of SYNC\_ISR. The maximum length of this routine is determined by the time it takes the pulse accumulator to overflow and therefore cause a request for service. If the maximum frequency of the V/F converter is assumed to be around 22KHz, this corresponds to about 3604 pulses per measuring interval of 163.84ms, therefore each overflow of the pulse accumulator corresponds to about 11.7ms. In the actual program SYNC\_ISR is never longer than 9ms. This time limit however long it might seem, can easily be exceeded when multiplication and division routines are extensively used. Enabling overflow interrupts within the SYNC\_ISR service routine has been avoided since it may upset the accurate timing set by the real time interrupt system and lead to accuracy loss of the measured quantities.

The flowchart for the pulse accumulator overflow interrupt service routine (named OVR\_ISR in the program), can be seen in figure 4.5.

#### **4.5 The subroutines of the program**

This section describes the various subroutines written as part of the program; also the various program sections forming part or whole tasks performed within each of the 32.768ms intervals are discussed too. Subroutines performing similar or closely related tasks will be discussed together. Also, subroutines used extensively by program sections within the 32.768ms intervals will be discussed with the latter. All program sections and subroutines dealing with measured conductivity and temperature data and processing it, have used integer arithmetic in a way that overcomes the limited

number range of 16 bits (unsigned) available on the 68HC11. Most numbers the program deals with are positive; when negative numbers have to be used, the sign is stored in another RAM variable. Besides, when the results of various operations are expected to be out of range, the numbers are broken into smaller parts and stored temporarily in separate RAM variables, so that no rollover with consequent loss of accuracy occurs. At first sight, this approach leads to some unjustified at a first look complexity of the program. An alternative method could be the development of full 32bit arithmetic routines (a 16x16 bit multiplication routine has already been written and used extensively in the program, though only the 16 lower bits of the result are used), although they would be considerably slower (especially a 32bit division routine) and could exceed the time limits within the measuring intervals if used extensively.

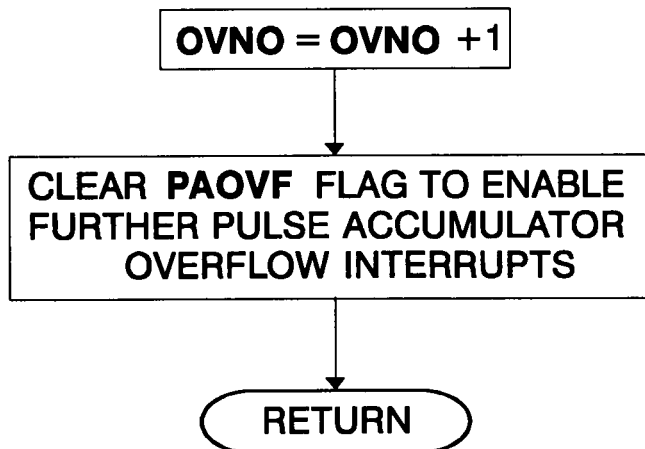


Figure 4.5 Pulse accumulator overflow interrupt service routine

#### 4.5.1 The keyboard handling routines

Two subroutines have been written to handle the keyboard; the first (called KBDBC in the program) provides debouncing for the switches of the keyboard and the second reads the keyboard and returns a code for each of the keys when pressed, as well as status information.

Mechanical keyswitches have key bounce associated with them; when a key is pressed, it usually exhibits open, closure, open, closure, and so on, before settling to a steady closed state. Usually the keyswitches' bouncing time does not exceed 10ms. Therefore if a keyswitch is examined at regular intervals of more than 10ms, we will be assured that even if the key was in the middle of bouncing the last time it was examined, it will have settled by this time. In the present application the key debouncing is handled by an algorithm (subroutine KBDBC) called soon after the start of each of the 32.768ms intervals used to synchronise the system's operation. This algorithm extends over many interrupts, and can be considered as a software implementation of a synchronous state machine, changing states (when needed) not more frequently than every 32.768ms.

The second subroutine discussed in this section (named FKCD in the program) actually "reads" the keyboard and returns predefined codes for the keys when each one of them is pressed, or other status information, like multiple key depression or no key depression. It will be discussed first, as it is extensively used by the key debouncing algorithm. This is the routine that actually deals with the keyboard and PORTC. It is used by KBDBC. The keyboard arrangement can be seen in figure 4.6. PORTC is a bidirectional port. Data direction is controlled by a data direction register (DDRC); an 1 written in an individual bit of DDRC configures the respective pin of PORTC as output, while a 0 as an input. In this application, pins 0 and 1 of PORTC are configured as inputs, while pins 2 and 3 as outputs. To check the keyboard for any key depressions, pins 2 and 3 are driven low; if no key has been pressed, reading PORTC yields xxxx0011. If some key has been pressed (indicated by a value of xxxx0010 or xxxx0001), the following test is carried out to resolve the row the key belongs to: DDRC is left as described above, PC2 is driven low, PC3 is driven high and PORTC is read again. If the value read is xxxx1001, this means that the [CNDY] key was pressed; if it is xxxx1010, the [TEMP] key was pressed. If this test fails, the second row is examined: PC2 is driven high, PC3 is driven low and PORTC is read again. If the value is xxxx0101, this



means that the [%] key was depressed; if it is xxxx0110, the [CS] key was depressed. The upper half of PORTC is masked out, therefore its value is irrelevant. The above described procedure also yields the code for each of the keyboard switches: the code for the [CNDY] key is \$09, for [TEMP] is \$0A, for [%] is \$05 and for [CS] it is \$06. Two keys of the same row pressed simultaneously give 0s at both PC0 and PC1. The flowchart of this subroutine can be seen in figure 4.7. On exit, ACCA holds the code for a single key pressed as mentioned above, or \$03 for no key depression. Finally, if two keys of the same row, column, or two diagonal keys are pressed simultaneously (however rare this might be, considering the rate of keyboard scanning) at the time the keyboard is read, ACCA is loaded with \$02 on subroutine exit, and the key debouncing algorithm then acts accordingly.

A flowchart showing the structure of the key debouncing algorithm can be seen in figure 4.8.

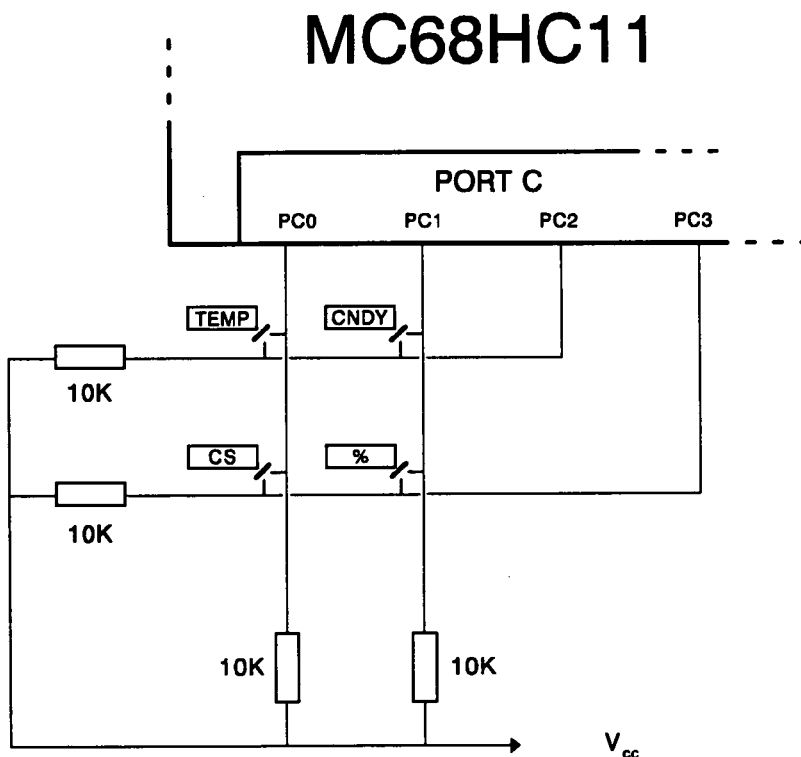


Figure 4.6 Keyboard connections to microcontroller

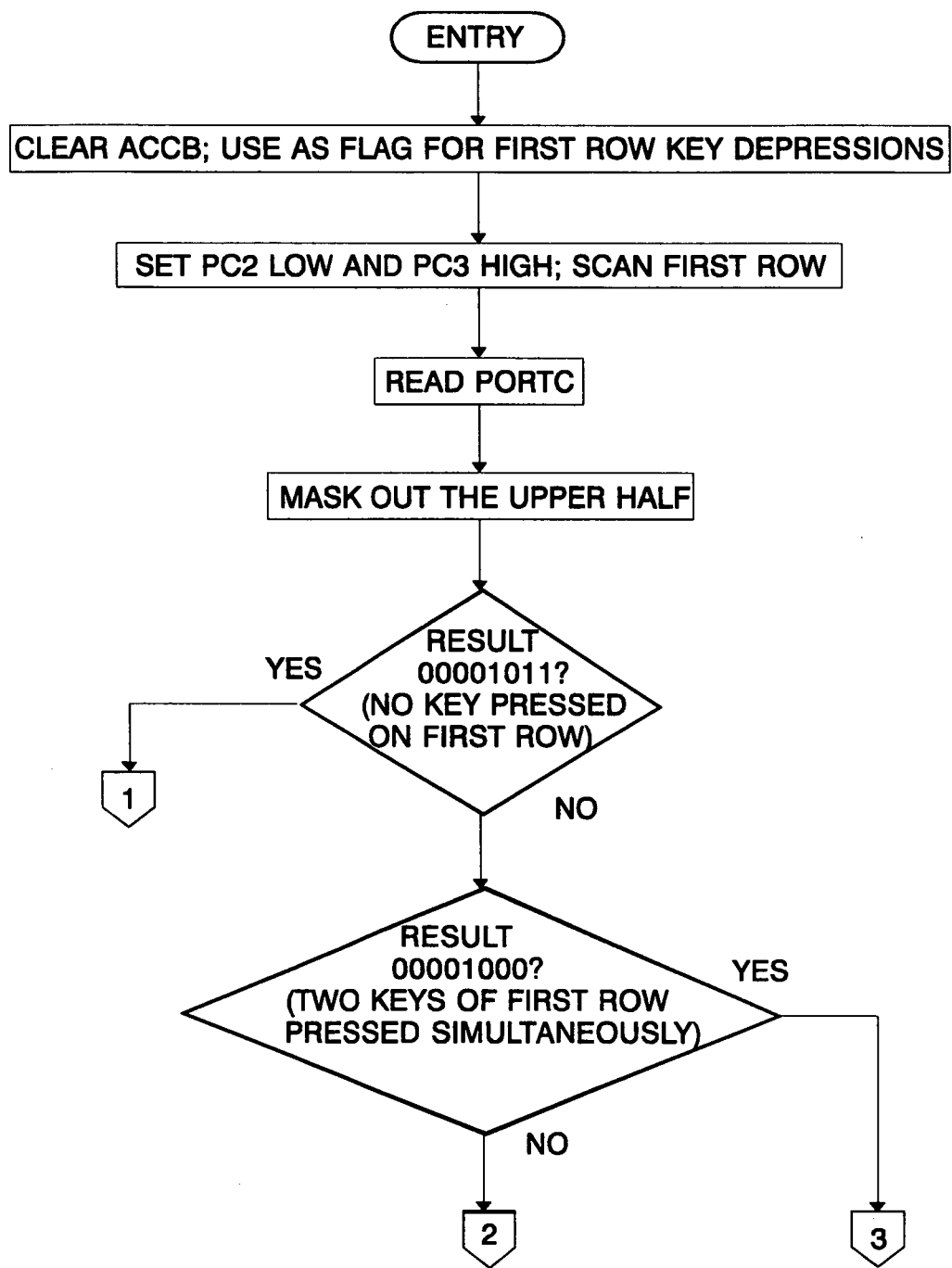


Figure 4.7 Keyboard scanning routine

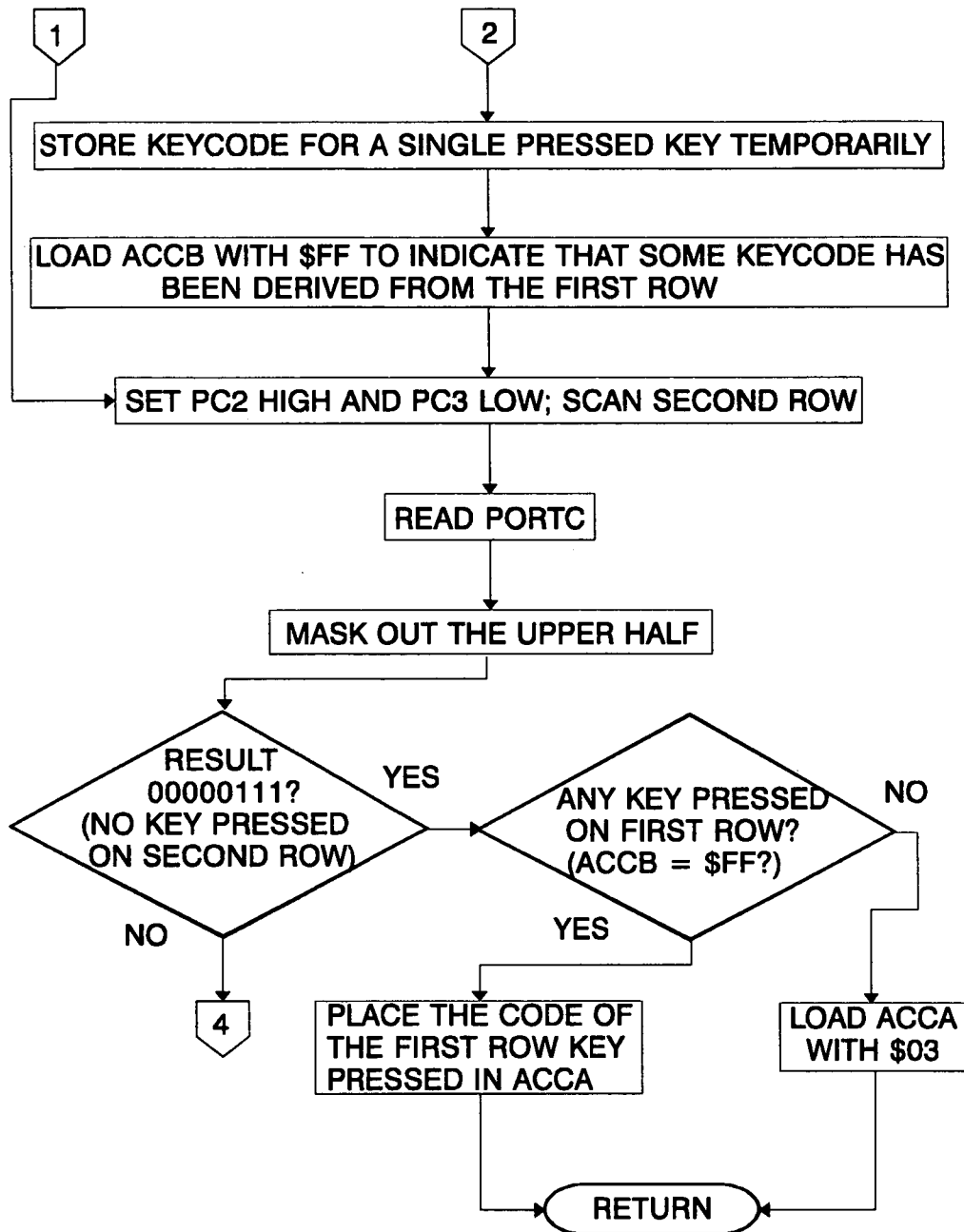


Figure 4.7 (Continued)

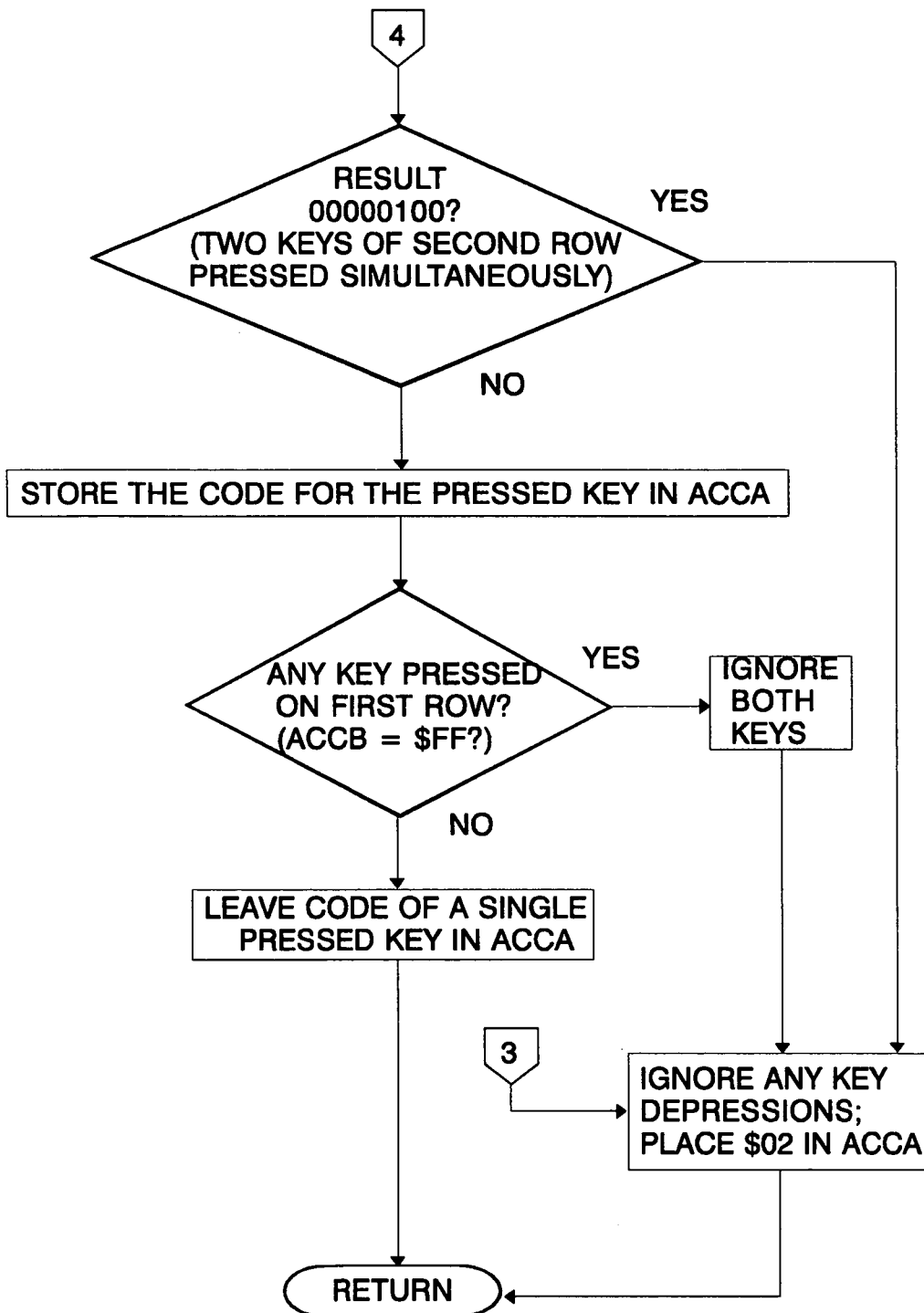


Figure 4.7 (Continued)

The main and most important variable used within this routine is KCDE (8 bits wide). In addition to holding the code for each of the keys pressed and indication for invalid key depressions, it is used to communicate status information to the key parsing algorithm about the stage of key depression processing.

When KCDE has the value of \$FF, the key debouncing algorithm is enabled to read the code for a newly pressed key, starting from state #0, that is when either the key parsing algorithm has serviced the previous key depression, or there has been no key depression to deal with. The value of \$0x where x is the code for each of the keys as mentioned above, is stored in KCDE while the algorithm is dealing with a newly pressed key until it is seen released; as long as this condition persists, the key parsing algorithm cannot be initiated. Therefore only when each key is released can the key parsing algorithm take appropriate action. In that case the KCDE variable is loaded with \$Fx to notify to the key parsing algorithm that it should take action. Finally, the key parsing algorithm cannot be initiated when KCDE has the value of \$FF, since there is no key depression to be serviced.

Another variable used by this algorithm is the KSTATE which holds the current state (possible values are 0,1,2 and 3). Finally the CSDF is a flag to indicate how many times the chemical curve select (CS) key has been pressed. It takes the value of \$00 when CS has been pressed once only and \$FF when it has been pressed twice in succession.

Referring now to figure 4.8 it can be seen that the test for entry to the algorithm (KCDE=\$FF) is performed after the test for state #0 of the algorithm. In this way, if the algorithm is dealing with some key depression (in which case KCDE holds the value of \$0x), control passes to the tests for all states other than 0, until it reaches state #3 and then back to #0, while for a key newly pressed the KCDE variable can only be altered immediately after the test for state #0 and \$FF in KCDE.

From figure 4.8, it can also be seen that for a key to be considered as pressed it has to be seen so twice in succession. In that case the algorithm goes

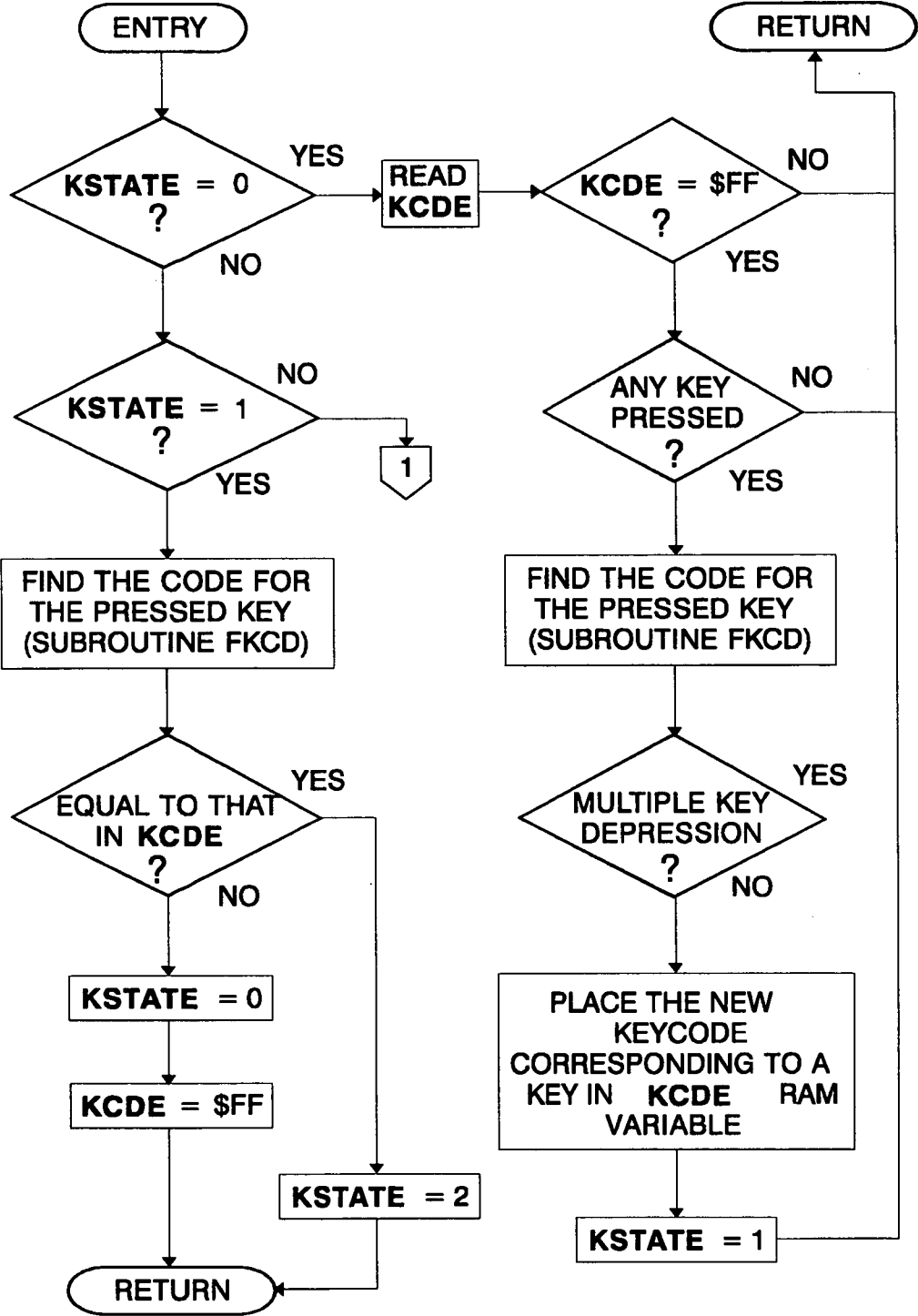


Figure 4.8 Key debouncing algorithm

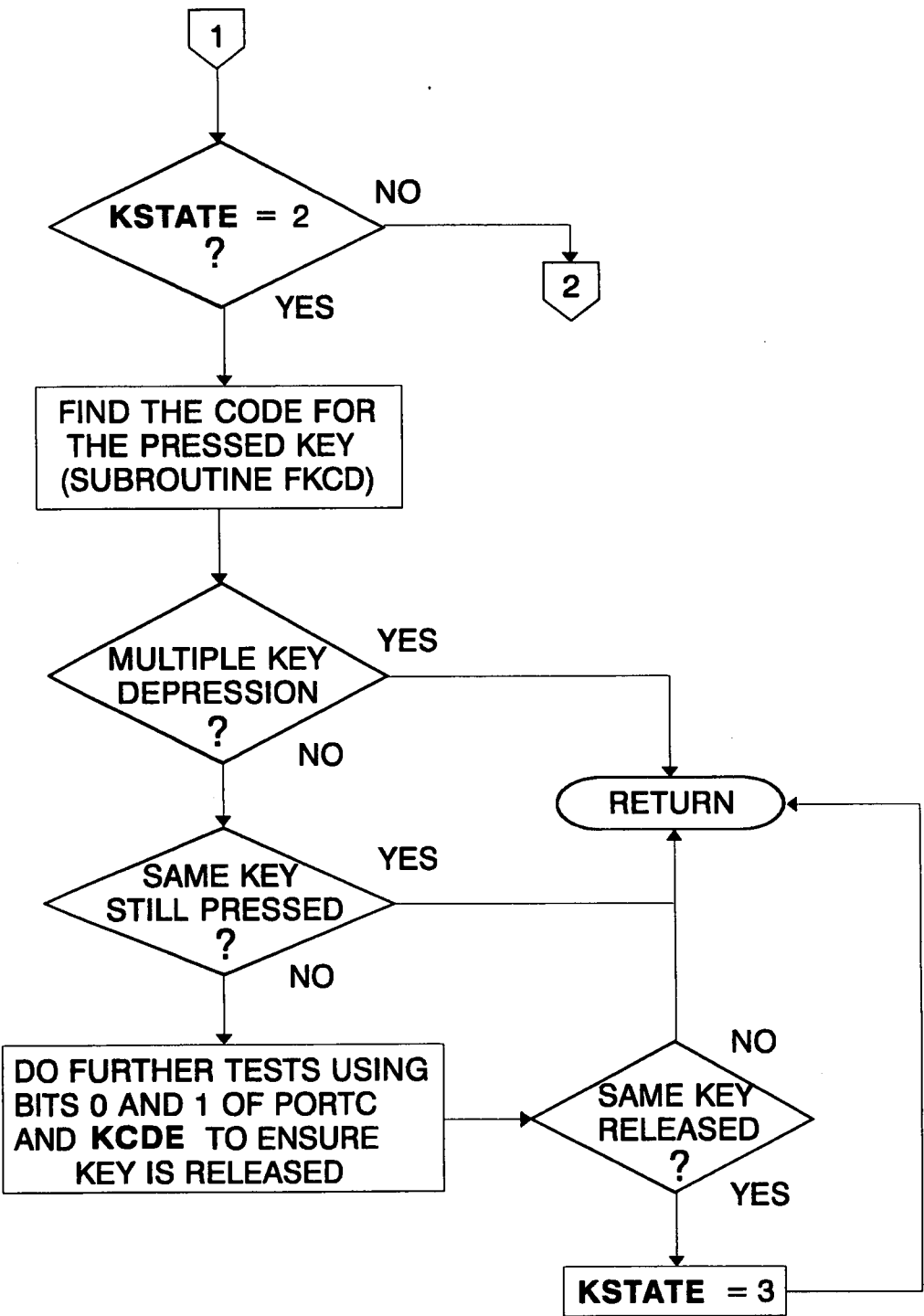


Figure 4.8 (Continued)

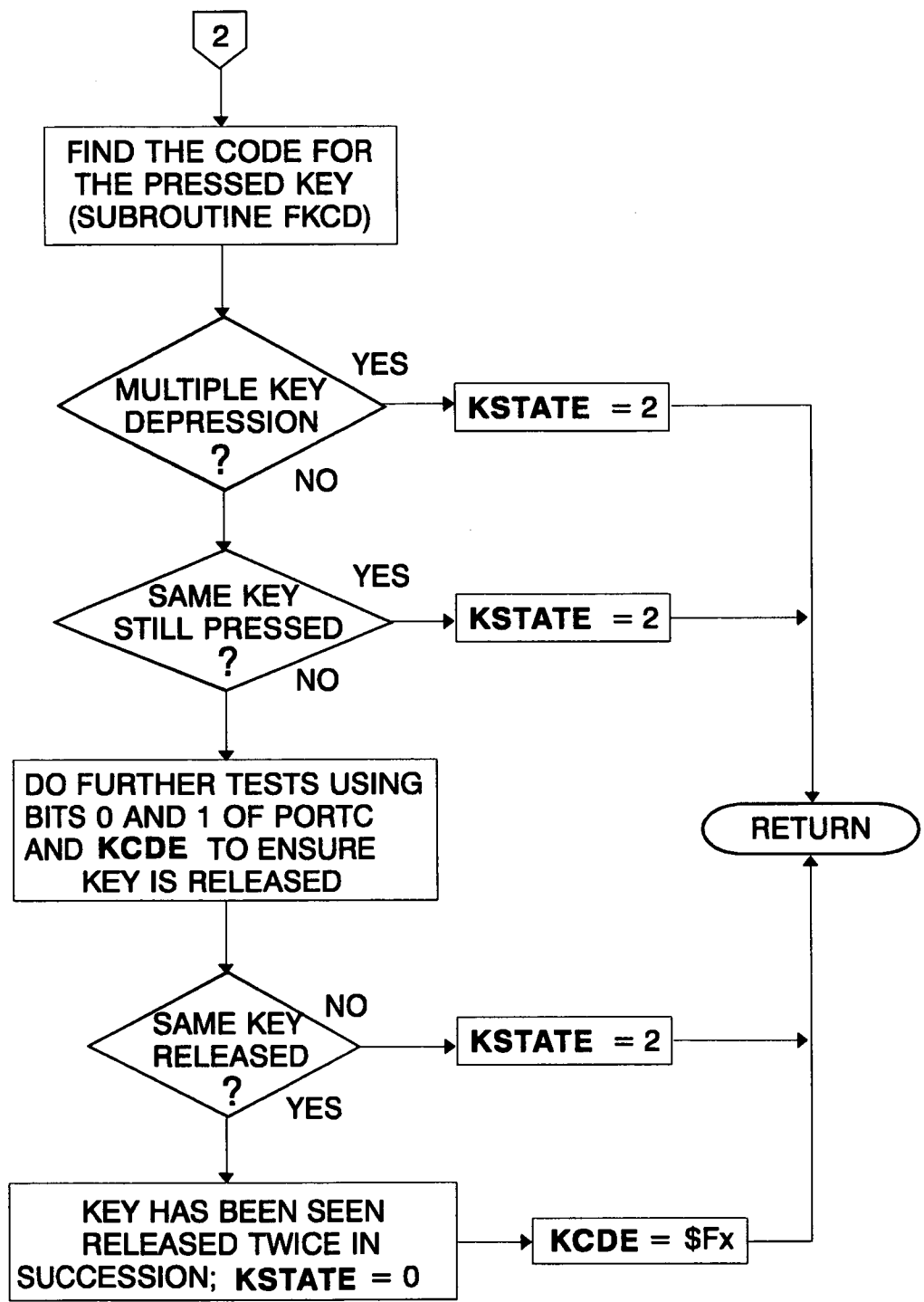


Figure 4.8 (Continued)



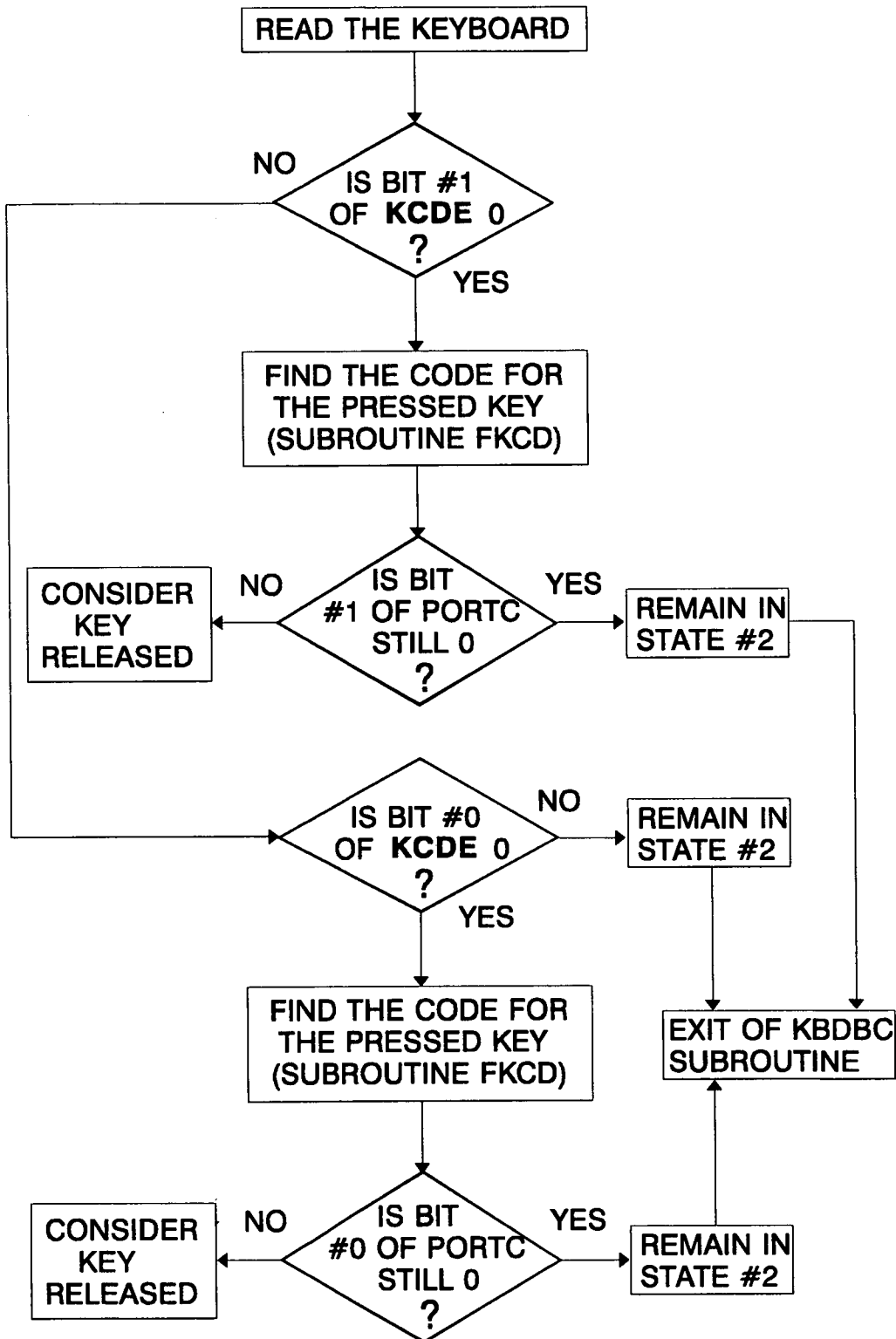


Figure 4.9 Key release test

to state #2 and stays there until this very key is detected as released for the first time. It then goes to state #3 after strict tests to ensure that the key is released indeed, and if it is again detected released in the immediately following interval, the key is considered definitely released. The algorithm then loads KCDE with \$Fx, so that the key parsing algorithm is allowed to take further action. The above mentioned test for released key is first carried out when from state #2 there is a mismatch between the value given by the keyboard reading and that in KCDE variable. This however is not a direct indication that the key has been released. It is quite possible that while the key in question is still pressed, other keys are pressed at the same time.

For this reason, a small program section checks separately the bits 1 and 0 of KCDE and PORTC respectively to conclude that the key has actually been released. This test is repeated after entry to both states #2 and #3. The structure of this program section can be seen in figure 4.9. Multiple key depressions have been dealt with before entry to this section as can be seen in figure 4.8, therefore it does not have to resolve again the row the examined key belongs to.

As far as initial conditions of the key debouncing algorithm are concerned, in the initialisation section \$FF is placed in KCDE and 0 in KSTATE. From the above discussion it can be seen that the key parsing and the key debouncing algorithm work in a closely linked manner as the one enables or disables the other. Also that only single key depressions are recognised each time and that if any key is pressed the time another depression is dealt with, the former is ignored until the latter key is seen released. This scheme has been found to work satisfactorily considering the small number of keys used, and also keeps the memory requirements low. Another method could acknowledge every key pressed at any time (using periodic polling or causing a hardware interrupt each time a key is pressed), keeping the keycodes in a queue and employ a different algorithm to interpret key depressions in a first in - first out basis. Such an algorithm though, would be more complicated than the one described here, and would demand more RAM (which is already very limited) for the queue realisation. A further alternative could be the use of a chip specifically

designed for key switch handling, like the MM74C923 from MOTOROLA. That would eliminate the subroutine described above, and all the associated involvement of the software with keyswitches. However the software method leads to reduction of components resulting to a more reliable and more maintainable design, which is a prime target of this work.

#### 4.5.2 The multiplication routines

The 68HC11 can only handle 8x8 bit hardware multiplication. This is insufficient for the needs of the program, so a 16x16 bit multiplication routine (named MULUL in the program), has been developed. This subroutine assumes that operands are 16bit unsigned numbers only. It uses a 32bit accumulator consisting of ACCD (high order part) and the concatenated RAM variables AML and AL (low order part) in the following order: ACCA, ACCB, AML, AL. On entry to this routine, the MPCND RAM variable holds the multiplicand while the multiplier is placed in AML:AL. On exit, the product is transferred in ACCD, as it is assumed that it is kept within the 16bit limits.

A flowchart showing the structure of this subroutine can be seen in figure 4.10. The choice of ACCD for the 32bit accumulator was not arbitrary. The rotation instruction of the 68HC11 uses only two cycles for the CPU registers ACCA and ACCB while six cycles are needed for AML and AL rotation; there is no direct addressing mode for rotation therefore extended mode has to be used. It is very important to keep the time consumed by the multiplication routine as short as possible, since it is used in numerous places in the program and in many cases it is called from within other subroutines. Its duration in the program is 626 cycles or 0,313ms assuming 8MHz clock frequency.

Another multiplication routine has been found necessary to develop. It is based on the routine described above, and multiplies any number with a 5-digit number of the form ABCDE (eg 0,6202, 1,0430, etc) with the decimal point

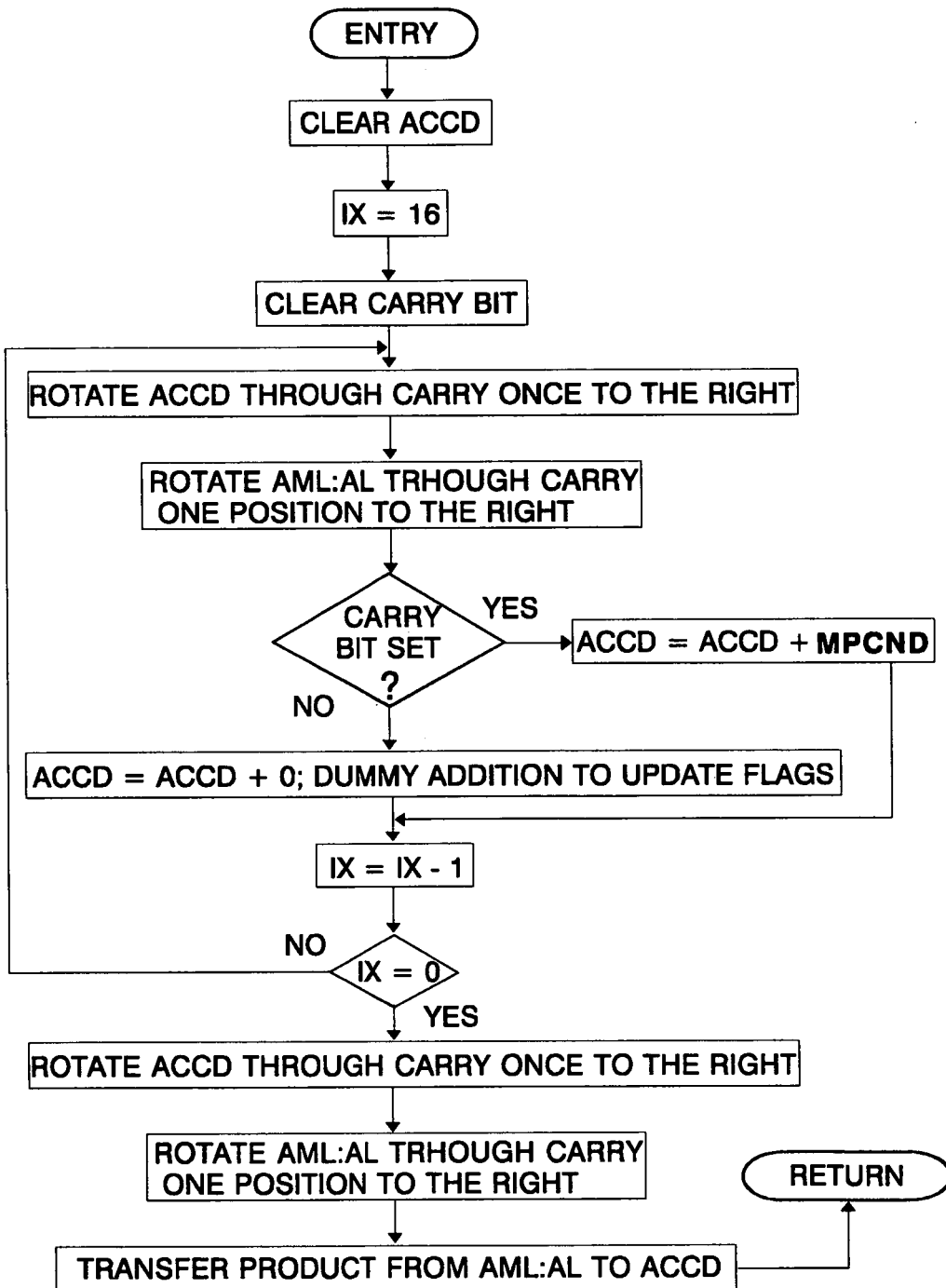


Figure 4.10 16x16 multiplication routine

assumed to be to the right of digit A. This routine (named FIND in the program) is mostly used in the derivation of final conductivity and temperature values. The above mentioned 5-digit number is usually a conversion factor. On entry, IX can hold any number (the multiplicand) and ACCD the 5-digit number. On exit, IX holds the result of multiplication. Some local RAM variables are also used by this subroutine (GPDB1, GPDB2 and GPDB3). Rounding is also carried out whenever division is performed within this subroutine, in order to produce more accurate results, since it deals directly with processed and displayed data.

The flowchart showing the structure of this subroutine can be seen in figure 4.11.

The following example outlines the process:

Suppose that the number 1646 (which could represent a number corresponding to conductivity or temperature measured pulses) has to be multiplied by 1,3257, which in the program is represented by 13257. The subroutine does the following:

$1646 \times 7 = 11522$ , divided by 10000 gives: 1, rounded to: 1.  
 $1646 \times 5 = 8230$ , divided by 1000 gives: 8, rounded to: 8.  
 $1646 \times 2 = 3292$ , divided by 100 gives: 32, rounded to: 33.  
 $1646 \times 3 = 4938$ , divided by 10 gives: 493, rounded to: 494.  
 $1646 \times 1 = 1646$ , divided by 1 gives: 1646, rounded to: 1646.

Adding all the rounded numbers, we find that the result is 2182, the same as we would find using normal multiplication. In fact experience shows that in most cases the results obtained using this method are very near the expected numbers. This example also shows a limitation of the method. The multiplicand cannot exceed the number 7281, as a digit 9 in the 5-digit multiplier will take the partial product above the 16bit limit (65535), resulting in rollover, and loss of accuracy. The duration of the subroutine is 4.201 cycles or 2.1ms assuming 8MHz clock rate; it is so prolonged because of the extensive use of the MULUL subroutine.

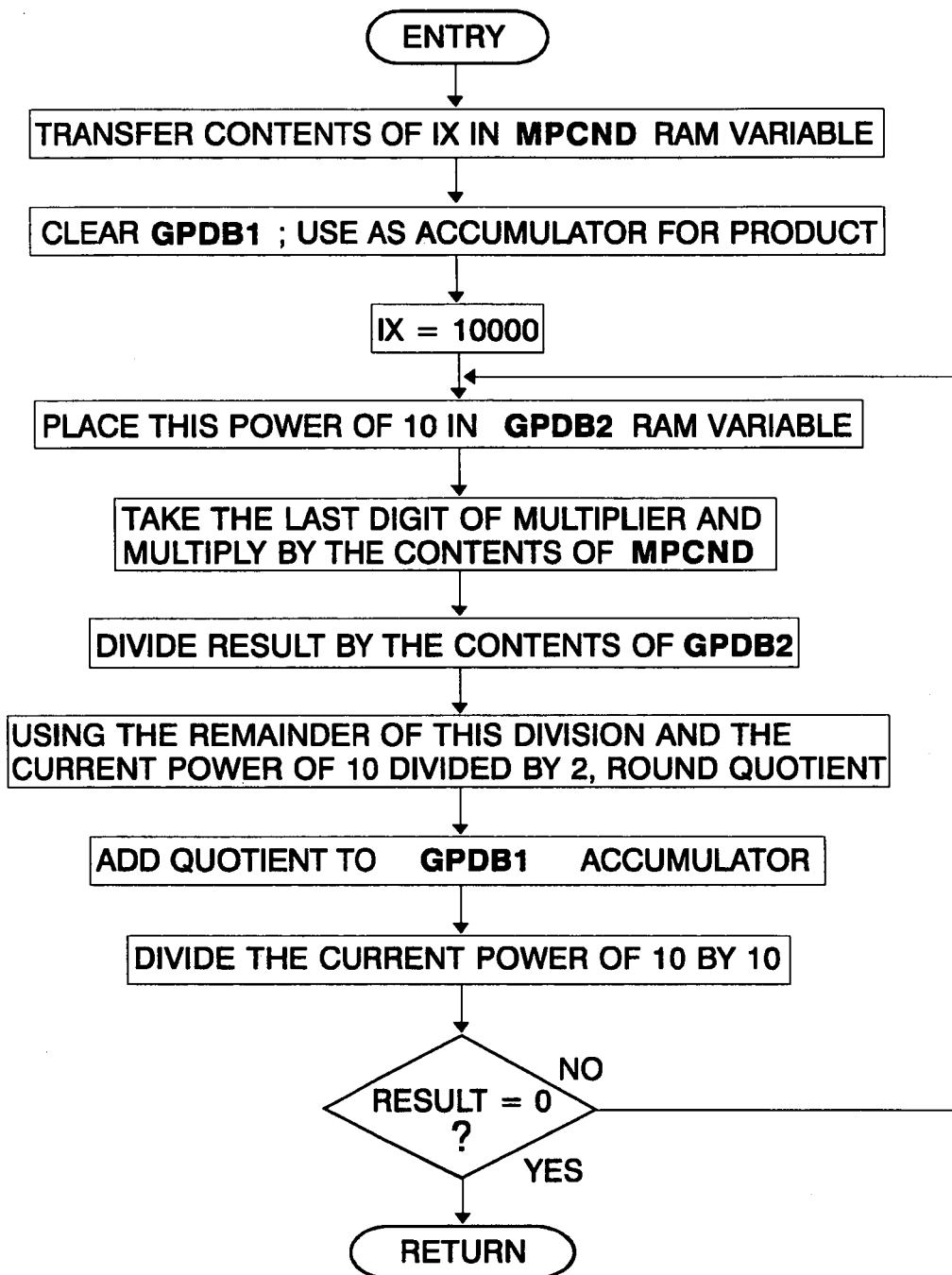


Figure 4.11

### 4.5.3 The display subroutines

There are three routines dealing with the display. The most important (named MDISR in the program), sends to the display any number between 0 and 1999, irrespective of decimal points or quantity displayed. This subroutine is used to display all temperature, conductivity and concentration values within their respective range. This routine does not deal with decimal points; this task is left to the key parsing algorithm action routines, which use each quantity's associated flags to turn on or off the necessary decimal points. An 8bit local RAM variable (GPB) is used for temporary data storage and also a small subroutine (named EDGE in the program) which sends the necessary low to high pulse to the display driver so that the display is updated. Referring to figure 3.3, it can be seen that bit 7 of PORTB is used to accomplish this task; also that pins 0, 1, 2 and 3 of PORTD are connected to the data pins and bits 4 and 5 to the digit select pins of the display driver. The data pins can take any value from \$0 to \$F while the digit select pins DS2 and DS1 select the digits D4, D3, D2 and D1 (starting from the left), when they take the values 00, 01, 10 and 11 (binary) respectively.

The procedure of updating one digit of the display is as follows:

- The value of the digit is written to the data pins.
- The digit selection code is written to the digit selection pins.
- The chip select pins are taken from low to high.

The display driver is designed to drive four full digits, while the display only has 3½ digits. If the 4th digit is to appear blank, the number \$C is written to the data lines and corresponding digit is updated. On entry to this routine the 16bit RAM variable DISDIG holds the number to be displayed. On exit, the display shows the number. A flowchart of this subroutine can be seen in figure 4.12.

Another subroutine dealing with the display (named DSPCC in the program) is the one that shows the code for the chemical curve selected by the user. The display in this case has the form CCx, CC for Chemical Curve and x for the number

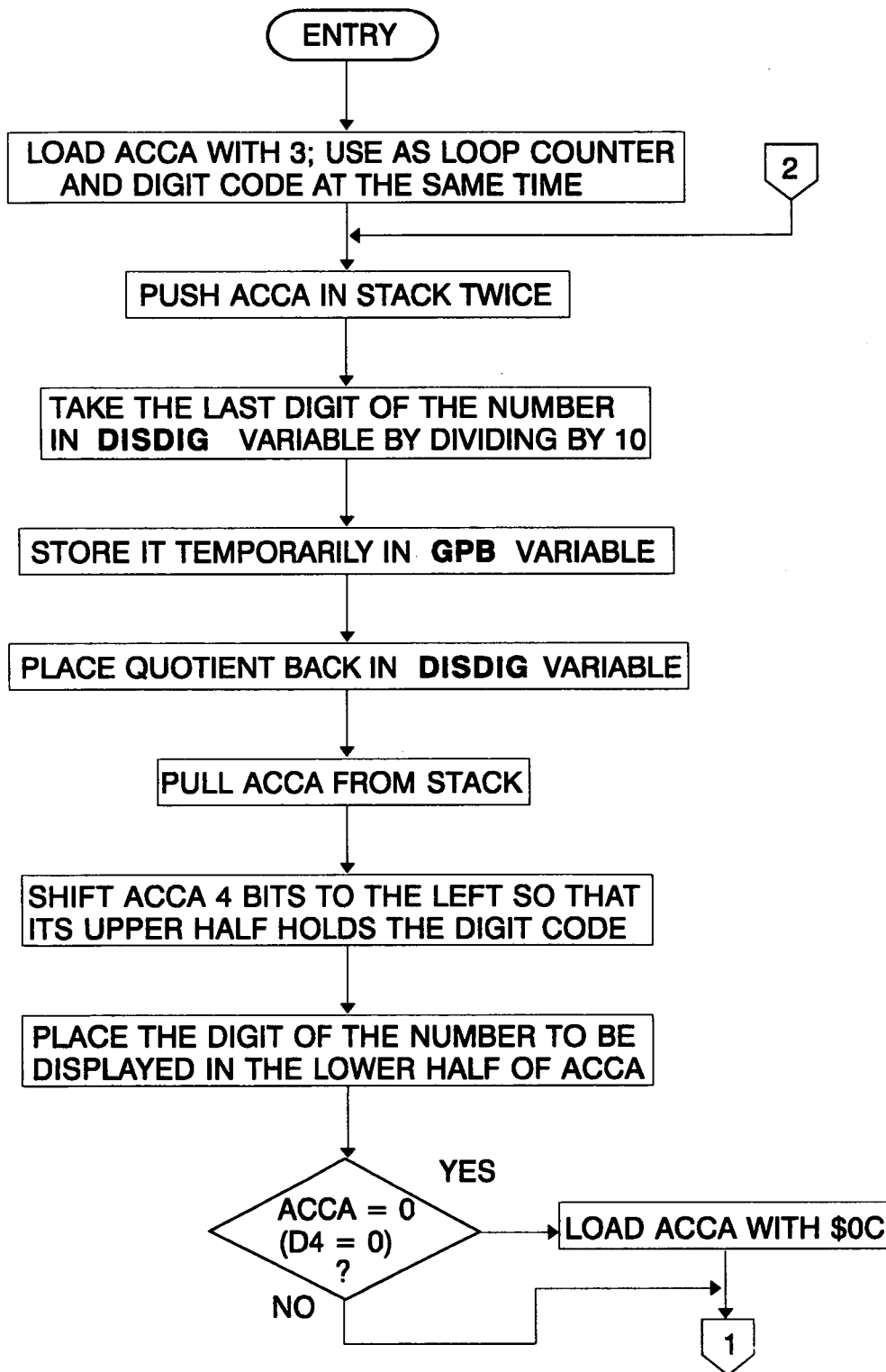


Figure 4.12 Main display routine



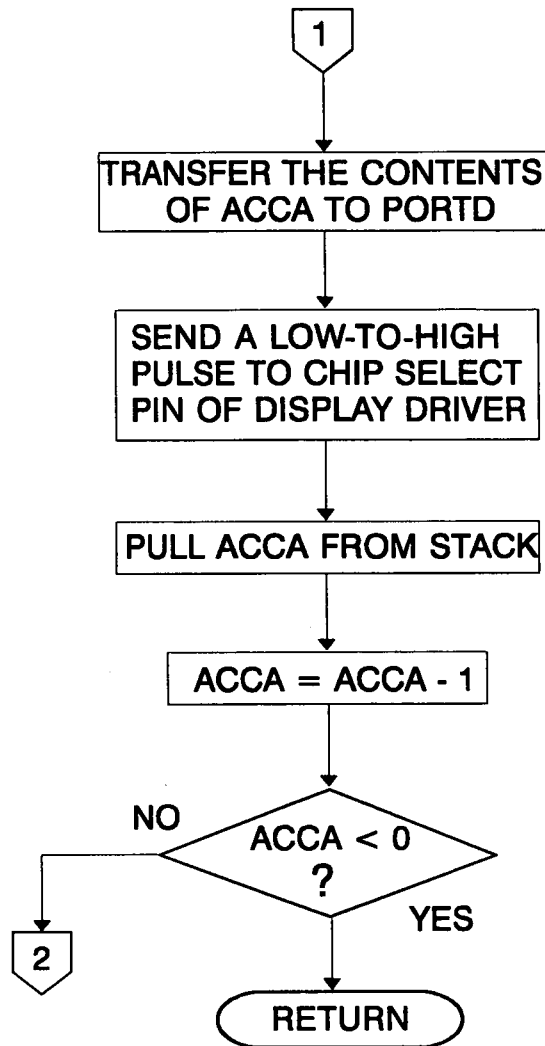


Figure 4.12 (Continued)

corresponding to a specific curve. This subroutine is used by the key parsing algorithm action routine dealing with [CS] key depressions. On entry to this routine, ACCA must hold the code for the chemical curve in the form \$0x, and on exit the display appears as described above.

The final subroutine for the keyboard (named DOOR in the program) is used whenever some of the displayed values goes out of range. Again, this subroutine is used by the key parsing algorithm and also during the initialisation section to indicate that the probe is out of the solution, therefore conductivity values are out of range. On exit, the display is filled with 3 Es, while the digit

D4 remains blank. Flowcharts for the last two subroutines are not given, since the procedure is the same as followed during the MDISR subroutine.

#### **4.5.4 Conductivity compensation against oscillator amplitude variations**

As has been mentioned in chapter 2 (equation 2.3.20), the amplitude of the sensor output varies linearly with the conductance linking the cores of the probe coils and the amplitude of the oscillator voltage, assuming that the frequency is stable. While conductivity measurement depends on the former, variations in the value of the latter can be a serious source of error. They can be caused by component tolerances, component aging or temperature variations, as has been mentioned in section 3.2.10. Therefore conductivity measurement should be done stable when oscillator amplitude varies within some reasonable limits.

One way can be to find the deviation of the oscillator amplitude from a preset value stored in EEPROM, and then add or subtract the same percentage of deviation from the measured conductivity value. Another way can be to divide the the number of conductivity pulses by a number of pulses corresponding to oscillator amplitude. The latter method needs less program space, needs no preset value for oscillator amplitude, thus making calibration of the device easier, and more important, it does not depend on the slope of the V/F converter characteristic. Implementing this method however in software is not straightforward, since the limited arithmetic capabilities of the 68HC11 have to be considered.

Both methods require the information of the amplitude of the oscillator voltage. This measurement is carried out during the initialisation section and every 10th measurement cycle thereafter. It is done by closing the switch IC5D (S5) in figure 3.2 and measuring the respective pulses for 163.84ms. To avoid signal conflict with consequent damage to the range selection amplifiers, switches IC5B (S3), IC3B and IC3C are opened, while IC3A and IC3D are kept closed for the time IC5D is closed.

The subroutine implementing the ratiometric method of compensation is called CCOMP in the program; on entry ACCD holds the number of pulses for

conductivity, and the 16bit RAM variable OA a value corresponding to oscillator amplitude. On exit, IX holds the ratio of the two above mentioned values. A flowchart showing the structure of CCOMP can be seen in figure 4.13.

In this routine the final result is the actual ratio multiplied by 1000. One more digit becomes available during the routine execution, although for overflow reasons it is not being used; the program section deriving it has been retained though for possible future use.

The following example illustrates the way the subroutine operates.

Suppose that 2851 pulses were collected for conductivity and 1732 for oscillator amplitude. The CCOMP subroutine then does the following:

$$2851 \times 10 = 28510 \div 1732 = 16 \times 1000 = 16000 \text{ (remainder 798).}$$

$$798 \times 10 = 7980 \div 1732 = 4 \times 100 = 400 \text{ (remainder 1052).}$$

$$1052 \times 10 = 10520 \div 1732 = 6 \times 10 = 60 \text{ (remainder 128).}$$

$$128 \times 10 = 1280 \div 1732 = 0 \times 1 = 0 \text{ (remainder 1280).}$$

Adding the partial results yields 16460. The last remainder is used to round the last digit:

$$1280 \times 10 = 12800 \div 1732 = 7 \geq 5 \rightarrow \text{final result} = 16461.$$

Dividing the final result by 10 and rounding gives 1646, which is the same as the expected up to the third decimal digit.

#### **4.5.5 Compensation of temperature measurement against reference voltage variations**

It has been shown in chapter 3 (section 3.2.8) that if ratiometric measurements are performed for the derivation of solution temperature, the final value can become independent of small changes in the voltage reference Z1 (see figure 3.2). Also, using this method several errors introduced by the subsequent stages to the microcontroller can be eliminated. The program section performing this compensation implements equation 3.2.3 with the usual handling of numbers that overcomes the 16-bit limit of the 68HC11.

On entry to this section ACCD holds the number of pulses corresponding to temperature value and the 16-bit RAM variable TREF a value corresponding to

the magnitude of the voltage reference Z1. On exit, TEMP variable holds the result of the operation -a number between 0 and 1000. The temperature conversion factor (stored in TSF EEPROM constant ) has the value of 2597 since the result of equation 3.2.3 has the same rate of change as that of the Pt1000 sensor.

The flowcart of this section can be seen in figure 4.14.

#### **4.5.6 The temperature compensation/concentration determination routines**

As has been mentioned in previous sections, measurement of conductivity takes place during intervals 4 to 0 (inclusive). This basic measurement, together with stored data for chemical solutions and the measured temperature of solution, are used to derive the concentration and conductivity referred to 18 °C for the chemical solution in question.

The solutions of strong electrolytes in general present a conductivity against concentration and temperature behaviour similar to that shown in figure 1.1. As seen in this figure, these curves have a turning point, which is the limit to the range of values that have been stored, since there is no way to distinguish different conductivity values for two concentration values lying symmetrically on either side of the turning point. For the purposes of this work, only data for the 18 °C curve has been stored for each one of the chemical solutions used. An initial thought was to approximate these curves with second degree polynomials and then derive temperature dependent coefficients. The limited arithmetic capabilities of the 68HC11 were however the main obstacle, as numbers of very wide range would have to be stored and handled. The method of partial straight line approximation has been found to be suitable for the purposes of this work.

The data block for the 18 °C curve starts with the number of points stored; then for each point the temperature coefficient, conductivity and concentration are stored consecutively. For each data item two bytes are allocated. These EEPROM data blocks are of the form shown in figure 4.15. Temperature coefficient (denoted by TC) is the percentage of change in conductivity, per degree. Two decimal points are stored in the reference curve; for example a TC

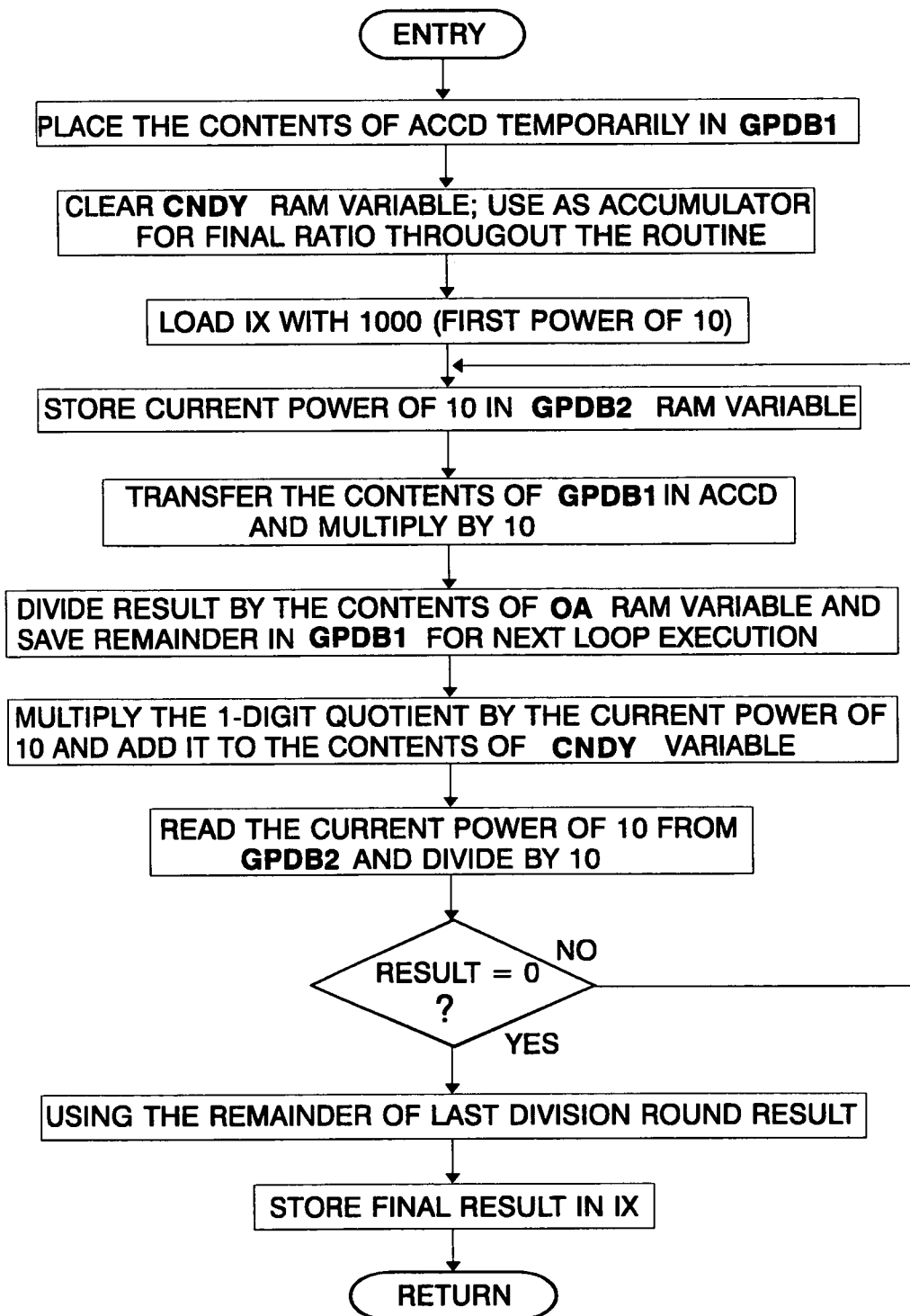


Figure 4.13 Conductivity compensation against oscillator amplitude variations

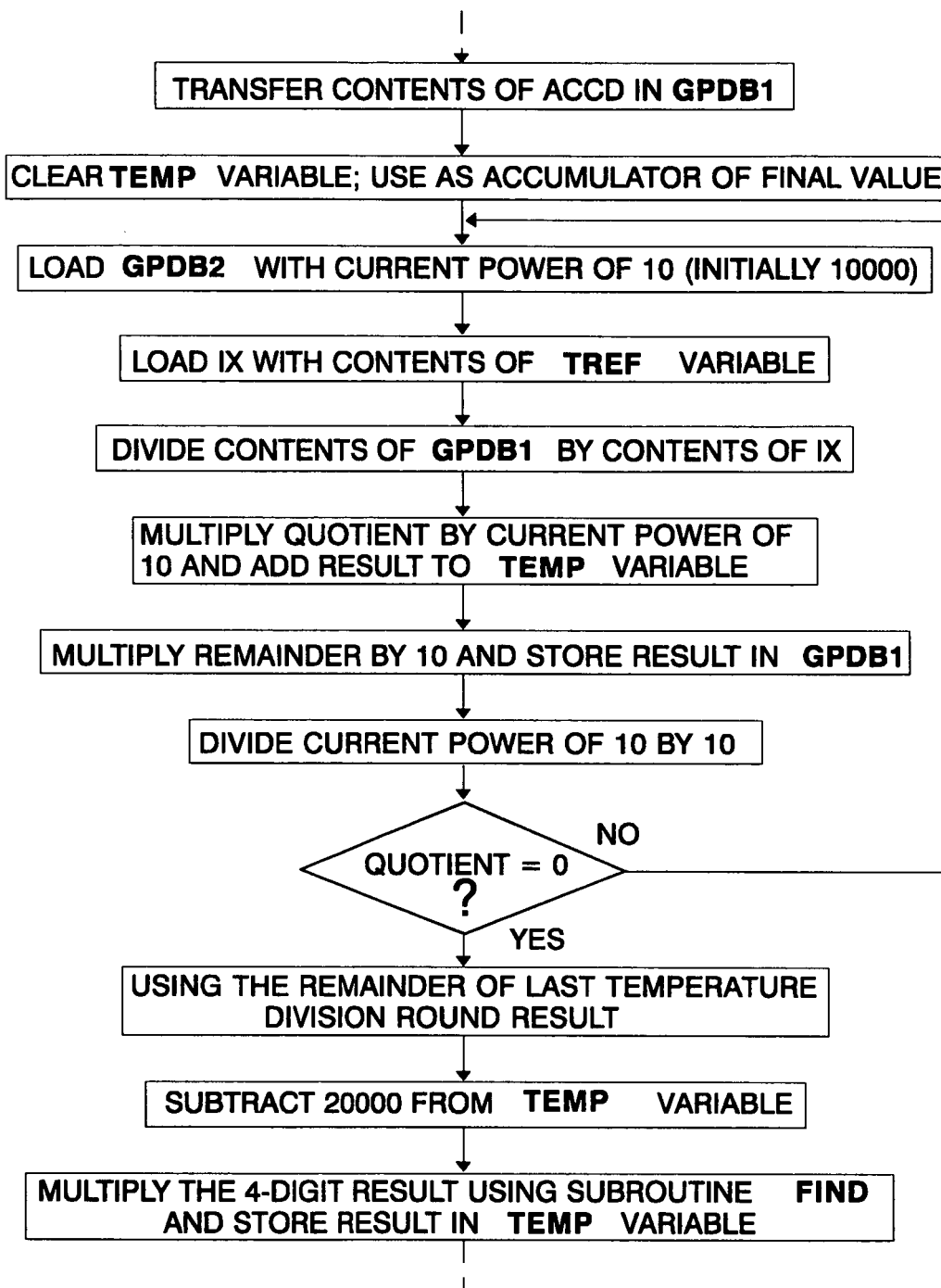


Figure 4.14 Temperature measurement compensation against voltage reference variations section

of 2.82% is stored as 282. Conductivity (denoted by  $\sigma$ ) is stored with one decimal digit of accuracy and it is assumed to be expressed in mS/cm. Concentration (denoted by  $c$ ) is stored with one decimal digit of accuracy, as only that was available in the conductivity tables used. It is assumed however that the next two are 0s, because it is necessary to obtain one more at least in the process of concentration determination. It is also assumed that for 0% concentration conductivity is 0.

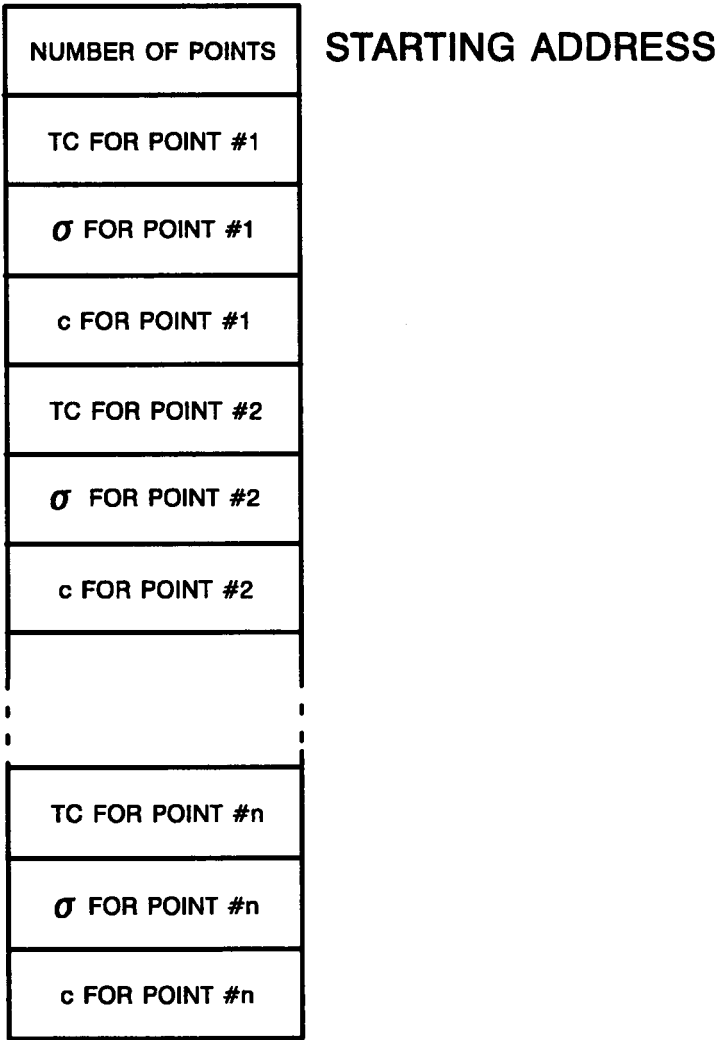


Figure 4.15 General structure of the memory block for storing chemical data of 18 °C curve

In addition to the tables of reference curves, there is also a table

holding the addresses of the first bytes of the reference chemical curves. This is referred to as CHTBL in the future. A 16bit pointer (CHPTR) is used to select the address of the current curve. Tables of chemical reference curves for the solutions used in this work can be found in APPENDIX 1.

The program section dealing with temperature compensation and concentration determination lies within interval #5 and is executed only when the user has selected some chemical for examination. This is indicated by a value different from 0 in CC RAM variable. After the beginning of the task for interval #5 the variable OSMC is checked to define whether oscillator amplitude will be measured in the place of conductivity. If this is the case, the RANGE flag is checked and the gain selection switches are moved in such a way, that at no time two operational amplifier outputs are connected together thus causing possible damage to the circuit; for each value of RANGE flag there is a corresponding bit pattern for the gain switches. In this case no calculations are performed and control passes to the next interval. In case conductivity is measured, a further check is carried out, to establish whether the user has selected some chemical curve. If not, control is again passed to the next interval. If yes, then the temperature compensation/concentration determination routine is executed, based on the conductivity value obtained during the previous measurement cycle.

The method for obtaining the concentration and conductivity at 18 °C is based on the reference curve of each chemical stored in EEPROM. Each of these curves can be thought to be of the same shape as that of figure 4.16, with conductivity on the horizontal rather than the vertical axis. For each of the points stored in EEPROM, the respective conductivity at the solution temperature is derived using a special subroutine (subroutine FNDST discussed later in this section). The conductivity derived from the analog interface (called measured conductivity thereafter) is compared to that given by FNDST, and if it is higher, the program goes on to examine the next point and so on; if it is lower, then the conductivity interval, in other words the segment between two successive points of the conductivity curve at the solution temperature has been established (see



figure 4.16). Once this has been done, data for its end points are transferred to a RAM buffer for ease of manipulation: the consecutively placed RAM variables UPS18, UPC, LPS18, LPC, UPST and LPST hold the upper point conductivity at 18 °C, the upper point concentration, the lower point conductivity at 18 °C, the lower point concentration, the upper point concentration at the solution temperature (denoted by  $\vartheta$  thereafter) and the lower point conductivity at the solution temperature respectively.

Concentration is then found using the following linear interpolation formula:

$$c_m = c_{i-1} + (c_{i+1} - c_{i-1}) \frac{\sigma_m - \sigma_{i-1}}{\sigma_{i+1} - \sigma_{i-1}} \quad (4.1)$$

This form is preferred in the calculations because only one multiplication is needed.

The final result of this operation is the actual concentration value multiplied by 1000.

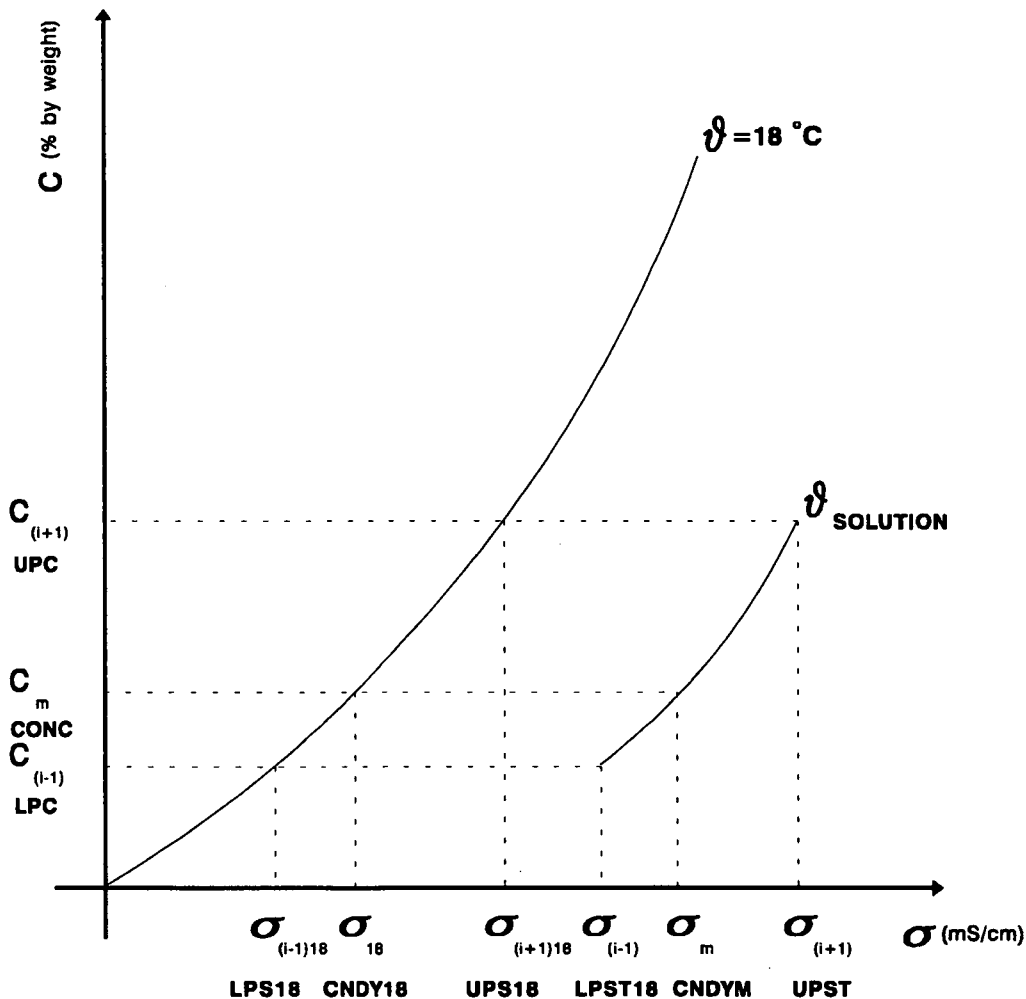


Figure 4.16

At the end of this program section this value is examined again to see if it is greater than 19.99%. If it is, two decimal digits are discarded after being used to round the result; if not, only the last digit is discarded. This is only done to adapt the numbers to the capabilities of the display.

Next the conductivity referred to 18 °C is calculated. The formula used is similar to that for concentration derivation:

$$\sigma_{18} = \sigma_{(i-1)18} + (\sigma_{(i+1)18} - \sigma_{(i-1)18}) \frac{c_m - c_{i-1}}{c_{i+1} - c_{i-1}} \quad (4.2)$$

This equation assumes that concentration is on the horizontal axis and conductivity on the vertical axis.

The fraction  $\frac{c_m - c_{i-1}}{c_{i+1} - c_{i-1}}$  has the same value as  $\frac{\sigma_m - \sigma_{i-1}}{\sigma_{i+1} - \sigma_{i-1}}$  therefore

it only has to be calculated once. When its value has been derived it is placed in the 16bit RAM variable FRACT.

The final result for  $\sigma_{18}$  is a value with only one decimal digit accuracy consequently ranges  $\times 10$  and  $\times 100$  are treated equally as far as range arrangements are concerned: RANGE18 flag takes the value 00000001 for the  $\times 1$  range and 00000010 for the  $\times 10$  and  $\times 100$  ranges, which reflects accordingly on the  $\sigma_{18}$  display format.

A flowchart showing the structure of this section can be seen in figure 4.17.

The last subject remaining to be discussed in this section is the method of calculating the points of conductivity curve at the solution temperature. This is done using the equation:

$$\sigma_{\theta} = \sigma_{18} + (\theta - 18) \times TC \times \sigma_{18} \quad (4.3)$$

The program uses the easier to implement formula

$$\sigma_{\vartheta} = [1 + TC \times (\vartheta - 18)] \times \sigma_{18} \quad (4.4)$$

This formula has been found to produce satisfactory results, comparable with these from other sources of conductivity data.

TC, as mentioned above, is a 3 digit number.  $\vartheta$  is a number between 0 and 999 (one digit of accuracy).  $\sigma_{18}$  can be any number between 0 and 19999.

The calculation is carried out by a separate subroutine called FNDST. On entry to this routine, the 16bit RAM variable TMPR must hold the current solution temperature and IX register must hold a pointer to the first byte of a data block holding information for a point. On exit, IX still holds the same pointer while ACCD holds the conductivity at  $\vartheta$  (value in TMPR), with no decimal points due to 16bit limit on the 68HC11. The lack of decimal points of accuracy is not critical in this case, as the values derived are only used as an indication of the conductivity interval and not for appearing on the display. A flowchart for this subroutine can be seen in figure 4.18.

In order that the conductivity interval comparisons are correct, the measured conductivity value (derived in the preceding measurement cycle) is adjusted according to the respective range of measurement. As the measured conductivity values always lie between 200 and 2000 (only one decimal point of accuracy), they are left as they are if range is  $\times 1$ , divided by 10 if range is  $\times 10$ , or divided by 100 if they are in the range  $\times 100$ . In each case division is performed, rounding of the final result is carried out. Also, since measured conductivity comes from the previous measurement cycle its range is also stored in the PRANGE flag; this is done because the autoranging algorithm located in the beginning of the task for interval #11 of the present measurement cycle may change the value of RANGE flag. For example, if the previous cycle gave a measurement of 2035 in the range  $\times 10$ , the autoranging algorithm will change the range to  $\times 1$  at interval #11 of this cycle, but will have retained the  $\times 10$  value in PRANGE flag; then the temperature compensation routine will correctly derive the value of 204mS/cm using the latter flag.

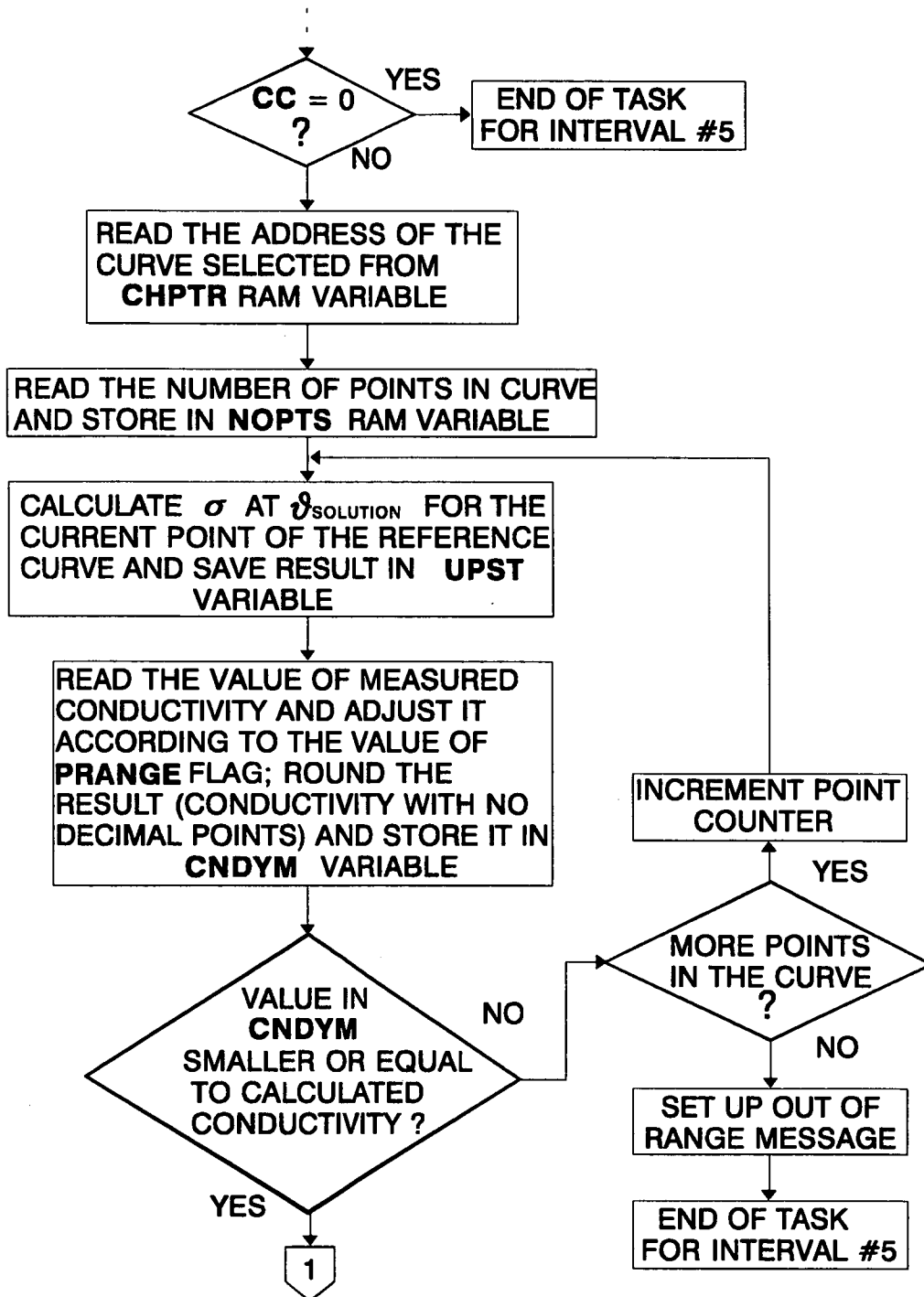


Figure 4.17 Temperature compensation/concentration determination section

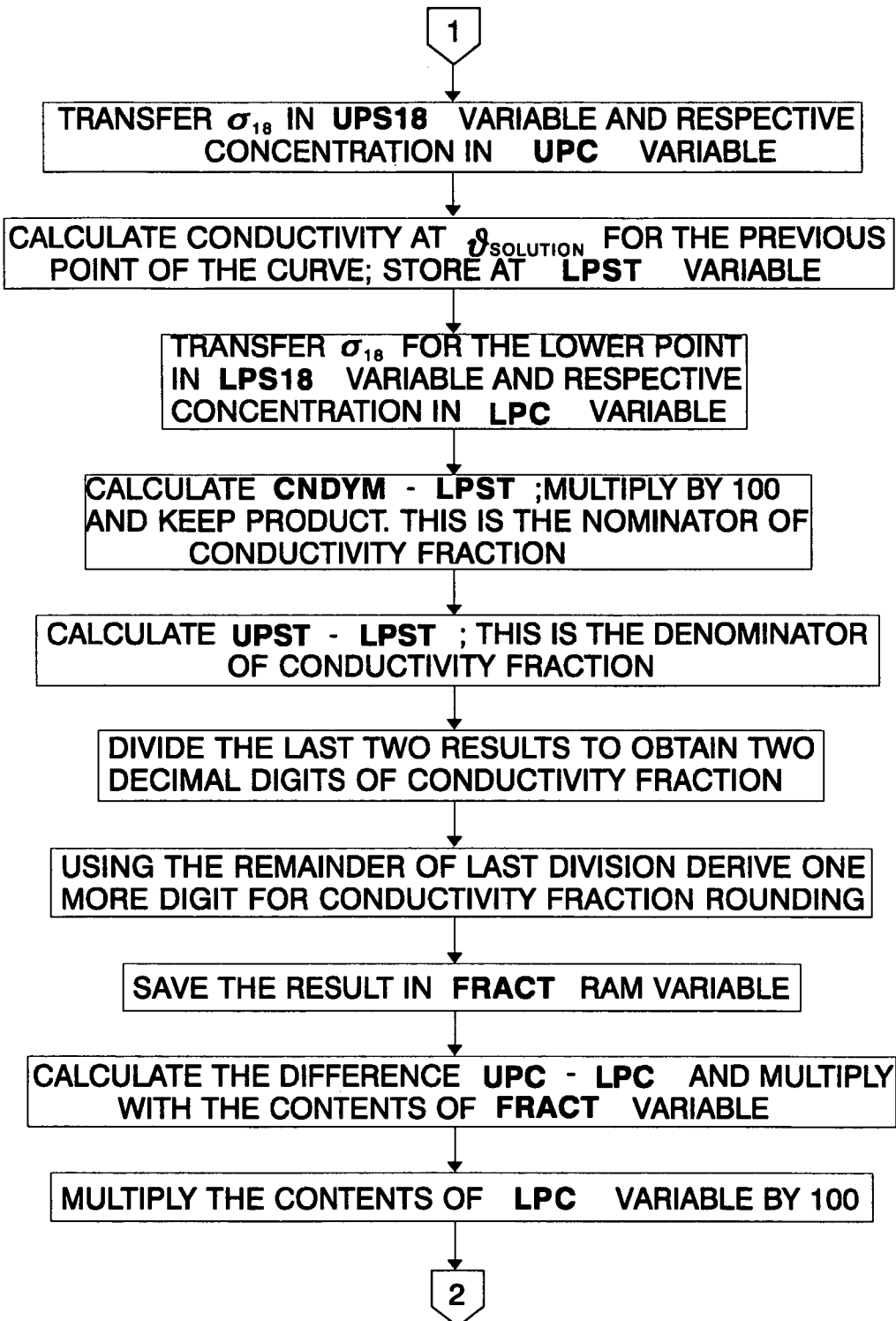


Figure 4.17 (Continued)

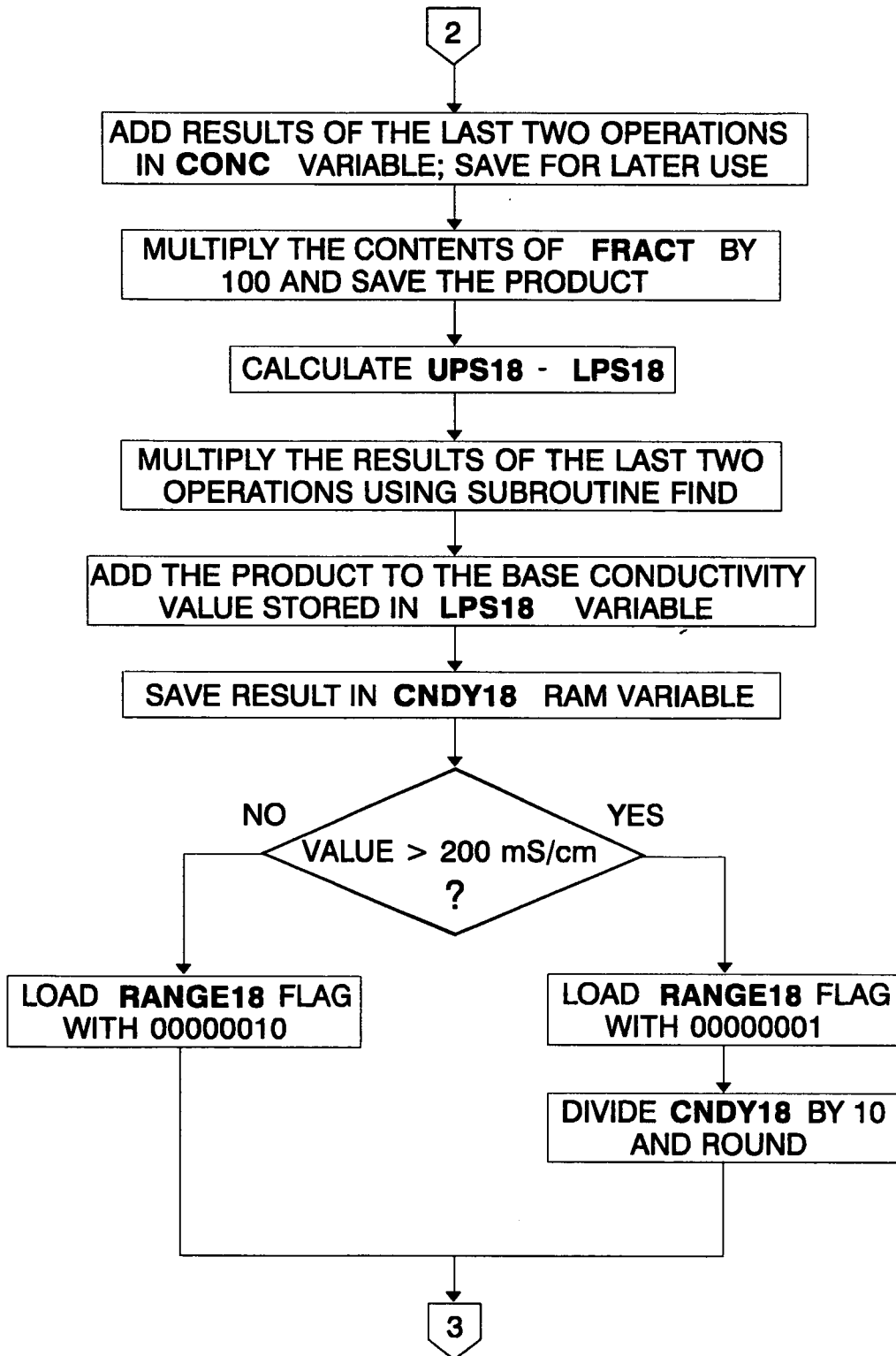


Figure 4.17 (Continued)

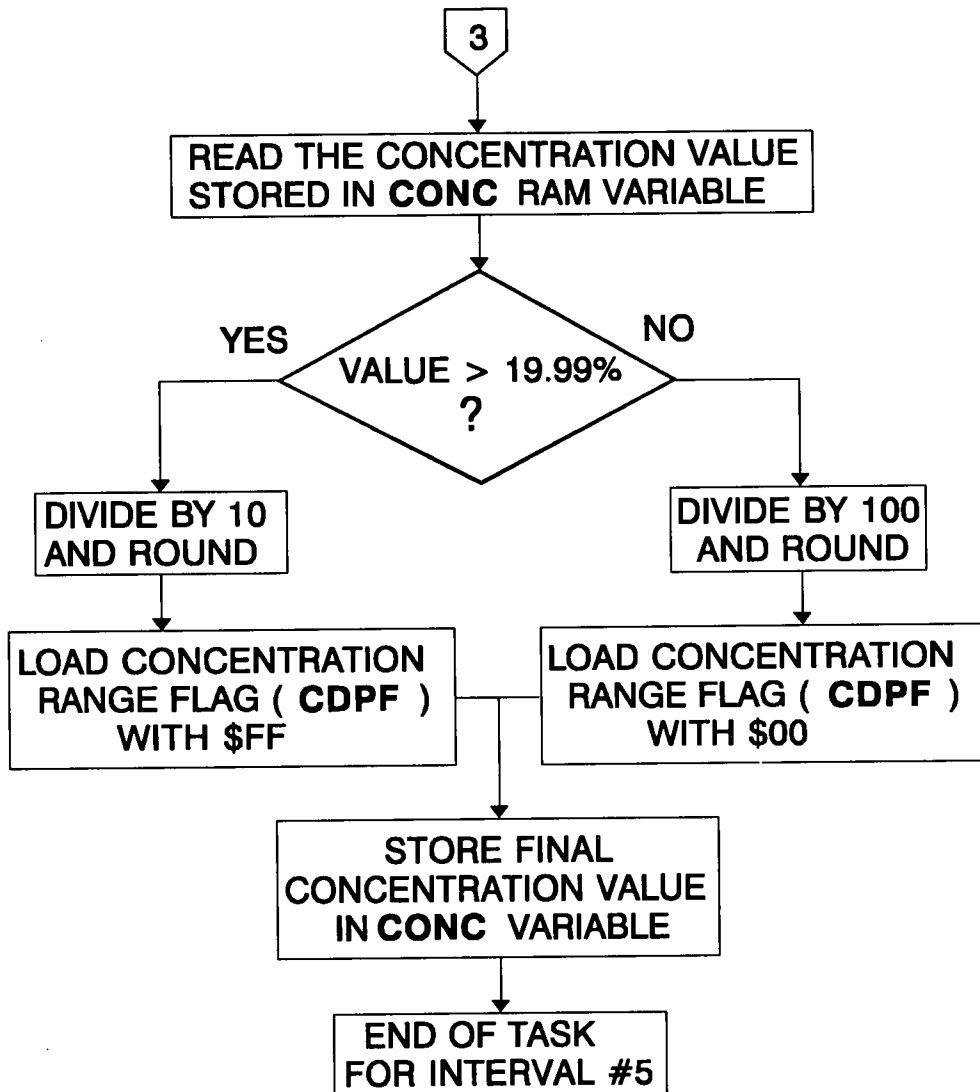


Figure 4.17 (Continued)

The following example best illustrates the procedures followed within the above described program section.

Suppose that a solution of HCl at 38.7 °C gives a measured conductivity value of 775mS/cm. Initially the measured conductivity is compared to the results of subroutine FNDST applied to each of the points of the stored reference curve in succession. At 38.7 °C the conductivity of HCl is found to be 834mS/cm for 10%

solution and 699mS/cm for 7,5% solution, therefore the conductivity interval has been established and the program sets up the necessary RAM variables as follows:

CNDYM : 775 (range  $\times 1$ )

UPST : 834 (no decimal points)

LPST : 699 (no decimal points)

UPC : 100 (1 decimal point)

LPC : 75 (1 decimal point)

UPS18 : 6302 (1 decimal point)

LPS18 : 5267 (1 decimal point)

Then the concentration formula (equation 4.1), is put to use:  $CNDYM-LPST=775-699=76$  and  $UPST-LPST=834-698=136$ ; the two results are divided after the first one is multiplied by 100, and the remainder is again used to round the second decimal digit. The result is 56, usually referred to as conductivity fraction in this work. It is saved in the RAM variable FRACT for later use. The concentration difference is found as  $UPC-LPC=100-76=24$ , which multiplied with the conductivity fraction gives a value of 1344 (1000 times the actual value). Adding the lower point concentration value after multiplying it by 100 gives:

$7500+1344=8844$  corresponding to 8.844%, which compares well with the hand calculated result of 8.915%. This is then stored in CONC RAM variable.

Next the conductivity at 18 °C has to be found using the equation 4.2. The interval fraction is read from FRACT and multiplied by 100:  $56 \times 100 = 5600$ . Then the magnitude of the conductivity interval at 18°C is found:  $UPS18-LPS18=6302-5267=1035$ . The last two results are then multiplied using the subroutine FIND: the fraction value is placed in ACCD and the interval magnitude in IX register. The result is 580 which added to the lower end of interval gives 5847, that is 584.7mS/cm, instead of an expected 585.2mS/cm. This result is larger than 2000 (corresponding to 200mS/cm), so it is divided by 10 and rounded and finally stored in CNDY18 RAM variable, ready to be sent to the display on request as 585mS/cm. Also, RANGE18 is loaded with 00000001



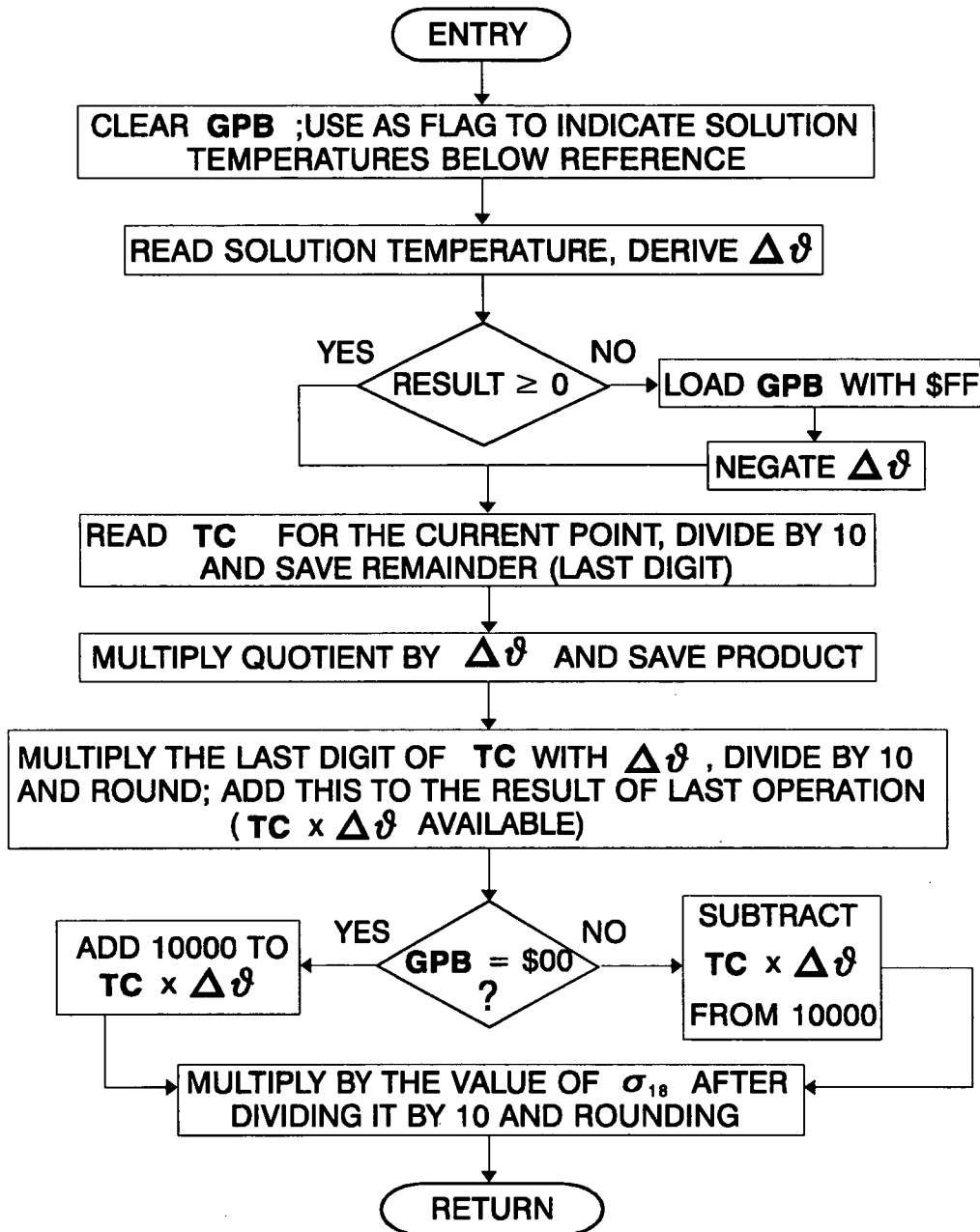


Figure 4.18 Subroutine for the calculation of conductivity at solution temperature using the stored reference curve.

to indicate that the result is in the  $\times 1$  range. Should the result of interpolation be under 2000, the last digit would be retained and **RANGE18** loaded with 00000010, to indicate  $\times 10$  or  $\times 100$  range.

Finally the range for calculated concentration is determined. The value of 8844 is read from CONC variable; as it is lower than 19999 (corresponding to 19.99%), the last digit is used to round the quotient of its division by 10 to 8.84%. At the same time CDPF flag is loaded with \$FF.

The order of the operations discussed above is not arbitrary; every care has been taken so that no intermediate result exceeds the 16 bit limit. If more curves have to be added, this point should carefully be observed. For example, concentration intervals must be kept short, preferably not more than 5% apart. This can be done by using the above mentioned linear interpolation formulas to derive intermediate points for the reference curve.

The next example illustrates the procedures followed in subroutine FNDST. Let's consider the 7.5% point corresponding to 526.7mS/cm on the reference curve for HCl, and a solution temperature of 38.7 °C. In the program these quantities are represented by the numbers 75, 5267 and 387 respectively. First the deviation from 18 °C is calculated:

$$\Delta\vartheta = 387 - 180 = 207.$$

Since  $\Delta\vartheta$  is positive, GPB flag is loaded with \$00. The value for TC at this point is 1.57% stored as 157. This is divided by 10 and the last digit is kept; both are then multiplied by  $\Delta\vartheta$ :  $207 \times 15 = 3105$  and  $207 \times 7 = 1449$  which divided by 10 and rounded gives 145. Adding the last two results yields 3250. By adding 10000 the result becomes 13250. This is finally multiplied by  $\sigma_{18}$ , after the latter has been divided by 10 and rounded to 527, using subroutine FIND as follows:

$$\begin{array}{llll} 527 \times 0 = & 0 \div 10000 & \text{gives} & 0 \text{ rounded to } 0 \\ 527 \times 5 = & 2635 \div 1000 & \text{gives} & 2 \text{ rounded to } 3 \\ 527 \times 2 = & 1054 \div 100 & \text{gives} & 10 \text{ rounded to } 11 \\ 527 \times 3 = & 1581 \div 10 & \text{gives} & 158 \text{ rounded to } 158 \\ 527 \times 1 = & 527 \div 1 & \text{gives} & 527 \text{ rounded to } 527 \end{array}$$

Adding the rounded results yields 699 instead of an expected 698.

#### 4.5.7 The autoranging algorithm

The autoranging algorithm is located within the interval #11, immediately after

the derivation of the actual conductivity value. The task of this program section is to read the conductivity derived during the previous measurement cycle, together with the associated range flag, and set the switches S1, S2 and S3 in a predefined sequence, so that they are ready for the measurement in the present cycle. Obviously, if the previous cycle was an oscillator amplitude/temperature reference measurement cycle, there is no point in executing this algorithm, therefore it is skipped.

Several flags are associated with this section:

- The RANGE flag, which takes the values 00000001 for  $\times 1$  range, 00000010 for  $\times 10$  range and 00000100 for  $\times 100$  range.
- The PRANGE flag, set up for the temperature compensation section, which holds the value of RANGE flag corresponding to the conductivity of the previous measurement cycle, in case the former has to be changed later in this section.
- The OOR flag, used by the output routines of the key parsing algorithm as an indication of out of range or not suitable to be displayed conductivity values. A value of \$00 indicates there is no range change. A value of \$FF indicates that there has been found an out of range value, but with a change in the gain switches positions conductivity can be brought again within range. The key parsing algorithm however does not change the display before the next measurement is taken as the present value cannot be displayed in most cases. Values of \$F0 and \$0F indicate conductivities larger than 2000mS/cm and smaller than 2mS/cm respectively; in such cases appropriate out of range messages are sent to the display.

The change in switch positions is done in a defined sequence in each of the possible range changes. In this way it is assured that at no time during changes two operational amplifier outputs are connected together, resulting in damage to the analog circuitry.

The structure of the autoranging algorithm can be seen in figure 4.19.

As far as initial conditions for the algorithm are concerned, the program has been designed so that on entry to interval #11, the autoranging algorithm cannot distinguish whether this is the first measurement cycle or others have been

executed in the past. Initial rough and then finer measurements of conductivity are carried out during the initialisation section, so that flags RANGE and OOR are set up according to the current solution conductivity.

#### 4.5.8 The key parsing algorithm

This section describes an algorithm designed to interpret key depressions. As mentioned in chapter 1 (section 1.5), four keys have been found to be adequate for the functions required by the conductivity meter. The following paragraphs describe how every key depression is expected to affect the displayed quantity.

- The TEMP key causes the current temperature of the solution to be shown on the display when pressed, irrespective of any previous key depressions.
- The CNDY key is used to display conductivity values. On reset, or when no particular chemical curve has been selected, pressing this key causes the uncompensated conductivity, that is not related to any chemical, to be displayed. When some chemical curve has been selected by the user (as described in the next paragraph), pressing this key causes the conductivity referred to 18 °C for this chemical to be sent to the display. Obviously, this key works in close relation with the CS key.
- The CS (chemical curve select) key, when pressed once displays a number corresponding to the currently used reference curve, in the form CCx. If x=0, this is an indication of no curve selection. The rest of the values for x denote the chemical reference curve as follows:

- 1:  $\text{HNO}_3$
- 2:  $\text{H}_2\text{SO}_4$
- 3:  $\text{HCl}$
- 4:  $\text{KCl}$
- 5:  $\text{NaOH}$
- 6:  $\text{NaCl}$

While the reference curve code is on the display, the next curve can be selected by pressing the CS key again. In case the present chemical code is 6, pressing the CS key returns its value back to 0. If, after pressing the CS key

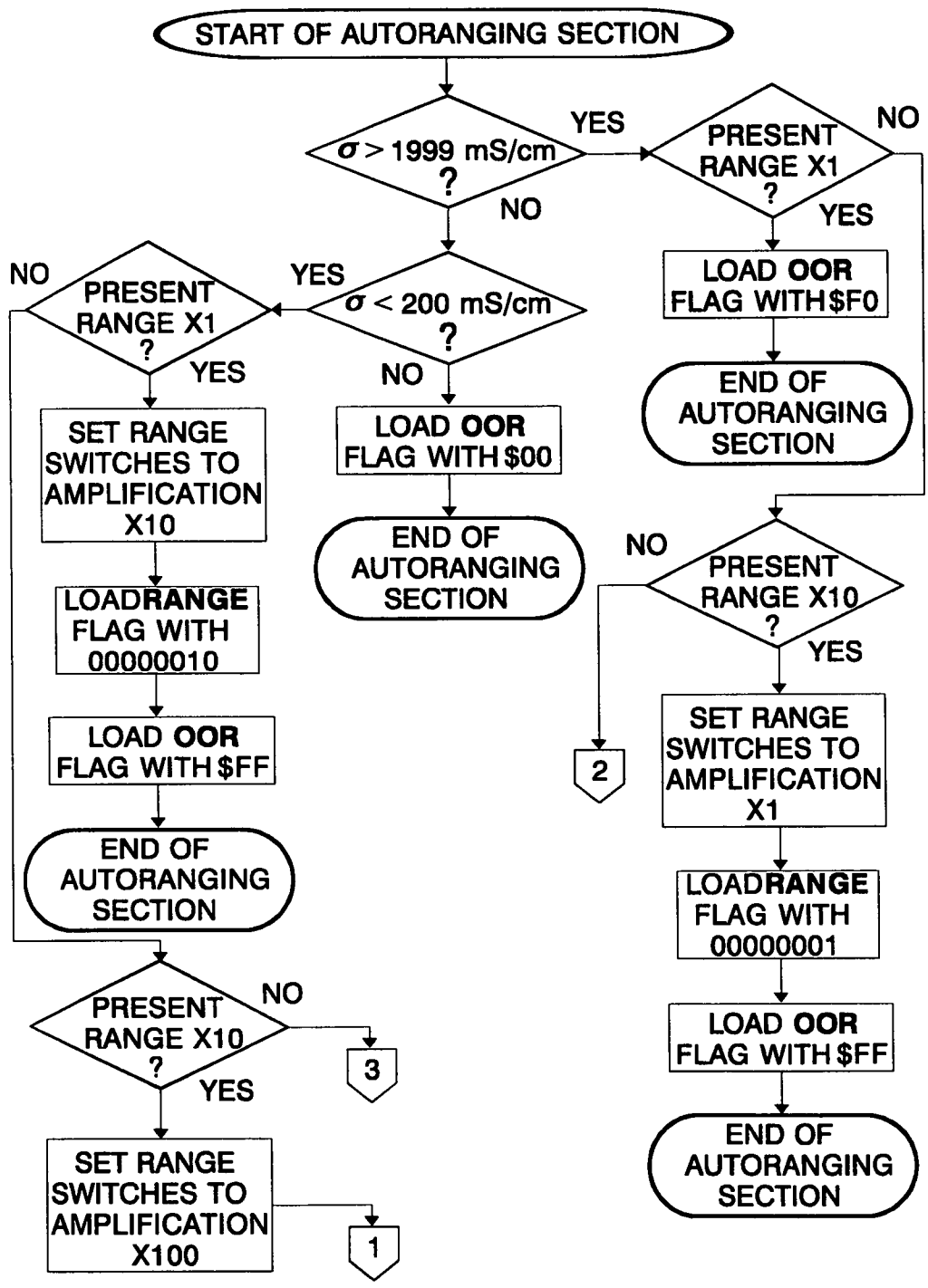


Figure 4.19 The autoranging algorithm

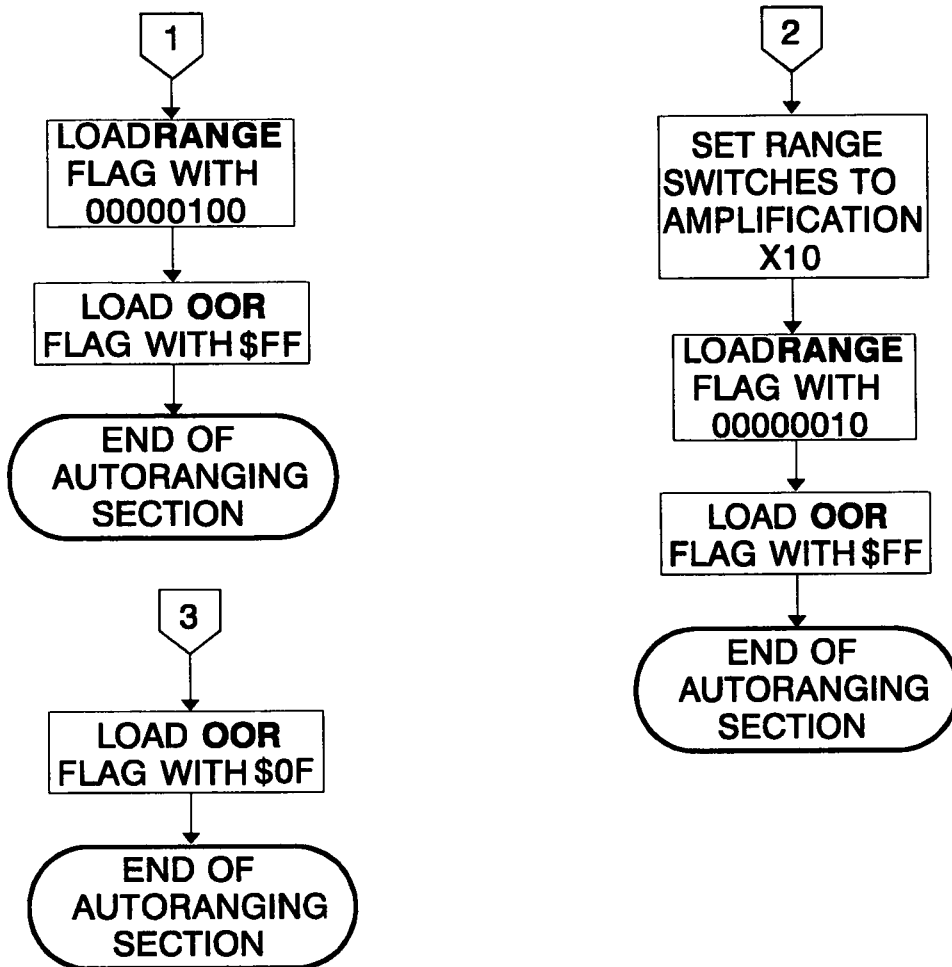


Figure 4.19 (Continued)

once, any of the other keys is pressed, and then CS is pressed again, no change of chemical curve occurs.

- The % key causes the concentration (by weight) of the chemical under examination to be displayed. It is obvious that when the chemical code is 0, a concentration value has no meaning, therefore % key depression in this case has no effect.

In order that the specifications just described are met, a program section employing a table driven algorithm has been developed. It assumes that at any given point in time, the system can only be in one of a predefined set of states, mainly determined by the last key depression and the value of some RAM

variables or flags. To move from one state to another, a key has to be pressed and some RAM variables/flags must have appropriate values; this approach again leads to a defined number of input codes. Also, for each of the stable states of the system there is a corresponding output (action) routine; this is executed as long as the system stays in that state.

As has been mentioned in section 4.5.1 this algorithm works in close relation with the key debouncing algorithm. The value held in KCDE RAM variable is checked on entry to this section, and if its value indicates that a key depression has given a valid keycode (in which case it is of the form \$Fx), the rest of the key parsing algorithm is executed, otherwise it is skipped. It is important that this check is carried out after the present state's action routine is called, so that the display is being updated continuously, with no apparent signs of the system halting in case this section cannot be executed.

The general structure of this program section (which is the task assigned to interval #1) can be seen in figure 4.20. Each of the parts will be fully described within the following paragraphs.

The CC RAM variable, holding the code for the chemical curve being used, plays a very important role in this program section. Together with the value being displayed determines the state the algorithm is in. Each state is given a unique identification number as follows:

- #0 Display of temperature with any value in CC.
- #1 Display of conductivity with CC=0 (uncompensated conductivity).
- #2 Display of conductivity with CC≠0 (temperature compensated conductivity for the chemical under examination).
- #3 Display of chemical curve code for no particular chemical (display shows CC0).
- #4 Display of chemical curve code with CC≠0.
- #5 Display of the percentage concentration with CC≠0.

Accordingly there are input conditions, defined by the code for the key just pressed, and the values in CC variable and the CSDF flag. The latter flag is used to indicate whether the CS key was the last to be pressed. A value of \$00

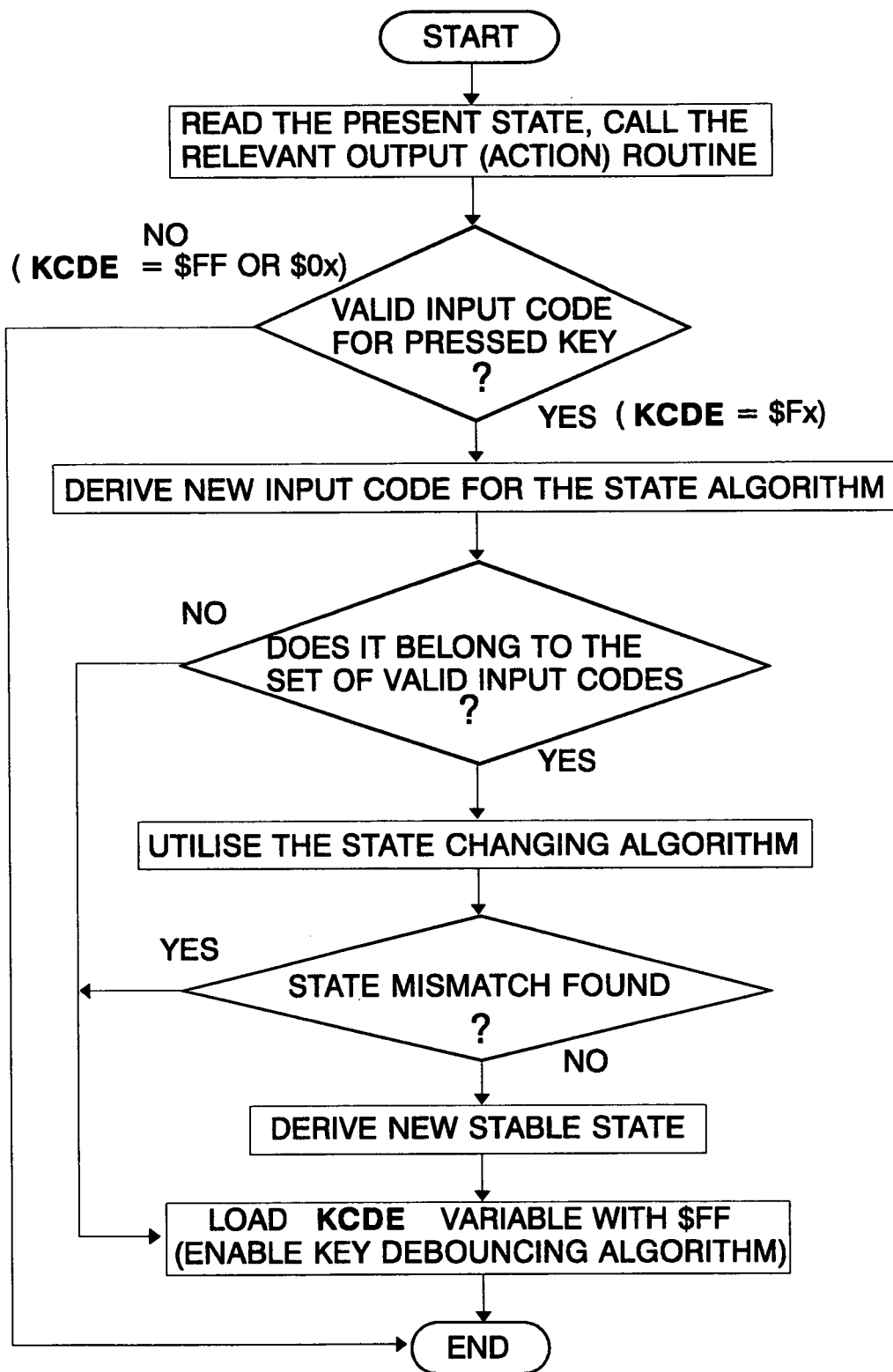


Figure 4.20 General structure of key parsing algorithm



indicates that the key has not been pressed, while a value of \$FF indicates that this key has been pressed at least once. Again, each input condition is given a unique identification number as follows:

- #0 TEMP key pressed, with CC and CSDF holding any values.
- #1 CNDY key pressed, with CC=0 and CSDF holding any value.
- #2 CNDY key pressed, with CC $\neq$ 0 and CSDF holding any value.
- #3 % key pressed, with CC $\neq$ 0 and CSDF holding any value.
- #4 CS key pressed, with CSDF=\$00 and CC=0.
- #5 CS key pressed, with CSDF=\$00 and CC $\neq$ 0.
- #6 CS key pressed, with CSDF=\$FF and CC+1 $\neq$ 0.
- #7 CS key pressed, with CSDF=\$FF and CC+1=0.

With the present states and input conditions defined, a table corresponding to the specifications set above can be constructed, like the one seen in figure 4.21. In that table squares corresponding to stable states are filled with the associated output (action) routine tasks. Squares containing a dash correspond to illegal states. The arrows indicate a valid transition, ending at the next stable state the algorithm enters to.

Software implementation of this state sequencing algorithm requires the existence of the following three tables:

**PTTBL** This is the permissible transitions table. Each entry is 8 bits wide; the upper part holds a stable state code number and the lower part an input code number. This table can be seen in figure 4.22.

**SSTBL** This is the table for the stable states. Again each entry is 8 bits wide, organised in the same way as PTTBL. This table can be seen in figure 4.23. In this table, states [3,7] and [4,6] are considered to be pseudo-stable as the system remains there only for the duration of a measurement cycle: their output routines cause then automatic transition to states [3,4] and [4,5] respectively.

**ACTTBL** This table holds the addresses of the output routines associated with each stable state. Each of the 8 entries in this table is 16 bits wide. This table is organised as seen in figure 4.24.

INPUT CODE STABLE STATE	#0 TEMP KEY CC: ANY CSDF: ANY	#1 CNDY KEY CC: 0 CSDF: ANY	#2 CNDY KEY CC: $\neq 0$ CSDF: ANY	#3 % KEY CC: $\neq 0$ CSDF: ANY	#4 CS KEY CC: 0 CSDF: \$00	#5 CS KEY CC: $\neq 0$ CSDF: \$00	#6 CS KEY CC+1: $\neq 0$ CSDF: \$FF	#7 CS KEY CC+1: 0 CSDF: \$FF
#0 SOLUTION DISPLAYED CC: ANY	DISPLAY CSD: \$00 CC: AS IS						—	—
#1 ABSOLUTE DISPLAYED CC: 0		DISPLAY ABSOLUTE CSD: \$00 CC: AS IS	—	—		—	—	—
#2 $\sigma_{16}$ DISPLAYED CC: $\neq 0$		—	DISPLAY $\sigma_{16}$ CSD: \$00 CC: AS IS	—		—	—	—
#3 CC: 0 DISPLAYED			—	—	DISPLAY CC CSD: \$FF	—	CHPTR = CHPTR + 1 CC = CC + 1	CHPTR = CHPTR + 1 CC = CC + 1
#4 CC: $\neq 0$ DISPLAYED		—			—	DISPLAY CC CSD: \$FF	CHPTR = CHPTR + 1 CC = CC + 1	
#5 VALUE OF c DISPLAYED CC: $\neq 0$		—		DISPLAY c CSD: \$00 CC: AS IS	—		—	—

INITIAL STATE ON RESET: (1,1)

Figure 4.21 Table driven algorithm for key depression interpretation

In addition to these tables, there is a 16 bit pointer named SSPTR in the program which holds an address in SSTBL, or more precisely, holds the address of the address of a subroutine at all times. This is the very variable (pointer) that determines which state the system is in.

Now that the building blocks of the algorithm have been presented, the program sections making use of them are discussed.

The first stage of the algorithm (see figure 4.20) calls the respective action routine. The value of SSPTR is read, and SSTBL address is subtracted from it; the result is then doubled to form an offset into ACTTBL. The relevant action routine is then called using double indirection.

The next stage is the examination of the KCDE; once it has been found to hold a value of the form \$Fx, the program proceeds to the resolution of the input conditions for the state sequencing algorithm. A flowchart of the latter program

section can be seen in figure 4.25.

As the input conditions have been defined, control is passed to the next section which derives the new state of the system. The structure of this section as well as

PTTBL	0	1	\$FFA0
	0	2	
	0	3	
	0	4	
	0	5	
	1	0	
	1	4	
	2	0	
	2	3	
	2	5	
	3	0	
	3	1	
	3	6	
	4	0	
	4	2	
	4	3	
	4	7	
	5	0	
	5	2	
	5	5	\$FFB3

Figure 4.22 Permissible transitions table

SSTBL

0	0	
1	1	
2	2	
3	4	
3	7	*
4	5	
4	6	*
5	3	

\$FFB4

\$FFBB

\* PSEUDO STABLE STATES

Figure 4.23 Stable state table

the method of determining the new state of the system can be seen in figure 4.26. The fact that for each column of the table in figure 4.21 there is only one stable state makes this algorithm much simpler to implement, as only an 8 entry, 8 bit wide table and no further checks are required for the derivation of the new stable state. SSTBL is considered part of PTTBL when searching for matching of the transition states, in order to allow for transitions between stable states belonging to the same row of the table in figure 4.21. This is the reason the two tables have to be placed consecutively in memory, so that the search-for-matching loop becomes shorter and simpler.

Next to be discussed are the action routines. The following paragraphs outline the task performed by each one of these routines:

ACT0: This routine displays the current solution temperature as derived from the analog interface, with one decimal point of accuracy. In case its value exceeds 99.9 °C, the display is filled with 3 Es, and both decimal points are turned on.

ACTTBL	ADDRESS OF ROUTINE ACT 0	\$FF90
	ADDRESS OF ROUTINE ACT 1	
	ADDRESS OF ROUTINE ACT 2	
	ADDRESS OF ROUTINE ACT 3	
	ADDRESS OF ROUTINE ACT 4	
	ADDRESS OF ROUTINE ACT 3	
	ADDRESS OF ROUTINE ACT 4	
	ADDRESS OF ROUTINE ACT 7	

Figure 4.24 Table of addresses of action routines of the key parsing algorithm

ACT1: This routine displays uncompensated conductivity, when OOR flag permits. In case the latter has the value of \$FF, the rest of the routine is skipped, leaving the display unchanged for this measurement cycle. When the OOR flag holds \$0F, the display is filled with 3 Es, with the decimal points turned off, as an indication that conductivity has gone under 2mS/cm. When OOR holds \$F0, the display is filled with 3 Es, and the decimal points are both turned on as an indication that conductivity has become larger than 2000mS/cm. Finally, when OOR holds \$00, normal conductivity is displayed, that is a value between 200 and 1999, together with the decimal points corresponding to the value of RANGE flag.

ACT2: This routine displays the conductivity referred to 18 °C for the chemical whose code is held in CC. Similar use of the OOR flag is done here, as an out of the instrument range conductivity value has no meaning in the calculation of a temperature compensated one. Again, the decimal points to appear on the

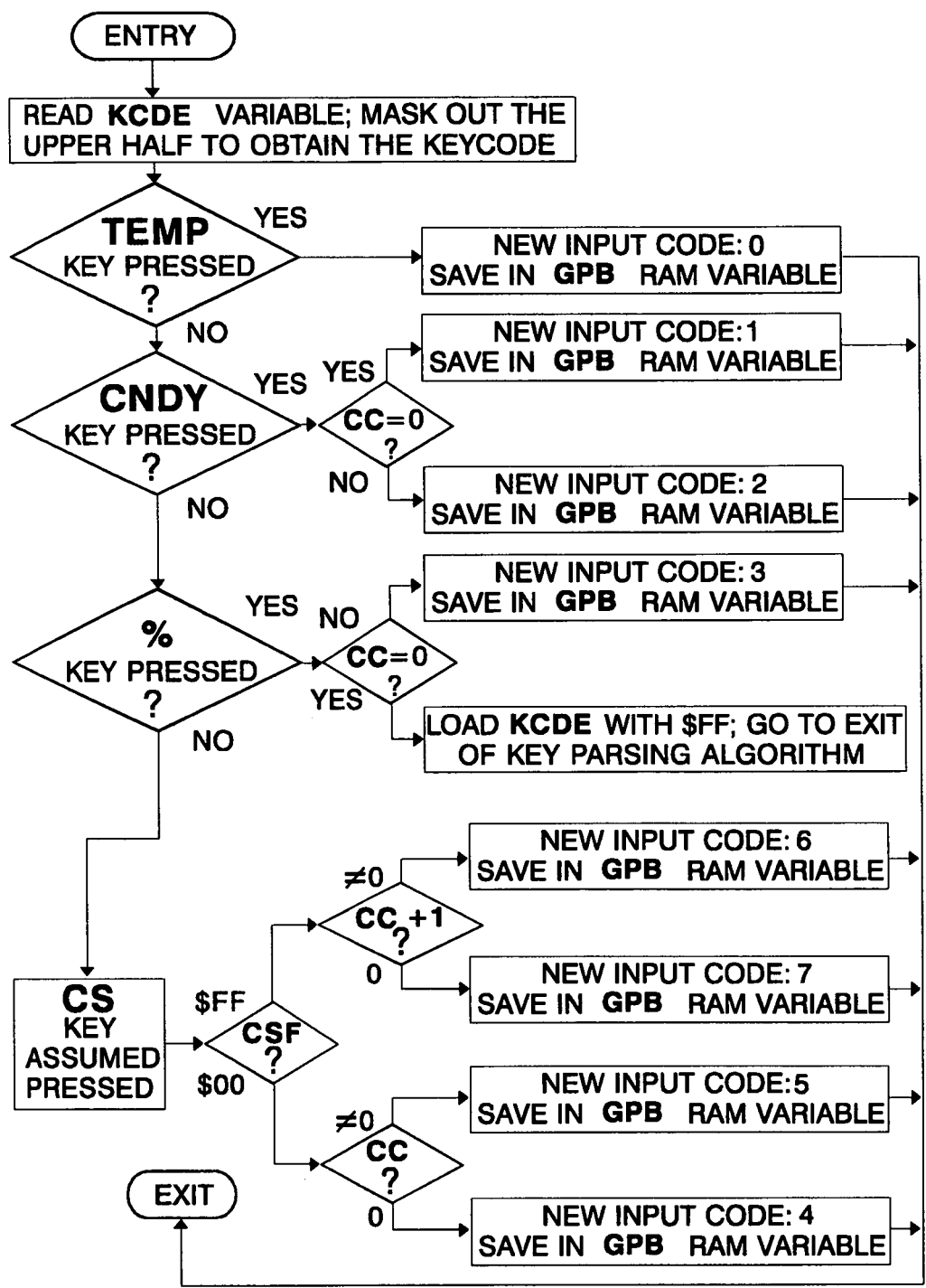


Figure 4.25 New input code derivation section of key parsing algorithm

display are determined by the value in RANGE18 flag.

ACT3: This short routine just displays the reference curve code held in CC variable, making use of DSPCC subroutine.

ACT4: This routine is the system's response to more than one successive depressions of the CS key. Its task is to update the value of CHPTR so that it corresponds to the value in CC variable. Besides it changes the value in SSPTR, so that transition to the just preceding state in SSTBL is caused. This routine does not deal directly with the display, but this task is left to the next state; this scheme causes a somewhat slower response of the display when the codes for the reference curves are changed.

ACT7: This routine displays the percentage by weight of the chemical under examination. It uses the CDPF flag to turn on the correct decimal points.

As seen from the above list there are no routines ACT5 and ACT6, as these would be the same as ACT3 and ACT4 respectively. Considering this, the form of ACTTBL shown in figure 4.24 can be fully understood.

The entry conditions to the key parsing algorithm are set during the initialisation section of the program. The CSDF flag is loaded with \$00, CC is cleared (start with no chemical curve selected), and SSPTR points to stable state [1,1]. Consequently the system after reset or switching on displays absolute (uncompensated) conductivity.

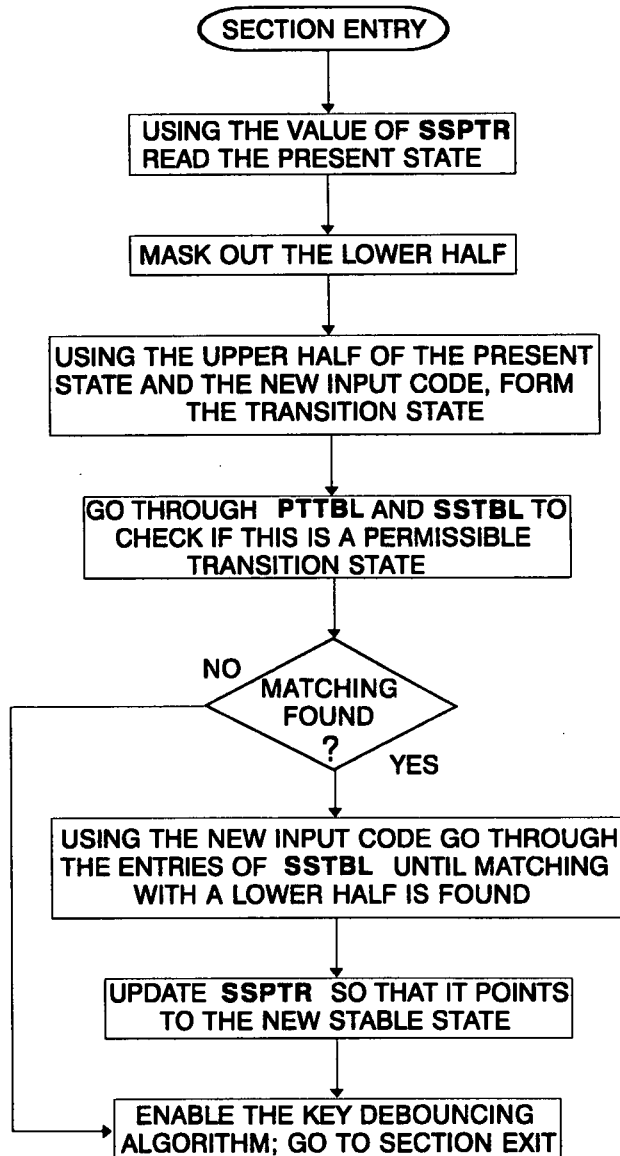


Figure 4.26 New stable state derivation section of key parsing algorithm



#### 4.6 Calibration procedure

Adjustment of the system can be effected as follows:

- The feedback resistor of IC1 (see figure 3.2) must have such value so that the output voltage at 2000mS/cm is around  $2.8V_{PP}$ . This can be achieved by placing a resistance corresponding to this conductivity value (using the value of cell constant) through the probe bore thus forming a closed conductive loop and adjusting the resistor value accordingly.
- The phase shifting network C20-R40 must bring the reference signal at the output of IC9A in phase with the oscillator signal. That would not be necessary if the components of this network had values matching to those of network C3-R9. Similarly, the network C9-R19 should bring the reference signal at the output of IC9B in phase with the conductivity signal. This is effected by observing the two signals on an oscilloscope display; in order that the conductivity signal is clear, a high conductivity signal should be used, preferably the same as in the previous step of adjustment. The use of oscilloscope is acceptable in this case, since the adjustment can be effected to an accuracy of tenths of a degree and the output of the phase sensitive detector is relatively immune to small deviations from the ideal of  $0^\circ$ .
- The characteristic of the V/F converter must be around 10000Hz/V. Exact adjustment is not critical since ratiometric measurements are performed. On a finished system it is difficult to measure the input voltage of this stage (pin 7 of IC11) as the input resistance is around 1 M $\Omega$ , but a proportional value of this voltage can be obtained at the input of the voltage level shifter (pin 10 of IC10C). The transfer function given by the manufacturer (equation 3.2.4) can give an indication of the values to be used.

Then the conversion factors for conductivity and temperature held in CSF and TSF EEPROM constants respectively remain to be adjusted. In the case of conductivity conversion factor a rough initial value can be placed in the EEPROM location, the system run, and then the value reprogrammed for finer adjustment. The unwanted offset in the measurement is automatically determined during the initialisation section of the program and subtracted from all the measured values

thereafter. This conversion factor needs only to be determined with the system in one range, provided that each of the range selection stages gives a precise amplification by 10, as is the case in the present application. In the case of temperature measurement the conversion factor is obvious since the result of equation 3.2.3 has the same rate of change as the value of the probe mounted temperature sensor. The conversion factor itself might not be stored in EEPROM since its value is fixed. It has been stored there though to allow for easy modification of the temperature measurement circuit.

On chip EEPROM programming is a very simple procedure. The 68HC11 evaluation board provides a socket for this purpose, and special commands in the monitor program for data copying, programming, erasing and verifying.

#### **4.7 Error consideration in uncompensated conductivity measurements**

Although theoretical error calculations of the measured quantities can be made, actual comparisons of measured against expected values give a better picture of the accuracy of the system.

The response of the system to several known values of conductivity for the three ranges of measurement can be seen in figures 4.27a to c, and the respective error plots in figures 4.28a to c.

In the latter figures the absolute fractional error is calculated ie

$$e = \frac{|\Delta \sigma|}{\sigma} \times 100\%$$

It can be seen from these figures that the error measured is much smaller than that predicted in section 3.2.11. As mentioned in that section, the calculations were made taking always into account the case that the individual errors always add instead of cancelling.

It is rather surprising and may be coincidental that the error is more or less equal on each of the ranges as this implies that the range amplifiers in the prototype circuit have amplification  $\times 10$  to an accuracy of greater than 1%.

# Instrument response curve

range: X1

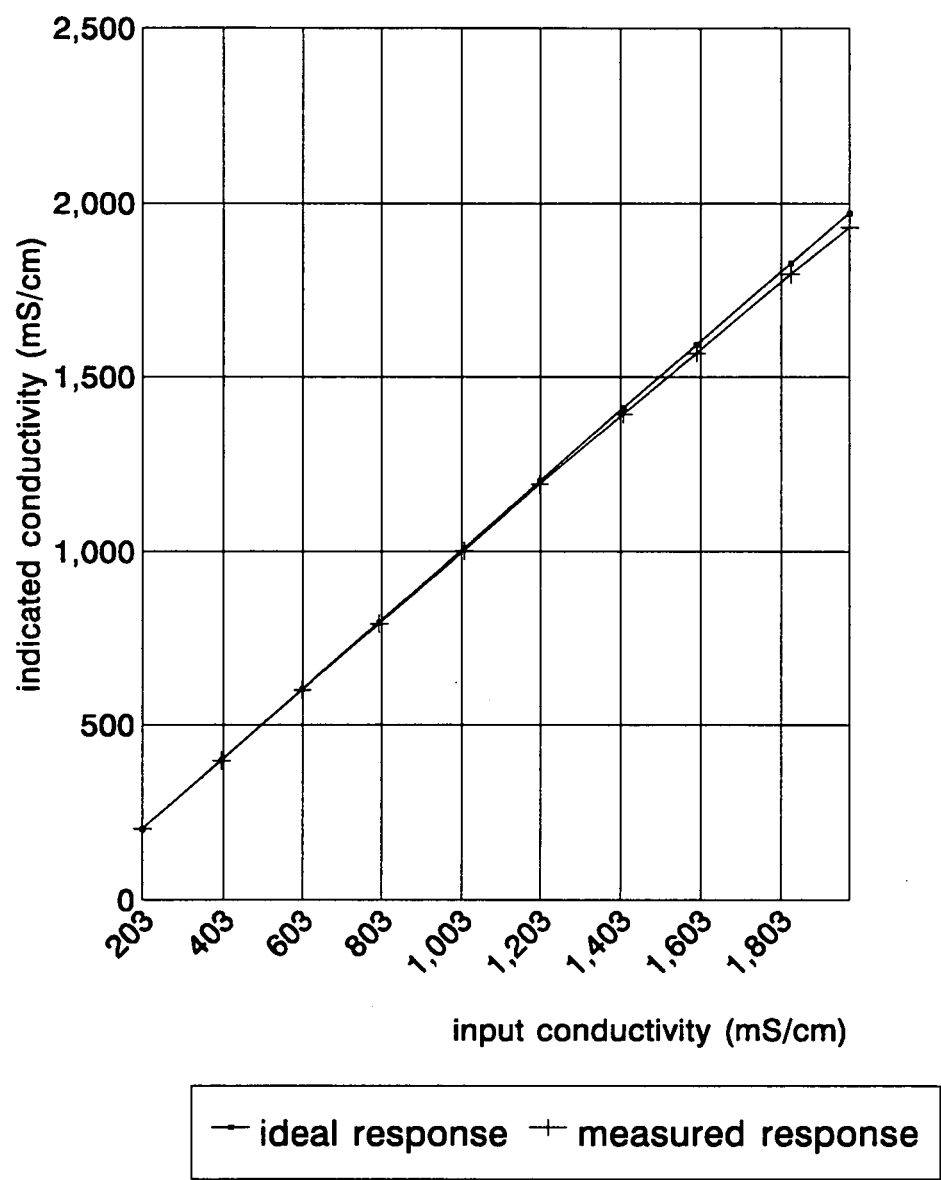


Figure 4.27a

# Instrument response curve

range: X10

---

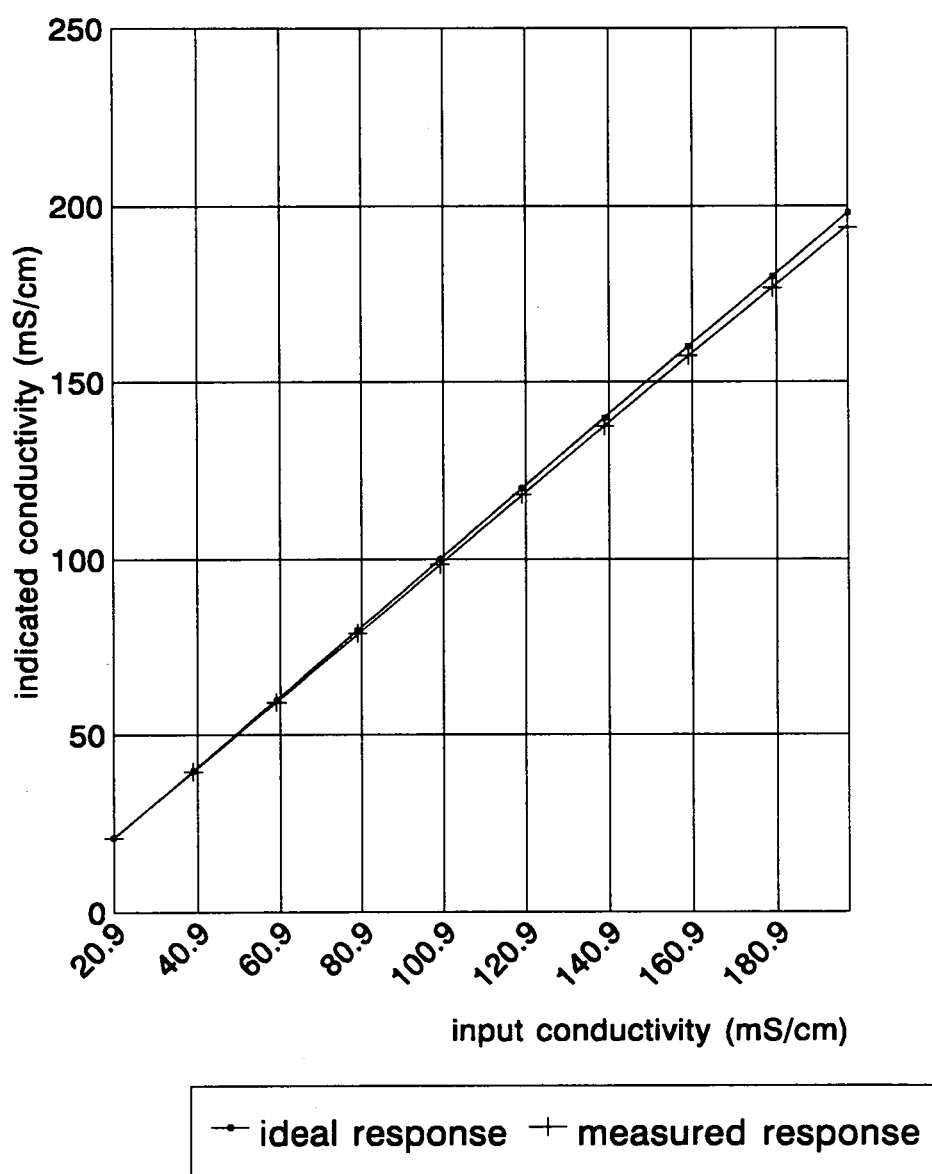


Figure 4.27b

# Instrument response curve

range: X100

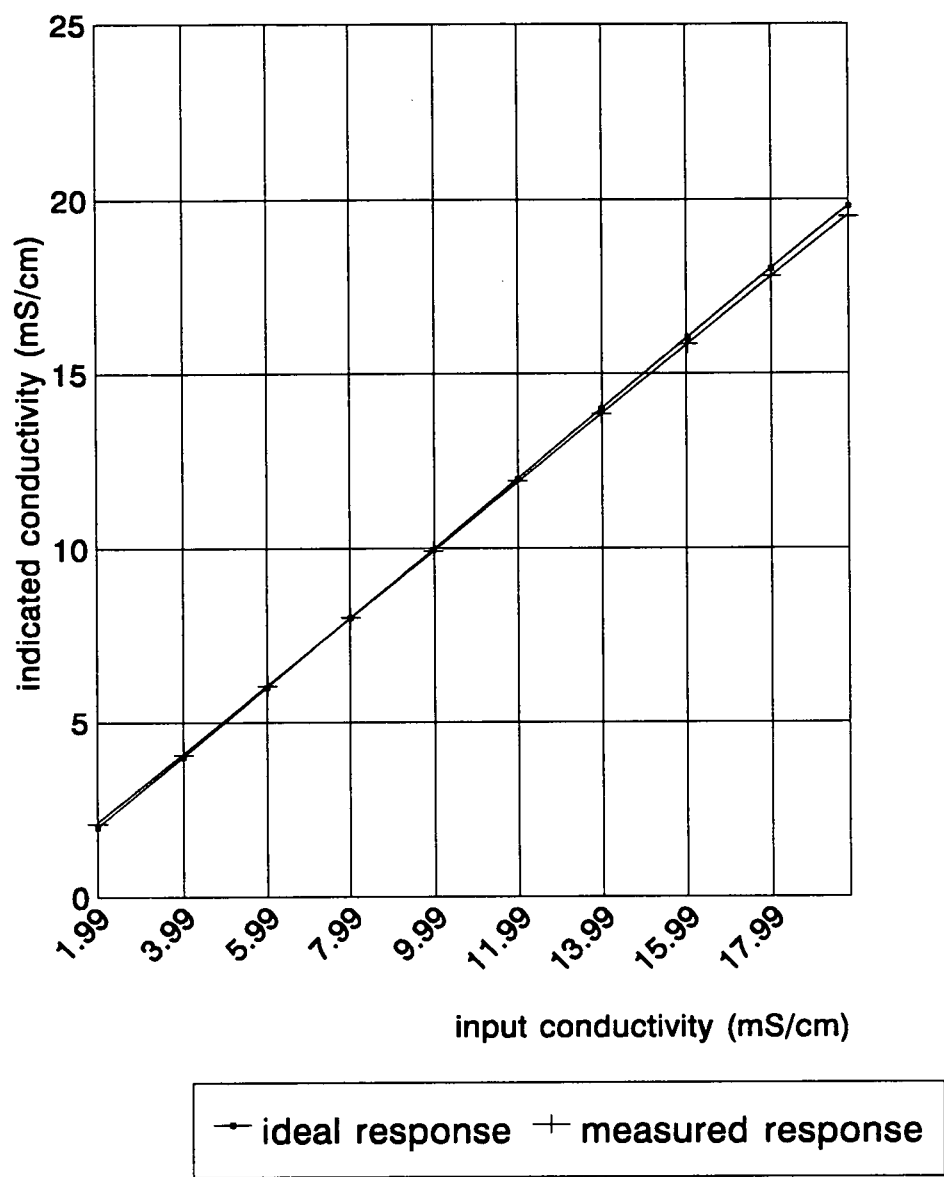


Figure 4.27c

# Instrument error curve

range: X1

---

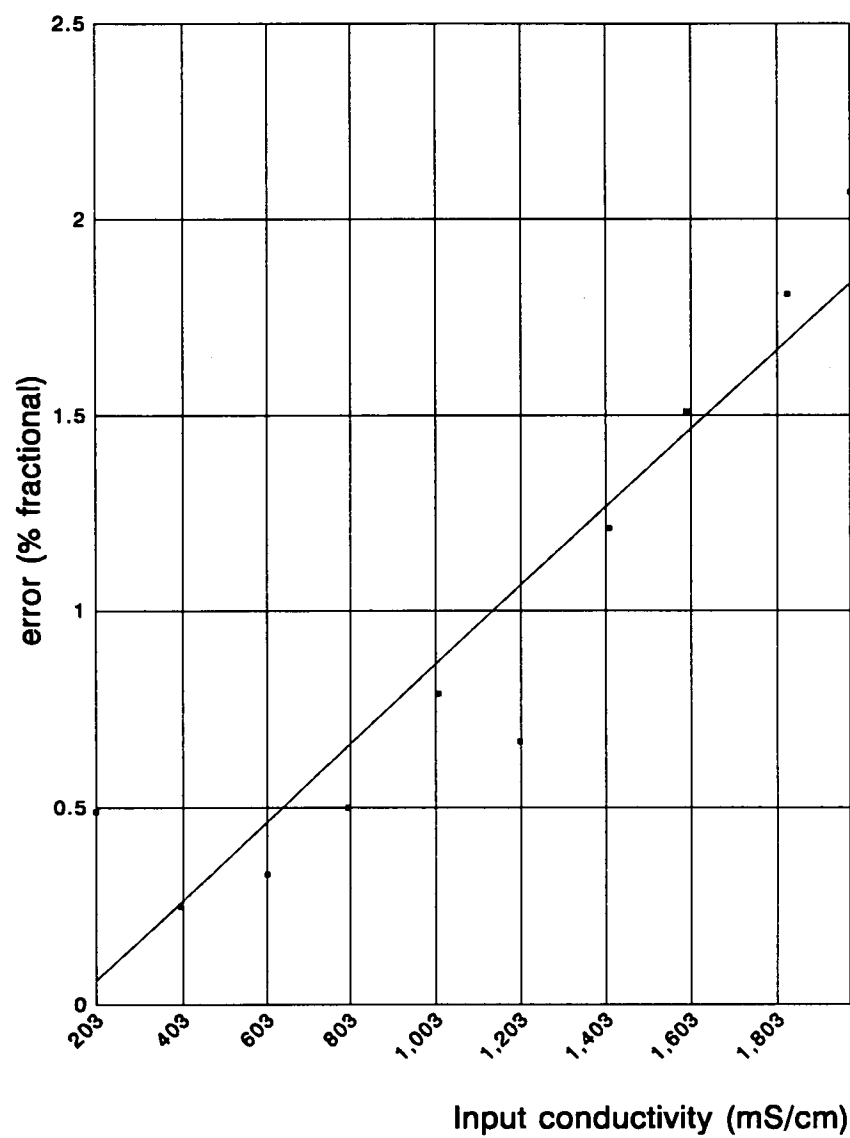


Figure 4.28a

# Instrument error curve

range: X10

---

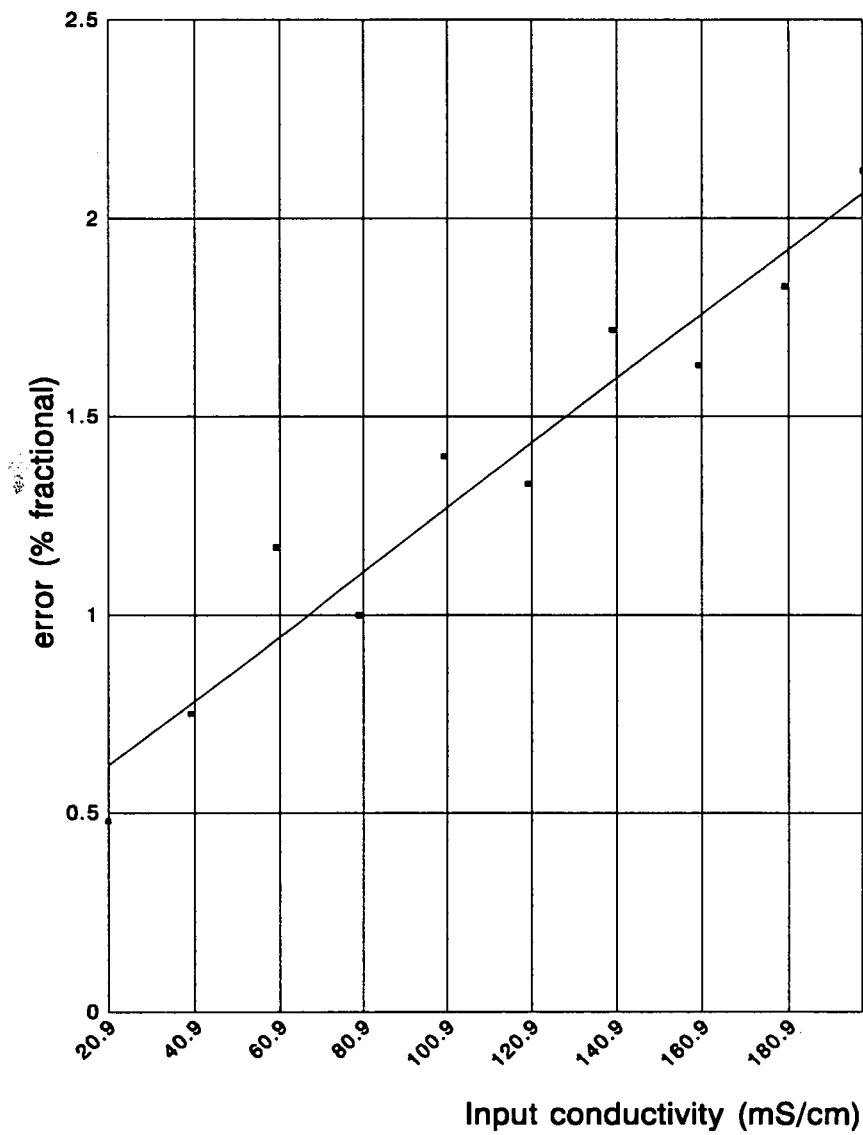


Figure 4.28b

# Instrument error curve

range: X100

---

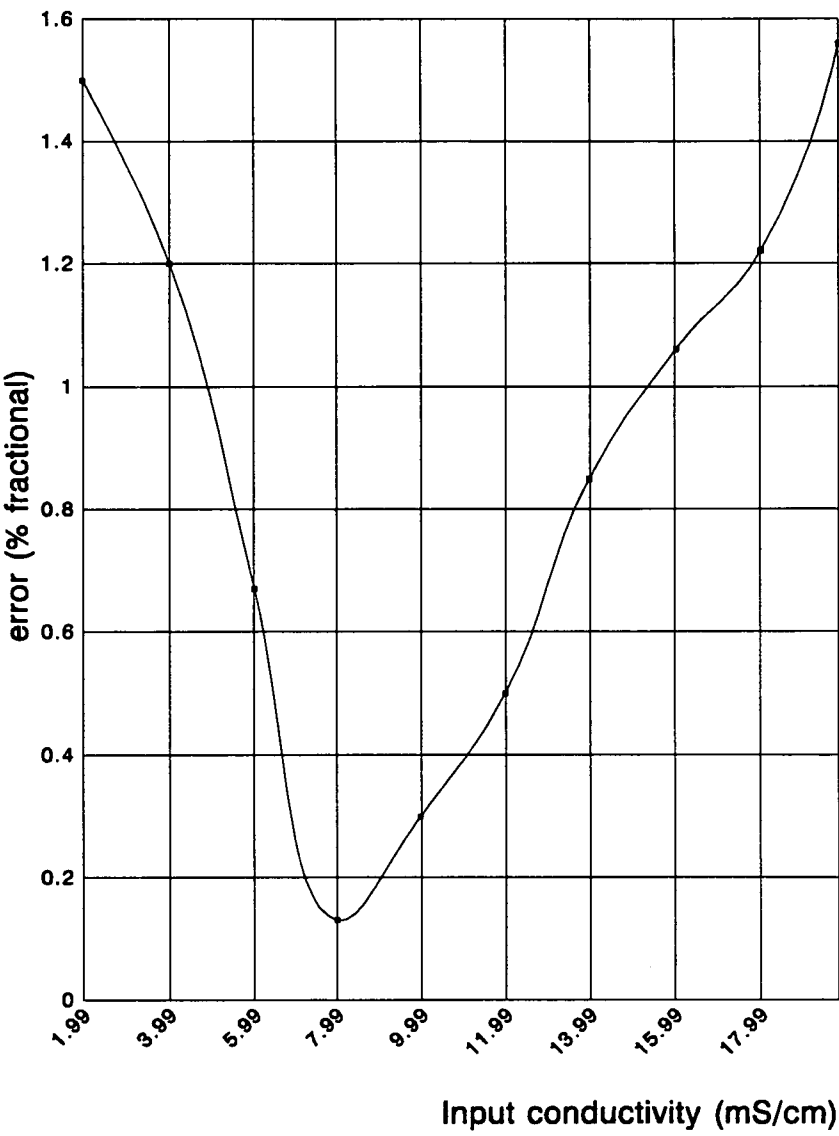


Figure 4.28c



# CHAPTER 5

## CONCLUSIONS

### 5.1 Summary

The method of electrodeless conductivity measurement, using two toroidally wound coils on high permeability ferrite cores in close proximity, has found extensive use in process control, mainly for the determination of solution concentration, due to its stability, ruggedness and maintenance free operation.

It has been shown (chapter 2) that if the magnetic field produced by the drive coil is considered to be entirely confined within the toroidal core (an assumption closely representing reality considering the high values of relative permeability of the toroidal cores) and the magnetic fields associated with currents in the electrolyte are ignored, the line integral of the electric field in the electrolyte is independent of the path of integration. These assumptions allow the deduction of current flow pattern in the electrolyte by solving an electrostatic field problem. Furthermore computations of currents and consequently resistances of the electrolyte can be performed. It has been shown that the dimensions of the conductivity probe and particularly those of the bore play the most important role in the values of resistances. This analysis showed that the total solution resistance can be broken into two parts, namely the bore resistance and that of the remaining solution resistance. The former was almost the same as that of any cylindrical conductor, while the latter was found to depend mainly on the radius of the bore and the cross section of the toroidal core. Hence an expression for the cell constant was derived.

It has been found that the conductivity probe can be represented by an equivalent electrical network comprising two transformers with the solution loop

forming the secondary winding of the first one and the primary winding of the second one. The effects of the transformer coupling coefficients, operating frequency and cable lengths on the magnitude and phase of the sensor output current have been examined. It was found that the effect of each of these factors is more evident on the phase, rather than the amplitude of the output current. It was also found that as the resistances approach 0 and coupling 100%, then the amplitude of the output current becomes a simple function of the oscillator amplitude, the number of turns of the toroidal coils and the conductance of the solution around the conductivity probe, while the phase difference with the oscillator drive voltage approaches  $0^\circ$ . Measurements of output current amplitude and phase for a typical electrodeless sensor gave values very close to ideal.

The other aim of this work was to build a portable, handheld conductivity meter, using an existing electrodeless sensor and based on microcontroller technology, that would be easy to manufacture, calibrate and use. Minimisation of components was a prime target for reduction of cost of production and power consumption, and increased reliability.

An analog part was required to condition the sensor output signal (temperature and conductivity) and convert it to a form readable by the microcontroller. As this signal was shown to vary linearly with the amplitude of the oscillator driving the sensor, it was clear that ratiometric measurements should be performed. In this way the oscillator amplitude can be allowed to vary around a centre value due to temperature variations, component tolerances and aging. Inclusion of the oscillator amplitude in the conductivity measurement also eliminates errors introduced by stages common to both signals. The same method has been employed for the measurement of solution temperature to eliminate variations in the value of the voltage reference. Since the measurement of conductivity is performed using AC signals, the DC offsets and their drifts with temperature and age in the amplification stages are eliminated using coupling capacitors, leading to increased accuracy.

The microcontroller employed (68HC11) holds and runs the program of the system. After an initialisation section during which all variables, devices and

parameters are set up and the offset in the conductivity measurement is determined, control is left to real time interrupts. These provide accurate time reference for the measurement cycles, themselves divided into measurement intervals during which all required tasks take place. The measurement intervals are of 396ms duration each, a response time much better than needed considering that the system is used for measurements in very slowly changing environments. Every 10th cycle is used for the measurement of the oscillator amplitude and the value of the voltage reference used in the temperature measurement circuit. In this way, any change in these sources due to external influences are rectified within 3.96s.

The system also performs calculations for compensated values of conductivity and respective concentration as related to specific chemical solutions, using EEPROM stored reference curves, the temperature and conductivity of the solution. In these calculations linear interpolation methods have been used.

Accuracy calculations for the analog circuit have been made. If worst case errors are considered (ie taking individual error signs in such a way that they always add instead of cancelling) there can be fractional errors of 2, 3.8 and 5.6% in the three ranges of conductivity measurement, not considering the inherent digitisation error. In real situations errors can possibly cancel; this was the case when actual measurements of conductivity showed almost in every case fractional error under 2% for the three ranges of measurement.

Apart from the calculations for the required quantities, other algorithms have been written to handle the debouncing of the keyboard, interpret the key depressions and update the display.

As far as power consumption is concerned, it has been found that the microcontroller used (68HC11), is the major limitation. Despite being an HCMOS device, it can draw a maximum current of 20mA.

## **5.2 Suggestions for further work**

The effect of electrolytic solution flowing around the probe on the sensor output current could be investigated; this is the case of using the sensor in

process control pipes.

The effect of changing the number of turns of the drive and pickup coil on the output current and its phase can also be investigated, using the two transformer equivalent network. In this case there is simultaneous change of the inductance and the resistance of the drive and pickup circuits.

It would be interesting to investigate whether the development and use of 32-bit multiplication and division routines can be feasible in this system considering the time restrictions imposed by the interrupt structure of the 68HC11. If that was made possible, future updating and expansion of the existing software would be made easier and more flexible. Alternatively, floating point routines could be developed; in that case, additional format conversion routines would have to be incorporated in the program. That would also make possible the use of an existing high level language compiler for microcontroller software development, if appropriate interface routines were available or developed.

Addition of an extended keyboard and a more sophisticated display (and display driver), could allow entry and storage of reference curves by the user. This would require extension of the key parsing algorithm and display routines, as well as addition of routines to program/erase parts of the EEPROM. The temperature coefficient, conductivity at 18°C and concentration could all be determined by the user by means of the existing conductivity meter and apparatus for solution temperature control and concentration determination.

The system described in chapters 3 and 4 could form the basis for a part of a distributed digital control system. The availability of an on chip serial port would allow communication with other computers in the system. Additional software would have to be developed for communication, diagnostic procedures, actuator handling, and possible keyboard expansion.

Measuring temperature with the probe immersed in melting ice (ie 0 °C) would give the offset in temperature measurement, allowing more precise temperature measurements. This however requires that this measurement is triggered in some way. This can be done by an additional key on the keyboard, resulting in the need to expand the key sequencing algorithm, or, alternatively a key inducing a

hardware interrupt.

Another small improvement in the temperature measurement could be the use of an AC signal (ie from the sinusoidal oscillator) instead of a voltage reference. In this case all the DC offsets (and their drifts with temperature and aging) could be eliminated with the use of coupling capacitors as in the conductivity measurement. In that case the temperature signal would have to be re-routed through the phase sensitive detector for rectification.

## REFERENCES

- [1] CAVENDISH, H.: Philosophical Transactions (1776) Vol. 46, p.296
- [2] MAXWELL, J.C.; LARMOR, J. (Editors) : "The scientific Papers Of The Honourable Henry Cavendish" University press, Cambridge, England (1921) Vol. 1, p.23
- [3] HORSFORD, E.N.: "Ann. der Physic" Vol. 70, p.238
- [4] KOHLRAUSCH, F.; HOLBORN, L.: "Das Leitvermögen der Electrolyte" Leipzig, Germany (1898)
- [5] WASHBURN, E.W.; BELL J.E.: Journal of American Chemical Society (1913) Vol. 35, p.177
- [6] MARIE, C. ; NOYES, W.A.: Journal of American Chemical Society (1921) Vol. 43, p. 1095
- [7] NEWBERRY, E.J.: Journal of Chemical Society (1918) Vol. 113, p.701
- [8] EASTMAN, E.D.: Journal of American Chemical Society (1920) Vol. 42, p. 1648
- [9] GUNNING, H.E.; GORDON, R.A.: Journal of Chemistry Physics (1942) Vol. 10, p.126
- [10] PUNGOR, E.: "Oscillometry and Conductometry" (1965) Pergamon Press, London

- [11] LIGHT, T.S.: "Electrodeless Conductivity" (1989) ACS Symposium Series, Vol. 390, p. 429
- [12] GUTHRIE, F.; Boys, C.V.: Philosophical Magazine (1880) Vol. 10, p.328
- [13] RUBEN, S.: US Patent 1,610,971 (1926)
- [14] RELIS, M.: MS Thesis, MIT, Cambridge, Massachusetts (1947)
- [15] PICCARD, A.; FRIVOLD, A.: (Swiss) Archives des Sciences Physiques et Naturelles (1920), series 5, Vol. 2, p.264
- [16] RELIS, M.: US Patent 2,542,057 (1951)
- [17] FIELDEN, J.E.: US Patent 2,709,785 (1955)
- [18] SPERRY, E.E.: US Patent 3,396,331 (1968)
- [19] ROSENTHAL, R.: US Patent 3,404,336 (1968)
- [20] KIDDER, R.J.: US Patent 3,404,335 (1968)
- [21] GROSS, T.A.O.: US Patent 3,806,798 (1974)
- [22] GROSS, T.A.O.: US Patent 4,220,920 (1980)
- [23] BROWN, N.L.: Deep Sea Research (1961) Vol. 8, p.65
- [24] KOSKI, O.H.: US Patent 3,867,688 (1975)
- [25] KOSKI, O.H.; DANIELSON, M.J.: Review of Scientific Instrumentation (1979)

Vol. 50, p.1433

- [26] ROSENBERGER, R.R.: US Patent 4,096,028 (1978)
  
- [27] EICHHOLDS, G.G.; BETTENS, A.H.: "Conductimetric Measurement and Control of Acid Concentration In Leach Pulps" (1960) CIM Bulletin, p.901
  
- [28] TIM, A.R.; LIEBENBERG, E.M.; ORMROD, G.T.W.; LOMBAARD, S.L.: "An Electrodeless Conductivity Meter Of Improved Sensitivity And Reliability", NIM, Instruments Division, Report #2003, Johannesburg, South Africa
  
- [29] QUEENEY, K.M.; DOWNEY, J.E. "Applications Of a Microprocessor Based Electrodeless Conductivity Monitor" (1986) ISA, paper # 86-2658
  
- [30] STOCK, J.T.: "Two Centuries Of Quantitative Electrolytic Conductivity" (1984) Analytical Chemistry, Vol. 56, p.561A
  
- [31] MC68HC11 Reference Manual (1989) Prentice Hall International
  
- [32] ALLEN, D.N.de G.: "Relaxation Methods" (1954) McGraw Hill, London
  
- [33] DE VAHL, DAVIS, G.: "Numerical Methods In Engineering Science" (1986) Allen & Unwin, London



# APPENDIX 1

## TABLES OF DATA FOR THE SOLUTIONS REFERENCE CURVES

1. HNO<sub>3</sub>

TC (°C <sup>-1</sup> )	σ <sub>18</sub> (mS/cm)	c (%)
0.0151	165.4	3.1
0.0147	312.3	6.2
0.0143	429.0	9.3
0.0142	541.8	12.4
0.0138	623.5	15.5
0.0137	690.1	18.6
0.0136	738.6	21.7
0.0137	767.6	24.8
0.0137	780.8	27.9
0.0145	781.9	31.0

2. H<sub>2</sub>SO<sub>4</sub>

TC (°C <sup>-1</sup> )	σ <sub>18</sub> (mS/cm)	c (%)
0.0116	107.5	2.5
0.0121	208.5	5.0
0.0124	303.4	7.5
0.0128	391.5	10.0
0.0133	472.3	12.5
0.0136	543.2	15.0
0.0141	603.5	17.5
0.0145	652.7	20.0
0.0149	690.6	22.5
0.0154	717.1	25.0
0.0158	732.9	27.5
0.0162	738.8	30.0

3. HCl

TC (°C <sup>-1</sup> )	σ <sub>18</sub> (mS/cm)	c (%)
0.0158	223.0	2.5
0.0158	394.8	5.0
0.0157	526.7	7.5
0.0156	630.2	10.0
0.0156	702.9	12.5
0.0155	745.3	15.0
0.0154	763.3	17.5

4. KCl

TC (°C <sup>-1</sup> )	$\sigma_{18}$ (mS/cm)	c (%)
0.0206	34.9	2.5
0.0201	69.0	5.0
0.0195	102.5	7.5
0.0188	135.9	10.0
0.0184	169.0	12.5
0.0179	202.0	15.0
0.0173	234.9	17.5
0.0168	267.7	20.0

5. NaOH

TC (°C <sup>-1</sup> )	$\sigma_{18}$ (mS/cm)	c (%)
0.0194	108.7	2.5
0.0201	196.9	5.0
0.0206	267.5	7.5
0.0217	312.4	10.0
0.0231	336.9	12.5
0.0249	346.3	15.0

6. NaCl

TC (°C <sup>-1</sup> )	$\sigma_{18}$ (mS/cm)	c (%)
0.0221	35.5	2.5
0.0217	67.2	5.0
0.0214	95.5	7.5
0.0214	121.1	10.0
0.0211	144.0	12.5
0.0212	164.2	15.0
0.0214	181.7	17.5
0.0216	195.7	20.0
0.0221	204.6	22.5
0.0227	213.5	25.0

# APPENDIX 2

## LIST OF COMPONENTS

The following list contains the components used in the analog and digital circuit. The prices quoted are for large quantity purchase. The cost of connectors, cables and IC sockets has not been included. The total component cost is £31.85, excluding the microcontroller whose prices depend on the version used; this figure is below the initially set maximum of £50.00.

### 1. Integrated circuits

2 × OP37	@ £ 1.50 each
1 × TL072	@ £ 0.26
1 × TL074	@ £ 0.39
1 × TLC3702	@ £ 0.65
1 × OP490	@ £ 3.73
1 × 40106	@ £ 0.20
1 × LM331	@ £ 3.08
2 × 4066	@ £ 0.16 each
1 × 4070	@ £ 0.11
1 × 7211	@ £ 1.76
1 × LS007 LCD	@ £ 4.73
1 × ULN2002A	@ £ 0.30
1 × TSC9491BJ	@ £ 0.70
1 × MC68HC11	(Prices starting from £8.00)

### 2. Diodes

2 × 1N914	@ £ 0.04 each
1 × 7.5V zener	@ £ 0.03

1 × 5.6V zener @ £ 0.03

### 3. Transistors

1 × J201 @ £ 0.24

1 × BC179 @ £ 0.19

2 × 2N3704 @ £ 0.16 each

### 4. Resistors

43 × 1% tolerance @ £ 0.023 each

1 × 4.7K variable resistor @ £ 0.14

### 5. Capacitors

25 × 100nF ceramic @ £ 0.186 each

1 × 100μF tantalum @ £ 1.32

2 × 1μF polyester @ £ 0.85 each

4 × 47μF electrolytic @ £ 0.05 each

2 × 10nF @ £ 0.13 each

3 × 3.3nF @ £ 0.15 each

3 × 100nF @ £ 0.38 each

2 × 10pF @ £ 0.09 each

### 6. Crystals

1 × MHz @ £ 0.70